Surface Modification of Cellulose Nanocrystals with CO_2-Responsive Polymers via Reversible Deactivation Radical Polymerization

by

Joaquin Arredondo-Luna

A thesis submitted to the Department of Chemical Engineering in conformity with the requirements for the Degree of Doctor of Philosophy

Queen's University

Kingston, Ontario, Canada

December, 2017

Abstract

Cellulose is the most abundant natural polymer on Earth. From cellulose, cellulose nanocrystals (CNC) can be obtained through various hydrolysis processes. There is interest in grafting different types of polymers onto CNC as their applications are limited due to their poor dispersibility in low polarity and non-polar systems. The potential versatility and value of modified CNC can be enhanced even further if the polymers used in the grafting process are CO_2-responsive, including for example poly(dimethylaminoethyl methacrylate) (PDMAEMA), poly(diethylaminoethyl methacrylate) (PDEAEMA) and poly(diisopropylaminoethyl methacrylate) (PDPAEMA), since stimuli responsive composites have shown promise in applications such as Pickering emulsifiers, water treatment and as polymer reinforcing agents.

In this work, reaction conditions for the homopolymerization of dialkylaminoethyl methacrlyates (DMAEMA, DEAEMA and DPAEMA) by Cu(0) and RAFT-mediated polymerizations were determine. Cu(0)-ATRP polymerization showed a linear evolution of M_n vs. conversion and first order kinetics; however, poor livingness of the macro-initiators was observed. RAFT-mediated polymerization showed good livingness and the M_n of exclusively the living chains of the macro-RAFT agents was determined by GPC-UV. These macro-RAFT agents were suitable to be used for the *grafting-to* approach.

The grafting of CNC surfaces via *grafting-from* and *grafting-to* using Cu(0)-mediated atom transfer radical polymerization (ATRP) and reversible addition fragmentation chain transfer (RAFT) radical polymerization is also reported. For the *grafting-from* approach, the CNC surfaces were first chemically modified with an ATRP initiating group or a RAFT

agent molecule capable of mediating the polymerization of dialkylaminoethyl methacrylates and their corresponding macro-RAFT agents. A *grafting-from* polymerization was then performed using the CO_2 switchable monomers DEAEMA, DMAEMA and DPAEMA via SI-Cu(0)-ATRP and SI-RAFT. For the *grafting-to* approach, the CNC surfaces were modified with a double bond containing molecule which was then reacted with fully characterized macro-RAFT agents.

All of the grafted products were found to be CO_2-responsive. Products made via *grafting-from* were colloidally stable under CO_2; whereas the products made via *grafting-to* were colloidally unstable under CO_2, but dispersible under mildly basic conditions. It was determined that both the M_n of the polymer grafts and graft densities play an important role on grafted CNC dispersibility.

Co-Authorship

The bulk of this research was conducted independently under the supervision of Dr. Michael F. Cunningham and Dr. Pascale Champagne at Queen's University.

The materials presented in Chapter 3 and 5 have been published in one paper in a peer-reviewed journal as described later on in this thesis. Manuscripts of Chapters 4 and 6 will be submitted as separate papers. Some of the work presented in Chapter 6 was conducted in collaboration with Nicole Woodcock who worked as a summer student in the laboratory.

A second paper mainly conducted and prepared by Dr. Omar Garcia-Valdez has been published as described later on, but it will not be discussed in this thesis.

Some of the work presented in Chapter 5 and 6 were included in a patent submission: Jessop, P.; Champagne, P.; Cunningham, M.; Boniface, K.; Arredondo, J.; Garcia-Valdez, O.; Wang, H.; Cormier, A.; Ge, S. Switchable Polysaccharides, Methods and Uses Thereof. Patent CA 2918904/ WO 2016149815, filed January 2016. Patent Pending.

Acknowledgments

First and foremost, I would like to thank to my supervisors Dr. Michael Cunningham and Dr. Pascale Champagne for giving me the opportunity to join their research group to pursuit my PhD degree. They were not just only guides during my research, but mentors in and outside academia, making their advices and experiences their most significant contribution to my personal development. I am greatly thankful for all the resources that were provided to me without hesitation to conduct all of my research and for the opportunity to explore an international environment.

Special thanks to my summer students, Nicole and Alisha for lending me their pair of hands and also for making the lab work even more enjoyable.

I am also fully grateful to all the CHEE staff. Brooke, Dawn, Elizabeth, Kelly, Laurie, Liann, Lynn, Megan, Tania, Ying. Their unreserved support and friendliness is highly appreciated, plus those great conversations we usually had after a hard day of work or during a tedious week, I will indeed miss you all.

Thanks to Aaron, Connor, Jan, Joe, Kevin, Olga, Omar, Sean, Sharmaine and Thomas for those fantastic research and not research related conversations.

Last but not least, to my family. To my father for always supporting me in my decisions. To my sister for taking care of my father in my absence during these past eight years. If it weren't for you, I'm sure I would not have come to Canada. To my love Yoli, for all your love, courage and patience for being far away from you during these past three and a half years. I know the road hasn't been easy, but I will make it up to you, I promise. I'm coming home!

Table of Contents

Abstract ..... **ii**

Co-Authorship ..... **iv**

Acknowledgments ..... **v**

LIST OF ABREVIATIONS ..... **xxii**

Chapter 1. Introduction **1**

1.1 THESIS OUTLINE 3

REFERENCES 5

Chapter 2. Background and Literature Review **6**

2.1 CELLULOSE NANOCRYSTALS 6

2.1.1 CNC properties *7*

2.1.2 CNC surface modification *8*

2.2 REVERSIBLE DEACTIVATION RADICAL POLYMERIZATION 11

2.2.1 Atom transfer radical polymerization *12*

Cu(0)-ATRP 13

2.2.2 Reversible addition-fragmentation chain transfer-mediated polymerization *15*

2.3 STIMULI-RESPONSIVE POLYMERS 19

2.4 CO_2-RESPONSIVENESS 22

REFERENCES 27

Chapter 3. Homopolymerization of Dialkylaminoethyl Methacrylates via Cu(0)-ATRP **32**

3.1 INTRODUCTION 32

3.2 EXPERIMENTAL 33

3.2.1 General procedure for homopolymerization of DMAEMA and DEAEMA *33*

3.2.2 General procedure for chain-extension of PDMAEMA and PDEAMA macro-initiators *34*

3.3 RESULTS AND DISCUSSION 35
3.3.1 Homopolymerization of DMAEMA and DEAEMA *35*
3.3.2 DMAEMA and DEAEMA Transesterification Analysis *39*
3.3.3 Conclusions *41*
REFERENCES 43

Chapter 4. Homopolymerization of Dialkylaminoethyl Methacrylates via RAFT-mediated Polymerization 45

4.1 INTRODUCTION 45
4.2 EXPERIMENTAL 48
4.2.1 General procedure for the homopolymerization of alkylaminoethyl methacrylates *48*
4.2.2 Chain-extension experiments *50*
4.3 RESULTS AND DISCUSSION 51
4.3.1 Homopolymerization of dialkylaminoethyl methacrylates *51*
4.3.2 Effect of the [CTA]/[I] Ratio *59*
4.3.3 Chain-extension of RAFT-mediated poly(dialkylaminoethyl methacrylates) *63*
4.4 CONCLUSIONS 67
REFERENCES 68

Chapter 5. Surface Modification of Cellulose Nanocrystals via SI-Cu(0)-ATRP and CO_2-Responsiveness. Grafting-from approach 70

5.1 INTRODUCTION 70
5.2 EXPERIMENTAL 74
5.2.1 CNC surface functionalization with α-bromo isobutyric acid *74*
5.2.2 Grafting-from approach by SI-Cu(0)-ATRP *75*
5.2.3 Procedure to test pH-responsiveness of CNC-grafted materials using HCl/NaOH as triggers *76*
5.2.4 Procedure to test the CO_2-responsiveness of the grafted CNC *76*
5.3 RESULTS AND DISCUSSION 77
5.3.1 CNC bromine functionalization *77*

5.3.2 Grafting-from via SI-Cu(0)-ATRP *82*

5.3.3 CO_2-responsiveness *85*

5.4 CONCLUSIONS 91

REFERENCES 92

Chapter 6. Surface Modification of Cellulose Nanocrystals via SI-RAFT-mediated Polymerization via *Grafting-to* and *Grafting-from* Approach and CO_2-Responsiveness 97

6.1 INTRODUCTION 97

6.2 EXPERIMENTAL 101

6.2.1 General procedure for the homopolymerization of alkylaminoethyl methacrylates *101*

6.2.2 General procedure for functionalizing of CNC with glycidyl methacrylate *102*

6.2.3 General procedure for grafting CNC via grafting-to approach by RAFT-mediated polymerization *103*

6.2.4 General procedure for functionalizing CNC with 4-cyanopentanoic acid dithiobenzoate *104*

6.2.5 General procedure for grafting CNC via grafting-from approach by SI-RAFT-mediated polymerization *106*

6.2.6 General procedure for CO_2-switching *106*

6.3 RESULTS AND DISCUSSION 107

6.3.1 Homopolymerization of dialkylaminoethyl methacrylates *107*

6.3.2 Grafting-to approach by RAFT-mediated approach *108*

Functionalization of CNC with glycidyl methacrylate 108

Grafting-to reaction of poly(dialkylaminoethyl methacrylate)s to CNC-GMA 110

Polymer loadings of grafted CNC using different molecular weights macro-RAFT agents 115

6.3.3 CO_2/pH-responsiveness of grafted CNC *117*

6.3.4 Grafting-from approach by SI-RAFT-mediated polymerization *134*

6.3.5 CO_2-responsive CNC as potential Pickering emulsifier agents *141*

6.4 CONCLUSIONS 145

REFERENCES 146

Chapter 7. Conclusions and Recommendations 149

7.1 CONCLUSIONS AND CONTRIBUTIONS 149

7.2 RECOMMENDATIONS FOR FUTURE WORK 151

Appendix.....153

A. Materials 153
A.I. ATRP 153
A.II. RAFT 153
A.III. Synthesis of 4-cyanopantanoic Acid Dithiobenzoate 154
B. Instrumentation 156
B.I. Gel Permeation Chromatography 156
B.II. ^{1}H and ^{13}C Nuclear Magnetic Resonance Spectroscopy 157
B.III. FT-Infrared Spectroscopy 157
B.IV. X-ray Photo Electron Spectroscopy 157
B.V. Elemental Analysis 158
B.VI. Thermogravimetric Analysis 158
B.VII. Atomic Force Microscopy 158
B.VIII. Zeta Potential and Auto-titrations 159
C. ATRP homopolymerization 159
D. RAFT homopolymerization 160
D.I. GPC-UV traces of macro-RAFT agents and chain-extensions 160
D.II. Multi-peak fitting 161
D.III. GPC-UV-RI of PDEAEMAs series 163
E. Grafting by SI-Cu(0)-ATRP 166
F. Grafting by RAFT 167
F.I. GPC-UV of DP# series macro-RAFT agents and their chain-extension 167
F.II. TGA plots of DE and DP grafting-to 168
F.III. Grafting Reproducibility 169
F.IV. pK_{aH} of Polymers 169
F.V. Grafting of CNC-DM# S2 171
F.VI. CO_2 switching of CNC-DM# S2 171
F.VII. ^{13}C NMR of grafting-from products 173
F.VIII. CNC stabilized macro-droplets of organic solvents 175
G. Grafting by FRP 178
G.I. Procedure to perform *grafting-from* approach via FRP 178

LIST OF FIGURES

Figure 2.1. Diagram illustrating different chemical surface modifications of CNC. Reprinted with permission from Peng *et al.*[11] Copyright 2011. Canadian Society for Chemical Engineering. 9

Figure 2.2. Illustration of the *grafting-to* and *grafting-from* approach for the immobilization of polymer chains on a solid surface. Reprinted with permission from Li *et al.*[12] Copyright 2013 Royal Society of Chemistry. 10

Figure 2.3. Classification of stimuli-responsive polymers.[49] 20

Figure 2.4. Illustration of the LCST and UCST of a polymer chain.[49] 21

Figure 2.5. Degree of protonation as a function of pK_{aH} and concentration at 0.1 Mbar of CO_2 and 25°C. Reprinted with permission from Alshamrani *et al.* [56] Copyright 2016 Royal Society of Chemistry 24

Figure 2.6. Chemical structures of diverse pH-responsive polyamines. Reprinted with permission from Cunningham and Jessop.[57] Copyright 2016 Elsevier Ltd.. 26

Figure 3.1. Ln($[M]_0/[M]$) vs. time plot of DMAEMA and DEAEMA homopolymerization by Cu(0)-ATRP using HMTETA as ligand at 60°C in MeOH. DMAEMA:$[CuBr_2]$:[L]:$[I]_0$:$[M]_0$= 1:100:91:5782. DEAEMA: $[CuBr_2]$:[L]:$[I]_0$:$[M]_0$= 1:100:107:5782. 36

Figure 3.2. . Reaction mixture in a sealed Schlenk tube at t=0 and after 60 min at 60°C in MeOH. DMAEMA: $[CuBr_2]$:[L]:$[I]_0$:$[M]_0$ = 1:100:91:5782. 36

Figure 3.3. M_n and Đ evolution vs. conversion of both PDMAEMA and PDEAEMA. DMAEMA:$[CuBr_2]$:[L]:$[I]_0$:$[M]_0$= 1:100:91:5782. DEAEMA: $[CuBr_2]$:[L]:$[I]_0$:$[M]_0$= 1:100:107:5782. 37

Figure 3.4. GPC traces of PDMAEMA and PDEAEMA as a function of conversion. DMAEMA:$[CuBr_2]$:[L]:$[I]_0$:$[M]_0$= 1:100:91:5782. DEAEMA: $[CuBr_2]$:[L]:$[I]_0$:$[M]_0$= 1:100:107:5782. 38

Figure 3.5. GPC trace of the chain-extension of PDMAEMA and PDEAEMA based macro-initiators via Cu(0)-ATRP. 39

Figure 3.6. Degree of transesterification MMA vs. time of DMAEMA and DEAEMA. Dialkylaminoethyl methacrylate:MeOH = 1:1 v/v at 60 C. 40

Figure 3.7. ^{1}H NMR spectra of DEAEMA (a) and DMAEMA (b) after 250 min of transesterification in methanol. 41

Figure 4.1. GPC-UV trace of a PDMAEMA-based macro-RAFT agent. Reprinted with permission from Sahnoun *et al.*[3] Copyright 2005 Wiley Periodicals, Inc. 47

Figure 4.2. Ln($[M]_0/[M]$) and conversion vs. time plots of DMAEMA (DM), DEAMA (DE), DPAEMA (DP) in bulk and in tert-butanol via RAFT polymerization at 70°C. DMAEMA: $[M]_0 : [CTP]_0 : [I]_0 = 318:5:1$. DEAEMA: $[M]_0 : [CTP]_0 : [I]_0 = 270:5:1$. DPAEMA: $[M]_0 : [CTP]_0 : [I]_0 = 234:5:1$. 52

Figure 4.3. Evolution of M_n vs. conversion of DMAEMA (DM), DEAMA (DE), DPAEMA (DP) in bulk and in tert-butanol via RAFT polymerization at 70°C. DMAEMA: $[M]_0 : [CTP]_0 : [I]_0 = 318:5:1$. DEAEMA: $[M]_0 : [CTP]_0 : [I]_0 = 270:5:1$. DPAEMA: $[M]_0 : [CTP]_0 : [I]_0 = 234:5:1$. 54

Figure 4.4. GPC UV-RI traces of the polymerization of DMAEMA in bulk and in tert-butanol via RAFT polymerization at 70°C. $[M]_0 : [CTP]_0 : [I]_0 = 318:5:1$.... 56

Figure 4.5. GPC UV-RI traces of the polymerization of DEAEMA in bulk and in tert-butanol via RAFT polymerization at 70°C. $[M]_0 : [CTP]_0 : [I]_0 = 270:5:1$.... 57

Figure 4.6. GPC UV-RI traces of the polymerization of DPAEMA in bulk and in tert-butanol via RAFT polymerization at 70°C. $[M]_0 : [CTP]_0 : [I]_0 = 234:5:1$.... 58

Figure 4.7. GPC UV-RI traces of the polymerization of DMAEMA in bulk and in tert-butanol via RAFT polymerization at 70°C. $[M]_0:[CTP]_0:[I]_0 = 318:10:1$. 61

Figure 4.8. GPC UV-RI traces of the polymerization of DEAEMA in bulk and in tert-butanol via RAFT polymerization at 70°C. DEAEMA: $[M]_0 : [CTP]_0 : [I]_0 = 270:10:1$. 62

Figure 4.9. GPC-UV traces of PDMAEMA macro-RAFT agents before and after chain-extension. [macro-RAFT]:[ACVA] = 5, in tert-butanol at 70°C. 64

Figure 4.10. GPC-UV-RI traces of DM1 macro-RAFT agent before and after chain-extension. [macro-RAFT]:[ACVA] = 5, in tert-butanol at 70°C after 16h. .. 66

Figure 4.11. GPC-UV-RI traces of DM2 macro-RAFT agent before and after chain-extension. [macro-RAFT]:[ACVA] = 5, in tert-butanol at 70°C after 16h. .. 66

Figure 4.12. GPC-UV-RI traces of DM3 macro-RAFT agent before and after chain-extension. [macro-RAFT]:[ACVA] = 5, in tert-butanol at 70°C after 16h. .. 67

Figure 5.1. FT-IR of native CNC, CNC-Br and polymer-grafted CNC. 78

Figure 5.2. Solid-state CP-MAS ^{13}C NMR spectra of native CNC and surface-modified CNC with BIBA, PDMAEMA and PDEAEMA. 79

Figure 5.3. Thermogravimetric analysis of native CNC, CNC-Br and polymer-grafted CNC. 80

Figure 5.4. High-resolution XPS spectra. a) carbon. b) bromine. 81

Figure 5.5. Grafting-from of PDEAEMA onto CNC-Br via SI-Cu(0)-ATRP 83

Figure 5.6. AFM micrographs of (a) native CNC, (b) CNC-Br, (c) CNC-g-PDEAEMA, (e) CNC-g-PDMAEMA. 84

Figure 5.7. HCl/NaOH cycles of CNC-g-PDMAEMA B1 ranging from pH 4-10. 86

Figure 5.8. CO_2/N_2 sparging cycles of CNC-g-DMAEMA B1 with no added base at initial conditions. 87

Figure 5.9. CO_2/N_2 sparging cycles of CNC-g-DMAEMA B2 with initial pH adjusted to 12 with 100 µL of 1M NaOH. 88

Figure 5.10. CO_2/N_2 sparging cycles of CNC-g-PDEAEMA B2 with initial pH adjusted at 12 with 100 µL of NaOH 1M. 89

Figure 5.11. CO_2-switchability of CNC-g-PDEAEMA B2 at ca. 0.4 wt.% under a full switching cycle. a) CNC-g-PDEAEMA dispersion in its original state. b)

Dispersed CNC-g-PDEAEMA after CO_2 sparging. c) CNC-g-PDEAEMA after N_2 sparging. 90

Figure 6.1 IR spectra of native CNC and CNC-GMA. The boxed region encloses the C=O stretching band at 1,700 cm^{-1} and the deformation vibration of residual water at 1,600 cm^{-1}..... 109

Figure 6.2. Thermogravimetric analysis of native CNC and CNC-GMA. 110

Figure 6.3. FT-IR spectra of PDMAEMA-grafted CNC (CNC-DM#) series. 112

Figure 6.4. FT-IR spectra of PDMAEMA-grafted CNC (CNC-DE#) series. 112

Figure 6.5. FT-IR spectra of PDMAEMA-grafted CNC (CNC-DP#) series..... 113

Figure 6.6. TGA analysis of native CNC, CNC-GMA and PDMAEMA-grafted CNC. 114

Figure 6.7. CO_2-switching of CNC-DM1 (0.4 wt.%) dispersed at neutral pH (a) and aggregated under CO_2 (b). 118

Figure 6.8. CO_2-switching of CNC-DP2 (0.4 wt.%) (a) under CO_2, (b) under N_2. 118

Figure 6.9. ζ-potential and ionic conductivity vs. pH of the CNC-DM# series (ca. 0.4 wt.%) going from pH 12 to 2 with 0.5 M HCl. The boxed region represents unreliable ζ-potential values as PDMAEMA-grafted CNC are aggregated at these pHs. 120

Figure 6.10. CNC-DM# dispersions (0.2 wt.%) at different pH values (DM1: pH 4-5, DM2: 7-8, DM3: 9-10) in a 50% v/v water chloroform mixture with Nile Red as hydrophobic dye..... 123

Figure 6.11. CNC-DM1 dispersion (0.2 wt.%) at three different pHs (4-5, 7-8, 9-10) in a 50% v/v water chloroform mixture with Nile Red as hydrophobic dye. A laser pointer beam was passed through the aqueous (left) an organic (right) phase. For the organic phase laser irradiation, of the dispersion in acidic pH was not shown due to a very strong light scattering of the organic phase. 123

Figure 6.12. CNC-DM2 dispersion (0.2 wt.%) at three different pHs (4-5, 7-8, 9-10) in a 50% v/v water chloroform mixture with Nile Red as hydrophobic dye. 124

Figure 6.13. CNC-DM3 dispersion (0.2 wt.%) at three different pHs (4-5, 7-8, 9-10) in a 50% v/v water chloroform mixture with Nile Red as hydrophobic dye. 125

Figure 6.14. ζ-potential and ionic conductivity vs. pH of the CNC-DE# series (0.4 wt.%) going from pH 12 to pH 2 with HCl 0.5M. The boxed region represents unreliable ζ-potential values as PDMAEMA-grafted CNC aggregate in this pH region 126

Figure 6.15. ζ-potential and ionic conductivity vs. pH of the CNC-DP# series (0.4 wt.%) going from pH 12 to pH 2 with HCl 0.5M..... 128

Figure 6.16. CNC-DP3 dispersion at different pHs covering the CO_2-N_2 pH range. A commercial laser pointer beam was directed through the aqueous phase in series showing the laser beam path due to light scattering generated by the CNC. The intensity of the scattered light in third vial is lower due to an attenuating effect caused by the first two vials. 128

Figure 6.17. Proposed phase diagram where CO_2 stability in aqueous dispersions depends on the graft density and the M_n of the polymer grafts. 131

Figure 6.18. CO_2-switching of CNC-DM1S2 (0.4 wt.%). Under CO_2 it forms a stable dispersion and it sediments under N_2. 133

Figure 6.19. Auto-titration curves of CNC-DM1 and CNC-DM1S2 (ca. 0.4 wt.%)..... 133

Figure 6.20. FT-IR of native CNC and CNC-CTP. The red box highlights corresponding to the carbonyl group of the CTP at 1,717 cm^{-1} structure and the aromatic skeletal vibrations at 1,590 cm^{-1} which overlaps the O-H signal at 1,640 cm^{-1}. The blue box highlights a signal at 1,268 cm^{-1} which is presumed to be an aromatic deformation vibration..... 135

Figure 6.21. TGA analysis of CTP, native CNC, CNC-CTP and grafted CNC products via SI-RAFT polymerization. 136

Figure 6.22. FT-IR of native CNC, CNC-CTP and polymer-grafted CNC via SI-RAFT polymerization. 138

Figure 6.23. Auto-titration curves of CNC-grafted products made by SI-RAFT polymerization (0.4 wt.%). 139

Figure 6.24. CO_2-switching cycles of CNC-DM. (0.4wt %). 140

Figure 6.25. CO_2-switching cycles of CNC-DE. (0.4wt %). 140

Figure 6.26. Toluene macro-droplets stabilized with CNC-DM1 (0.2 wt.%) using Nile red as dye. pH was adjusted with 0.5 M HCl and NaOH in the CO_2-N_2 pH switching range. (a) 5-6, (b) 7-8, (c) 9-10. 142

Figure 6.27. Toluene macro-droplets stabilized with CNC-DM3 (0.2 wt.%) using Nile red as dye. The pH was adjusted with 0.5 M HCl and NaOH in the CO_2-N_2 pH switching range. (a) 5-6, (b) 7-8, (c) 9-10. 143

Figure 6.28. High viscosity emulsions of different organic solvents (chloroform, hexanes and toluene) after sonication of CNC-DM1 and CNC-DM3 aqueous dispersions (ca. 0.2 wt.%) at a pH between 7-8. The pH was not adjusted. 144

Figure A.1. ^{1}H NMR of synthesized CTP. 155

Figure A.2. ^{13}C NMR of synthesized CTP. 156

Figure C.1. Conversion vs. time profiles of DEAEMA polymerization using Me_6TREN as ligand. [$CuBr_2$]:[Me_6TREN] = 1:100, BIBA=0.2 mmol, DEAEMA= 10.8 mmol. Me_6TREN= 0.37 mmol. 159

Figure C.2. DEAEMA polymerization using Me_6TREN as ligand in DMSO. [$CuBr_2$]:[Me_6TREN] = 1:100, BIBA=0.2 mmol, DEAEMA= 10.8 mmol. Me_6TREN= 0.37 mmol. 160

Figure D.1. GPC-UV traces of PDEAEMA macro-RAFT agent series and their chain-extension. 160

Figure D.2. GPC-UV traces of PDEAEMA macro-RAFT agent series and their chain-extension. 161

Figure D.3. Multi-peak fitting of the RI chain-extension trace of DM1..... 161

Figure D.4. Multi-peak fitting of the RI chain-extension trace of DM2..... 162

Figure D.5. Multi-peak fitting of the RI chain-extension trace of DM3..... 162

Figure D.6. GPC-UV-RI of DE1 macro-RAFT agent and its chain-extension. 163

Figure D.7. GPC-UV-RI of DE2 macro-RAFT agent and its chain-extension. 163

Figure D.8. GPC-UV-RI of DE3 macro-RAFT agent and its chain-extension. 164

Figure D.9. GPC-UV-RI of DP1 macro-RAFT agent and its chain-extension. 164

Figure D.10. GPC-UV-RI of DP2 macro-RAFT agent and its chain-extension. 165

Figure D.11. GPC-UV-RI of DP2 macro-RAFT agent and its chain-extension. 165

Figure F.1. GPC-UV of DP# series macro-RAFT agents and their chain-extension. 167

Figure F.2. TGA analysis of CNC-DE# series. 168

Figure F.3. TGA analysis of CNC-DP# series..... 168

Figure F.4. Titration of PDMAEMA for pK_{aH} determination. $M_{n\ MHS}$: 14,900 Da. 169

Figure F.5. Titration of PDEAEMA for pK_{aH} determination. $M_{n\ MHS}$: 12,700 Da. 170

Figure F.6. Titration of PDPAEMA for pK_{aH} determination. $M_{n\ PMMA}$: 7,100 Da. 170

Figure F.7. CO_2-N_2 switching of CNC-DM1S2. 171

Figure F.8. CO_2-N_2 switching of CNC-DM2S2. 172

Figure F.9. CP-MAS ^{13}C NMR of native CNC (black) and CNC-CTP (red). 173

Figure F.10. CP-MAS ^{13}C NMR of CNC-DM. 173

Figure F.11. CP-MAS ^{13}C NMR of CNC-DE. 174

Figure F.12. CP-MAS ^{13}C NMR of CNC-DP..... 174

Figure F.13. Mixture of chloroform and water with Nile Red as a hydrophobic dye. Both phases show a certain level of light scattering (left). 175

Figure F.14. CNC-DM2 dispersions (0.2 wt.%) in dyed toluene (left) and chloroform (center) and hexanes (right) with unmodified pH. The vial on the left with each solvent was not stirred. The vial on the right was hand-shaken. No sonication. 176

Figure F.15. CNC-DE3 dispersion (0.2 wt.%) in dyed toluene. The pH was adjusted with 0.5 M NaOH to a value of 9-10 (left). No sonication. 176

Figure F.16. CNC-DE1 dispersion (0.2 wt.%) in dyed toluene. The pH was adjusted with 0.5 M HCl to a value of 2-3 (left). No sonication. 177

Figure F.17. Sonicated CNC-DM1, CNC-DM2, CNC-DM3 and CNC-DE2 dispersion (0.2 wt.%) in dyed toluene. The pH was adjusted with 0.5 M HCl to a value of 4-5 only for CNC-DE2 (right). The rest dispersions are at neutral pH. 177

Figure G.1. TGA analysis of CNC-GMA, FRP grafted CNC and physical mixtures of CNC-GMA with homopolymers of DMAEMA, DEAEMA and DPAEMA. 178

LIST OF SCHEMES

Scheme 2.1. ATRP general mechanism of propagation. 12

Scheme 2.2. SARA/SET ATRP mechanism. Reprinted with permission from Konkolewicz *et al.*[33] Copyright 2014 Royal Society of Chemistry 14

Scheme 2.3. General RAFT polymerization mechanism showing initiation, propagation, reversible chain transfer, reinitiation, chain equilibration and termination steps.[39] 16

Scheme 2.4. RAFT agent structures. Dithioesters (a), trithiocarbonates (b), xanthates (c) and dithiocarbamates (d). Reprinted with permission from Keddie, D.[43] Copyright 2013 Royal Society of Chemistry. 17

Scheme 2.5. Radical propagating species in the form of methacrylate, vinyl acetate or methyl methacrylate. Reprinted with permission from Keddie, D.[42] Copyright 2012 American Chemical Society 18

Scheme 2.6. Guideline for the selection of Z group for RAFT polymerization according to monomer activity. Reprinted with permission from Keddie, D.[42] Copyright 2012 American Chemical Society 19

Scheme 2.7. Guideline for the selection of Z group for RAFT polymerization according to monomer activity. Reprinted with permission from Keddie, D.[42] Copyright 2012 American Chemical Society 19

Scheme 2.8. Schematics representing the deprotonation of a protonated polyamine (pK_{aH}). 22

Scheme 2.9. Reversible protonation of a polyamine with CO_2. 23

Scheme 3.1. Cu(0)-ATRP of DMAEMA and DEAEMA. DMAEMA [$CuBr_2$]: [L]:[$I]_0$:[$M]_0$ = 1:100:91:5782. DEAEMA:[$CuBr_2$]:[L]:[$I]_0$:[$M]_0$=1:100:107:5782. 33

Scheme 4.1. RAFT-mediated polymerization of dialkylaminoethyl methacrylates in bulk or solution at 70°C using 4-cyanopantanoic acid dithiobenzoate as RAFT agent and 4,4 -azobis(4-cyanopentanoic acid) as initiator..... 48

Scheme 5.1 CO_2-responsive poly(dialkylaminoethyl methacrylate). 72

Scheme 5.2 Grafting-from approach for modifying CNC with CO_2-switchable polymers. 73

Scheme 5.3. CNC functionalization reaction with BIBA and CDI at room temperature. BIBA= 111 mmol, CDI= 111.5 mmol, OH= 37 mmol. 77

Scheme 5.4. Grafting-from approach via SI-Cu(0)-ATRP. DMAEMA:$[CuBr_2]$:[L]:$[I]_0$:$[M]_0$=1:100:91:5782. DEAEMA:$[CuBr_2]$:[L]:$[I]_0$:$[M]_0$= 1:100:107:5782. 82

Scheme 6.1. Attachment of CTA to the substrate determines the mechanism of polymerization. If the substrate is attached through the R-group, grafting-from operates. Conversely, transfer-to is the mechanism if the CTA is attached through the Z-group.[12] 99

Scheme 6.2. CNC surface modification via *grafting-from* and *grafting-to* approaches. 101

Scheme 6.3. CNC functionalization with GMA under acidic conditions (pH= 3). OH= 36.54 mmol, GMA= 74 mmol at 65°C. 108

Scheme 6.4. *Grafting-to* of CNC-GMA with poly(dialkylaminoethyl methacrylates) based macro-RAFT agents in tert-butanol. [macro-RAFT]:[ACVA] = 5:1 at 70°C. 111

Scheme 6.5. CNC functionalization reaction with CTP and CDI at room temperature. CTP= 111 mmol, CDI= 111.5 mmol, OH= 37 mmol. 134

Scheme 6.6. *Grafting-from* via SI-RAFT polymerization. CNC-CTP (0.25 g), DMAEMA (12.72 mmol), DEAMA (10.77 mmol), DPAEMA (9.39 mmol), ACVA (0.07 mmol) in tert-butanol at 70°C. 137

LIST OF TABLES

Table 2.1. pK_{aH} of pH-responsive polymers and monomers. Adapted with permission from Cunningham and Jessop.[57] Copyright 2016 Elsevier Ltd. 26

Table 4.1. Polymerization recipe for the synthesis of macro-RAFT agents. 49

Table 4.2. Characteristics of macro-RAFT agents and recipe for chain-extension experiments. 50

Table 4.3. Comparison of M_n and Đ values of macro-RAFT agents synthesized in bulk and in solution. 62

Table 4.4. GPC UV-RI data of macro-RAFT agents and after chain-extension. 63

Table 5.1. Atomic and mass composition of bromine-functionalized CNC by XPS analysis. 80

Table 5.2. Elemental Analysis of CNC-grafted products. 84

Table 6.1. Recipes for synthesizing 4 g of different macro-RAFT agents of DMAEMA, DEAMA and DPAEMA at 50% monomer conversion in solution 4mL of tert-butanol. 102

Table 6.2. Recipe for the grafting of CNC-GMA using pre-synthesized PDMAEMA, PDEAMA and PDPAEMA based macro-RAFT agents. [macro-RAFT]:[ACVA] = 5. 104

Table 6.3. Characteristics of macro-RAFT agents used for chain-extension experiments and CNC grafting. 107

Table 6.4. Elemental analysis, polymer content and graft densities of the CNC-DM#, CNC-DE# and CNC-DP# series. 115

Table 6.5. CO_2-N_2 switching of an aqueous dispersion of CNC-DM1 (0.4 wt.%). Initial pH was adjusted with 0.5 M NaOH. 117

Table 6.6. Graft characteristics of PDEADMA-grafted CNC via RAFT and NMP..... 130

Table 6.7. Elemental analysis and graft densities of CNC-DM1 and CNC-DM1S2..... 132

Table 6.8. Elemental analysis results of CNC-grafted products via SI-RAFT polymerization. 138

Table F.1 Elemental analysis of grafting-to replicates of DM2 macro-RAFT agent 169

Table F.2. Elemental Analysis of CNC-DM#S2 series. 171

LIST OF ABREVIATIONS

ζ	Zeta potential
[I]	Initiator concentration
[L]	Ligand concentration
[M]	Monomer concentration
ACVA	4,4 -Azobis(4-cyanopentanoic acid)
AFM	Atomic force microscopy
AGUs	Anhydroglucose units
ARGET	Activators regenerated by electron transfer
ATRP	Atom transfer radical polymerization
BIBA	Bromo isobutyric acid
CDI	Carbonyl diimidazole
CNC	Cellulose nanocrystals
CNC-Br	Bromine functionalized CNC product
CNC-CTP	4-cyanopantanoic acid dithiobenzoate functionalized CNC
CNC-DE	PolyDEAEMA functionalized CNC
CNC-DM	PolyDMAEMA functionalized CNC
CNC-DP	PolyDPAEMA functionalized CNC
CNC-GMA	Glycidyl methacrylate functionalized CNC
CTA	Chain transfer agent
CTP	4-cyanopantanoic acid dithiobenzoate
Đ	Molecular weight dispersity defined as M_n/M_w
DEAEMA	Diethyl aminoethyl methacrylate
DLS	Dynamic light scattering
DMAEMA	Dimethyl aminoethyl methacrylate
DMAPMAM	Dimethyl aminopropyl methacrylamide
DMF	Dimethyl formamide
DMSO	Dimethyl sulfoxide
DPAEMA	Diisiopropy aminoethyl methacrylate
DP_n	Degree of polymerization
FRP	Free radical polymerization
FT-IR	Fourier-transformed infrared spectroscopy
GMA	Glycidyl methacrylate
GPC	Gel permeation chromatography
GPC-UV-RI	Gel permeation chromatography couple to UV and RI detector
HMTETA	1,1,4,7,10,10-Hexamethyltriethylenetetramine
ICAR	Initiators for continuous activator regeneration
k_{add}	Rate coefficient of addition in the RAFT mechanism
k_{deact}	Deactivation constant in ATRP equilibrium

$k_{p\ app}$	Apparent rate coefficient of propagation
k_p	Propagation rate coefficient
LCST	Lower critical solution temperature
MA	Methacrylic acid
Me_6TREN	Tris[2-(dimethylamino)ethyl]amine
MeOH	Methanol
M_n	Number average molecular weight
mV	Millivolt
M_n	Number average molecular weight
M_w	Weight average molecular weight
NMR	Nuclear magnetic resonance
NMP	Nitroxide mediated polymerization
PAA	Polyacrylic acid
PDEAEMA	Poly(diethylaminoethyl methacrylate)
PDMAEMA	Poly(dimethylaminoethy methacrylate)
PDMAPMAm	Poly(dimethylaminopropyl methacrylamide)
PDPAEMA	Poly(diisiopropyaminoethyl methacrylate)
pK_a	Acidity constant in $\log_{10}$ scale
pK_{aH}	The pK_a of the protonated form of an amine
PMA	Polymethacrylic acid
PMMA	Poly(methyl methacrylate)
P_n	Propagating chain with “n” monomer units
PNIPAM	Poly(N-isopropylacrylamide)
PRE	Persistent radical effect
RAFT	Reversible addition fragmentation chain transfer
RDRP	Reversible deactivation radical polymerization
RI	Refractive index
R_p	Rate of polymerization
SARA	Supplemental activator and reducing agent
SET	Single electron transfer
SI-Cu(0)-ATRP	Surface-initiated copper mediated atom transfer radical polymerization
SI-RAFT	Surface-initiated RAFT polymerization
TGA	Thermogravimetric analysis
THF	Tetrahydrofuran
UCST	Upper critical solution temperature
UV	Ultraviolet
XPS	X-ray photoelectron microscopy

Chapter 1. Introduction

Cellulose is the most abundant natural and renewable biopolymer on earth having an estimated annual production of 7.5 x 10^{10} tons.[1] As a raw material, it has traditionally been used extensively in the form of fibers or chemically modified derivatives for a wide spectrum of products which have a critical role in modern applications. Recently, cellulose has regained the interest of the scientific community mainly due to its highly crystalline allomorph commonly known as cellulose nanocrystals (CNC). Published papers related to CNC have grown at an exponential trend since 2000 (4 papers published) compared to present times (almost 12,776 papers published in 2016) (Web of Science, 2017). While the physical, chemical, and mechanical properties of CNC are comparable to other reinforcing nanomaterials, the recent attention CNC have garnered may also be attributed to its natural abundance, renewability, low toxicity, and relatively low cost. With future research, CNC are poised to become a major reinforcing material in nanocomposites, amongst other applications.[2]

Possible applications for CNC are currently being studied, covering a wide spectrum of areas and focusing mainly on reinforcing materials. However, applications in the biomedical, drug delivery, optical, coatings, water treatment and other areas are being developed as well. Nevertheless, there is one main obstacle to the development of these applications, which is the highly hydrophilic character of CNC, beneficial for biomedical applications,[3-4] but a limitation as a reinforcing material.[5] In consequence, the introduction of unmodified CNC are therefore limited to highly polar systems (solvents or polymer blends) unless surface modifications are made to the CNC surfaces. One approach to address this limitation is to functionalize one or more of the free hydroxyl groups with

different types of chemical groups, which can range from small molecules to relatively high molecular weight molecules or polymers, through different functionalization strategies.

Stimuli-responsive polymers derived from vinyl pyridine or dialkylaminoethyl methacrylates, for which CO_2 could be used as a trigger are of particular interest for surface modification of CNC, as the responsive polymer properties could be incorporated to enhance the desirable CNC properties. Properties such as pH-responsive hydrophobicity and electrostatic positive charges could result in a CNC-based material with fully reversible switching hydrophobicity and the ability to produce redispersible colloidal systems, which could contribute to the development of new applications such as pH-responsive flocculants[6], or Pickering pH-responsive emulsifiers.[7-9]

Therefore, taking into account CNC's limitations (strong hydrophilic character), along with the switchable hydrophobicity of tertiary polyamines, and their capability of providing positive surface charges, the primary objective of this research is to surface-modify CNC with CO_2-responsive polymers using reversible deactivation radical polymerization (RDRP) techniques, such as surface-initiated copper mediated atom transfer radical polymerization (SI-Cu(0)-ATRP) and surface-initiated reversible addition-fragmentation chain transfer radical polymerization (SI-RAFT), and analyze their CO_2-responsiveness for potential applications. The specific research objectives are summarized below:

1. Determine suitable homopolymerization conditions for DMAEMA, DEAEMA via Cu(0)-ATRP.

2. Determine suitable homopolymerization conditions for DMAEMA, DEAEMA and DPAEMA via RAFT-mediated polymerization.

3. Graft CNC with PDMAEMA, PDEAEMA and PDPAEMA via *grafting-from* and *grafting-to* approach using Cu(0)-ATRP and RAFT polymerization techniques.

4. Assess CO_2-responsiveness of the grafted materials.

5. Analyze the effect of different molecular weights of the polymer grafts in the CO_2-switching of grafted CNC.

1.1 ***Thesis outline***

Chapter 2 provides background on CNC and the present techniques available on how to surface-modify them. It also describes the fundamentals of Cu(0)-ATRP and RAFT-mediated polymerization techniques that were employed in this research. Finally, it gives an overview of the different kinds of stimuli-responsive polymers showing why they are of great interest for producing composite materials and finishes with the description of the principles of CO_2-switching of pH-responsive polymers.

Chapter 3 discusses the homopolymerization kinetics and conditions for suitable polymerization of dialkylaminoethyl methacrylates in solution via Cu(0)-ATRP. It discusses monomer incompatibilities with the catalyst as well as side reactions with the solvent which are not usually taken into account in existent reports. Livingness was also assessed by chain-extension experiments.

Chapter 4 discusses the homopolymerization kinetics and conditions of dialkylaminoethyl methacrylates via RAFT-mediated polymerization in bulk and in solution. It shows the advantages of using RAFT to polymerize dialkylaminoethyl methacrylates compared to Cu(0)-ATRP and NMP, where homopolymers can be easily obtained with good control and livingness. Chain-end functionality and livingness were drastically improved compared to Cu(0)-ATRP.

Chapter 5 summarizes the surface modification of CNC with ATRP-capable initiator and poly(dialkylaminoethyl methacrylates) via a *grafting-from* approach using SI-Cu(0)-ATRP. It also describes the CO_2-responsiveness of grafted CNC with two different dialkylaminoethyl methacrylates as well as the advantages and disadvantages of CO_2-switching compared to conventional acid and bases.

Chapter 6 summarizes the surface modification of CNC with reactive double bonds and with a RAFT agent capable of mediating RAFT polymerization. The grafting of poly(dialkylaminoethyl methacrylates) via *grafting-to* and *grafting-from* approaches and the effects of grafting density and molecular weight of the polymer grafts on CO_2-switching are also discussed. Potential applications as surfactants are briefly addressed.

Chapter 7 is a summary and highlights the contributions of this research, suggesting further approaches to help further understanding the behaviour of these CO_2-switchable materials.

References

1.French, A. D.; Bertoniere, N. R.; Brown, R. M.; Chanzy, H.; Gray, D.; Hattori, K.; Glasser, W., Cellulose. In *Kirk-othmer encyclopedia of chemical technology*, John Wiley & Sons, Inc.: 2000.

2.Kovacs, T.; Naish, V.; O'Connor, B.; Blaise, C.; Gagné, F.; Hall, L.; Trudeau, V.; Martel, P., An ecotoxicological characterization of nanocrystalline cellulose (ncc). *Nanotoxicology* **2010,** *4* (3), 255-270.

3.Morandi, G.; Thielemans, W., Synthesis of cellulose nanocrystals bearing photocleavable grafts by ATRP. *Polymer Chemistry* **2012,** *3* (6), 1402-1407.

4.Lin, N.; Huang, J.; Dufresne, A., Preparation, properties and applications of polysaccharide nanocrystals in advanced functional nanomaterials: A review. *Nanoscale* **2012,** *4* (11), 3274-3294.

5.Capadona, J. R.; Van Den Berg, O.; Capadona, L. A.; Schroeter, M.; Rowan, S. J.; Tyler, D. J.; Weder, C., A versatile approach for the processing of polymer nanocomposites with self-assembled nanofibre templates. *Nat Nano* **2007,** *2* (12), 765-769.

6.Kan, K. H. M.; Li, J.; Wijesekera, K.; Cranston, E. D., Polymer-grafted cellulose nanocrystals as pH-responsive reversible flocculants. *Biomacromolecules* **2013,** *14* (9), 3130-3139.

7.Tang, J.; Berry, R. M.; Tam, K. C., Stimuli-responsive cellulose nanocrystals for surfactant-free oil harvesting. *Biomacromolecules* **2016,** *17* (5), 1748-1756.

8.Tang, J.; Lee, M. F. X.; Zhang, W.; Zhao, B.; Berry, R. M.; Tam, K. C., Dual responsive Pickering emulsion stabilized by poly[2-(dimethylamino)ethyl methacrylate] grafted cellulose nanocrystals. *Biomacromolecules* **2014,** *15* (8), 3052-3060.

9.Tang, J.; Quinlan, P. J.; Tam, K. C., Stimuli-responsive Pickering emulsions: Recent advances and potential applications. *Soft Matter* **2015,** *11* (18), 3512-3529.

Chapter 2. Background and Literature Review

2.1 *Cellulose nanocrystals*

Cellulose is Earth's most abundant natural and renewable biopolymer. As a raw material, it is widely used in the form of fibers or as chemically modified derivatives for a wide spectrum of products. Lately, cellulose has become the subject of widespread interest to the scientific community primarily due to its renewability and, more recently, due to its highly crystalline allomorph known as cellulose nanocrystals (CNC).[1]

Cellulose nanocrystals are comprised of cellulose crystallites with at least one dimension of 100 nm.[2] CNC are produced via the acid hydrolysis of cellulose fibers. Interestingly, CNC can be easily obtained from any cellulosic source including bacteria, plants or marine species containing cellulose fibers.[1] These fibers are mainly composed of a cellulosic amorphous outer layer which is hydrolyzed leaving the crystalline surface intact and yielding crystals of 200 to 400 nm long and a width ranging from 10-20 nm, depending on the acid hydrolysis process and the cellulose source.[3] Depending on the acid selected for this process, the CNC surfaces could end up with different moieties, in addition to the hydroxyl groups, at the end of the hydrolysis process.

The most common acid used for obtaining CNC is sulfuric acid which, during the hydrolysis process, will functionalize a small fraction of the hydroxyl groups with half sulfate ester groups which will in turn confer to the CNC surface a negative electrostatic charge, making the CNC readily dispersible in high polarity solvents resulting from electrostatic repulsion. If desired, these sulfate half-ester moieties could be also removed with further mild alkaline treatments.[4] Other hydrolysis processes can be performed either

with hydrochloric acid, which yields 100% unmodified CNC, or phosphoric acid hydrolysis, which yields slightly phosphorylated CNC, both of which are more thermally stable than sulfated CNC.[5]

2.1.1 *CNC properties*

CNC have interesting mechanical, optical and chemical properties.[6] CNC mechanical properties can be directly compared to single walled carbon nanotubes, which are much more toxic and expensive to produce than CNC, which is nontoxic, biodegradable and relatively easy to obtain.[7] In terms of Young's modulus and tensile strength, CNC are usually on the order of GPa (134 GPA and 7 GPa respectively),[8] which are slightly lower than the values associated with single walled carbon nanotubes (320-1,470 GPa and 10-52 GPa respectively).[9] This similarity in mechanical properties, with respect to carbon nanotubes, is mainly due the highly ordered crystalline structure.

The thermal stability of CNC will depend on the process employed in its synthesis. It is well known that CNC produced by hydrolysis using sulfuric acid will be less thermally stable as the half sulfate ester groups are thermally labile compared to the CNC obtained with hydrochloric acid, where no functional groups are attached to the CNC surface. However, CNC generally have a high thermal stability, decomposing above 250°C.[5] These mechanical and thermal properties could enhance the performance of materials when using CNC as a reinforcing material for several applications involving the design of new materials.

In terms of optical properties, CNC obtained through the sulfuric acid hydrolysis process exhibits self-assembly in aqueous media, similar to liquid crystalline arrangements

or chiral nematic ordering.[1] This means that in a dilute regime, CNC crystals are randomly oriented (isotropic phase). However, when a critical CNC concentration is achieved, unidirectional self-orientation of the CNC can be induced forming a chiral nematic phase. This liquid crystalline behaviour could be advantageous as CNC could have potential applications in the field of electronics.[1]

2.1.2 *CNC surface modification*

As previously noted, the highly hydrophilic character of CNC restricts their dispersibility in low polarity systems. In recent decades, several chemical surface modification strategies for regular cellulose have been developed. These strategies have included esterification, oxidation, silylation, polymer grafting or a combination of the above, which could also be applied for the modification of the CNC surfaces (Figure 2.1).[10-11] The main objective of such strategies is to successfully attach functional groups or polymer chains of interest to the CNC surfaces, while preserving the integrity of the crystals and CNC morphology.

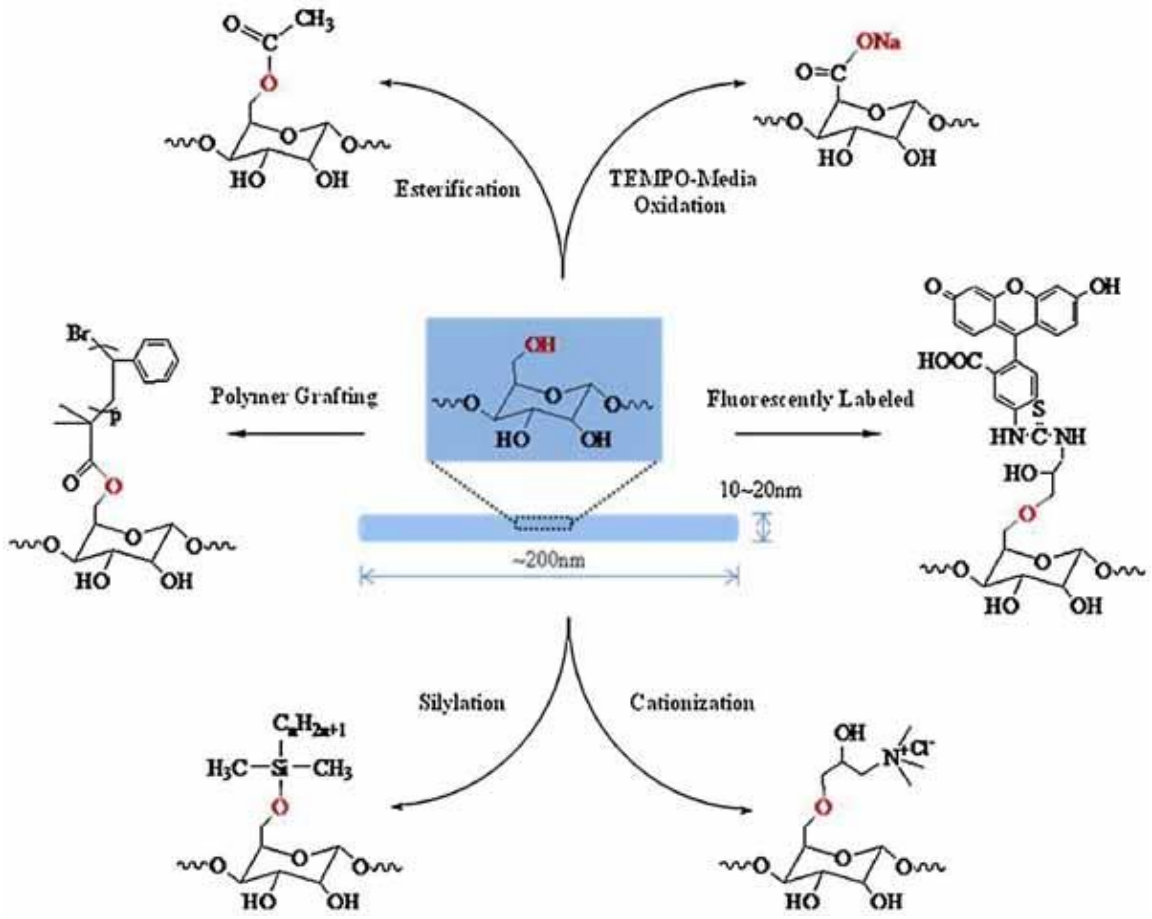

Figure 2.1. Diagram illustrating different chemical surface modifications of CNC. Reprinted with permission from Peng *et al.*[11] Copyright 2011. Canadian Society for Chemical Engineering.

Grafting polymers onto CNC surfaces represents a viable and advantageous approach to increase the compatibility of CNC with low polarity systems, as well to enhance the mechanical and responsive properties of CNC. In order to graft polymers onto the CNC surfaces, several strategies have extensively studied. These strategies are based on two main approaches: a *grafting-from* approach, which refers to starting a polymerization using surface groups as initiation loci; and the *grafting-to* approach where previously polymerized and fully characterized polymer chains are attached to the CNC surfaces

through the reaction of functional groups between the pre-formed polymer chain and the CNC surface (Figure 2.2).

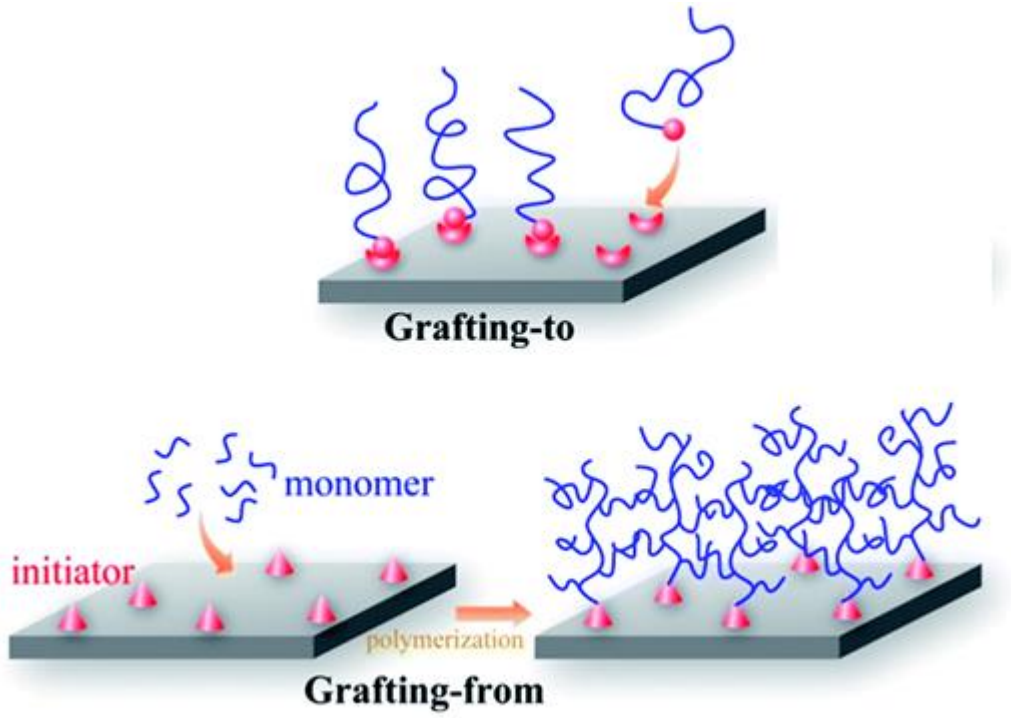

Figure 2.2. Illustration of the *grafting-to* and *grafting-from* approach for the immobilization of polymer chains on a solid surface. Reprinted with permission from Li *et al.*[12] Copyright 2013 Royal Society of Chemistry.

Both approaches offer distinct characteristics to the final grafted product. In the *grafting-from* approach, a higher grafting density is usually obtained. However, knowledge of the molecular weight of the grafted chains in commonly unknown if the polymer chains cannot be cleaved from the substrate without degrading the polymer. This represents a considerable disadvantage that can be easily overcome by using the *grafting-to* approach. In this approach, preformed polymer chains can be fully characterized and then grafted onto the substrate. However, due to the steric effects of longer chains, grafting densities will generally be lower than that achieved with the *grafting-from* approach.

During the last decade, the grafting of regular cellulose or CNC by free radical polymerization (FRP)[13-14] along with reversible deactivation radical polymerization (RDRP) techniques such as atom transfer radical polymerization (ATRP) in different variants[15-19], nitroxide-mediated polymerization (NMP)[20-22] and reversible addition-fragmentation chain transfer (RAFT)[23-25] have been reported. These reports include the incorporation of conventional polymers such as polystyrene (PS) and poly(methyl methacrylate) (PMMA), plus one particular class of polymers denominated as stimuli-responsive polymers such as poly(N-isopropylacrylamide) (PNIPAM), poly(dimethylaminoethyl methacrylate) (PDMAEMA) and poly(diethylaminoethyl methacrylate) (PDEAEMA). RDRP techniques allow for the grafting of a variety of polymers by either grafting approach with a good control of molecular weight and molecular weight dispersities. This is important from a proof of concept point of view if feature properties are to be analyzed as a function of molecular weight or degree of polymerization or molecular architecture.

2.2 ***Reversible deactivation radical polymerization***

Early in the 1990s, the radical polymerization field saw increased interest as new polymerization chemistries were developed allowing high chain-end functionality along with good control in molecular weight and molecular weight dispersity (Đ). A few years ago, these different chemistries were still referred to as "living radical" or "controlled/living radical" polymerization reactions. Recently, IUPAC discouraged the use of those terms in favor of reversible deactivation radical polymerization (RDRP).[26] The most important and common of these polymerization chemistries are NMP, ATRP and

RAFT-mediated polymerization. Consistent with the scope of this project, only ATRP and RAFT will be reviewed.

2.2.1 *Atom transfer radical polymerization*

One of the most common and well-studied RDRP is ATRP. This system consists of an organic halide, catalyst or coordination complex and monomers. As with other types of RDRP chemistries, ATRP is comprised of one main equilibrium step between "dormant" and "active" species (Scheme 2.1). The rate of polymerization (R_p) according to this equilibrium is shown in equation (1), where R_p is proportional to the monomer concentration [M], the organic halogen or initiator [RX] and to the ratio of the coordination complexes $Mt^nL/Mt^{n+1}X$.[27]

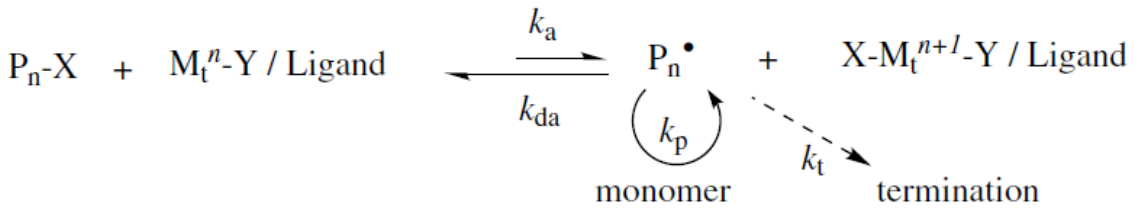

Scheme 2.1. ATRP general mechanism of propagation.

$$R_p = -\frac{d[M]}{dt} = k_p[M][P^*] = k_p[M]K_{ATRP}[RX]\left[\frac{\left[\frac{Mt^n}{L}\right]}{\left[\frac{Mt^{n1+}X}{L}\right]}\right] \qquad (1)$$

As with other RDRP chemistries, termination reactions in between active species and side reactions, such as chain transfer reactions, cannot be completely suppressed. Consequently, particularly in ATRP, the concentration of the $Mt^{n+1}X$ species increases

leading to a decrease in the R_p, resulting in a shift to the dormant state in the ATRP system equilibrium. This effect on the system is called the persistent radical effect (PRE).[28] To alleviate this rate reduction in ATRP systems, variants have been developed, such as activators regenerated by electron transfer (ARGET) and initiators for continuous activator regeneration (ICAR), where reducing organic molecules or organometallic compounds (eg. tin octanoate) have been used to regenerate the Mt^n species.[29] However, these techniques usually require high concentration of the reducing agents, which could be both expensive and difficult to remove from the final product. Another variant related to these techniques involves the usage of Cu(0) (wire form) as the reducing agent. Currently, there is debate in the literature regarding the nature of the mechanism of this ATRP variant more commonly known as either SET or SARA ATRP[30-34]. Consequently, throughout this work, this technique will be referred to solely as Cu(0)-ATRP.

Cu(0)-ATRP

Cu(0)-ATRP has several advantages including that it can be performed at room temperature (25-30°C), yields uncolored solutions (low metal content), and allows for good control of the molecular weight, low Đ and high chain-end functionality polymers.[32] Moreover, what makes this technique attractive for the purposes of this research, is that this system requires minimal amounts of copper (ppm range) and the copper wire catalyst can be easily removed from the reaction medium. This represents an important benefit as CNC can physically adsorb different types of dissolved constituents in solution including some metals in high concentrations.[35]

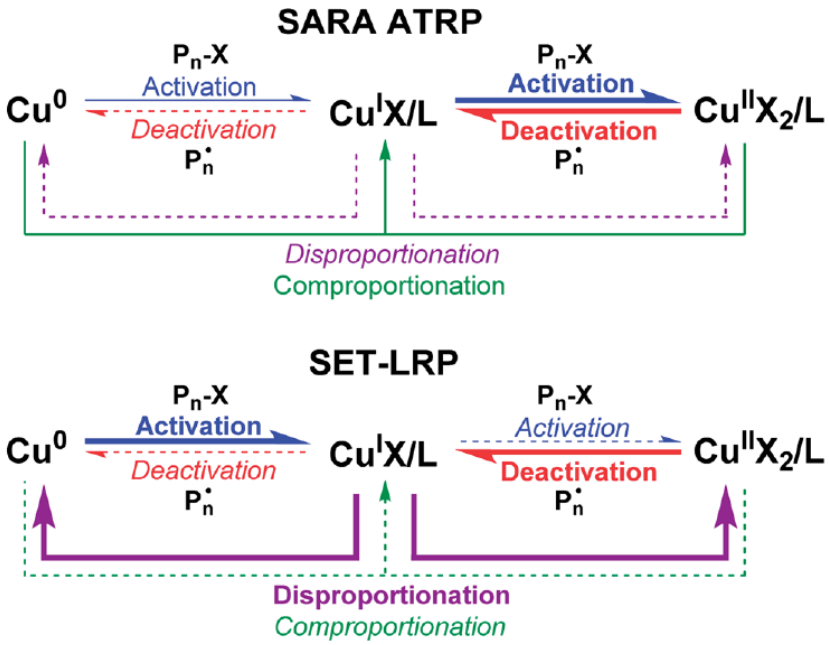

Scheme 2.2. SARA/SET ATRP mechanism. Reprinted with permission from Konkolewicz *et al.*[33] Copyright 2014 Royal Society of Chemistry

Cu(0)-ATRP involves the basic ATRP mechanism for propagation and deactivation of active species as shown in Scheme 2.1. The difference between Cu(0)-ATRP with other ATRP techniques like ARGET or ICAR ATRP, is the mechanism by which Cu^{1+} is regenerated. In the literature, there are currently two models describing how Cu(0) mediates an ATRP reaction. These two models are commonly known as supplemental activator and reducing agent (SARA-ATRP)[34,36] and single electron transfer (SET-ATRP).[32,37]. The main difference between these mechanisms is the role and the extent to which the reactions involved in the disproportionation and comproportionation of copper species contribute to the activation/deactivation of the alkyl halides.[33] These mechanisms are illustrated in Scheme 2.2. Both theories demonstrate evidence supporting the origin of their respective mechanism; however, because the nature of the Cu(0) mechanism is not

within the scope of this project, this particular system will be referred to simply as Cu(0)-ATRP.

As already mentioned, the primary advantage of Cu(0)-ATRP is the very low copper content required to achieve good molecular weight control and high chain-end functionality. The Cu(0) catalyst in the form of a wire is much easier to remove from the reaction mixture than Cu^{1+} and Cu^{2+} salts, negating the need for post-reaction treatment to reduce the copper level in the polymer product. In conventional ATRP, Cu^{1+} and Cu^{2+} are typically added at much higher concentrations than when Cu(0) is employed. In principle, Cu^{1+} and Cu^{2+} can be removed from solution, however the methods used for copper removal (e.g. silica columns) are often not readily scalable or suitable for CNC grafting.

2.2.2 *Reversible addition-fragmentation chain transfer-mediated polymerization*

RAFT-mediated polymerization is commonly documented as the most effective and versatile method for attributing living characteristics to radical polymerizations. This effectiveness is mainly attributed to the ability of this technique to polymerize under mild conditions with high tolerance to monomers with functional groups, giving living character to the final product (low Đ, good control in molecular weight).[38]

RAFT polymerization relies on the RAFT mechanism proposed by Rizzardo's group as shown in Scheme 2.3.[39] In addition to initiation and radical-radical termination, in a RAFT system at the early stages of reaction, the addition of a propagating radical to the thiocarbonylthio compound (a.k.a. RAFT agent or as chain transfer agent [CTA]), followed by fragmentation of the intermediate radical provides a polymeric "dormant" chain with a

dithiocarbonyl moiety and a new radical R$^{\bullet}$ capable of generating a new propagating radical. A rapid equilibrium between the active propagating radicals ($P_n^{\bullet}$ and $P_m^{\bullet}$) and the dormant dithiocarbonyl chains provides equal probability for all chains to grow and allows for the synthesis of polymers with narrow molecular weight distributions.[40] At the end of the reaction, most of the chains retain the dithiocarbonyl end group which can be either used for further chain-end modifications with different types of chemistries, or for performing chain-extension reactions in block copolymer synthesis.[41] The inclusion of the RAFT agent will ideally not have a direct influence on the reaction kinetics (initiation, propagation and termination), and the narrowing of the molecular weight distributions will be only due to chain transfer reactions as with any other CTA in an FRP.

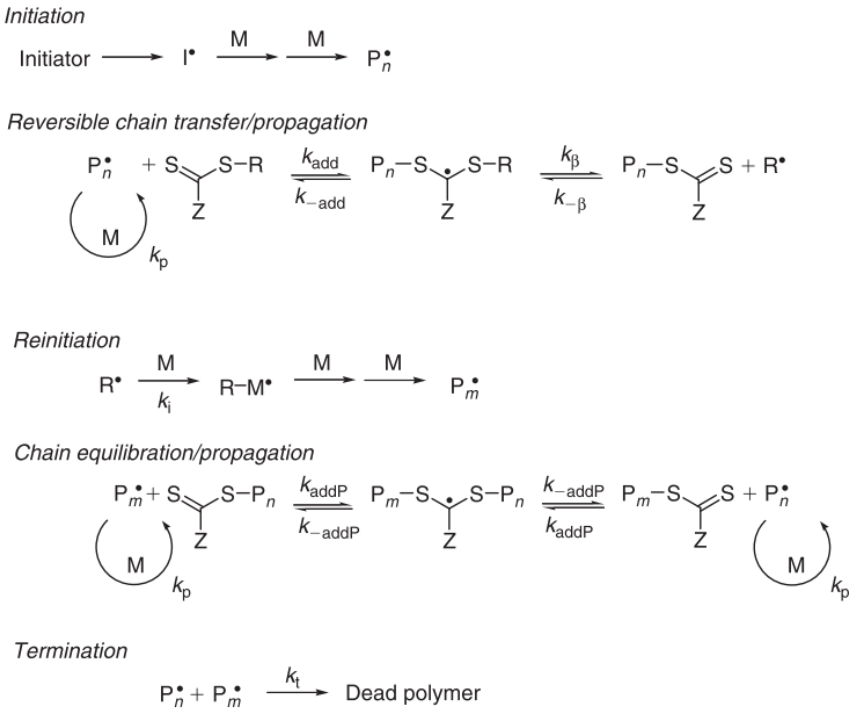

Scheme 2.3. General RAFT polymerization mechanism showing initiation, propagation, reversible chain transfer, reinitiation, chain equilibration and termination steps.[39]

There are different types of RAFT agents (Scheme 2.4) such as dithioesters, trithiocarbonates, xanthates and dithiocarbamates. An important consideration regarding the different classes of RAFT agents, is that not all of them will show the same performance when used in the polymerization of different types of monomers. Hence, good control and living character in RAFT reactions require the selection of the appropriate RAFT agent for specific monomers. The efficiency of the RAFT agent will be determined by the Z and R groups, which play different roles in the addition-transfer steps during the polymerization, and the reactivity of the monomer propagating radicals.[42]

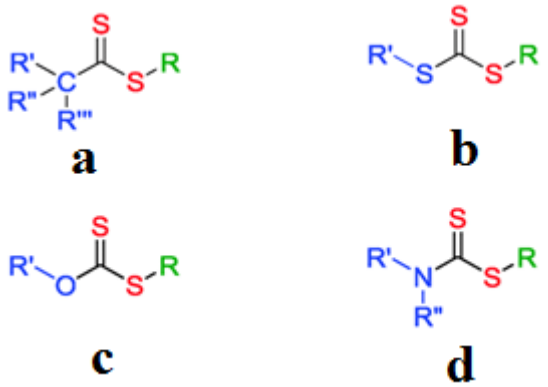

Scheme 2.4. RAFT agent structures. Dithioesters (a), trithiocarbonates (b), xanthates (c) and dithiocarbamates (d). Reprinted with permission from Keddie, D.[43] Copyright 2013 Royal Society of Chemistry.

Monomers in general are catalogued in two different groups. The "more activated monomers" (MAMs), where the double bond is conjugated with any other pi-system like an aromatic ring (i.e. styrene), a carbonyl group (i.e. (meth)acrylates, (meth)acrylamides); and the "less activated monomers" (LAMs), where the double bond is adjacent to an electron rich system such as an oxygen or nitrogen lone pair (vinyl esters, vinylamides) or an heteroaromatic ring (N-vinylcarbazole).[43] These classifications refer to the manner in which monomers will react in a free radical environment, where MAMs are more promptly

to react with a radical than LAMS. Nevertheless, the relative reactivity of the propagating radicals does not agree with these classifications. Because of electronic group stabilization (resonance or electron donating groups) along with additional steric factors, MAMs produce more stable radicals and therefore less reactive propagating species than LAMs.[42-44] A clear example of this case is depicted in Scheme 2.5, where the acrylate radical, is less reactive than a vinyl acetate radical due to resonance stability of the radical with the adjacent carbonyl group, but it is more reactive than a methyl methacrylate radical in which the additional methyl group adds a steric factor, in addition to some inductive effects.

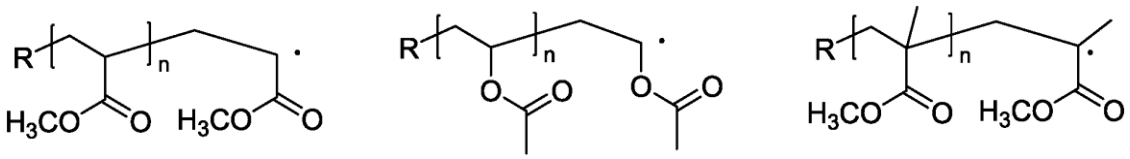

Scheme 2.5. Radical propagating species in the form of methacrylate, vinyl acetate or methyl methacrylate. Reprinted with permission from Keddie, D.[42] Copyright 2012 American Chemical Society.

In other words, MAMs are less reactive in radical addition (lower k_p, lower k_{add}) and therefore, they require the more active RAFT agents (dithioesters, trithiocarbonates and aromatic dithiocarbamates as Z groups) to achieve good control. LAMs on the other hand, are highly reactive in radical addition (higher k_p higher k_{add}) so they require less active transfer agents (Z groups) (dithiocarbamates and xanthates) as summarized in Scheme 2.6.[45]

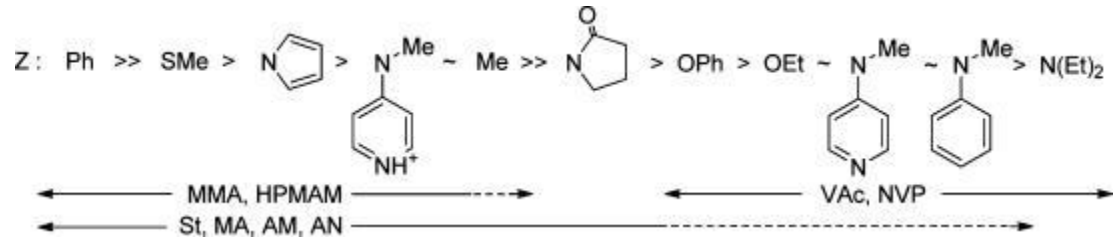

Scheme 2.6. Guideline for the selection of Z group for RAFT polymerization according to monomer activity. Reprinted with permission from Keddie, D.[42] Copyright 2012 American Chemical Society.

The role of the R group on the RAFT agent is important as it has the role of reinitiating the propagation of species. If the R radical is not stable, the ability to reinitiate propagation could be compromised and retardation is likely to occur. Therefore, the R group needs to be a good homolytic leaving group with respect to $P_n^{\bullet}$. In the case of methacrylates and methacrylamides polymerization, the R groups on the RAFT agents need to comprise one tertiary carbon to stabilize the new initiating radical, whereas LAMs (acrylates, acrylamides, vinyl esters) require primary or secondary radicals as tertiary radicals are inefficient in reinitiating monomer propagation (Scheme 2.7).[42-43]

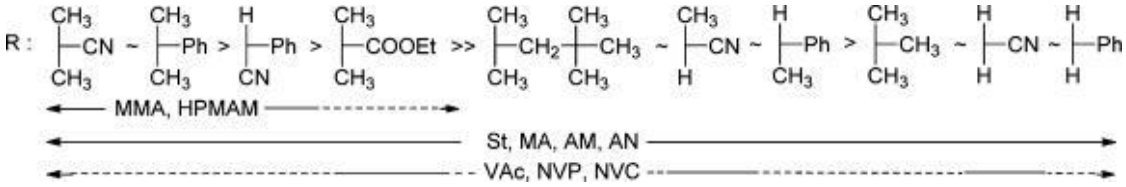

Scheme 2.7. Guideline for the selection of Z group for RAFT polymerization according to monomer activity. Reprinted with permission from Keddie, D.[42] Copyright 2012 American Chemical Society.

2.3 ***Stimuli-responsive polymers***

Stimuli-responsive polymers are materials whose physical-chemical properties change in the presence of an applied stimulus.[46] Recently, these materials have become the subject of intense study as they have several potential applications, including the biomedical field

and drug delivery systems to more traditional areas such as coatings, colloids and emulsions.[47-48] Stimuli-responsive polymers are commonly classified in three categories: physical, chemical or biological, although certain polymers can exhibit multiple responsiveness such as pH and temperature (chemical and physical). (Figure 2.3)[49]

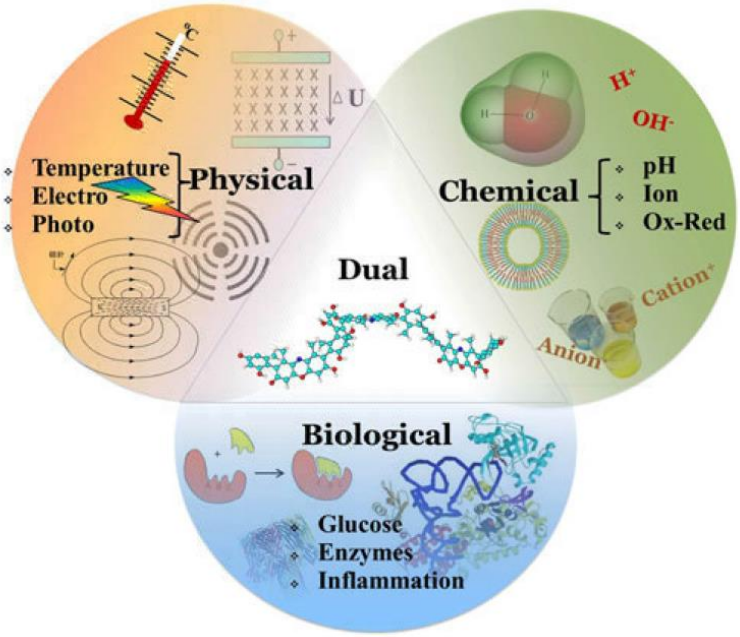

Figure 2.3. Classification of stimuli-responsive polymers.[49]

Temperature-responsive polymers are characterized by a critical solution temperature at which the polymer interactions can drastically change, either becoming hydrophobic or hydrophilic with respect to the medium in which they are dissolved, within a small temperature range.[49] Usually, these type of polymers exhibit an upper critical solution temperature (UCST), or a lower critical solution temperature (LCST) (Figure 2.4). The UCST is the minimum temperature at which one polymer phase exists and below this temperature, polymer phase separation will occur; whereas the LCST is the maximum temperature at which the polymer will remain in solution and above this LCST, phase

separation will occur as well. In general, these kinds of materials exist in the form of copolymers such as (L-lactic acid)-poly(ethylene glycol)-poly(L-lactic acid) (PLLA-PEG-PLLA) triblock copolymers, and poly (ethylene oxide)-b-poly(propylene oxide)-b-poly (ethylene oxide) triblock copolymers (PEO–PPO–PEO).[49]

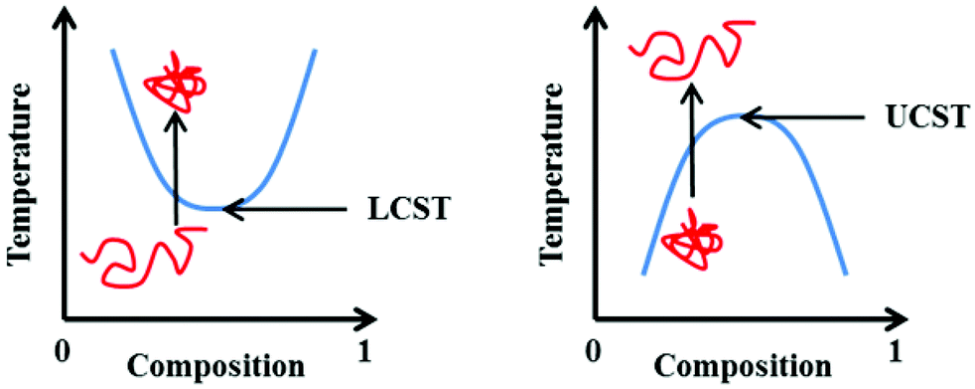

Figure 2.4. Illustration of the LCST and UCST of a polymer chain.[49]

Another type of responsive polymer within the chemically dependent stimuli category involves pH-responsive polymers. These polymers are of great interest as pH is an important parameter in biomedical applications for drug delivery, but they could also be applied in a wide variety of applications such as industrial coatings, oil exploration, colloidal suspension stabilization, and water treatment. The pH-responsiveness is usually obtained by incorporating pH-responsive moieties to the polymeric backbone.[50] These moieties allow the polymer physical properties such as solubility, volume, configuration and conformation to be reversibly adjusted by pH adjustments. This pH-triggered responsiveness could result in the design of "smart" materials with potential applications in drug delivery, viscosity modifiers, self-assembly products, which would be applied in the coatings industry.

The most common pH-responsive polymers are homopolymers of tertiary amine methyl methacrylates such as PDMAEMA and PDEAEMA, some acrylates like PAA, PMA, poly (maleic anhydride) and some block copolymers, where usually one block is hydrophobic and the other block is pH-responsive.[51] The main characteristic of these polymers is that they have ionizable groups which are usually carboxylic acids or amines. These ionizable polymers, which can be catalogued as weak Bronsted acids or bases, can be identified or catalogued based in their pK_a values. In general, pH-responsive polymers with pK_{aH} values (the pK_a of the protonated form, Scheme 2.8) between 3 and 10 are good candidates for pH-responsiveness.[52]

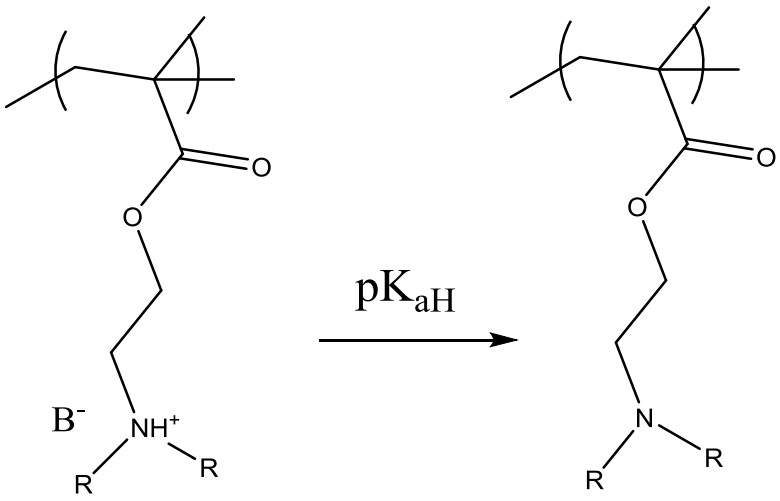

Scheme 2.8. Schematics representing the deprotonation of a protonated polyamine (pK_{aH}).

2.4 *CO_2-responsiveness*

Recently, CO_2 has attracted considerable attention as a trigger for pH-responsive polymers.[53] In using CO_2 as a trigger, rather than common liquid acid/base triggers, the need for further purification or removal of neutralization by-products can be eliminated, as CO_2 can be easily removed by using a constant flow of any non-acidic gas (e.g. air,

nitrogen, argon) and/or by gently heating the solution. Furthermore, CO_2 is an attractive trigger due to its benign nature, low cost and availability.[54]

The concept of CO_2-switching is based on the chemistry of carbonic acid in water and the reaction with neutral amines, amidines or guanidines resulting in the protonated species and a bicarbonate anion (Scheme 2.9). This reaction converts the hydrophobic amines, amidines or guanidines into their bicarbonate salt, which is hydrophilic, and it could be reversibly regenerated by removing the CO_2 out of solution through sparging a non-acidic gas into the solution.

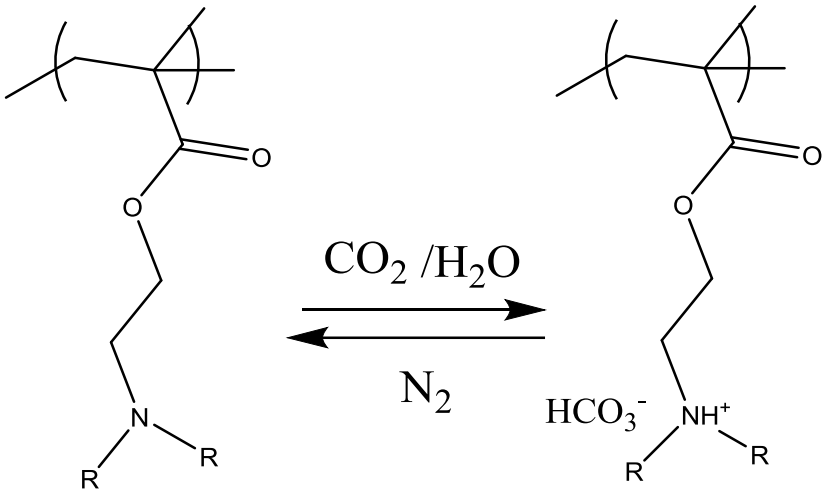

Scheme 2.9. Reversible protonation of a polyamine with CO_2.

Experimental data on CO_2 solubility shows that at standard temperature and pressure (275 K and 1 atm), the molar fraction of CO_2 in water equals to 0.62×10^{-3},[55] which represents 1.52 g CO_2 / L H_2O, resulting in a minimum theoretical pH of 3.9 with CO_2. However, not all amines, amidines or guanidienes are good candidates for CO_2-switching. Alshamrani *et al.* determined the required pK_{aH} for a base to have a specific degree of protonation, when mixed with neutral and carbonated water as a function of the base

concentration when both, the protonated and not protonated form of the base are water soluble at 25°C and 0.1 MPa of CO_2.[56] In Figure 2.5, the dashed lines represent the of protonation of any base in just neutral water and the solid lines represent the degree of protonation of any base in carbonated water. In order to maximize the switchability and the change in properties of the CO_2-responsive molecule at a concentration of 1 mM (going from low % protonation to high % protonation), the pK_{aH} value of the base of interest should be between the red dashed line and the solid blue line. This will ensure that without CO_2, the degree of protonation of the molecule of interest will be ca. 5% and, under CO_2, the degree of protonation will be ca. 95%.

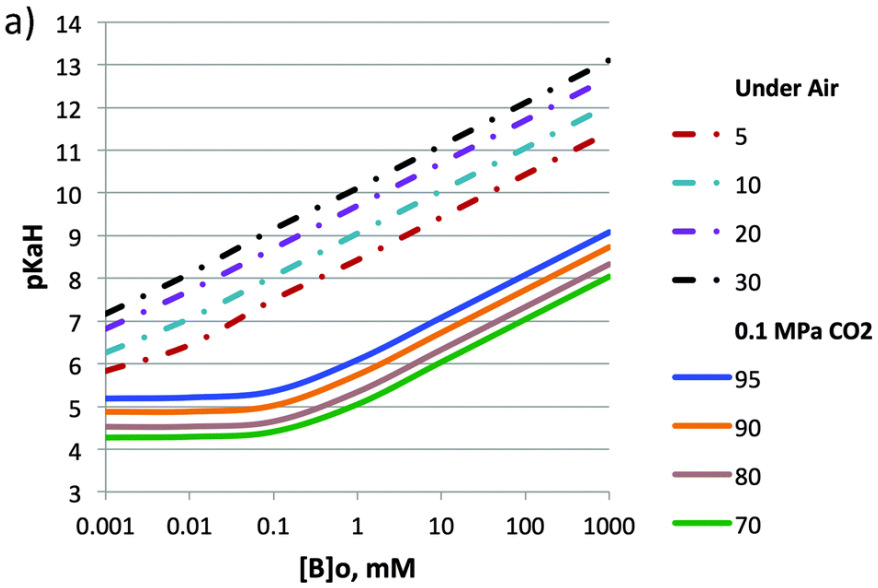

Figure 2.5. Degree of protonation as a function of pK_{aH} and concentration at 0.1 Mbar of CO_2 and 25°C. Reprinted with permission from Alshamrani *et al.* [56] Copyright 2016 Royal Society of Chemistry

It is worth noting that the former model only applies to small molecules with single protonable sites and if both the ionized and non-ionized version of the molecule are water soluble. For most polyamines, this is not the case as most of them will become water

insoluble in their neutral form. However, as polyamines do follow the general trends shown in this model, it can still be a used as a guide for choosing determined switchable groups to be incorporated in CO_2-swtitchable polymeric materials (Figure 2.5). For example, stronger bases (higher pK_{aH} values, Figure 2.5) are required if high concentrations of the polymer will be used, or mildly basic (medium pK_{aH} values Figure 2.5) if low concentrations of the polymers will be used.

Table 2.1 shows the pK_{aH} values of few polyamines and their monomers, mainly methyl methacrylates. Figure 2.6 shows their corresponding structure. From Table 2.1, it can be observed that the range of pK_{aH} goes from slightly basic (P2VP) up to mildly basic (PDMAPMAm). One thing to note is that the pK_{aH} values of the polymers are lower than their corresponding monomers. This means that polymers are more difficult to protonate mainly due to charge density accumulation. In this research, three polymers were chosen: PDMAEMA, PDEAEMA and PDPAEMA. For the first two, the reported pK_{aH} values (Table 2.1), are almost identical, while for PDPAEMA, the pK_{aH} is 1.3 units lower (PDMAEMA = 7.0, PDEAEMA = 6.9, PDPAEMA = 5.7). The reason these polymers were selected, was that their pK_{aH} values make them suitable for CO_2-switching in the range 0.1 and 1 mM of polyamine, as well as the commercial availability of their corresponding monomers.

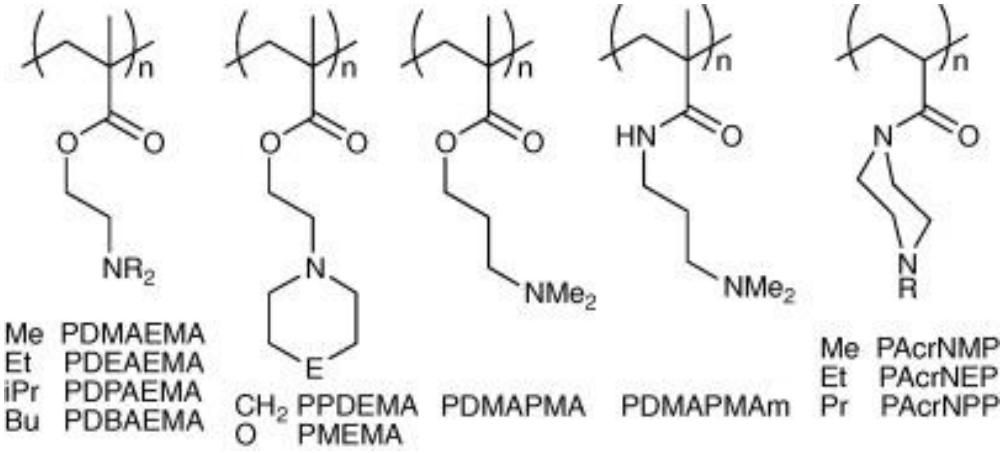

Figure 2.6. Chemical structures of diverse pH-responsive polyamines. Reprinted with permission from Cunningham and Jessop.[57] Copyright 2016 Elsevier Ltd.

Table 2.1. pK_{aH} of pH-responsive polymers and monomers. Adapted with permission from Cunningham and Jessop.[57] Copyright 2016 Elsevier Ltd.

Polymer	pK_{aH}	pK_{aH} of monomer
PDMAPMAm	8.6 [58]	9.2 [58]
PDMAPMA	8.4 [58]	9.1 [58]
PDMAEMA	7.0 [58]	8.3 [58]
PDEAEMA	7.5 [58]	8.8 [58]
PPDEMA	6.9 [59]	8.9 [59]
PDPAEMA	6.3 [59]	8.5 [59]
PDBAEMA	5.1 [60]	6.9 [59]
PMEMA	4.9 [60]	---
PAcNPP	4.6 [60]	---
P2VP	4.2 [61]	4.9 [62]

References

1.Habibi, Y.; Lucia, L. A.; Rojas, O. J., Cellulose nanocrystals: Chemistry, self-assembly, and applications. *Chem. Rev.* **2010,** *110* (6), 3479-3500.

2.Filson, P. B.; Dawson-Andoh, B. E., Sono-chemical preparation of cellulose nanocrystals from lignocellulose derived materials. *Bioresour. Technol.* **2009,** *100* (7), 2259-2264.

3.Yi, J.; Xu, Q.; Zhang, X.; Zhang, H., Chiral-nematic self-ordering of rodlike cellulose nanocrystals grafted with poly(styrene) in both thermotropic and lyotropic states. *Polymer* **2008,** *49* (20), 4406-4412.

4.Beck, S.; Bouchard, J., Auto-catalyzed acidic desulfation of cellulose nanocrystals. *Nordic Pulp & Paper Research Journal* **2014,** *29* (1), 6-14.

5.Camarero Espinosa, S.; Kuhnt, T.; Foster, E. J.; Weder, C., Isolation of thermally stable cellulose nanocrystals by phosphoric acid hydrolysis. *Biomacromolecules* **2013,** *14* (4), 1223-1230.

6.Khoshkava, V.; Kamal, M. R., Effect of drying conditions on cellulose nanocrystal (CNC) agglomerate porosity and dispersibility in polymer nanocomposites. *Powder Technol.* **2014,** *261*, 288-298.

7.Kovacs, T.; Naish, V.; O'Connor, B.; Blaise, C.; Gagné, F.; Hall, L.; Trudeau, V.; Martel, P., An ecotoxicological characterization of nanocrystalline cellulose (NCC). *Nanotoxicology* **2010,** *4* (3), 255-270.

8.Elmabrouk, A. B.; Wim, T.; Dufresne, A.; Boufi, S., Preparation of poly(styrene-co-hexylacrylate)/cellulose whiskers nanocomposites via miniemulsion polymerization. *J. Appl. Polym. Sci.* **2009,** *114* (5), 2946-2955.

9.Coleman, J. N.; Khan, U.; Blau, W. J.; Gun'ko, Y. K., Small but strong: A review of the mechanical properties of carbon nanotube–polymer composites. *Carbon* **2006,** *44* (9), 1624-1652.

10.Roy, D.; Semsarilar, M.; Guthrie, J. T.; Perrier, S., Cellulose modification by polymer grafting: A review. *Chem. Soc. Rev.* **2009,** *38* (7), 2046-2064.

11.Peng, B. L.; Dhar, N.; Liu, H. L.; Tam, K. C., Chemistry and applications of nanocrystalline cellulose and its derivatives: A nanotechnology perspective. *Can. J. Chem. Eng.* **2011,** *89* (5), 1191-1206.

12.Li, D.; Zheng, Q.; Wang, Y.; Chen, H., Combining surface topography with polymer chemistry: Exploring new interfacial biological phenomena. *Polymer Chemistry* **2014,** *5* (1), 14-24.

13.Kan, K. H. M.; Li, J.; Wijesekera, K.; Cranston, E. D., Polymer-grafted cellulose nanocrystals as pH-responsive reversible flocculants. *Biomacromolecules* **2013,** *14* (9), 3130-3139.

14.Tang, J.; Lee, M. F. X.; Zhang, W.; Zhao, B.; Berry, R. M.; Tam, K. C., Dual responsive Pickering emulsion stabilized by poly[2-(dimethylamino)ethyl methacrylate] grafted cellulose nanocrystals. *Biomacromolecules* **2014,** *15* (8), 3052-3060.

15.Majoinen, J.; Walther, A.; McKee, J. R.; Kontturi, E.; Aseyev, V.; Malho, J. M.; Ruokolainen, J.; Ikkala, O., Polyelectrolyte brushes grafted from cellulose nanocrystals using Cu-mediated surface-initiated controlled radical polymerization. *Biomacromolecules* **2011,** *12* (8), 2997-3006.

16.Morandi, G.; Thielemans, W., Synthesis of cellulose nanocrystals bearing photocleavable grafts by ATRP. *Polymer Chemistry* **2012,** *3* (6), 1402-1407.

17.Dupayage, L.; Save, M.; Dellacherie, E.; Nouvel, C.; Six, J.-L., PMMA-grafted dextran glycopolymers by atom transfer radical polymerization. *J. Polym. Sci., Part A: Polym. Chem.* **2008,** *46* (23), 7606-7620.

18.Wang, H.-D.; Roeder, R. D.; Whitney, R. A.; Champagne, P.; Cunningham, M. F., Graft modification of crystalline nanocellulose by Cu(0)-mediated SET living radical polymerization. *J. Polym. Sci., Part A: Polym. Chem.* **2015,** *53* (24), 2800-2808.

19.Hatton, F. L.; Kedzior, S. A.; Cranston, E. D.; Carlmark, A., Grafting-from cellulose nanocrystals via photoinduced Cu-mediated reversible-deactivation radical polymerization. *Carbohydr. Polym.* **2017,** *157*, 1033-1040.

20.Daly, W. H.; Evenson †, T. S.; Iacono, S. T.; Jones, R. W., Recent developments in cellulose grafting chemistry utilizing barton ester intermediates and nitroxide mediation. *Macromolecular Symposia* **2001,** *174* (1), 155-164.

21.Garcia-Valdez, O.; Brescacin, T.; Arredondo, J.; Bouchard, J.; Jessop, P. G.; Champagne, P.; Cunningham, M. F., Grafting CO_2-responsive polymers from cellulose nanocrystals via nitroxide-mediated polymerisation. *Polymer Chemistry* **2017,** *8* (28), 4124-4131.

22.Roeder, R. D.; Garcia-Valdez, O.; Whitney, R. A.; Champagne, P.; Cunningham, M. F., Graft modification of cellulose nanocrystals via nitroxide-mediated polymerisation. *Polymer Chemistry* **2016,** *7* (41), 6383-6390.

23.Roy, D.; Guthrie, J. T.; Perrier, S., Graft polymerization: Grafting poly(styrene) from cellulose via reversible addition−fragmentation chain transfer (RAFT) polymerization. *Macromolecules* **2005,** *38* (25), 10363-10372.

24.Hernández-Guerrero, M.; Davis, T. P.; Barner-Kowollik, C.; Stenzel, M. H., Polystyrene comb polymers built on cellulose or poly(styrene-co-2-

hydroxyethylmethacrylate) backbones as substrates for the preparation of structured honeycomb films. *Eur. Polym. J.* **2005,** *41* (10), 2264-2277.

25.Zeinali, E.; Haddadi-Asl, V.; Roghani-Mamaqani, H., Nanocrystalline cellulose grafted random copolymers of n-isopropylacrylamide and acrylic acid synthesized by RAFT polymerization: Effect of different acrylic acid contents on LCST behavior. *RSC Advances* **2014,** *4* (59), 31428-31442.

26.Jenkins Aubrey, D.; Jones Richard, G.; Moad, G., Terminology for reversible-deactivation radical polymerization previously called "controlled" radical or "living" radical polymerization (IUPAC recommendations 2010). *Pure Appl. Chem.* **2009,** *82* (2), 483-491.

27.Matyjaszewski, K. D., T., *Handbook of radical polymerization*. Wiley Iinterscience: USA, 2002.

28.Fischer, H., The persistent radical effect in controlled radical polymerizations. *J. Polym. Sci., Part A: Polym. Chem.* **1999,** *37* (13), 1885-1901.

29.Matyjaszewski, K., Atom transfer radical polymerization (ATRP): Current status and future perspectives. *Macromolecules* **2012,** *45* (10), 4015-4039.

30.Levere, M. E.; Nguyen, N. H.; Leng, X.; Percec, V., Visualization of the crucial step in SET-LRP. *Polymer Chemistry* **2013,** *4* (5), 1635-1647.

31.Lligadas, G.; Rosen, B. M.; Bell, C. A.; Monteiro, M. J.; Percec, V., Effect of Cu(0) particle size on the kinetics of SET-LRP in DMSO and Cu-mediated radical polymerization in MeCN at 25 °c. *Macromolecules* **2008,** *41* (22), 8365-8371.

32.Rosen, B. M.; Percec, V., Single-electron transfer and single-electron transfer degenerative chain transfer living radical polymerization. *Chem. Rev.* **2009,** *109* (11), 5069-5119.

33.Konkolewicz, D.; Wang, Y.; Krys, P.; Zhong, M.; Isse, A. A.; Gennaro, A.; Matyjaszewski, K., SARA ATRP or SET-LRP. End of controversy? *Polymer Chemistry* **2014,** *5* (15), 4396-4417.

34.Konkolewicz, D.; Wang, Y.; Zhong, M.; Krys, P.; Isse, A. A.; Gennaro, A.; Matyjaszewski, K., Reversible-deactivation radical polymerization in the presence of metallic copper. A critical assessment of the SARA ATRP or SET-LRP mechanisms. *Macromolecules* **2013,** *46* (22), 8749-8772.

35.Yu, X.; Tong, S.; Ge, M.; Wu, L.; Zuo, J.; Cao, C.; Song, W., Adsorption of heavy metal ions from aqueous solution by carboxylated cellulose nanocrystals. *J Environ Sci* **2013,** *25* (5), 933-43.

36.Matyjaszewski, K.; Coca, S.; Gaynor, S. G.; Wei, M.; Woodworth, B. E., Zerovalent metals in controlled/"living" radical polymerization. *Macromolecules* **1997,** *30* (23), 7348-7350.

37.Percec, V.; Popov, A. V.; Ramirez-Castillo, E.; Monteiro, M.; Barboiu, B.; Weichold, O.; Asandei, A. D.; Mitchell, C. M., Aqueous room temperature metal-catalyzed living radical polymerization of vinyl chloride. *JACS* **2002,** *124* (18), 4940-4941.

38.Vana, P., Kinetic aspects of RAFT polymerization. *Macromolecular Symposia* **2007,** *248* (1), 71-81.

39.Destarac, M., On the critical role of raft agent design in reversible addition-fragmentation chain transfer (RAFT) polymerization. *Polymer Reviews* **2011,** *51* (2), 163-187.

40.Moad, G.; Rizzardo, E.; Thang, S. H., Living radical polymerization by the RAFT process – a second update. *Aust. J. Chem.* **2009,** *62* (11), 1402-1472.

41.Moad, G.; Rizzardo, E.; Thang, S. H., Living radical polymerization by the RAFT process—a first update. *Aust. J. Chem.* **2006,** *59* (10), 669-692.

42.Keddie, D. J.; Moad, G.; Rizzardo, E.; Thang, S. H., RAFT agent design and synthesis. *Macromolecules* **2012,** *45* (13), 5321-5342.

43.Keddie, D. J., A guide to the synthesis of block copolymers using reversible-addition fragmentation chain transfer (RAFT) polymerization. *Chem. Soc. Rev.* **2014,** *43* (2), 496-505.

44.Foster, J. C.; Radzinski, S. C.; Matson, J. B., Graft polymer synthesis by RAFT transfer-to. *J. Polym. Sci., Part A: Polym. Chem.* **2017,** *55* (18), 2865-2876.

45.Perrier, S., 50th anniversary perspective: RAFT polymerization—a user guide. *Macromolecules* **2017**.

46.Schacher, F.; Muellner, M.; Schmalz, H.; Mueller, A. H. E., New block copolymers with poly(N,N-dimethylaminoethyl methacrylate) as a double stimuli-responsive block. *Macromol. Chem. Phys.* **2009,** *210* (3-4), 256-262.

47.Cao, P.-F.; Mangadlao, J. D.; Advincula, R. C., Stimuli-responsive polymers and their potential applications in oil-gas industry. *Polymer Reviews* **2015,** *55* (4), 706-733.

48.Schmalz, A.; Hanisch, M.; Schmalz, H.; Müller, A. H. E., Double stimuli-responsive behavior of linear and star-shaped poly(N,N-diethylaminoethyl methacrylate) in aqueous solution. *Polymer* **2010,** *51* (6), 1213-1217.

49.Cabane, E.; Zhang, X.; Langowska, K.; Palivan, C.; Meier, W., Stimuli-responsive polymers and their applications in nanomedicine. *Biointerphases* **2012,** *7* (1-4), 1-27.

50.Dai, S.; Ravi, P.; Tam, K. C., pH-responsive polymers: Synthesis, properties and applications. *Soft Matter* **2008,** *4* (3), 435-449.

51.Schmaljohann, D., Thermo- and pH-responsive polymers in drug delivery. *Advanced Drug Delivery Reviews* **2006,** *58* (15), 1655-1670.

52.Siegel, R., Hydrophobic weak polyelectrolyte gels: Studies of swelling equilibria and kinetics. *Responsive Gels: Volume Transitions I* **1993,** *109*, 233-267.

53.Darabi, A.; Jessop, P. G.; Cunningham, M. F., CO_2-responsive polymeric materials: Synthesis, self-assembly, and functional applications. *Chem. Soc. Rev.* **2016,** *45* (15), 4391-436.

54.Lin, S.; Theato, P., CO_2-responsive polymers. *Macromol. Rapid Commun.* **2013,** *34* (14), 1118-1133.

55.Carroll, J. J.; Slupsky, J. D.; Mather, A. E., The solubility of carbon dioxide in water at low pressure. *J. Phys. Chem. Ref. Data* **1991,** *20* (6), 1201-1209.

56.Alshamrani, A. K.; Vanderveen, J. R.; Jessop, P. G., A guide to the selection of switchable functional groups for CO_2-switchable compounds. *PCCP* **2016,** *18* (28), 19276-19288.

57.Cunningham, M. F.; Jessop, P. G., An introduction to the principles and fundamentals of CO_2-switchable polymers and polymer colloids. *Eur. Polym. J.* **2016,** *76*, 208-215.

58.van de Wetering, P.; Moret, E. E.; Schuurmans-Nieuwenbroek, N. M. E.; van Steenbergen, M. J.; Hennink, W. E., Structure−activity relationships of water-soluble cationic methacrylate/methacrylamide polymers for nonviral gene delivery. *Bioconjugate Chem.* **1999,** *10* (4), 589-597.

59.Zhou, K.; Wang, Y.; Huang, X.; Luby-Phelps, K.; Sumer, B. D.; Gao, J., Tunable, ultrasensitive pH-responsive nanoparticles targeting specific endocytic organelles in living cells. *Angew. Chem. Int. Ed. Engl.* **2011,** *50* (27), 6109-14.

60.Roshan Deen, G.; Gan, L. H., Influence of amino group pKa on the properties of stimuli-responsive piperazine-based polymers and hydrogels. *J. Appl. Polym. Sci.* **2008,** *107* (3), 1449-1458.

61.Morse, A. J.; Armes, S. P.; Mills, P.; Swart, R., Stopped-flow kinetics of pH-responsive polyamine latexes: How fast is the latex-to-microgel transition? *Langmuir* **2013,** *29* (49), 15209-15216.

62.Pietrzyk, A.; Wiley, R.; McDaniel, D., Notes - base strength of monovinylpyridines. *The Journal of Organic Chemistry* **1957,** *22* (1), 83-84.

Chapter 3. Homopolymerization of Dialkylaminoethyl Methacrylates via Cu(0)-ATRP

Some of the work presented in this chapter was published in *Green Chem.* 2017, 19, 4141. For the purpose of this thesis, its content was modified and combined with some unpublished work. All the materials along with the characterization methods and specifications can be found in the Appendices A.I and B. respectively.

3.1 ***Introduction***

In order to perform grafting reactions of DMAEMA and DEAEMA, suitable conditions for the polymerization of these monomers needed to be first determined. Previous reports on classic ATRP have been published regarding the polymerization of DEAEMA[1-4] and DMAEMA[5-9], where ratios of [CuX]:[L]:[I] employed were 1:1:1 or higher, providing relatively good control of the M_n (number averaged molecular weight) and molar mass dispersities (Đ). However, these ratios employed high concentrations of metal which should be avoided in CNC grafting procedures, since CNC could physically adsorb excess metal giving colour to the final material and could limit its application in other fields (e.g. biomedical) due to high metal concentration.[10-11]

Homopolymerization of DMAEMA and DEAEMA by ATRP has been reported using different types of solvents such as THF,[8] anisole and dichlorobenzene[12-13] and methanol-water mixtures[6,9] where classic ATRP procedures or ARGET ATRP were employed. However, non-polar solvents like THF, anisole or dichlorobenzene are not good solvents to disperse CNC. Furthermore, solvent system mixtures containing water can lead to the hydrolysis of DEAEMA (as a function of pH) as previously reported by our group.[14]

Because CNC needs to be well dispersed to achieve homogenous grafting over the CNC surface, a sufficiently polar solvent is needed to adequately disperse the CNC; therefore methanol was selected, although it should be noted that the transesterification of some dialkylaminoethyl methacrylates can occur in methanol.[15] To the best of our knowledge, the kinetic behaviour of these monomers via Cu(0)-ATRP had not been previously reported. As such, we first studied the polymerization kinetics of the monomers in methanol (Scheme 3.1) to establish appropriate conditions for the grafting procedure, and the amount of PMMA incorporated in the final polymers due to the *in-situ* formation of MMA as a consequence of the transesterification of the dialkylaminoethyl methacrylates with methanol.

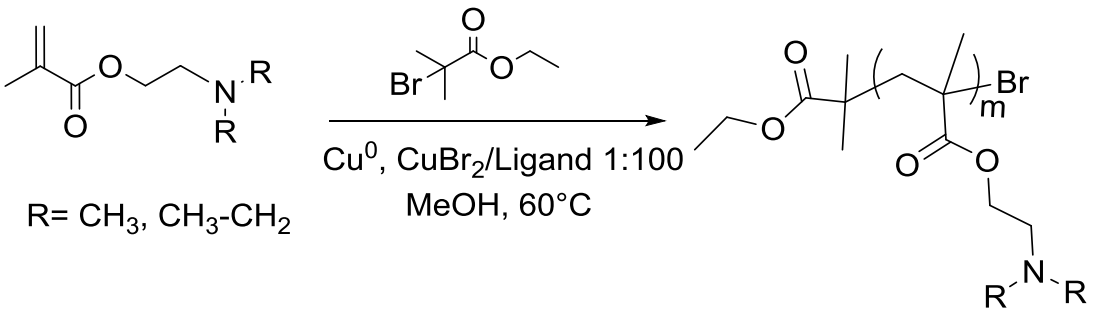

Scheme 3.1. Cu(0)-ATRP of DMAEMA and DEAEMA. DMAEMA [$CuBr_2$]: [L]:[I]$_0$:[M]$_0$ = 1:100:91:5782. DEAEMA:[$CuBr_2$]:[L]:[I]$_0$:[M]$_0$=1:100:107:5782.

3.2 ***Experimental***

3.2.1 *General procedure for homopolymerization of DMAEMA and DEAEMA*

To a 10 mL Schlenk tube, 3 mL of methanol were added along with DMAEMA or DEAEMA (12.7 mmol), 38 or 45 mg (0.20 or 0.23 mmol) of ethyl 2-bromo isobutyrate

(BIBA), 51.5 mg (0.22 mmol) of HMTETA, 0.5 mg (0.002 mmol) of $CuBr_2$**,** three copper wires (50 mm, gauge 14) pre-treated with HCl rinsed with methanol, and 300 µL of DMF as internal standard for ^1H NMR conversion analysis. The tube was degassed by three freeze-pump-thaw cycles and sealed with a rubber septum under argon atmosphere. Subsequently, it was submerged in an oil bath at 25°C or 60°C. Samples were taken every 10 minutes and quenched by exposure to oxygen. Samples were analyzed by ^1H NMR for conversion; afterwards, samples were diluted with THF, passed through a basic alumina column and analyzed by GPC.

3.2.2 *General procedure for chain-extension of PDMAEMA and PDEAMA macro-initiators*

In a 10 mL Schlenk tube, 50 mg of PDMAEMA/PDEAEMA based macro-initiator were solubilized in 6 mL of methanol. Then, DMAEMA (0.37 mmol) or DEAEMA (0.32 mmol), 1.47 mg (6.4E-3 mmol) of HMTETA, 0.14 mg (6.46E-5 mmol) of $CuBr_2$**,** one copper wires (50 mm, gauge 14) pre-treated with HCl rinsed with methanol. The tube was degassed by three freeze-pump-thaw cycles and sealed with a rubber septum under argon atmosphere. Subsequently, it was submerged in an oil bath 60°C. The reactions were quenched by exposing them to air. $CuBr_2$ was removed and samples were analyzed by GPC.

3.3 ***Results and discussion***

3.3.1 *Homopolymerization of DMAEMA and DEAEMA*

Several trials using DEAEMA were performed at both 25°C and 60°C using Me_6TREN as the ligand. However, monomer conversions after 3 hours were below 25% and 39% respectively (Figure C.1). These low conversions suggested that the monomer may be competing with the ligand for complexation with the copper, thereby destabilizing the ligand/monomer complex and resulting in low conversions as has been reported elsewhere.[16]

HMTETA was then assessed as an alternative ligand, as there are a few reports of polymerizing DEAEMA by ATRP using HMTETA in solvents other than methanol.[1,3-4,17] Figure 3.1 depicts the kinetic plots for the Cu(0)-ATRP of DMAEMA and DEAEMA at 60°C. It can be seen from the $Ln([M]_0/[M])$ vs. time plot that for both monomers, conversion follows pseudo-first order kinetics indicating a near constant concentration of growing radicals during polymerization with no apparent induction time. It can also be observed that the DMAEMA polymerization rate ($k_{p\ app}$ = 0.020 min^{-1}) was almost twice as fast as the DEAEMA polymerization rate ($k_{p\ app}$ = 0.011 min^{-1}). This is likely because DEAEMA is more basic than DMAEMA, which suggests that DEAEMA has a stronger affinity for the copper ions than the ligand, resulting in a decrease in available catalyst, which directly impacts the polymerization rate. Additionally, Figure 3.2 shows the initial appearance of the reaction mixture, which has a light blue due to the 100 ppm of added Cu^{2+}; whereas after 60 min, the final reaction product is colorless showing the advantages of this particular technique.

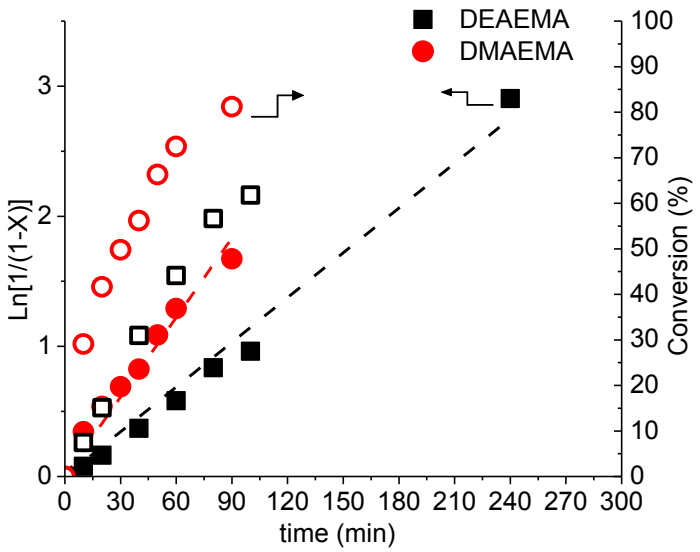

Figure 3.1. Ln($[M]_0/[M]$) vs. time plot of DMAEMA and DEAEMA homopolymerization by Cu(0)-ATRP using HMTETA as ligand at 60°C in MeOH. DMAEMA:$[CuBr_2]:[L]:[I]_0:[M]_0$= 1:100:91:5782. DEAEMA: $[CuBr_2]:[L]:[I]_0:[M]_0$= 1:100:107:5782.

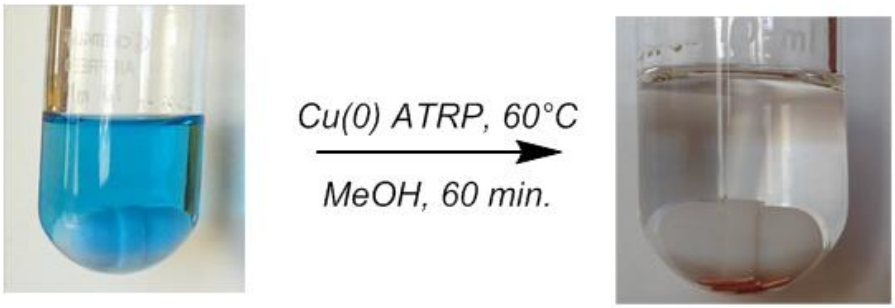

Figure 3.2. . Reaction mixture in a sealed Schlenk tube at t=0 and after 60 min at 60°C in MeOH. DMAEMA: $[CuBr_2]:[L]:[I]_0:[M]_0$ = 1:100:91:5782.

Figure 3.3 illustrates the M_n and Đ evolution as a function of monomer conversion during the polymerization of DMAEMA and DEAEMA. For each monomer, a rapid increase in M_n in the early stages of the polymerizations was observed, reflecting a lower than the theoretically expected number of chains being initiated early in the polymerization. This may be due to the interaction of the monomers with the copper catalyst affecting the

activation/deactivation equilibrium of propagating and dormant species. A near-linear trend in the evolution of M_n was observed for PDMAEMA and PDEAEMA. Đs were maintained below 1.6 throughout the course of each monomer polymerization, yielding a reasonable level of control over Đ for both monomers.

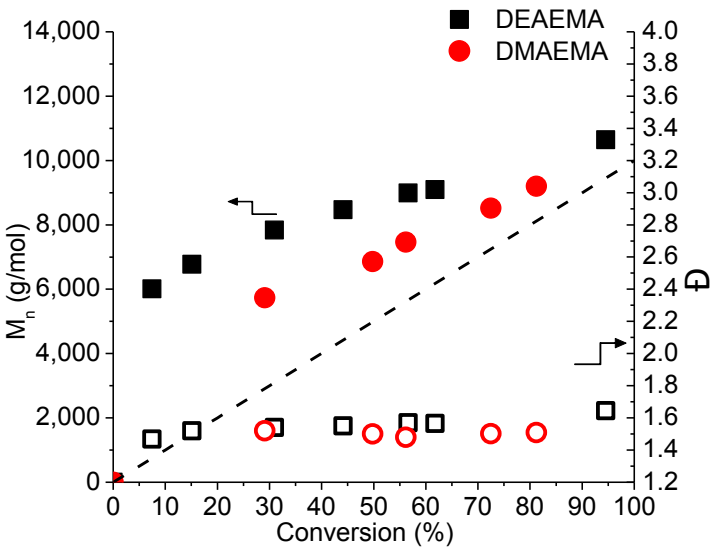

Figure 3.3. M_n and Đ evolution vs. conversion of both PDMAEMA and PDEAEMA. DMAEMA:[$CuBr_2$]:[L]:[I]$_0$:[M]$_0$= 1:100:91:5782. DEAEMA: [$CuBr_2$]:[L]:[I]$_0$:[M]$_0$= 1:100:107:5782.

Figure 3.4 shows the GPC traces for PDMAEMA and PDEAEMA as a function of conversion. The GPC traces for each polymer show livingness during the polymerization, as noted by the evident shift to higher molecular weights with increasing monomer conversion. Nevertheless, both traces show a shoulder at conversions of ~50 % for PDMAEMA and ~31% for PDEAEMA, which would suggest the presence of dead chains. For PDEAEMA, the shoulder was more pronounced, which would support the hypothesis that DEAEMA competes more strongly for the copper catalyst than DMAEMA due to their difference in basicity.

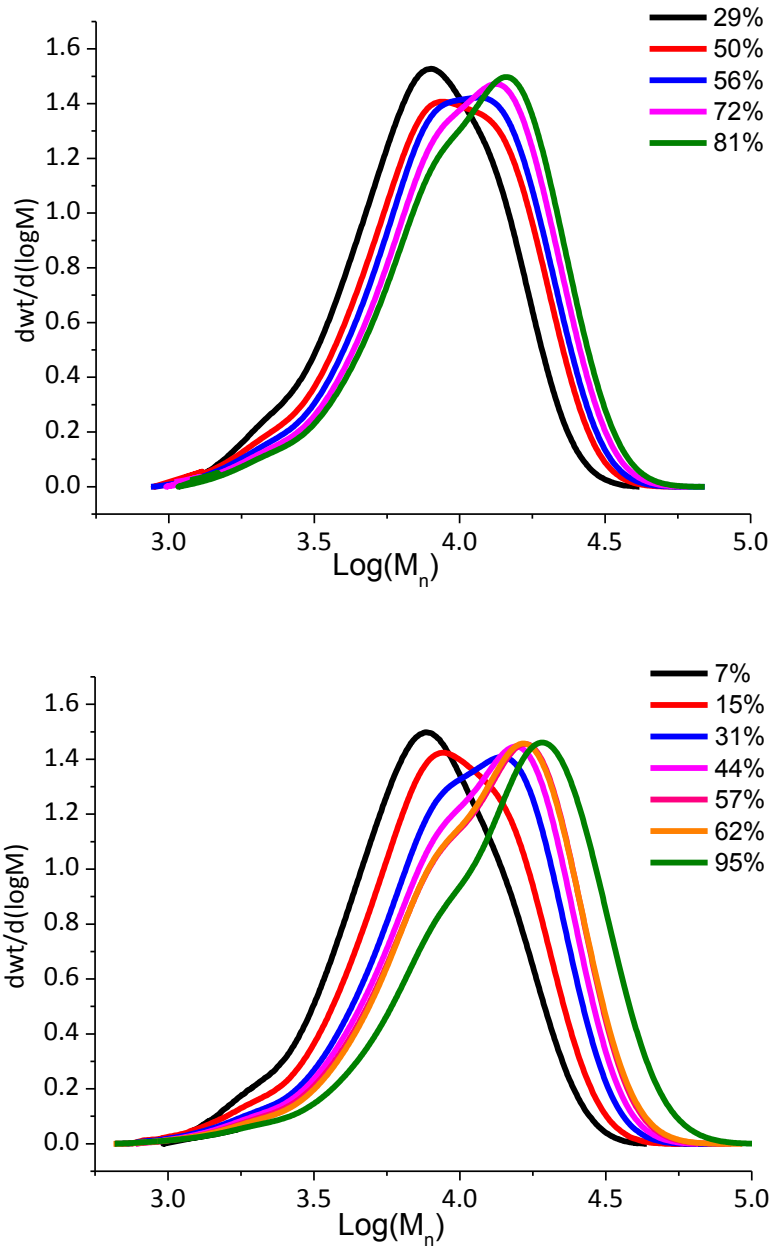

Figure 3.4. GPC traces of PDMAEMA and PDEAEMA as a function of conversion. DMAEMA:[$CuBr_2$]:[L]:[I]$_0$:[M]$_0$= 1:100:91:5782. DEAEMA: [$CuBr_2$]:[L]:[I]$_0$:[M]$_0$= 1:100:107:5782.

Chain-extensions were performed for both systems and the GPC traces are presented in Figure 3.5. It can be noted that in the PDEAEMA chain-extension, the fraction of dead chains was higher than the fraction of dead PDMAEMA chains. As already mentioned in

the homopolymerization discussion, it would support the hypothesis that DEAEMA competes more strongly than DMAEMA for the copper catalyst, resulting in a more deficient deactivation of propagating chains. In consequence, PDEAEMA chain-end functionality appeared to be lower than PDMAEMA. Having a fraction of irreversibly terminated polymer chains does not represent a concern in terms of the *grafting-from* approach as a high-chain end functionality of the polymers grafted from the CNC is not required for the purposes of this work. Nevertheless, polymerization of these monomers using this technique may not be ideal to produce macroinitiators for the purpose of CNC grafting via *grafting-to* approach.

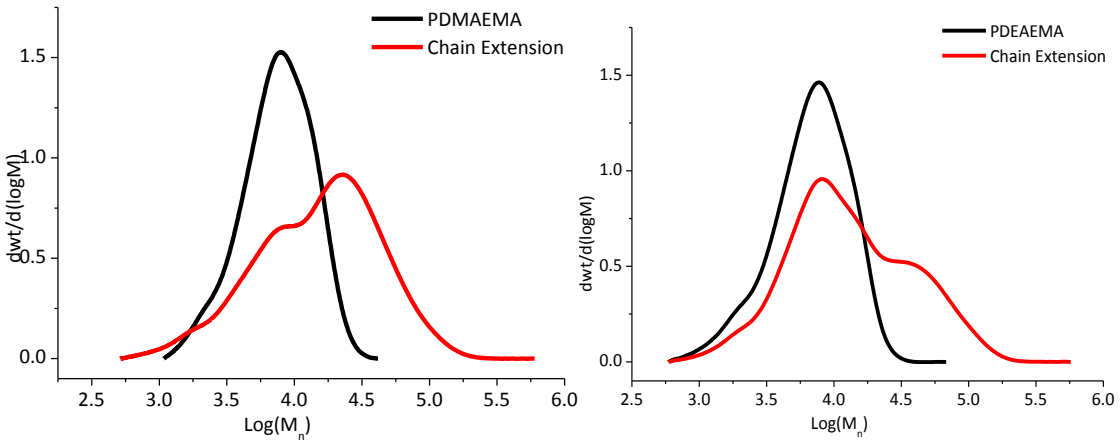

Figure 3.5. GPC trace of the chain-extension of PDMAEMA and PDEAEMA based macro-initiators via Cu(0)-ATRP.

3.3.2 *DMAEMA and DEAEMA Transesterification Analysis*

Both DMEAEMA and DEAEMA can self-catalyze their transesterification with methanol at room temperature resulting in the formation of MMA during the polymerization. Boriez-Azeau and Armes[15] reported the transesterification of DMAEMA in methanol; after 18 h at room temperature, the final PMMA content on the final

copolymer was approximately 2 mol% using conventional ATRP. We determined the degree of transesterification of each monomer as a function of time in methanol at 60°C (Figure 3.6). It was determined that after 60 min, DMAEMA and DEAEMA conversions to MMA were less than 7.4% and 20% respectively, and after 250 minutes the transesterification conversions were 22% and 50%, respectively. As DEAEMA is more basic than DMAEMA, it can self-catalyze its transesterification faster than DMAEMA resulting in a higher degree of transesterification.

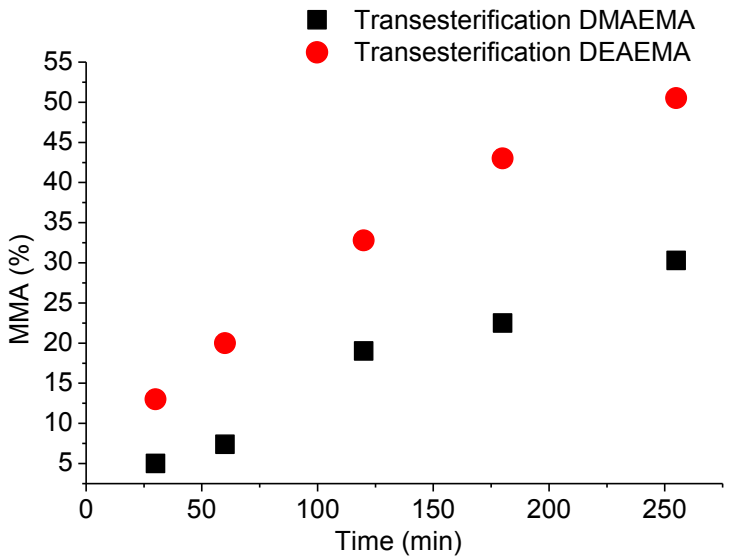

Figure 3.6. Degree of transesterification MMA vs. time of DMAEMA and DEAEMA. Dialkylaminoethyl methacrylate:MeOH = 1:1 v/v at 60 C.

^{1}H NMR analyses of PDEAEMA and PDMAEMA synthesized by Cu(0)-ATRP after 60 minutes (Figure 3.6) show that the final PDMAEMA and PDEAEMA products contained 8 mol% and 0.6 mol% MMA, respectively, which was consistent with the observations reported by Boriez-Azeau and Armes.[15] Previous reports on the polymerization of DMAEMA and DEAEMA via any variation of ATRP in methanol/water

mixtures have generally not considered the *in situ* formation of MMA, although it seems likely that some transesterification would take place. Although the homopolymerization kinetics in methanol showed that the MMA content could be as high as ~8 mol% in methyl esters on the final grafts, we considered this as an acceptable trade-off that allowed the use of methanol as a solvent capable of effectively dispersing CNC during the grafting process.

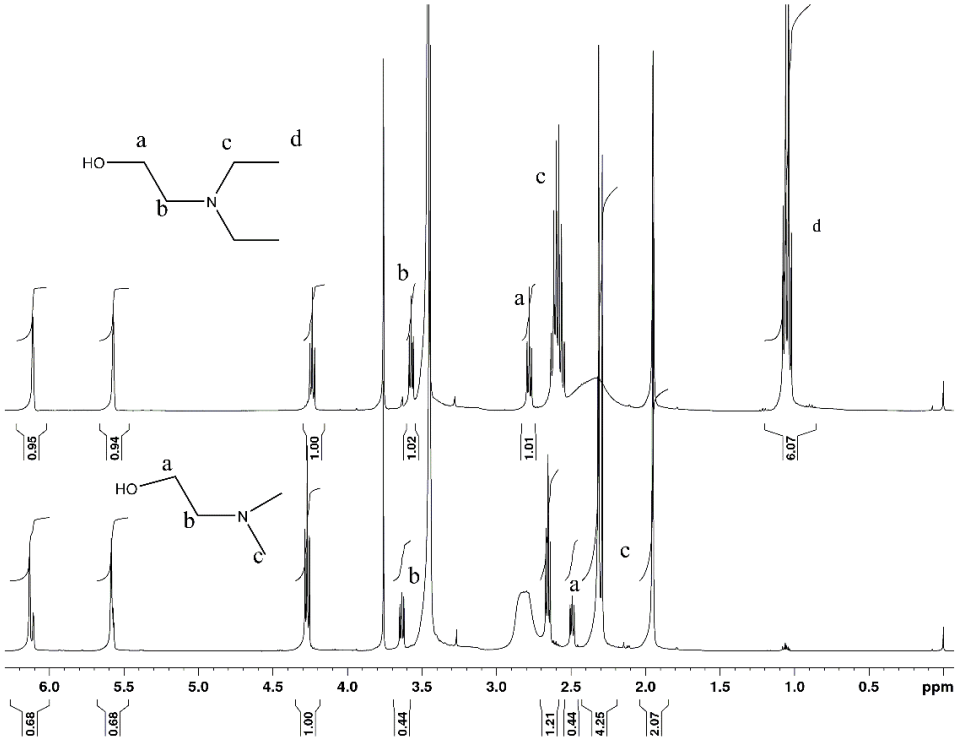

Figure 3.7. ^{1}H NMR spectra of DEAEMA (a) and DMAEMA (b) after 250 min of transesterification in methanol.

3.3.3 *Conclusions*

In this work we reported, for the first time, a homopolymerization kinetic analysis of the two dialkylaminoethyl methacrylates, DMAEMA and DEAEMA, via Cu(0)-ATRP in methanol, to determine favorable conditions to perform a *grafting-from* approach on CNC with these CO_2-responsive monomers in a polar solvent. Fair control of the molecular

weight and molar mass distributions were obtained. Although chain-extension experiments showed that a high fraction of chain-end functionality was lost due to strong interactions of the amino groups with the copper catalyst. Kinetics analysis showed a near constant concentration of growing radicals during the polymerization and an almost linear trend in M_n evolution. Polymers made by Cu(0)-ATRP in methanol showed a PMMA content of 8 mol% for PDMAEMA and 0.6 mol% for PDEAEMA resulting from transesterification of the monomer, which was deemed a reasonable amount of PMMA content as it permitted the use of methanol as a solvent when polar solvents are needed.

As the *grafting-to* approach is also considered in this work due to the advantage of being capable to graft well-characterized the polymers, Cu(0)-ATRP is not the best option for this purpose, as the macroinitiators contain a significant fraction of dead chains. Due to the presence of these dead chains, the real molecular weight of the macroinitiators to be grafted will be considerably overestimated, as only a fraction of the polymer chains has the potential to chain-extend. For the case of NMP, the polymers made with this technique are mostly statistical copolymers containing ca. 10 mol% styrene which could affect the hydrophobicity of the final products. Therefore, to be able to obtain and graft 100% poly(dialkylaminoethyl methacrylates) onto CNC surfaces, homopolymerization of these monomers was also studied by the RAFT polymerization technique.

References

1.Gan, L.-H.; Ravi, P.; Mao, B. W.; Tam, K.-C., Controlled/living polymerization of 2-(diethylamino)ethyl methacrylate and its block copolymer with tert-butyl methacrylate by atom transfer radical polymerization. *J. Polym. Sci., Part A: Polym. Chem.* **2003,** *41* (17), 2688-2695.

2.Kitayama, Y.; Takeuchi, T., Synthesis of CO_2/N_2-triggered reversible stability-controllable poly(2-(diethylamino)ethyl methacrylate)-grafted-aunps by surface-initiated atom transfer radical polymerization. *Langmuir* **2014,** *30* (42), 12684-12689.

3.Mao, B. W.; Gan, L. H.; Gan, Y. Y.; Tam, K. C.; Tan, O. K., Controlled one-pot synthesis of pH-sensitive self-assembled diblock copolymers and their aggregation behavior. *Polymer* **2005,** *46* (23), 10045-10055.

4.Mori, H.; Walther, A.; André, X.; Lanzendörfer, M. G.; Müller, A. H. E., Synthesis of highly branched cationic polyelectrolytes via self-condensing atom transfer radical copolymerization with 2-(diethylamino)ethyl methacrylate. *Macromolecules* **2004,** *37* (6), 2054-2066.

5.Lee, S. B.; Russell, A. J.; Matyjaszewski, K., Atrp synthesis of amphiphilic random, gradient, and block copolymers of 2-(dimethylamino)ethyl methacrylate and n-butyl methacrylate in aqueous media. *Biomacromolecules* **2003,** *4* (5), 1386-1393.

6.Mao, B. W.; Gan, L. H.; Gan, Y. Y., Ultra high molar mass poly[2-(dimethylamino) ethyl methacrylate] via atom transfer radical polymerization. *Polymer* **2006,** *47* (9), 3017-3020.

7.Zeng, F. Q.; Shen, Y. Q.; Zhu, S. P.; Pelton, R., Rapid communication - atom transfer radical polymerization of 2-(dimethylamino)ethyl methacrylate in aqueous media. *J. Polym. Sci., Part A: Polym. Chem.* **2000,** *38* (20), 3821-3827.

8.Zeng, F. Q.; Shen, Y. Q.; Zhu, S. P.; Pelton, R., Synthesis and characterization of comb-branched polyelectrolytes. 1. Preparation of cationic macromonomer of 2-(dimethylamino)ethyl methacrylate by atom transfer radical polymerization. *Macromolecules* **2000,** *33* (5), 1628-1635.

9.Mao, B. W.; Gan, L. H.; Gan, Y. Y.; Li, X. S.; Ravi, P.; Tam, K. C., Controlled polymerizations of 2-(dialkylamino)ethyl methacrylates and their block copolymers in protic solvents at ambient temperature via atrp. *J. Polym. Sci., Part A: Polym. Chem.* **2004,** *42* (20), 5161-5169.

10.Yu, X.; Tong, S.; Ge, M.; Wu, L.; Zuo, J.; Cao, C.; Song, W., Adsorption of heavy metal ions from aqueous solution by carboxylated cellulose nanocrystals. *J Environ Sci* **2013,** *25* (5), 933-43.

11.Cai, J.; Kimura, S.; Wada, M.; Kuga, S., Nanoporous cellulose as metal nanoparticles support. *Biomacromolecules* **2009,** *10* (1), 87-94.

12.Zhang, X.; Xia, J.; Matyjaszewski, K., Controlled/"living" radical polymerization of 2-(dimethylamino)ethyl methacrylate. *Macromolecules* **1998,** *31* (15), 5167-5169.

13.Dong, H.; Matyjaszewski, K., Arget atrp of 2-(dimethylamino)ethyl methacrylate as an intrinsic reducing agent. *Macromolecules* **2008,** *41* (19), 6868-6870.

14.Darabi, A.; Shirin-Abadi, A. R.; Jessop, P. G.; Cunningham, M. F., Nitroxide-mediated polymerization of 2-(diethylamino)ethyl methacrylate (deaema) in water. *Macromolecules* **2015,** *48* (1), 72-80.

15.Bories-Azeau, X.; Armes, S. P., Unexpected transesterification of tertiary amine methacrylates during methanolic atrp at ambient temperature: A cautionary tale. *Macromolecules* **2002,** *35* (27), 10241-10243.

16.Lad, J.; Harrisson, S.; Mantovani, G.; Haddleton, D. M., Copper mediated living radical polymerisation: Interactions between monomer and catalyst. *Dalton Transactions* **2003,** (21), 4175-4180.

17.Schmalz, A.; Hanisch, M.; Schmalz, H.; Müller, A. H. E., Double stimuli-responsive behavior of linear and star-shaped poly(n,n-diethylaminoethyl methacrylate) in aqueous solution. *Polymer* **2010,** *51* (6), 1213-1217.

Chapter 4. Homopolymerization of Dialkylaminoethyl Methacrylates via RAFT-mediated Polymerization

All the materials along with the characterization methods and specifications can be found in the Appendices A.II and B. respectively.

4.1 ***Introduction***

As mentioned in Chapter 2, RAFT polymerization is one of the most versatile RDRP techniques as it is suitable for polymerizing monomers containing functional groups in different types of solvents and it does not require extreme reaction conditions (e.g. extreme monomer and solvent purity or air-free conditions). In Chapter 3, it was shown that Cu(0)-ATRP is not ideal for polymerizing dialkylaminoethyl methacrylates due to interaction of these monomers with the copper catalyst resulting in low chain-end functionality polymers. High chain-end functionality is of great importance for the scope of this project as one of the objectives is to assess whether there is an effect of molecular weight on the final CO_2-switching properties of grafted-CNC via the *grafting-to* approach. To accomplish this assessment, fully characterized polymers with the ability to be chain-extended are needed. Therefore, an alternative to Cu(0)-ATRP was required and the RAFT approach is a convenient alternative as it is compatible with monomers containing different functional groups and requires only mild reaction conditions.

There are only a few reports on the homopolymerization of DMAEMA, DEAEMA and DPAEMA by RAFT-mediated polymerization where kinetics, molecular weight control and livingness are reported. These reports describe the homopolymerization and copolymerization of these monomers in non-polar solvents (e.g. 1,4 dioxane, toluene)[1-5] which are not good solvents for CNC surface modification. In other reports on the

polymerization of DMAEMA, methanol was used as a solvent having reaction times up to 24 h at 70°C.[6-7] In Chapter 3, it was demonstrated that 22% of DMAEMA is converted to MMA in methanol at 60°C after 4 h which immediately discards the usage of short-chain primary alcohols as a suitable solvents. Secondary alcohols like isopropanol can undergo chain transfer when used as a solvent in free radical polymerization.[8-9] Xiong *et al.*[10] reported the RAFT-mediated polymerization of DMAEMA in water at 70°C using 4-cyanopantanoic acid dithiobenzoate (CTP) as CTA. Pseudo-first-order kinetic plots and a linear increase of M_n were observed. However, as CTP degrades in water at 70°C,[11] chain-end functionality of the final product could have been significantly compromised as neither chain-extensions experiments nor GPC-UV analyses were performed to demonstrate livingness.

Other non-acidic polar organic solvents like DMF or DMSO are not good options for various reasons; in the case of DMF, it is a difficult solvent to remove following polymerization because of its high boiling point (153°C). In the case of DMSO, our experiments showed that PDEAEMA is hydrophobic enough to phase separate during its polymerization in DMSO (Figure C.2). Consequently, viable options to polymerize these monomers are in bulk or in solution with a tertiary alcohol as a solvent. Tert-butanol is not subjected to side reactions like the ones previously mentioned and it is polar enough to sufficiently disperse CNC. In addition, poly(dialkylaminoethyl methacrylates) proved to be fully soluble in tert-butanol.

The work reported by Sahnoun *et al.*[3] (RAFT-mediated polymerization of DMAEMA) presents one GPC-UV trace analyzing the fraction of polymer chains retaining the dithiobenzoate moiety in the chain-ends after chain-extension (Figure 4.1). They report a

significant shoulder of the macro-RAFT agent in the GPC-UV trace that did not shift towards higher molecular weights, showing a low reinitiation efficiency. Even though the authors analyzed the macro-RAFT agent with MALDI-TOF mass spectrometry, conclusions on the nature of that shoulder could not be formulated due to possible fragmentation or degradation of the dithiobenzoate group under analytical conditions.

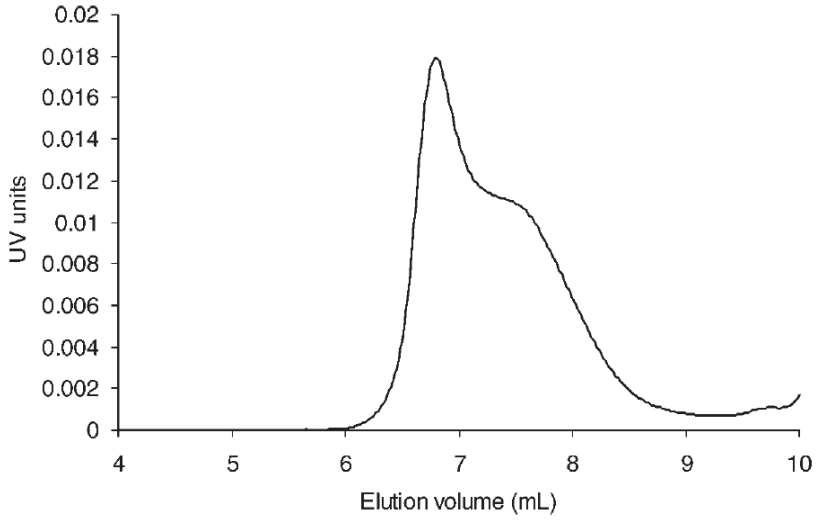

Figure 4.1. GPC-UV trace of a PDMAEMA-based macro-RAFT agent. Reprinted with permission from Sahnoun *et al.*[3] Copyright 2005 Wiley Periodicals, Inc.

Due to the limited information regarding the synthesis and livingness of PDMAEMA, PDEAEMA and PDPAEMA-based macro-RAFT agents in polar solvents, where CNC can be dispersed in the absence of side reactions (transesterification of monomers), kinetic studies via RAFT-mediated polymerization of DMAEMA, DEAMA and DPAEMA using CTP as CTA were performed in bulk and tert-butanol (Scheme 4.1). Once the polymerization conditions were determined, a set of three different molecular weights were synthesized for each polymer and their livingness were assessed by chain-extension experiments via GPC-UV-RI detection.

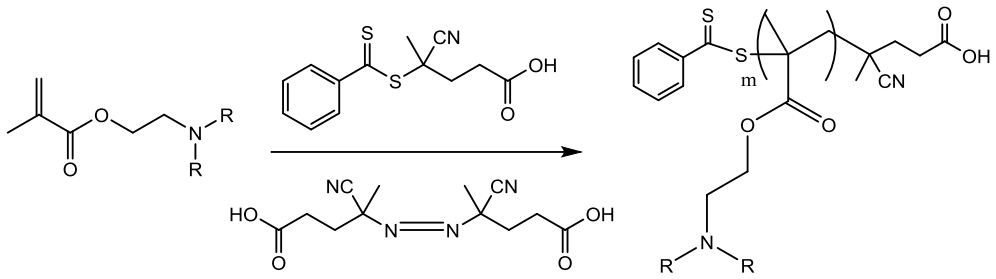

Scheme 4.1. RAFT-mediated polymerization of dialkylaminoethyl methacrylates in bulk or solution at 70°C using 4-cyanopantanoic acid dithiobenzoate as RAFT agent and 4,4 -azobis(4-cyanopentanoic acid) as initiator.

4.2 ***Experimental***

4.2.1 *General procedure for the homopolymerization of alkylaminoethyl methacrylates*

Stocks solutions of each monomer were prepared by adding 3.5 g of DMAEMA (22.25 mmol), DEAEMA (18.88 mmol) or DPAEMA (16.40 mmol), to 97.78 mg (0.35 mmol) of CTP. The stock solution was then divided into six vials containing 250 mg of the mixture for the polymerization in bulk. To each vial, 1.4 mg (0.005 mmol) of 4,4 -Azobis(4-cyanopentanoic acid) (ACVA) were added along with a magnetic stir bar. For the experiments performed in solution, 250 mg of tert-butanol was added as the solvent. Next, the vials were degassed by bubbling nitrogen for 3 minutes and sealed. The vials were then immersed in an oil bath at 70°C and were sequentially quenched by cooling them down to -10°C and exposing them to air. The vials were taken out of the oil bath at a predetermined reaction time. In the case of the vials run in bulk, they were taken out of the oil bath right after the stir bar started to skip rotations due to high viscosity. Samples were collected for ^{1}H NMR and GPC analysis. Larger batches were made under the same conditions to be used as macro-RAFT agents for the chain-extension experiments (Table 4.1). All three

polymers were precipitated three times. PDMAEMA was precipitated in cold hexanes, while PDEAEMA and PDPAEMA were precipitated in ice water. Finally, the three polymers were dried in a vacuum oven at 50°C.

Table 4.1. Polymerization recipe for the synthesis of macro-RAFT agents.

	Monomer (g)	Macro-RAFT (mmol)	ACVA (mmol)	tBuOH (g)	Target M_n[a] (Da)
PDMAEMA					
	4	1.00	0.20	4	2,280
	4	0.50	0.10	4	4,280
	4	0.33	0.07	4	6,280
PDEAEMA					
	4	1.00	0.20	4	2,280
	4	0.50	0.10	4	4,280
	4	0.33	0.07	4	6,280
PDPAEMA	4				
	4	1.00	0.20	4	2,280
	4	0.50	0.10	4	4,280
	4	0.33	0.07	4	6,280

[a] Target M_n at 50% monomer conversion. Target M_n = conversion x ([mon]/[CTA]) x $M_{w\ mon}$+$M_{w\ CTA}$. $M_{w\ mon}$ is the molecular weight of the monomer and $M_{w\ CTA}$ is the molecular weight of the CTA.

4.2.2 *Chain-extension experiments*

Table 4.2 shows the recipes for different chain-extension experiments where three different molecular weights for each polymer (PDMAEMA, PDEAEMA, PDPAEMA) were used. First, the macro-RAFT agent was put in a 5 mL vial. Then, tert-butanol was added, adjusting the solution to a final solids content of 50%. Then, the monomer was added and the vials were stirred until complete dissolution of the polymer and monomer was observed. Finally, initiator was added from a prepared stock solution via syringe ([macro-RAFT]/[I] =5) and the vial was degassed by bubbling nitrogen gas for 5 minutes. The vial was sealed and then put into an oil bath at 70°C for 16 h.

Table 4.2. Characteristics of macro-RAFT agents and recipe for chain-extension experiments.

	M_n[a] (Da)	Đ	Macro-RAFT (mmol)	ACVA (mmol)	Monomer (mg)	tBuOH (mg)	Target M_n (Da)
PDMAEMA							
	2,500	1.20	2.50E-02	4.1E-03	246	297	12,000
	6,800	1.19	7.99E-03	1.6E-03	136	189	17,000
	7,800	1.20	6.59E-03	1.32E-03	119	170	18,000
PDEAEMA							
	3,700	1.22	1.39E-02	2.78E-03	194	244	14,000
	5,800	1.22	1.03E-02	2.06E-03	165	225	16,000
	8,600	1.21	5.95E-03	1.19E-03	113	165	19,000
PDPAEMA							
	3,600	1.16	1.56E-02	3.12E-03	219	277	14,000
	5,900	1.11	9.92E-03	1.98E-03	159	218	16,000
	7,100	1.11	7.18E-03	1.44E-03	122	173	17,000

[a]M_n was determined by GPC-UV-RI. For PDMAEMA and PDEAEMA, absolute molecular weights were obtained by universal calibration using Mark-Houwnik parameters published elsewhere.[12] M_n of PDPAEMA was determined using PMMA equivalents.

4.3 ***Results and discussion***

4.3.1 *Homopolymerization of dialkylaminoethyl methacrylates*

Kinetics analyses were required for each monomer to determine the conditions and conversions under which the homopolymerization of DMAEMA, DEAEMA and DPAEMA could be performed to obtain good control and livingness. Figure 4.2 shows the $Ln([M]_0/[M])$ and conversion vs. time plots of the polymerization of DMAEMA, DEAEMA and DPAEMA. In all three plots, an induction period of ca. 60 min can be observed. This is to be expected for systems where dithiobenzoates are used as CTA in RAFT polymerization.[13-14]

For the case of the polymerizations performed in solution, pseudo-first order kinetics were observed for all three monomers indicating a nearly constant radical concentration during the polymerization until approximately 8 h of reaction time. After 8 hours, a curvature or second stage in the semi-logarithmic plots can be observed. This behavior is mainly due to a decrease in the concentration of reactive radicals as the initiator half-life at 70°C is ca. 10 h. Therefore, after 8 h, the initiator concentration was almost at 50% of its initial value (in RAFT polymerization, R_p is still dependent on the initiator concentration).

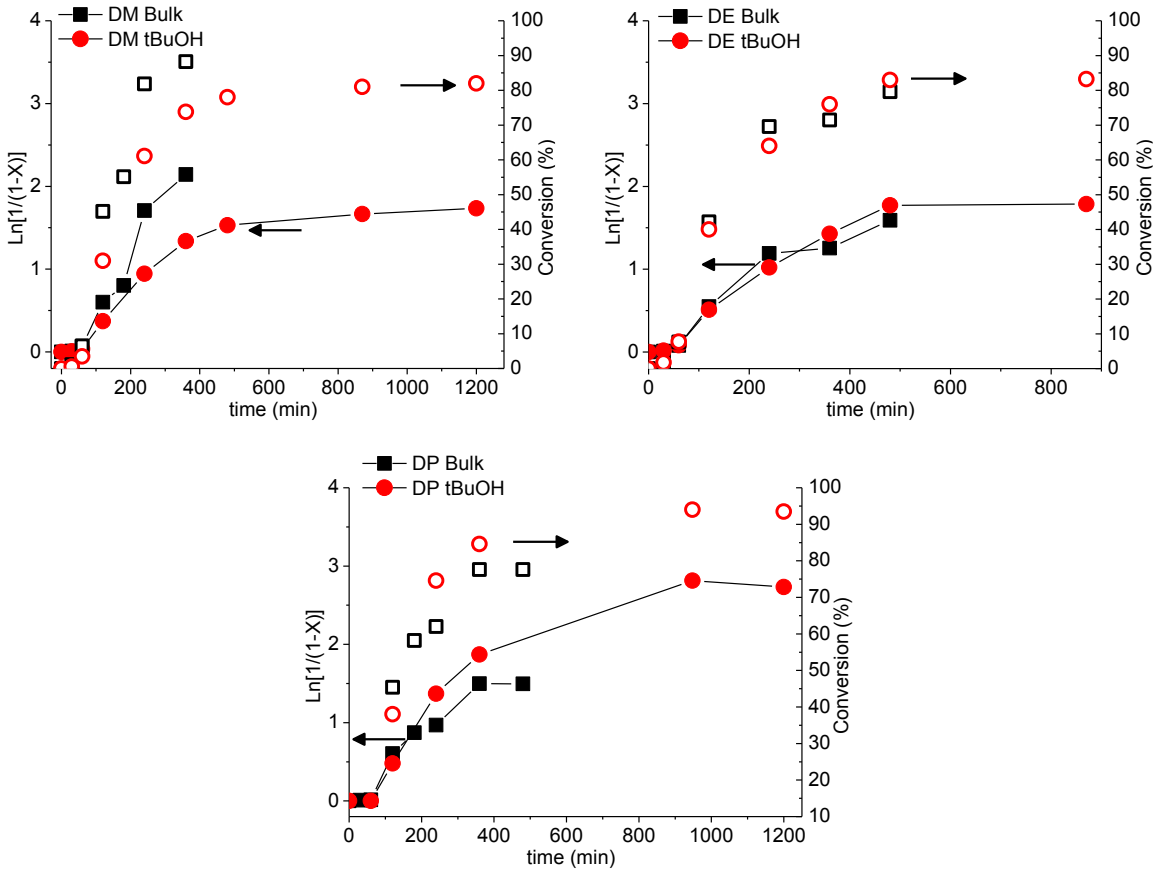

Figure 4.2. Ln($[M]_0/[M]$) and conversion vs. time plots of DMAEMA (DM), DEAMA (DE), DPAEMA (DP) in bulk and in tert-butanol via RAFT polymerization at 70°C. DMAEMA: $[M]_0 : [CTP]_0 : [I]_0 = 318:5:1$. DEAEMA: $[M]_0 : [CTP]_0 : [I]_0 = 270:5:1$. DPAEMA: $[M]_0 : [CTP]_0 : [I]_0 = 234:5:1$.

For the polymerization of the monomers in bulk, a linear trend observed at the early stages of the reactions, indicated pseudo-first order kinetics (Figure 4.2). In the case of DMAEMA, a sudden increase in conversion (and therefore in the concentration of radicals) was observed at 55% conversion. A reasonable explanation could be that at ~55% monomer conversion in bulk, the system was too viscous for the magnetic stir bar to efficiently stir the reaction mixture. Still, M_n increased linearly with conversion and narrow

molecular weight distributions are obtained throughout the reaction ($Đ \leq 1.2$) suggesting livingness and good control for all the systems (Figure 4.3).

The linear trend in the evolution of M_n vs. conversion suggests a living process during the polymerization of all three monomers. However, this trend does not guarantee that most of the chains have a dithiobenzoate moiety at the chain-end (Scheme 4.1). To confirm the presence of the RAFT moieties at the polymer chain-ends and therefore their potential to be chain-extended, samples from the kinetic study were analyzed by GPC with both UV and RI detectors (GPC-UV-RI). The population of polymer chains containing a RAFT moiety at their chain-end are UV-active. In an ideal RAFT polymerization, every chain should contain one dithiobenzoate moiety which is UV active at a $\lambda = 310$ nm.[3] The GPC-UV traces represent the living chains (as number based distributions) that have a dithiobenzoate moiety at their chain-end. If (nearly) all of the polymer chains contain a dithiobenzoate group, the UV and RI traces will be almost identical. An increasing fraction of dead chains (i.e. those not containing a dithiobenzoate moiety at their end) will result in greater deviation between the UV and RI traces. To allow for direct comparison in between traces (UV and RI), all of the RI traces were transformed to number based distributions.

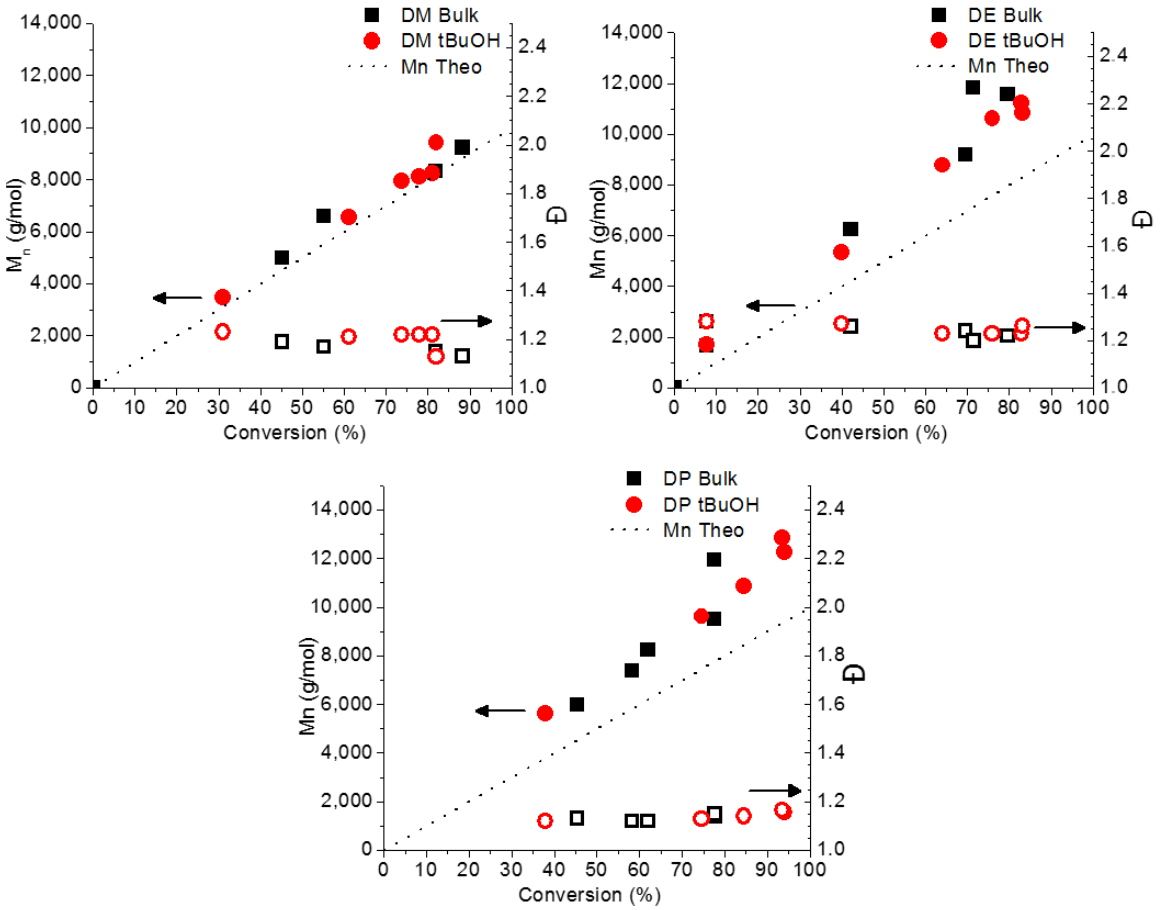

Figure 4.3. Evolution of M_n vs. conversion of DMAEMA (DM), DEAMA (DE), DPAEMA (DP) in bulk and in tert-butanol via RAFT polymerization at 70°C. DMAEMA: $[M]_0 : [CTP]_0 : [I]_0 = 318:5:1$. DEAEMA: $[M]_0 : [CTP]_0 : [I]_0 = 270:5:1$. DPAEMA: $[M]_0 : [CTP]_0 : [I]_0 = 234:5:1$.

From the GPC traces shown in Figures 4.4-4.6, it can be seen that for all three monomers in bulk and solution, the UV and RI traces are almost identical at conversions lower than 50%. This would imply that most of the polymer chains are functionalized with a dithiobenzoate group making them suitable to be chain-extended. For all of the polymerizations in both systems (bulk and solution), high conversions were also achieved. However, at higher monomer conversions, higher fractions of dead chains were noted to appear as a low- molecular weight tails on the RI traces. These fractions of polymer chains did not contain a dithiobenzoate group and therefore did not appear in the UV trace. From these kinetic analyses, it could be concluded that good control and possibly good livingness, can be achieved either in bulk or solution polymerization. However, in order to obtain polymers with a desired molecular weight and to maximize the chain-end functionality, the targeted monomer conversions should be less than ~50%.

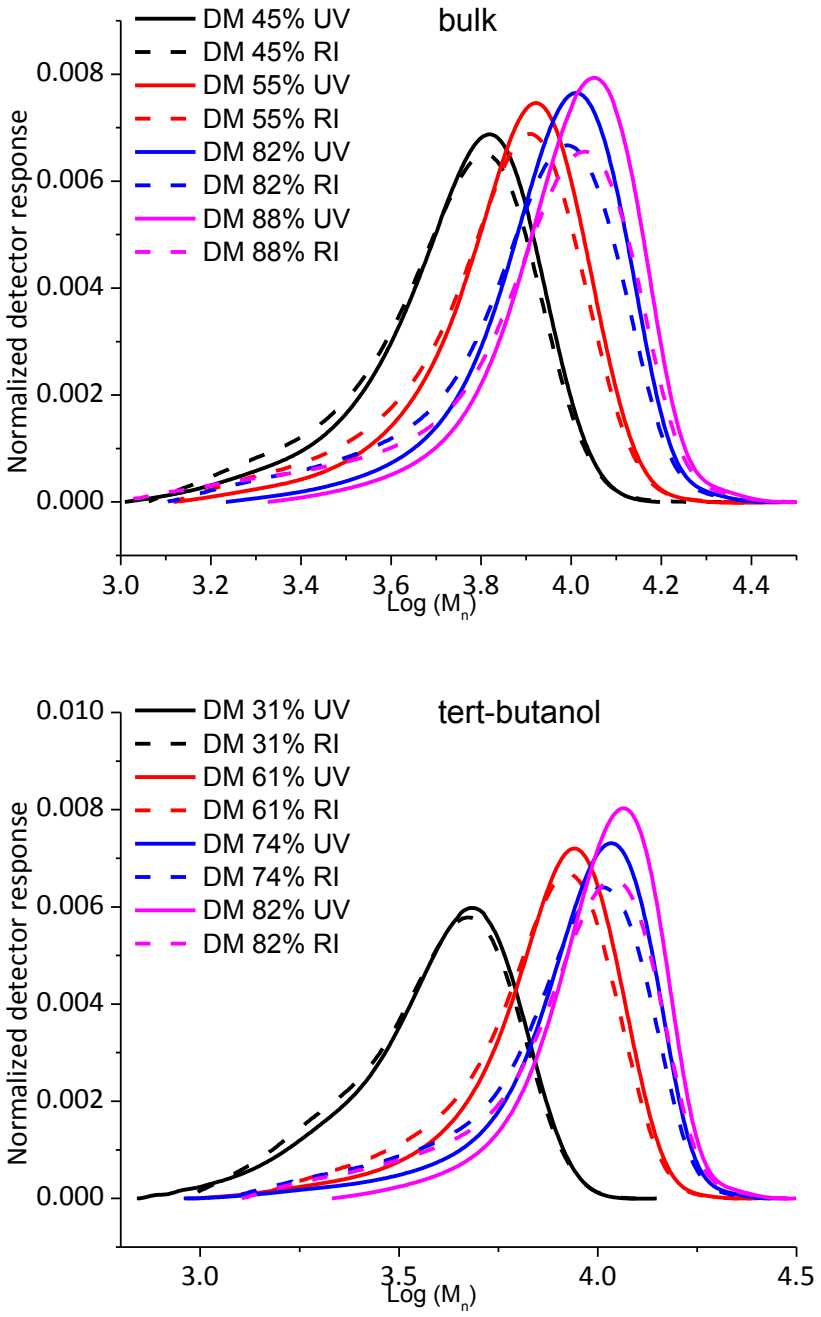

Figure 4.4. GPC UV-RI traces of the polymerization of DMAEMA in bulk and in tert-butanol via RAFT polymerization at 70°C. $[M]_0 : [CTP]_0 : [I]_0 = 318:5:1$.

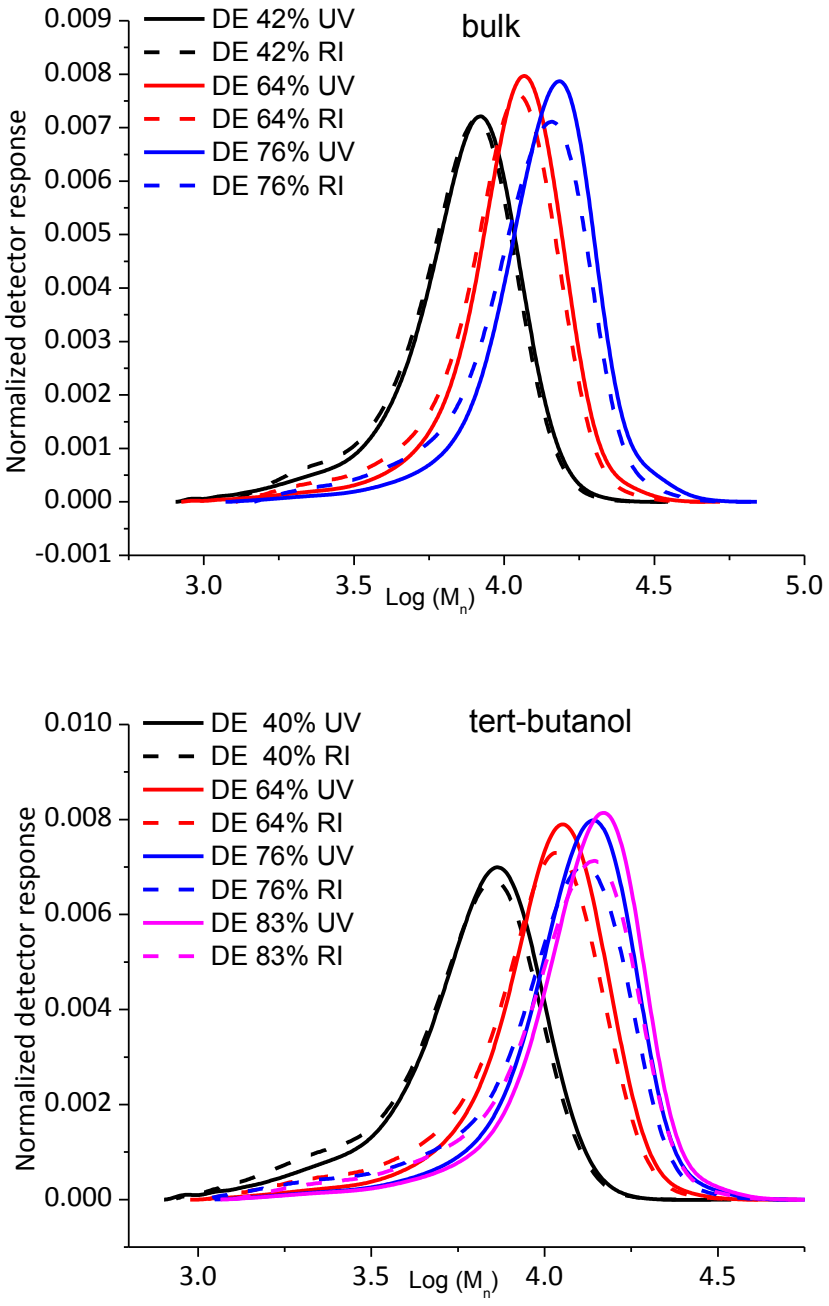

Figure 4.5. GPC UV-RI traces of the polymerization of DEAEMA in bulk and in tert-butanol via RAFT polymerization at 70°C. $[M]_0 : [CTP]_0 : [I]_0 = 270:5:1$.

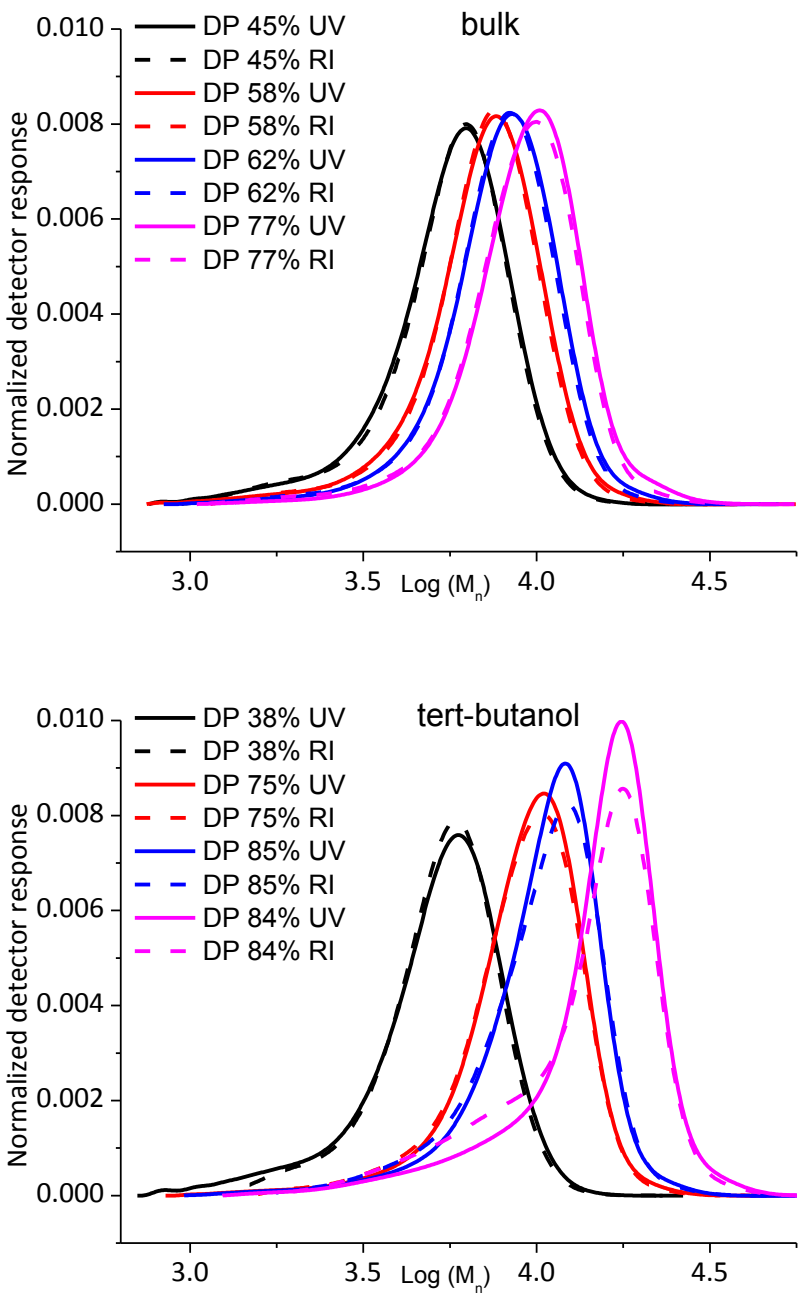

Figure 4.6. GPC UV-RI traces of the polymerization of DPAEMA in bulk and in tert-butanol via RAFT polymerization at 70°C. $[M]_0 : [CTP]_0 : [I]_0 = 234:5:1$.

4.3.2 *Effect of the [CTA]/[I] Ratio*

For any RDRP technique (ATRP, NMP, RAFT), it is well known that to minimize the number of dead chains formed by irreversible radical termination, the concentration of active species during the polymerization should be as low as possible while maintaining an acceptable overall polymerization rate.[15] In the case of RAFT polymerization, the active species concentration can be adjusted by modifying the initiator concentration, which also directly affects R_p. The number of living polymer chains is determined by the amount of CTA, but the R_p is influenced by the initiator concentration.[16] Molecular weight, dispersity and R_p are determined by the [CTA]/[I] ratio in addition to the initiator half-life. Depending on the type of monomer, a [CTA]/[I] of ~5-10 is commonly employed for RAFT-mediated polymerization. Having higher [CTA]/[I] ratios results in very good control and high chain-end functionality, but at the expense of much lower polymerization rates. Conversely, having lower [CTA]/[I] ratios could significantly increase the polymerization rates, but a higher dead polymer fraction (lower chain-end functionality) and poor control could also occur. These aspects are much dependent on the type of monomer. So, to verify that the [CTA]/[I] ratio of 5 used for the kinetic experiments of DMAEMA and DEAEMA in this study did not lead to high fractions of dead polymers chains at conversions higher than 50%, polymerization experiments were also conducted applying a [CTA]/[I] ratio of 10 at similar conversion.

Figure 4.7 and Figure 4.8 show the GPC traces of the polymerization in bulk and solution (tert-butanol) of DMAEMA and DEAEMA, respectively, using a [CTA]/[I] ratio of 10. In the case of PDMAEMA, tailing can be noticed on the RI trace for the polymerizations in both bulk and in solution, despite having less initiator compared to the

experiment with a [CTA]/[I] ratio of 5 (Figure 4.4). Moreover, the monomer conversions were 44% and 48% respectively after 10.5 h, whereas, with a [CTA]/[I] ratio of 5, monomer conversions were ≥80% after the same reaction time. These experiments confirmed that the [CTA]/[I] ratio of 5 was not a significant causal factor in the formation of dead polymer chains at the low-end of the molecular weight distributions and it can be used to have faster polymerization rates.

GPC-UV traces of PDMAEMA made in bulk and solution are also shown in Figure 4.7. It can be noted that the PDMAEMA macro-RAFT agent made in bulk, had a higher molecular weight (ca. 3,000 Da, Table 4.3) than the one made in tert-butanol, even though the monomer conversion was lower in bulk (44%) than in solution (48%). For the case of the PDEAEMA-based macro-RAFT agent, the monomer conversion and the UV traces (bulk and solution, Figure 4.8) were almost identical. With respect to the RI traces, it can be noted that for the case of PDEAMA-based macro-RAFT agents, RI traces exhibited a good agreement with the UV traces indicating that most of the polymer chains contained a dithiobenzoate groups. However, for the case of PDMAEMA in bulk analyzed by RI, a pronounced low molecular weight shoulder could be observed. This shoulder would indicate the presence of low molecular weight dead chains.

In the kinetic analysis of the DMAEMA polymerization (Figure 4.2), an increase in the radical population in the bulk system at ca. 55% conversion was observed; as well as in the polymerization rate, which was also consistent with the sudden increase in monomer conversion in bulk. These kinetics results, along with the difference in molecular weight (ca. 3 kDa) observed in the GPC-UV traces, suggest a lower rate of deactivation of the propagating chains during the polymerization of DMAEMA in bulk; and would hence

suggest, an auto-accelerating effect, producing chains with higher molecular weights when compared to the polymerization in solution. The low molecular tail was likely formed due to new propagating radicals that continued to be generated by the initiator ($t_{1/2}$ = 10 h), which irreversibly terminated as they were not found to be UV-active.

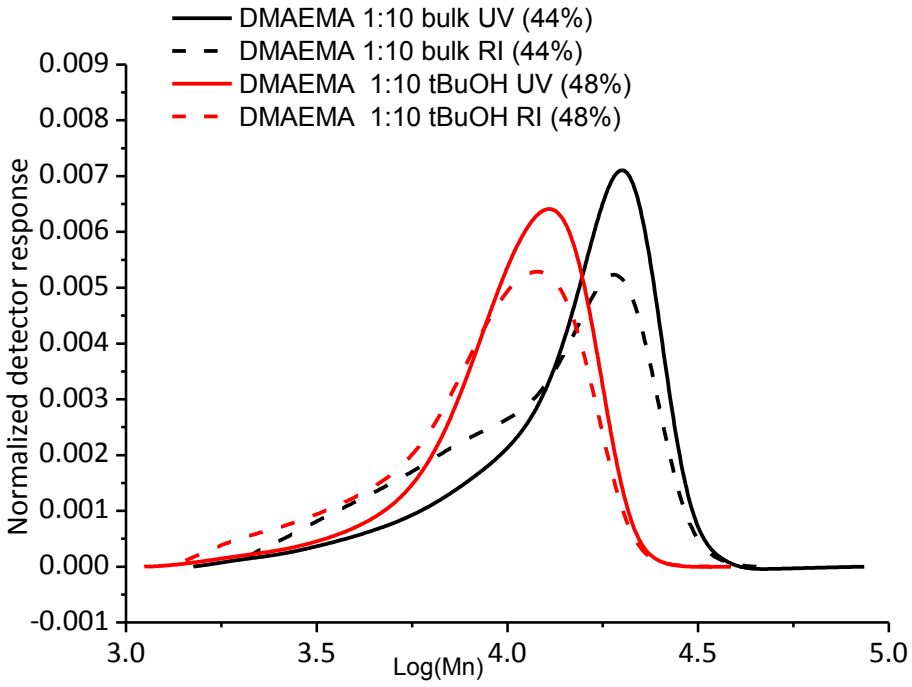

Figure 4.7. GPC UV-RI traces of the polymerization of DMAEMA in bulk and in tert-butanol via RAFT polymerization at 70°C. $[M]_0:[CTP]_0:[I]_0$ = 318:10:1.

With respect to PDEAEMA, tailing at the low end of the molecular weight distribution was barely noticeable in both bulk and in solution (Figure 4.8). Monomer conversions were 56% and 58%, respectively, after 10.5 h, whereas when using a [CTA]/[I] ratio of 5, ≥80% conversions were obtained after 11 h. Similarly, as for PDMAEMA, these experiments confirmed that a [CTA]/[I] ratio of 5 could be used without affecting chain-end functionality and Đs, or lowering the R_p. Table 4.3 summarizes the molecular weight and Đ values of PDMAEMA and PDEAEMA synthesized using both [CTA]/[I] ratios.

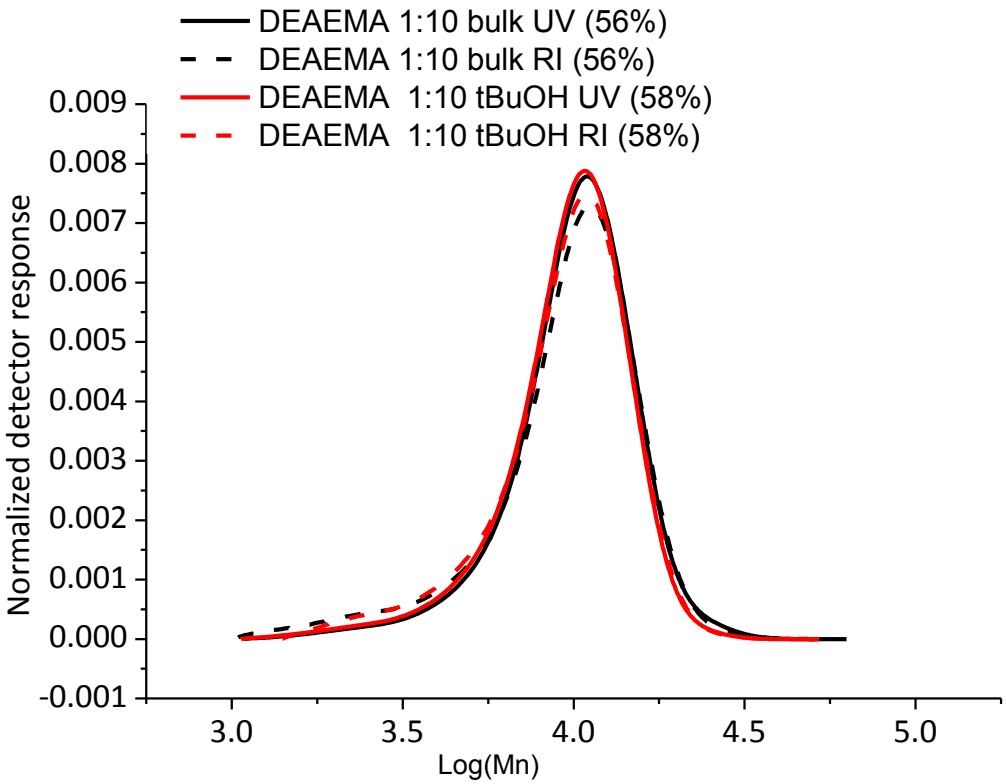

Figure 4.8. GPC UV-RI traces of the polymerization of DEAEMA in bulk and in tert-butanol via RAFT polymerization at 70°C. DEAEMA: $[M]_0 : [CTP]_0 : [I]_0 = 270:10:1$.

Table 4.3. Comparison of M_n and Đ values of macro-RAFT agents synthesized in bulk and in solution.

	Reaction Time (h)	Monomer Conversion (%)	[CTA]/[I]	Theoretical M_n[a] (Da)	M_n[b] (Da)	Đ
PDMAEMA						
Bulk	8	81	5	10,280	8,300	1.15
Bulk	19	44	10	10,280	11,900	1.35
Solution	8	78	5	10,280	8,100	1.22
Solution	19	48	10	10, 280	8,800	1.26
PDEAEMA						
Bulk	8	80	5	10,280	11,600	1.22
Bulk	19	56	10	10,280	8,900	1.21
Solution	8	83	5	10,280	10,800	1.23
Solution	19	58	10	10,280	8,500	1.26

[a] Theoretical M_n at 100% conversion. [b] M_n was determined by GPC-UV-RI. For PDMAEMA and PDEAEMA, absolute molecular weights were obtained by universal calibration using Mark-Houwnik parameters published elsewhere.[9]

4.3.3 *Chain-extension of RAFT-mediated poly(dialkylaminoethyl methacrylates)*

The main purpose of analyzing the macro-RAFT agents by GPC-UV-RI was to determine the molecular weights of the polymer chains that would be grafted on the CNC surface (i.e. the living chains). To assess the livingness of the macro-RAFT agents, chain-extension experiments were performed for each of the polymers presented in Table 4.2. Table 4.4 shows the M_n values and Đs after the chain-extension experiments.

Table 4.4. GPC UV-RI data of macro-RAFT agents and after chain-extension.

Macro-RAFT Agents	M_n[a] (Da)	Đ	$M_{n\ theo}$[b] (Da)	Chain-extension M_n[a] (Da)	Đ
PDMAEMA					
DM1	2,500	1.20	12,000	10,200	1.39
DM2	6,800	1.19	17,000	14,400	1.74
DM3	7,800	1.20	18,000	14,700	1.55
PDEAEMA					
DE1	3,700	1.22	14,000	13,600	1.47
DE2	5,800	1.22	16,000	12,500	1.40
DE3	8,600	1.21	19,000	12,400	1.33
PDPAEMA					
DP1	3,600	1.16	14,000	8,600	1.22
DP2	5,900	1.11	16,000	8,000	1.10
DP3	7,100	1.11	19,000	11,700	1.10

[a]M_n were determined by GPC-UV-RI. For PDMAEMA and PDEAEMA, absolute molecular weights were obtained by universal calibration using Mark-Houwnik parameters published elsewhere.[9] [b] Theoretical M_n at 100% conversion.

Figure 4.9 shows the GPC-UV traces of the chain-extensions of all three PDMAEMA-based macro-RAFT agents. Tailing at the low-end of the molecular weight distributions was noted and consequently, higher Đ values were observed. For the case of DM2 and DM3, it would appear that a fraction of polymer chains did not undergo chain-extension. This was likely because the re-initiation efficiency was not 100%. It could not be attributed

to dead polymer chains as these chains did contain dithiobenzoate groups (UV active). The PDEAEMA and PDPAEMA series exhibited a similar behaviour and their GPC-UV traces are shown in Figure D.1and Figure D.2 in Appendix D.I.

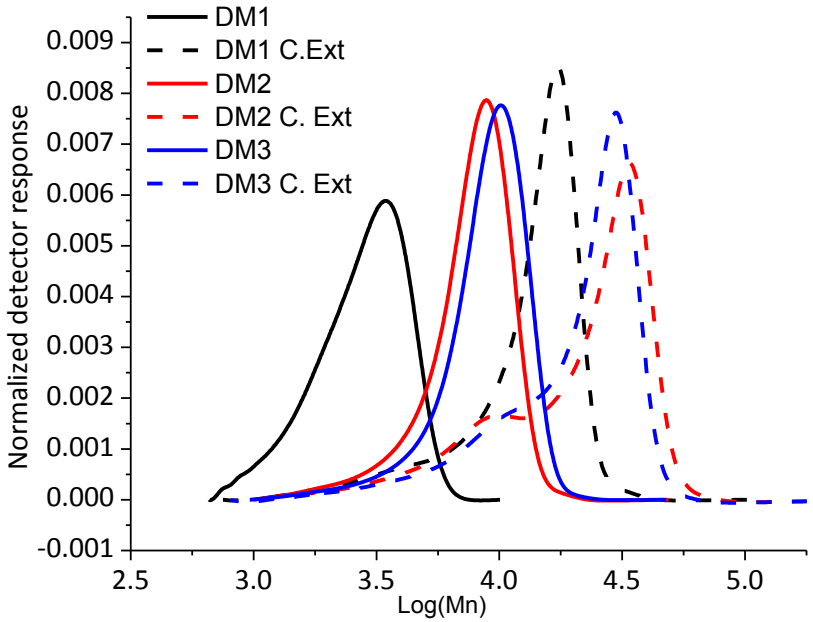

Figure 4.9. GPC-UV traces of PDMAEMA macro-RAFT agents before and after chain-extension. [macro-RAFT]:[ACVA] = 5, in tert-butanol at 70°C.

Figures 4.9-4.11 show the overlapped UV-RI traces of DM1, DM2 and DM3 macro-RAFT agents and their corresponding chain-extensions. All of the number-based RI chain-extension traces showed a considerable fraction of chains that were not UV active and therefore did not contain the dithiobenzoate group. These dead chains were likely a product of FRP polymerization of the monomer without being deactivated by the macro-RAFT agent as suggested by its lack of UV absorbance. The formation of these dead polymer chains could have been caused by a low reinitiation efficiency of the macro-RAFT agents, suggesting that the accessibility of the dithioester group was limited to the shorter propagating radicals that were formed due to the continuous formation of primary radicals

from the ACVA. Additionally, it could be noted that reinitiation efficiency decreased as a function of the M_n of the macro-RAFT agent. The causes for this observed behaviour are still unclear. However, a similar trend was also observed and reported elsewhere suggesting steric effects due to the longer chains containing the dithiobenzoate groups.[17]

In Figure 4.10, it can be noted that in the number-based RI trace, most of the DM1 shifted to higher molecular weights after chain-extension when compared to DM2 and DM3 chain-extensions. For the case of DM2 and DM3, it was observed in their corresponding UV traces that most of polymer chains containing the dithiobenzoate group (UV active), did shift towards higher molecular weights and would indicated livingness and good control during the synthesis of the macro-RAFT agents. However, their corresponding RI traces show a considerable fraction of dead chains. A rough estimation of the fraction of dead chains on the RI traces was performed by multi-peak fitting and the areas of the resultant distributions were compared (curve fitting plots are shown in Appendix D.II). For DM2 and DM3, it was estimated that ca. 70% of the RI signal corresponded to dead chains. These dead chains did not shift towards higher molecular weights and they were not visible by the UV detector. As previously suggested, the formation of these dead chains was primarily due FRP of the monomer. Additionally, incomplete reinitiation efficiency was observed as there were small fractions in the UV traces that did not shift towards higher molecular weights. However, because these fractions were still UV-active, it indicates that they did not reinitiate during the chain-extension experiments. The same behaviour was observed for the PDEAEMA and PDPAEMA macro-RAFT agents and their GPC-UV-RI traces are shown in the Appendix D.III.

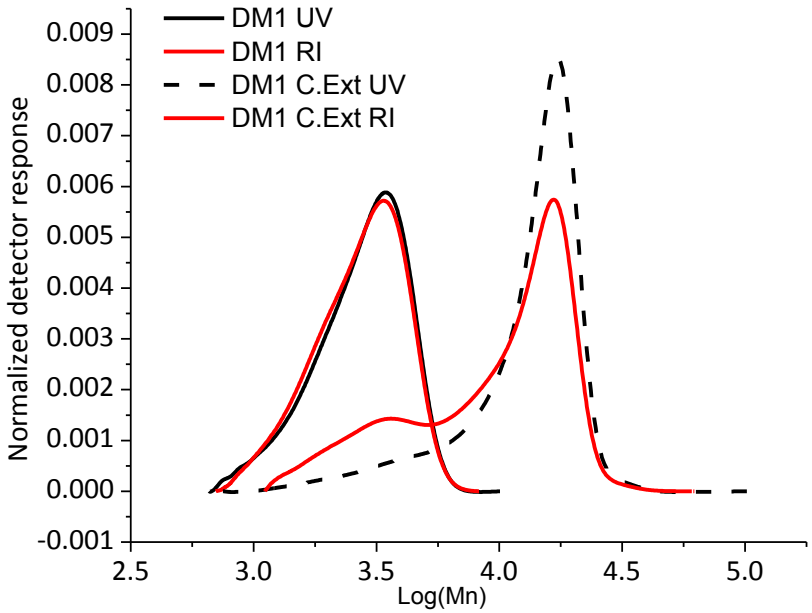

Figure 4.10. GPC-UV-RI traces of DM1 macro-RAFT agent before and after chain-extension. [macro-RAFT]:[ACVA] = 5, in tert-butanol at 70°C after 16h.

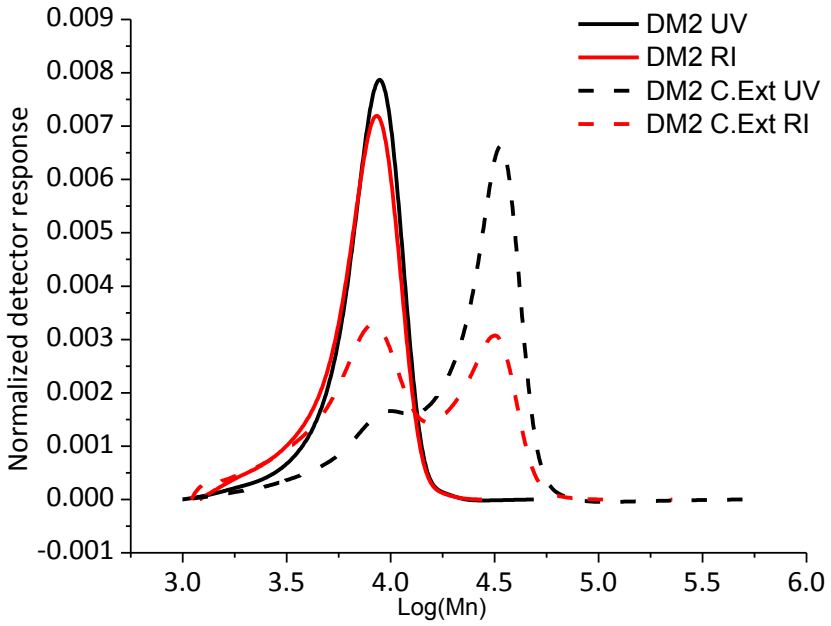

Figure 4.11. GPC-UV-RI traces of DM2 macro-RAFT agent before and after chain-extension. [macro-RAFT]:[ACVA] = 5, in tert-butanol at 70°C after 16h.

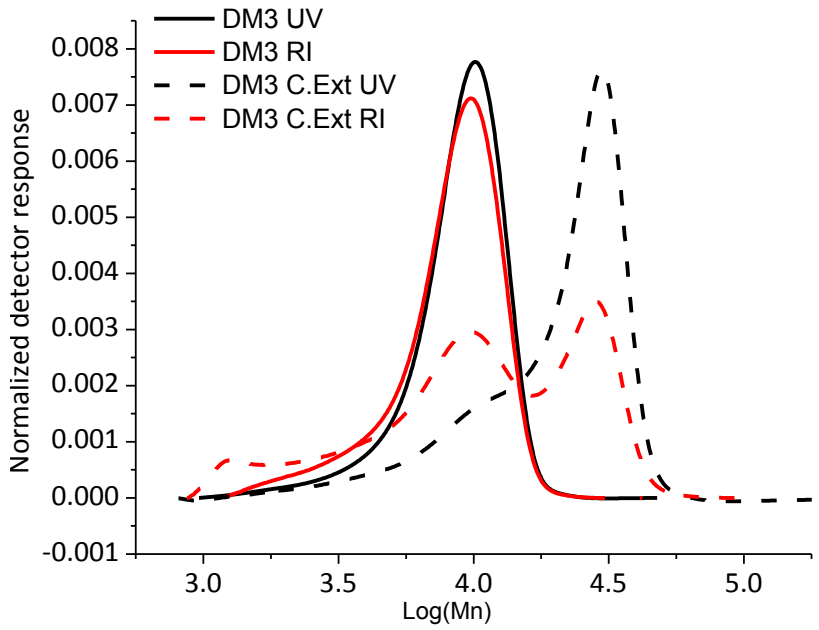

Figure 4.12. GPC-UV-RI traces of DM3 macro-RAFT agent before and after chain-extension. [macro-RAFT]:[ACVA] = 5, in tert-butanol at 70°C after 16h.

4.4 ***Conclusions***

In this work, we report the kinetic analysis in bulk, and for the first time in a relative polar solvent (tert-butanol), of the polymerization of three different dialkylaminoethyl methacrylates via RAFT-mediated polymerization. Tert-butanol minimizes the occurrence of side reactions during polymerization. Good control and high chain-end functionality were obtained for all three monomers in bulk and in solution. GPC analyses showed good agreement in between UV and RI traces confirming a high chain-end functionality for all three monomers. A higher degree of chain-end functionality was obtained at conversions below ~50% with minimum tailing towards low molecular weights. Conversely, at higher monomer conversion, tailing due to the formation of dead polymer chains was more evident. Macro-RAFT agents proved to be living and successfully chain-extended confirming their ability to produce block copolymers, to be further reacted with macromers

or to be grafted onto a substrate surface. However, reinitiation efficiency was not 100%. Additionally, GP-UV-RI traces suggested that the higher the molecular weight of the macro-RAFT agents, the higher the fraction of dead chains formed mainly by a FRP mechanism due to a lower reinitiation efficiency. Finally, GPC-RI-UV was used to determine the molecular weight of the living chain fraction of a macro-RAFT agent, which would be useful as macro-RAFT agents used for post-reactions, grafting reactions or block copolymers synthesis.

References

1.Smith, A. E.; Xu, X.; Abell, T. U.; Kirkland, S. E.; Hensarling, R. M.; McCormick, C. L., Tuning nanostructure morphology and gold nanoparticle "locking" of multi-responsive amphiphilic diblock copolymers. *Macromolecules* **2009,** *42* (8), 2958-2964.

2.Liu, L.; Wu, C. L.; Zhang, J. C.; Zhang, M. M.; Liu, Y. W.; Wang, X. J.; Fu, G. Q., Controlled polymerization of 2-(diethylamino)ethyl methacrylate and its block copolymer with n-isopropylacrylamide by raft polymerization. *J. Polym. Sci., Part A: Polym. Chem.* **2008,** *46* (10), 3294-3305.

3.Sahnoun, M.; Charreyre, M. T.; Veron, L.; Delair, T.; D'Agosto, F., Synthetic and characterization aspects of dimethylaminoethyl methacrylate reversible addition fragmentation chain transfer (RAFT) polymerization. *J. Polym. Sci., Part A: Polym. Chem.* **2005,** *43* (16), 3551-3565.

4.Hu, Y. Q.; Kim, M. S.; Kim, B. S.; Lee, D. S., RAFT synthesis of amphiphilic (a-ran-b)-b-c diblock copolymers with tunable pH-sensitivity. *J. Polym. Sci., Part A: Polym. Chem.* **2008,** *46* (11), 3740-3748.

5.Zhu, L. P.; Powell, S.; Boyes, S. G., Synthesis of tertiary amine-based pH-responsive polymers by raft polymerization. *J. Polym. Sci., Part A: Polym. Chem.* **2015,** *53* (8), 1010-1022.

6.Ting, S. R. S.; Min, E. H.; Lau, B. K. F.; Hutvagner, G., Acetyl-α-d-mannopyranose-based cationic polymer via raft polymerization for lectin and nucleic acid bindings. *J. Appl. Polym. Sci.* **2017,** *134* (24).

7.Zhang, L.; Nguyen, T. L. U.; Bernard, J.; Davis, T. P.; Barner-Kowollik, C.; Stenzel, M. H., Shell-cross-linked micelles containing cationic polymers synthesized via the RAFT

process: Toward a more biocompatible gene delivery system. *Biomacromolecules* **2007,** *8* (9), 2890-2901.

8.Bhattacharyya, B. R.; Nandi, U. S., Determination of chain transfer of alcohols by end group estimation. *Die Makromolekulare Chemie* **1968,** *116* (1), 8-13.

9.Bhattacharyya, S. N.; Maldas, D., Radiation-induced graft copolymerization of mixtures of styrene and acrylamide onto cellulose acetate. I. Effect of solvents. *J. Polym. Sci. Polym. Chem. Ed.* **1982,** *20* (4), 939-950.

10.Xiong, Q. F.; Ni, P. H.; Zhang, F.; Yu, Z. Q., Synthesis and characterization of 2-(dimethylamino)ethyl methacrylate homopolymers via aqueous raft polymerization and their application in miniemulsion polymerization. *Polym. Bull.* **2004,** *53* (1), 1-8.

11.Smith, A. E.; Xu, X.; McCormick, C. L., Stimuli-responsive amphiphilic (co)polymers via raft polymerization. *Prog. Polym. Sci.* **2010,** *35* (1), 45-93.

12.Kockler, K. B.; Fleischhaker, F.; Barner-Kowollik, C., Free radical propagation rate coefficients of n-containing methacrylates: Are we family? *Macromolecules* **2016,** *49* (22), 8572-8580.

13.Barner-Kowollik, C.; Buback, M.; Charleux, B.; Coote, M. L.; Drache, M.; Fukuda, T.; Goto, A.; Klumperman, B.; Lowe, A. B.; Mcleary, J. B.; Moad, G.; Monteiro, M. J.; Sanderson, R. D.; Tonge, M. P.; Vana, P., Mechanism and kinetics of dithiobenzoate-mediated RAFT polymerization. I. The current situation. *J. Polym. Sci., Part A: Polym. Chem.* **2006,** *44* (20), 5809-5831.

14.Buback, M.; Vana, P., Mechanism of dithiobenzoate-mediated RAFT polymerization: A missing reaction step. *Macromol. Rapid Commun.* **2006,** *27* (16), 1299-1305.

15.Braunecker, W. A.; Matyjaszewski, K., Controlled/living radical polymerization: Features, developments, and perspectives. *Prog. Polym. Sci.* **2007,** *32* (1), 93-146.

16.Favier, A.; Charreyre, M.-T., Experimental requirements for an efficient control of free-radical polymerizations via the reversible addition-fragmentation chain transfer (RAFT) process. *Macromol. Rapid Commun.* **2006,** *27* (9), 653-692.

17.Zhao, W.; Gody, G.; Dong, S.; Zetterlund, P. B.; Perrier, S., Optimization of the raft polymerization conditions for the in situ formation of nano-objects via dispersion polymerization in alcoholic medium. *Polymer Chemistry* **2014,** *5* (24), 6990-7003.

Chapter 5. Surface Modification of Cellulose Nanocrystals via SI-Cu(0)-ATRP and CO_2-Responsiveness. Grafting-from approach

The work presented in this chapter was published in *Green Chem.* 2017, 19, 4141.

5.1 ***Introduction***

In the last decade, there has been increasing interest in modifying or functionalizing CNC using polymer-grafting approaches, in particular via reversible deactivation radical polymerization (RDRP). Conventional atom transfer radical polymerization (ATRP)[1-7] is the most commonly used RDRP technique, with only a few reports on CNC graft-modification using nitroxide mediated polymerization (NMP)[8-9] or reversible addition fragmentation chain transfer (RAFT) polymerization.[10-11] The main disadvantage with conventional ATRP is the large amount of copper catalyst required (≥1000 ppm) to achieve good control, fast polymerization rates and high chain-end functionality.[12] Variants of the ATRP approach such as activators regenerated by electron transfer (ARGET) and initiators for continuous activator regeneration (ICAR) ATRP have been extensively studied, allowing the polymerization of a variety of monomers using less than 100 ppm Cu(II) by employing reducing agents.[13-14] However, most commercial products require much lower residual copper levels (<~10 ppm) for health and safety reasons. Therefore, post-polymerization removal of the copper is usually required, an undesirable and expensive step that reduces the potential economic viability of using ATRP on a commercial scale. There is another ATRP variant which uses zero valent metals such as Cu(0) as a reducing agent,[15] commonly known as either Supplemental Activator and Reducing Agent ATRP (SARA-ATRP)[16-21] or Single Electron Transfer ATRP (SET-

ATRP).[22-26] This variant also requires very low amounts of metal catalyst during the polymerization, for example a small piece of copper wire that can be easily removed from the reaction media. A typical polymer made using Cu(0) may have less than 10 ppm residual copper. Furthermore, polar protic and aprotic solvents can be used, achieving good molecular weight control and high chain-end functionality.[19-20,23-25] While there have been a limited number of reports related to the grafting of common polymers such as polystyrene,[1,27] N-isopropylacrylamide[3,28] and some natural biopolymers[7,29] on CNC using ATRP, the potential versatility and value of modified CNC could be further enhanced if the polymers used for the grafting step were CO_2 stimuli-responsive.

Our group has previously reported the use of CO_2-switchable systems such as CO_2-responsive solvents[30-33] for chemical manufacturing and separation processes, CO_2-switchable surfactants,[34-37] and CO_2-switchable polymer nanoparticle latexes.[38-42] In addition to these applications, CO_2-switchable polymers have demonstrated potential for a broad range of applications such as forward osmosis for water desalination, the fabrication of hydrogels for potential enhanced oil recovery purposes, or the generation of CO_2-responsive vesicles that could be used for controlled drug delivery among others.[43] Monomers with tertiary amine groups such as dimethylaminoethyl methacrylate (DMAEMA, pK_{aH}: 8.3; PDMAEMA, pK_{aH}:7.4)[44] and diethylaminoethyl methacrylate (DEAEMA pK_{aH}: 8.8; PDEAEMA pK_{aH}: 7.5)[44] are CO_2-responsive and can be employed to prepare CO_2-responsive polymers that can then be used to produce redispersible colloidal systems (Scheme 5.1).[38,45-48] These two monomers may appear to be similar but, in fact, the polymers behave quite differently. PDEAEMA is significantly more hydrophobic than PDMAEMA and has a T_g of -20°C,[49] whereas PDMAEMA has a T_g of

26°C.[49] In addition to the CO_2-responsiveness, it has also been reported that PDEAEMA and PDMAEMA have different pH-dependent lower critical solution temperatures (LCST)[50] (80°C and 40°C, respectively at pH=7) making these polymers multi-responsive materials, which may enhance their potential applications as dual-responsive materials.

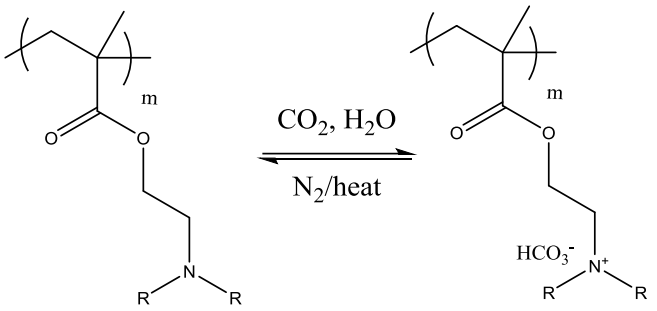

Scheme 5.1 CO_2-responsive poly(dialkylaminoethyl methacrylate).

Our objectives in undertaking this study were to develop a greener approach in making high performance, stimuli-responsive nanomaterials for composite applications via polymer grafting-modification using a form of RDRP that requires very low metal catalyst loadings and does not require post-reaction treatment for catalyst recovery. In addition, the stimulus required to trigger property changes is a benign alternative to liquid acids and bases. CNC was selected as the solid substrate due to its renewability and promise as a new nanomaterial with unique properties, specifically addressing the inherent challenges with respect to the poor compatibility of CNC with most polymers. Therefore, a different approach for grafting CO_2-responsive polymers onto CNC was explored with the intent of enhancing CNC compatibility with a broader range of solvents and polymer matrices.

In this chapter, the surface modification of CNC with PDMAEMA and PDEAEMA applying a *grafting-from* approach via surface-initiated copper(0)-mediated polymerization (SI-Cu(0)-ATRP) is reported (Scheme 5.2). First, the CNC surfaces were

modified with α-bromo isobutyric acid (BIBA) to yield a bromine-functionalized CNC (CNC-Br) as macroinitiator. Subsequently, a *grafting-from* approach was employed to graft DMAEMA and DEAEMA from the CNC surface using the experimental conditions that were outlined in Chapter 3. The grafting of the CNC was confirmed by CP-MAS ^{13}C NMR, FT-IR, TGA and elemental analysis, while the CO_2-responsiveness of the materials was demonstrated via ζ-potential measurements. The grafted CNC CO_2-responsiveness was also assessed over multiple cycles.

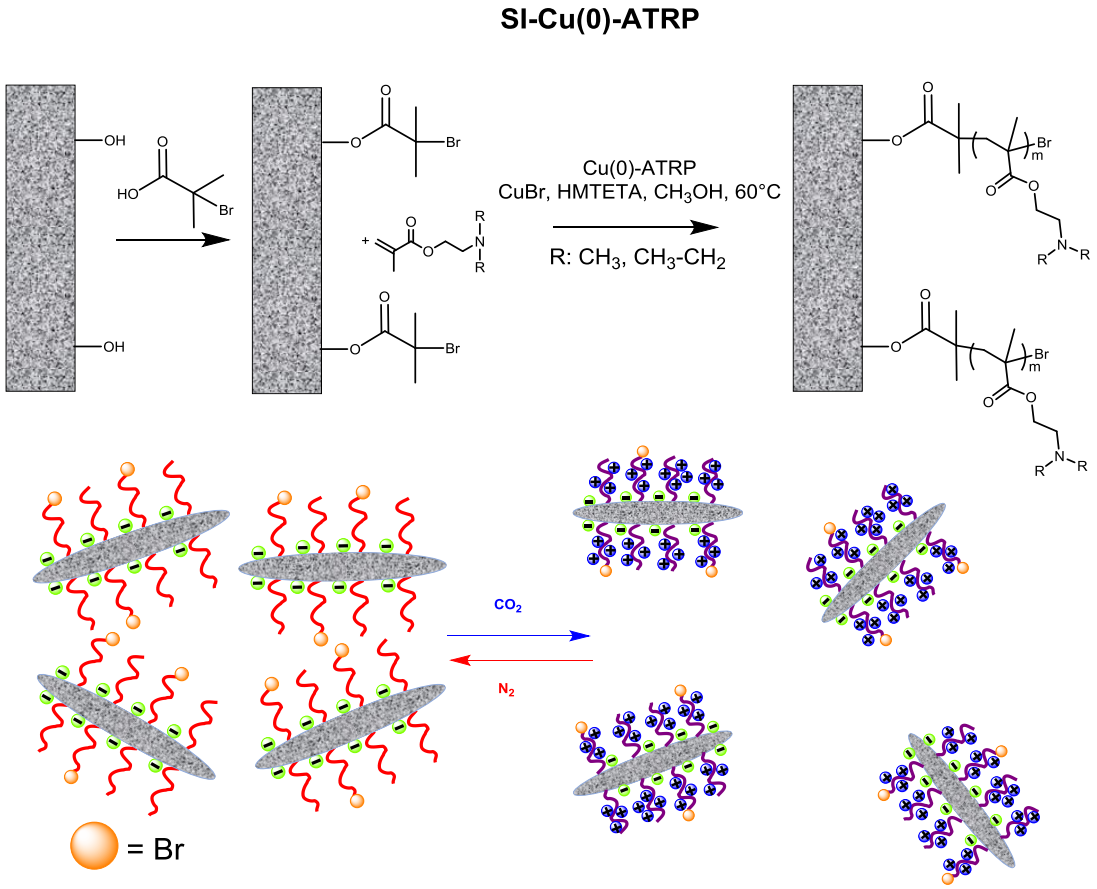

Scheme 5.2 Grafting-from approach for modifying CNC with CO_2-switchable polymers.

5.2 ***Experimental***

5.2.1 *CNC surface functionalization with α-bromo isobutyric acid*

CNC functionalization was performed following a similar procedure previously reported by our group.[51] Briefly, 18 g (111 mmol) of carbonyl diimidazole (CDI) was added to a 250 mL three-necked round-bottomed flask with an addition funnel attached. Next, 15 mL of freshly distilled anhydrous dichloromethane (DCM) was added via cannula. BIBA (111 mmol) was dissolved in freshly distilled anhydrous DCM in a septum-sealed vial and the solution was transferred to the addition funnel via cannula. The solution was added dropwise with constant stirring under nitrogen atmosphere at room temperature. The reaction was maintained under inert atmosphere and was stopped after 4 h when CO_2 was no longer released as a by-product (pot 1). Following the initial reaction between the CDI and BIBA, 2.2 g (37 mmol OHs) of CNC were dispersed in 20 mL of freshly distilled anhydrous dimethyl sulfoxide (DMSO) and vortexed in a 50 mL centrifuge tube until the CNC were completely dispersed. Freshly distilled anhydrous DCM (30 mL) was added to the CNC dispersion, then vortexed, centrifuged (6,000*g* force) and decanted. The CNC cake was redispersed in 30 mL of DCM and then transferred with a cannula to a three-necked round-bottom flask equipped with an addition funnel and a condenser (pot 2). Next, the reaction solution from the first step (pot 1) was transferred via cannula to the addition funnel coupled to the three-necked round bottom flask containing the dispersed CNC in DCM (pot 2) and added dropwise under constant stirring and nitrogen atmosphere at room temperature. Then, the reaction was stirred for three days followed by a solvent exchange with acetone. The final CNC cake was placed into a frit glass thimble inside a Soxhlet apparatus and left under constant acetone reflux for five days to remove any excess

reactants and side products. After completion of the Soxhlet extraction, the product was stored in ethanol at 4°C and a portion of the sample was freeze-dried for characterization.

5.2.2 *Grafting-from approach by SI-Cu(0)-ATRP*

Approximately 0.4 g CNC-Br (0.3 mmol Br, determined by XPS) was added into a 100 mL round-bottom flask with 25 mL of MeOH and sonicated until CNC aggregates were no longer visible in the suspension. Afterwards, the suspension was transferred into a 250 mL round-bottom Schlenk flask equipped with a stir bar and an additional 25 mL of MeOH was added. Then, under argon atmosphere, 0.5 mg ($2.0x10^{-3}$ mmol) of $CuBr_2$, 0.5 mg (0.22 mmol) HMTETA and 12.72 mmol of monomer (DMAEMA, DEAEMA), 300 µL of DMF and three 1 cm length copper wires (14 gauge) were added. Copper wires were pre-treated with 35% HCl and rinsed with methanol. Finally, the Schlenk flask was degassed by three freeze-pump-thaw cycles, sealed under vacuum and put in an oil bath at 60°C for 24 h. After a specified reaction time, the methanolic solution was removed via cannula under argon atmosphere to prevent Cu^+ from oxidizing and staining the final product. More degassed methanol was added to wash the product, and subsequently removed via cannula. Next, the product was exhaustively washed with THF to remove any free monomer/polymer and then centrifuged. Finally, the product was stored in ethanol and a small portion was freeze-dried for further analyses.

5.2.3 *Procedure to test pH-responsiveness of CNC-grafted materials using HCl/NaOH as triggers*

A dispersion of ca. 0.4 wt.% of polymer-grafted CNC was prepared in 10 mL of deionized water in a 25 mL sample tube. Using a Malvern multipurpose auto-titrator (MPT-2), the dispersion was titrated starting from a pH of 4±0.3 to a final pH of 10±0.3. A disposable folded capillary cell was connected to the auto-titrator, and the ζ-potential and conductivity were measured automatically at each data point.

5.2.4 *Procedure to test the CO_2-responsiveness of the grafted CNC*

Polymer-grafted CNC dispersions (ca. 0.4 wt.%) were prepared in 25 mL of deionized water containing ca. 0.13 mmol and 0.10 mmol of amine groups of DMAEMA (sample CNC-g-DMAEMA B2) and DEAEMA (sample CNC-g-DEAEMA B2), respectively. A three-necked round-bottom flask was adapted with a pH meter, a gas dispersion tube with a porous fritted glass tip, and a stir bar. Each gas was sparged through the mixture until pH readings were stable for more than 10 minutes (~20 min for CO_2; ~1 h for N_2). The round-bottom flask was submerged in an oil bath at 25°C to maintain constant temperature.

5.3 ***Results and discussion***

5.3.1 *CNC bromine functionalization*

CNC were treated with BIBA and CDI to convert the CNC into cellulose-based macroinitatiors (Scheme 5.3). In Figure 5.1, the FT-IR spectrum of CNC-Br is shown where the appearance of the carbonyl stretching signal can be clearly observed at 1,700 cm^{-1}. CP-MAS ^{13}C NMR spectroscopy (Figure 5.2) also shows the carbonyl signal at 180 ppm corroborating the successful surface functionalization of CNC. CP-MAS ^{13}C NMR was employed to determine whether the crystallinity of CNC had been affected by the modification process by monitoring the crystalline and amorphous peaks (labelled as C4 and C4'). As reported elsewhere by our group, this particular surface modification has been noted not to affect CNC crystallinity.[51]

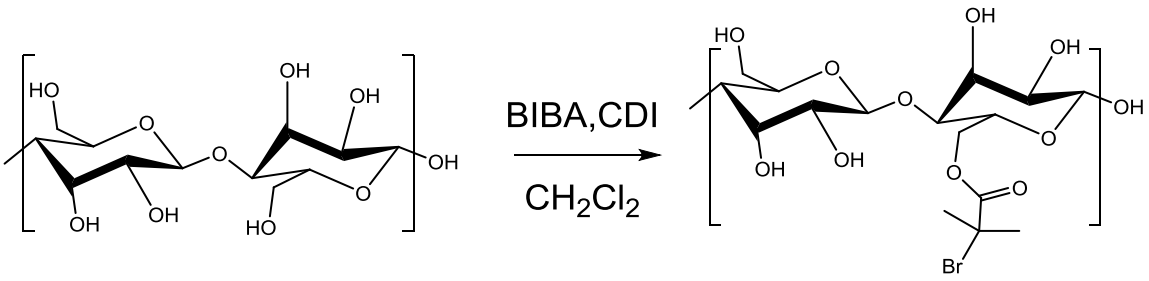

Scheme 5.3. CNC functionalization reaction with BIBA and CDI at room temperature. BIBA= 111 mmol, CDI= 111.5 mmol, OH= 37 mmol.

To further confirm the formation of bromine surface-modified CNC and that no traces of the bromine precursor remained, TGA analyses were performed. Figure 5.3 shows that no residual BIBA was left in any of the modified CNC samples, as BIBA starts decomposing at 45°C, CNC-Br decomposes at 200°C, while native CNC decompose at 300°C. The decrease in the thermal sample stability of CNC-Br compared to the native CNC was expected as the tertiary bromine of the BIBA is a thermally labile group. In addition, it can be noted that grafted CNC products exhibited a different thermal profile compared to both the native and functionalized CNC.

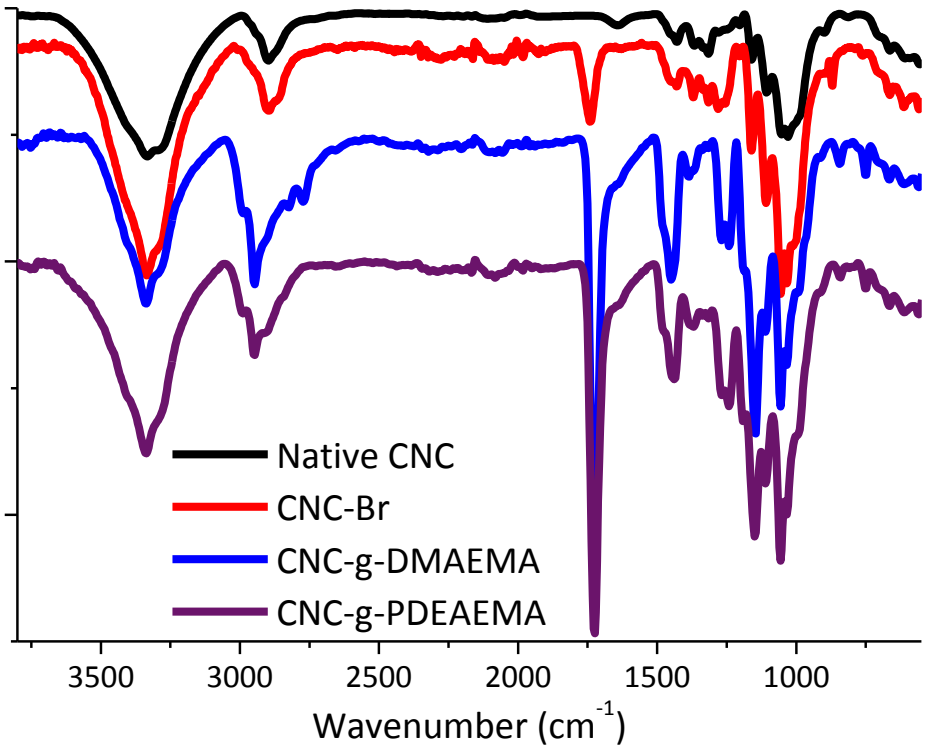

Figure 5.1. FT-IR of native CNC, CNC-Br and polymer-grafted CNC.

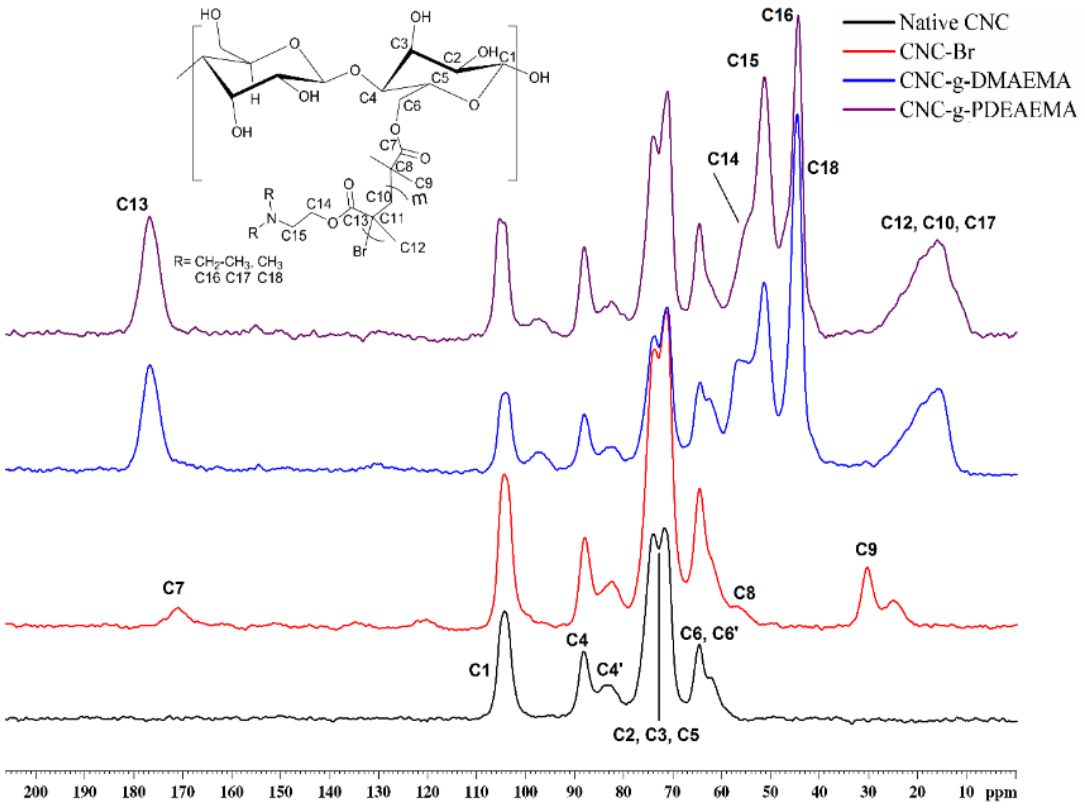

Figure 5.2. Solid-state CP-MAS ^{13}C NMR spectra of native CNC and surface-modified CNC with BIBA, PDMAEMA and PDEAEMA.

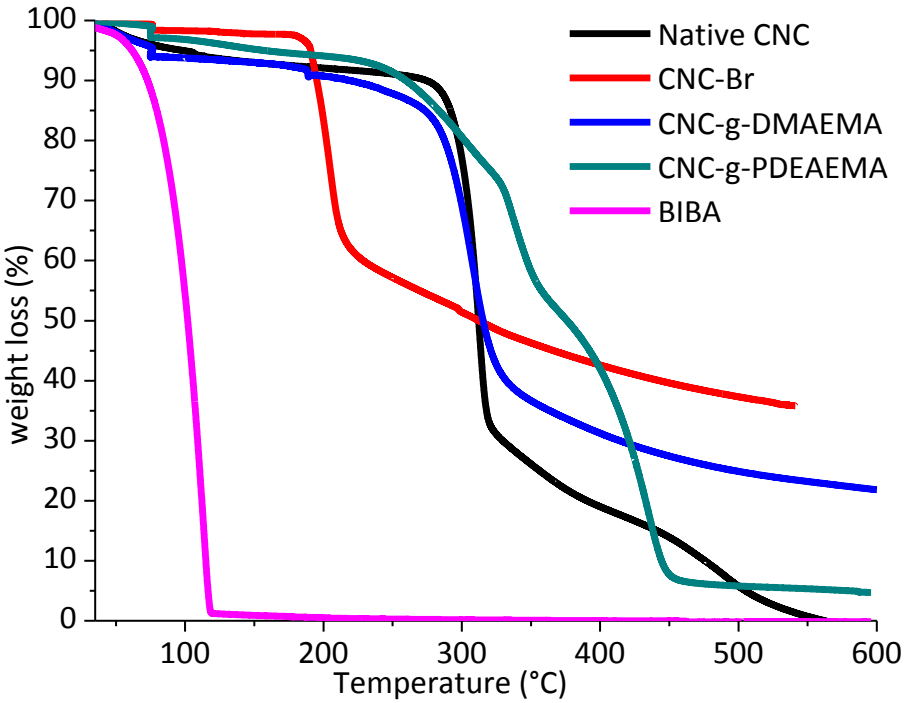

Figure 5.3. Thermogravimetric analysis of native CNC, CNC-Br and polymer-grafted CNC.

Table 5.1. Atomic and mass composition of bromine-functionalized CNC by XPS analysis.

CNC-Br	C	O	Br
Batch 1			
Atomic	55.85±0.34	43.15±0.27	1.10±0.07
Mass	46.27±0.28	47.66±0.22	6.07±0.06
Batch 2			
Atomic	55.55±0.77	42.90±0.57	1.54±0.21
Mass	45.16±0.63	46.50±0.46	8.34±0.17
Batch 3			
Atomic	53.21±0.09	45.71±0.90	1.09±0.19
Mass	43.80±0.75	50.20±0.74	6.00±0.15

Error represents the standard deviation of measurements ran in triplicate at different locations on the sample

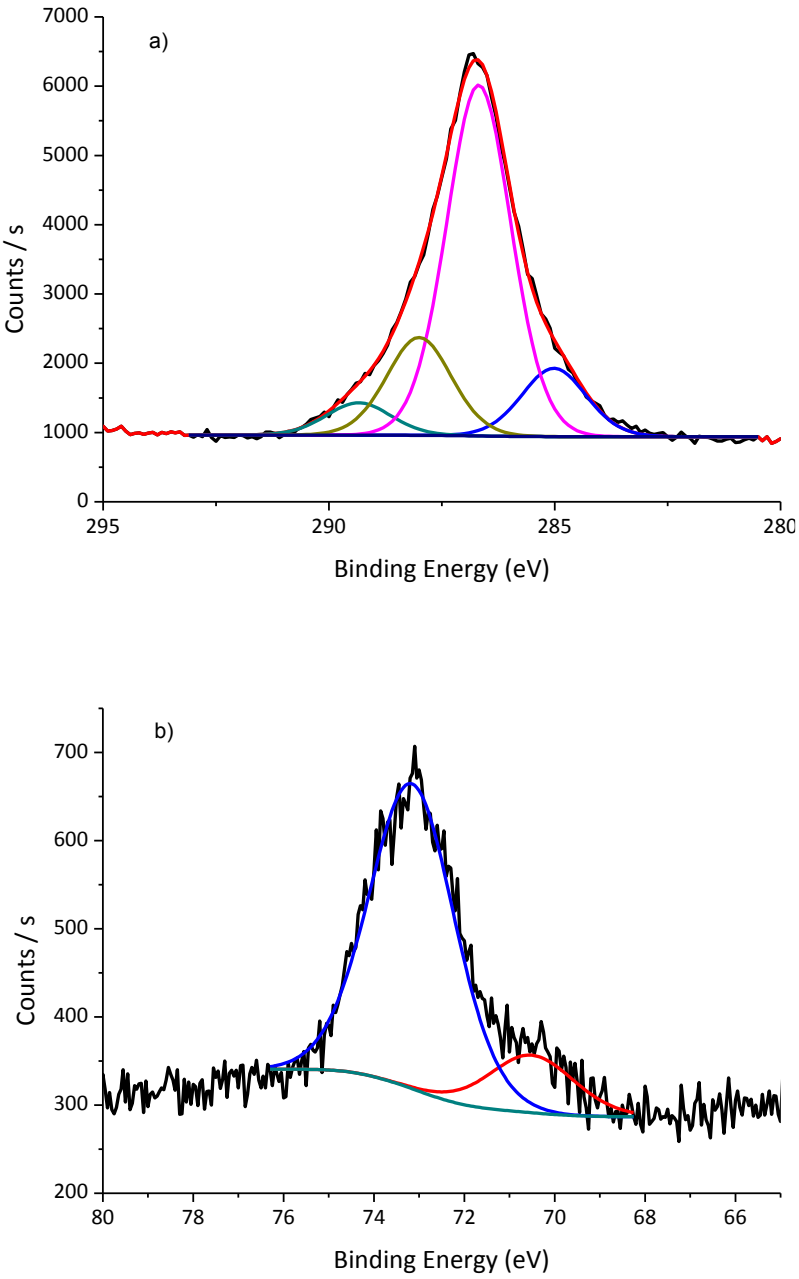

Figure 5.4. High-resolution XPS spectra. a) carbon. b) bromine.

XPS analysis was performed to confirm the presence of bromine atoms on the CNC surfaces. The high-resolution spectrum of carbon C1s (Figure 5.4) shows the different types of carbon bonds. At 298 eV, the C=O signal can be readily identified suggesting a successful esterification of BIBA on the CNC surfaces. Additionally, in the high-resolution

spectrum of Br3d (Figure 5.4), the typical signal for covalent bromine C-Br can be observed at 73 eV. Different batches of CNC-Br were synthesized with good bromine content reproducibility, as determined by XPS. Table 5.1 summarizes the atomic and elemental mass composition of three different batches of bromine-functionalized CNC.

5.3.2 *Grafting-from via SI-Cu(0)-ATRP*

The CNC-Br was used as a macroinitiator to polymerize DMAEMA and DEAEMA from the CNC surface using the conditions previously determined for the homopolymerization of the monomers via SI-Cu(0)-ATRP (Scheme 5.4). The resulting dispersions were colorless (Figure 5.5) suggesting a low concentration of copper (II) in solution. After the purification of the grafted CNC by vortexing and centrifugation to remove unreacted monomer and dissolved copper, samples were further analyzed by FT-IR, solid-state CP-MAS ^{13}C NMR, TGA, elemental analysis and AFM.

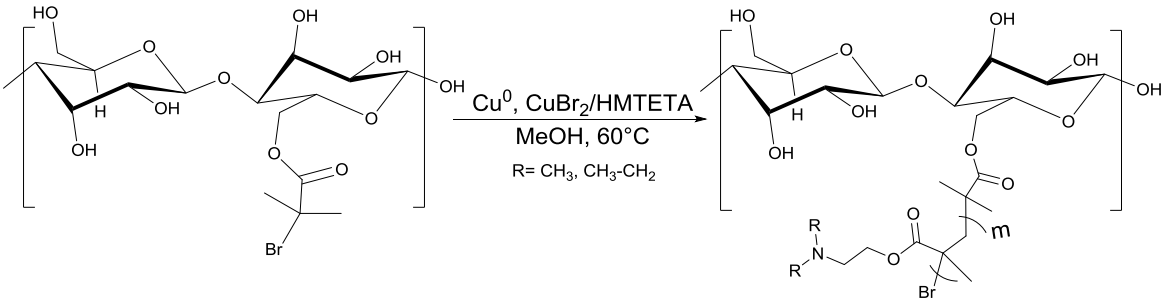

Scheme 5.4. Grafting-from approach via SI-Cu(0)-ATRP. DMAEMA:$[CuBr_2]$:[L]:$[I]_0$:$[M]_0$=1:100:91:5782. DEAEMA:$[CuBr_2]$:[L]:$[I]_0$:$[M]_0$= 1:100:107:5782.

The grafting of PDMAEMA and PDEAEMA was confirmed spectroscopically as shown in Figure 5.1 where an intense carbonyl signal of the polymer backbone at 1,700

cm^{-1} by FT-IR spectroscopy and the peak at 178 ppm in the ^{13}C NMR spectrum (Figure 5.2) can be identified, along with the complementary polymer backbone signals. After an exhaustive washing procedure to ensure that the final products were not a physical mixture of CNC, CNC-Br and grafted CNC, TGA analysis was performed of the three different materials as shown in Figure 5.3. The weight loss traces of the grafted CNC with both polymers show that CNC-Br and free BIBA were not detectable, which confirms that the new product was successfully grafted.

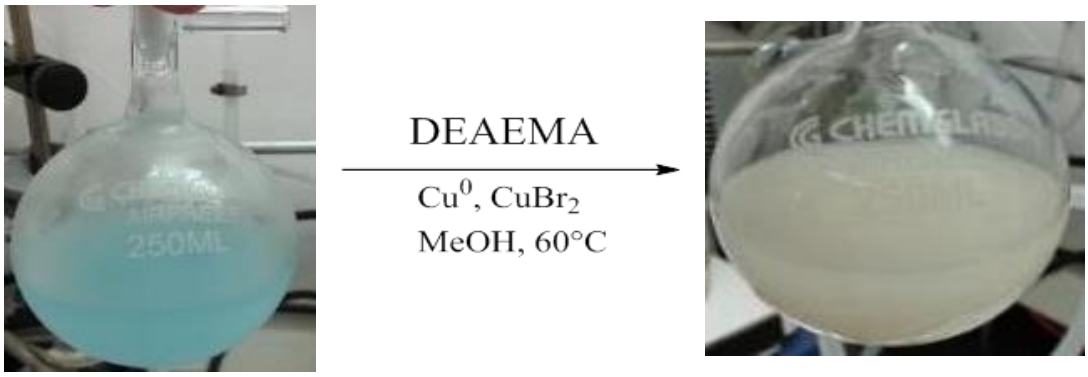

Figure 5.5. Grafting-from of PDEAEMA onto CNC-Br via SI-Cu(0)-ATRP

All CNC products were analyzed by elemental analysis for CHN content. The results are summarized in Table 5.2. The nitrogen results confirm the presence of PDMAEMA and PDEAEMA-grafted on the CNC. The weight percent of grafted polymer relative to the total mass of modified CNC was calculated from the nitrogen content as reported elsewhere[52] and the amount of PMMA was calculated from the excess of carbon content compared to the expected amount of carbon for a 100% polyamine graft. From Table 5.2, it can be seen that CNC-g-DEAEMA contained more PMMA as DEAEMA transesterifies faster than DMAEMA. It can also be noted that PDMAEMA- and PDEAEMA-grafted CNC showed similar contents of polyamine obtained for a particular CNC-Br batch

suggesting good reproducibility. AFM microscopy (Figure 5.6) revealed that the CNC rod -like shape and the crystallinity of the final material was preserved as was also demonstrated by the solid-state ^{13}C NMR spectrum. Differences in size of the crystals shown in the AFM images could be due to aggregation either during the grafting procedure or during sample preparation for analysis.

Table 5.2. Elemental Analysis of CNC-grafted products.

	C%	%H	%N	%O[a]	N mmol/ g of CNC	wt.% of polyamine/ g of CNC[b]	wt.% of PMMA/ g of CNC[c]
CNC-g-DEAEMA B1	54.1±0.1	7.9±0.04	1.7±0.1	36.2	1.6±0.1	20.2	13.8
CNC-g-DEAEMA B2	52.9±0.1	7.5±0.03	1.2±0.01	38.3	1.1±0.1	14.3	14.1
CNC-g-DMAEMA B1	53.7±0.1	7.7±0.1	2.4±0.02	36.1	2.3±0.02	26.8	12.2
CNC-g-DMAEMA B2	46.7±0.2	7.7±0.1	1.6±0.03	44	1.5±0.03	18.6	3.3
Native CNC	40.8±0.1	6.2±0.02	0.0±0.1	53.1	---	---	---

[a] The remaining wt.% was assumed to be oxygen
[b] Calculated based on nitrogen content as reported by Hemraz *et al.*[5]
[c] Calculated from the excess of carbon wt.% as compared to the expected mass of carbon obtained from the amount of 100% polyamine graft. (See Appendix E.)

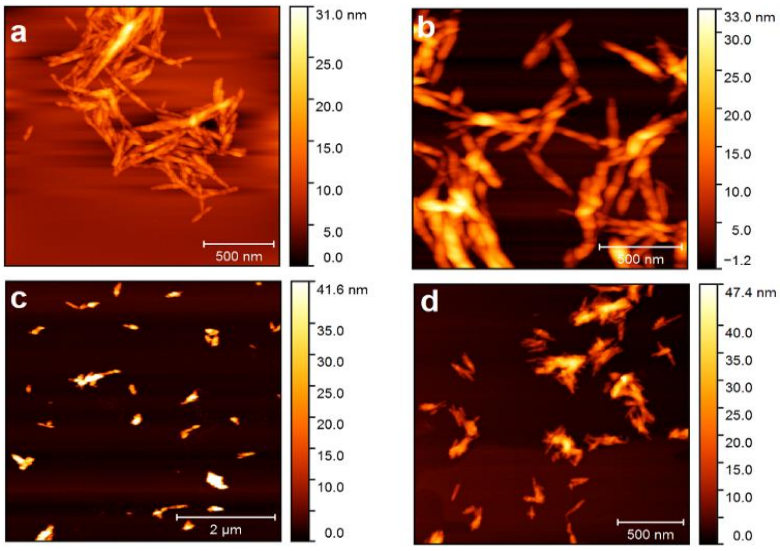

Figure 5.6. AFM micrographs of (a) native CNC, (b) CNC-Br, (c) CNC-g-PDEAEMA, (e) CNC-g-PDMAEMA.

5.3.3 *CO_2-responsiveness*

PDMAEMA and PDEAEMA are high interest polymers for switching systems as they have pK_{aH} of 7.4 and 7.5, respectively,[50] making them good candidates for CO_2-switching.[48] Switchability of the grafted CNC was analyzed via ζ-potential measurements. The ζ-potential values reported in this paper are not intended to represent an actual potential on the CNC surface as this analysis assumes spherical particles. However, trends in ζ-potential measurements do provide valuable information regarding the effect of varying solution conditions on the CNC surface charge. As mentioned before, the advantage of CO_2-switchable over conventional acids and bases is the low salt accumulation. To illustrate this feature, CNC-g-PDMAEMA was subjected to conventional acid-base switching cycles. Figure 5.7 shows several switching cycles of CNC-g-PDMAEMA triggered by HCl and NaOH 1.0 M. A pH range of 4-10 was chosen to simulate a CO_2/N_2 system at ambient pressure. By using a strong acid and base, it is possible to obtain good control on the pH values within cycles, while interference due to mass transfer or CO_2/N_2 diffusion effects would be negligible. Figure 5.7 illustrates how ζ-potential responded to changes in pH where the maximum positive value decreased as the grafted CNC was subjected to an increasing number of switching cycles. This decrease in the maximum ζ-potential throughout the switching cycles was likely due to salt accumulation, as also evidenced by the conductivity values, which exhibited a positive trend increasing approximately 3 mS/cm per cycle.

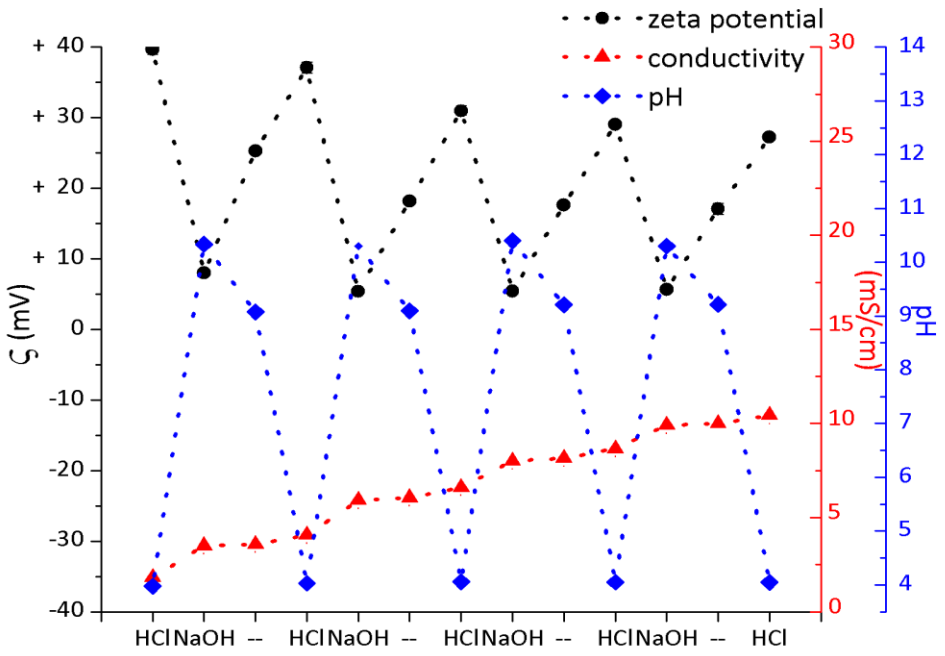

Figure 5.7. HCl/NaOH cycles of CNC-g-PDMAEMA B1 ranging from pH 4-10.

Colloidal destabilization is known to occur with increasing salt concentration as evident in Figure 5.7, in which after four switching cycles, the maximum ζ-potential had decreased by almost 10 units. This decrease in the maximum ζ-potential value can be avoided if CO_2 and N_2 are used instead of acid and base for the switching of the surface properties. Figure 5.8 shows a preliminary experiment where two cycles of CO_2/N_2 were performed using sample CNC-g-PDMAEMA B1. After dispersing the grafted CNC in water, it was observed that the pH became slightly basic and ζ-potential was +15 mV. This positive ζ-potential was attributed to the protonation of the amine groups after dispersing the material in water as the polymer is slightly basic (pK_{aH}: 7.5[44]) giving an initial pH value of 8.4. Figure 5.8 illustrates that even with N_2 sparging for over 2 hours, little decrease in ζ-potential was observed with a final pH value of 8.4. We then realized that CNC-g-PDMAEMA and CNC-g-PDEAEMA could not be fully deprotonated solely by sparging

N_2 into a dispersion of CNC added to neutral water. Because the pK_{aH} values of both polymers were similar to the maximum pH value that could be achieved by N_2 sparging in water (pH~8), the amine groups on the polymeric backbone would only be ~50% protonated. Complete deprotonation requires the solution pH to be >~2 pH units above the pK_{aH}. Therefore, negative or near zero ζ-potential values cannot be achieved with CO_2/N_2 cycles when grafted CNC are added to neutral water. In contrast, the HCl/NaOH system (Figure 5.7) reached pH values of ~10 with the addition of NaOH, sufficiently higher than the pK_{aH} allowing for a (near) complete deprotonation, which resulted in a significant decrease in the ζ-potential.

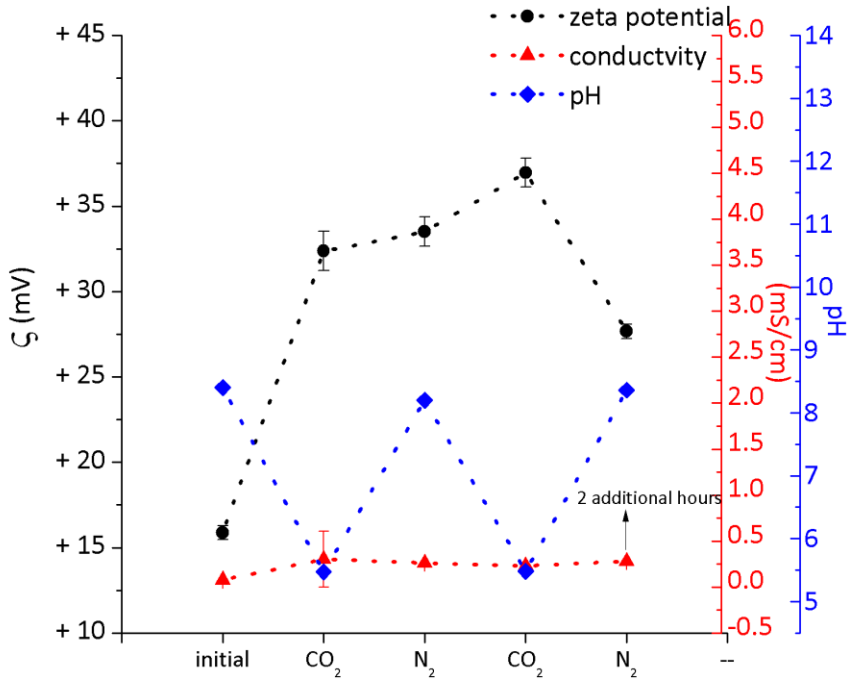

Figure 5.8. CO_2/N_2 sparging cycles of CNC-g-DMAEMA B1 with no added base at initial conditions.

In order to overcome this issue, an adjustment to the initial pH to a higher value such that the range of pH attained with alternating CO_2/N_2 cycling would yield effective protonation and deprotonation of the polymer grafts was required. The initial pH was

therefore adjusted to 12 through the addition of 100 µL 1M NaOH to the CNC-g-PDMAEMA B2 and CNC-g-PDEAEMA B2 dispersions. Figure 5.9 and Figure 5.10 illustrate the variations in ζ-potential values of the CNC-g-PDMAEMA B2 and CNC-g-PDEAEMA B2 dispersions as a function of pH triggered by CO_2/N_2 sparging cycles. In both cases, the grafted CNC clearly exhibited reversible CO_2-responsive behaviour obtaining ζ-potential values around +30 mV. In the particular case of CNC-g-PDMAEMA B2 (Figure 5.9), the ζ-potential values obtained under N_2 were not lower than +10 mV, suggesting that the PDMAEMA grafts are still slightly protonated.

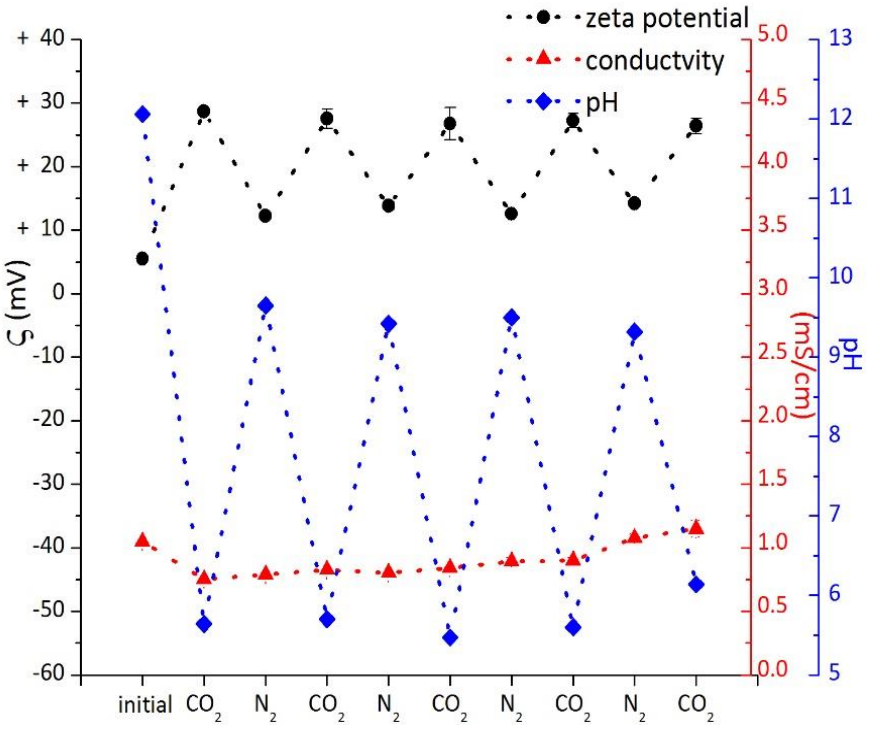

Figure 5.9. CO_2/N_2 sparging cycles of CNC-g-DMAEMA B2 with initial pH adjusted to 12 with 100 µL of 1M NaOH.

For the case of CNC-g-PDEAEMA B2 in the presence of CO_2 (Figure 5.10), ζ-potential values were +27-31 mV, while sparging with N_2 reduced the ζ-potential values to ~+5 mV exhibiting reversible aggregation/dispersion capabilities (Figure 5.11). In the last N_2

sparging cycle, N_2 gas was bubbled for three additional hours compared to previous cycles. It is worth noting that after three hours of N_2 sparging, the ζ-potential value decreased to -12 mV. This behaviour was likely due to the fact that protonation of the amine groups is an exothermic reaction; hence, the system could require longer N_2 sparging times or heat to fully deprotonate the polymer grafts. If a high degree of deprotonation is desired, dispersions could be heated in between 60-80°C to assist in the removal of remaining dissolved CO_2. Consequently, a high degree of deprotonation leads to a negative ζ-potential due to the presence of half-ester sulfate groups on the CNC surface arising from the acid-hydrolysis process used in the CNC manufacturing process. Because native CNC has a ζ-potential of about -40 mV, fully deprotonating the polymer grafts on the CNC surface would have resulted in a negative surface charge on the grafted CNC.

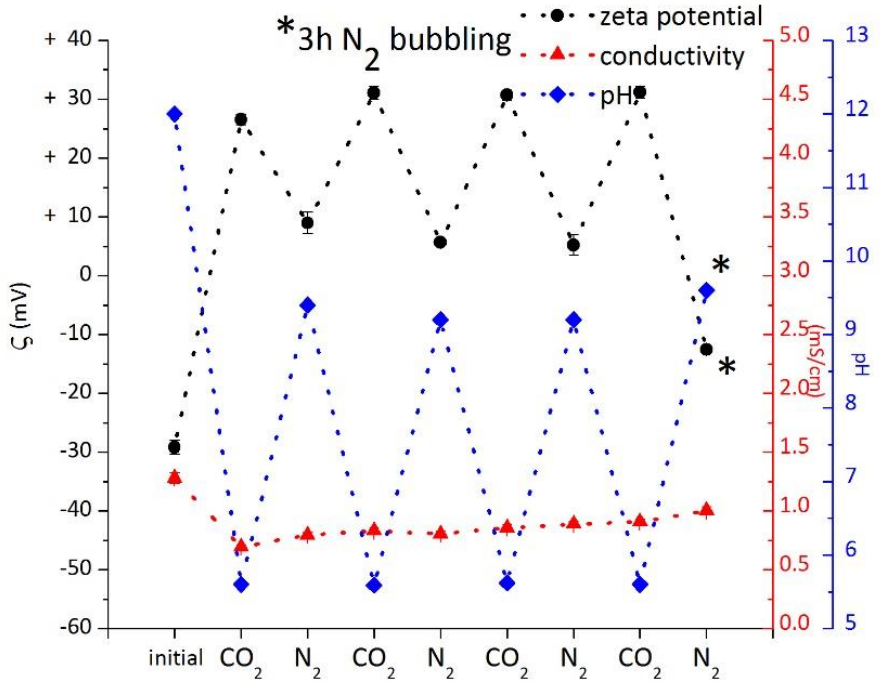

Figure 5.10. CO_2/N_2 sparging cycles of CNC-g-PDEAEMA B2 with initial pH adjusted at 12 with 100 µL of NaOH 1M.

The observed variation in the ζ-potential reflects a change in the surface properties that could have important implications. The protonated CNC are highly hydrophilic, and will disperse well in aqueous systems. However, when the polymer is deprotonated, the CNC surface will become quite hydrophobic in the case of PDEAEMA, making it more compatible with hydrophobic polymers. Varying the polymer type and/or the extent of protonation would provide fully tunable CNC whose surface properties could be tailored for specific applications.

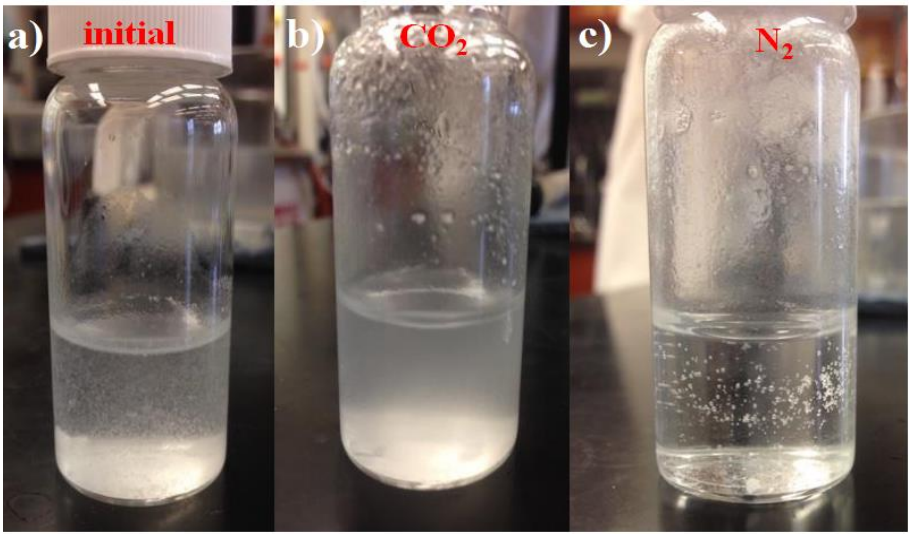

Figure 5.11. CO_2-switchability of CNC-g-PDEAEMA B2 at ca. 0.4 wt.% under a full switching cycle. a) CNC-g-PDEAEMA dispersion in its original state. b) Dispersed CNC-g-PDEAEMA after CO_2 sparging. c) CNC-g-PDEAEMA after N_2 sparging.

5.4 ***Conclusions***

Renewably-sourced CO_2-responsive cellulose nanocrystals were prepared using a polymer graft-modification process that requires only low copper concentrations, and benign triggers for the switching process. DMAEMA and DEAEMA were then grafted from bromine-functionalized CNC via SI-Cu(0)-ATRP to yield CO_2-responsive CNC. Solid-state CP-MAS ^{13}C NMR spectroscopy and elemental analysis confirmed the presence of amino groups grafted on the CNC surfaces. CNC-g-PDMAEMA and CNC-g-PDEAEMA were subjected to CO_2/N_2 sparging cycles where both products showed near fully reversible CO_2-responsiveness over four switching cycles with no signs of destabilization or the increase in conductivity resulting from salt accumulation associated with the HCl/NaOH system. The ability to make the CNC surface tunable using benign triggers, varying from hydrophilic when the grafted polymer is protonated to hydrophobic when the polymer is deprotonated, addresses the critical challenge of effectively dispersing CNC into a range of polymers with varying hydrophobicity.

References

1.Yin, Y.; Tian, X.; Jiang, X.; Wang, H.; Gao, W., Modification of cellulose nanocrystal via SI-ATRP of styrene and the mechanism of its reinforcement of polymethylmethacrylate. *Carbohydr. Polym.* **2016,** *142,* 206-212.

2.Morandi, G.; Thielemans, W., Synthesis of cellulose nanocrystals bearing photocleavable grafts by ATRP. *Polymer Chemistry* **2012,** *3* (6), 1402-1407.

3.Zoppe, J. O.; Habibi, Y.; Rojas, O. J.; Venditti, R. A.; Johansson, L.-S.; Efimenko, K.; Österberg, M.; Laine, J., Poly(n-isopropylacrylamide) brushes grafted from cellulose nanocrystals via surface-initiated single-electron transfer living radical polymerization. *Biomacromolecules* **2010,** *11* (10), 2683-2691.

4.Boujemaoui, A.; Mongkhontreerat, S.; Malmstrom, E.; Carlmark, A., Preparation and characterization of functionalized cellulose nanocrystals. *Carbohydr. Polym.* **2015,** *115*, 457-64.

5.Majoinen, J.; Walther, A.; McKee, J. R.; Kontturi, E.; Aseyev, V.; Malho, J. M.; Ruokolainen, J.; Ikkala, O., Polyelectrolyte brushes grafted from cellulose nanocrystals using Cu-mediated surface-initiated controlled radical polymerization. *Biomacromolecules* **2011,** *12* (8), 2997-3006.

6.Tizzotti, M.; Charlot, A.; Fleury, E.; Stenzel, M.; Bernard, J., Modification of polysaccharides through controlled/living radical polymerization grafting—towards the generation of high performance hybrids. *Macromol. Rapid Commun.* **2010,** *31* (20), 1751-1772.

7.Yu, J.; Liu, Y.; Liu, X.; Wang, C.; Wang, J.; Chu, F.; Tang, C., Integration of renewable cellulose and rosin towards sustainable copolymers by "grafting from" atrp. *Green Chemistry* **2014,** *16* (4), 1854-1864.

8.Roeder, R. D.; Garcia-Valdez, O.; Whitney, R. A.; Champagne, P.; Cunningham, M. F., Graft modification of cellulose nanocrystals via nitroxide-mediated polymerisation. *Polymer Chemistry* **2016,** *7* (41), 6383-6390.

9.Garcia-Valdez, O.; Brescacin, T.; Arredondo, J.; Bouchard, J.; Jessop, P. G.; Champagne, P.; Cunningham, M. F., Grafting CO_2-responsive polymers from cellulose nanocrystals via nitroxide-mediated polymerisation. *Polymer Chemistry* **2017,** *8* (28), 4124-4131.

10.Anžlovar, A.; Huskić, M.; Žagar, E., Modification of nanocrystalline cellulose for application as a reinforcing nanofiller in PMMA composites. *Cellulose* **2016,** *23* (1), 505-518.

11.Zeinali, E.; Haddadi-Asl, V.; Roghani-Mamaqani, H., Nanocrystalline cellulose grafted random copolymers of n-isopropylacrylamide and acrylic acid synthesized by RAFT

polymerization: Effect of different acrylic acid contents on LCST behavior. *RSC Advances* **2014,** *4* (59), 31428-31442.

12.Mendonca, P. V.; Konkolewicz, D.; Averick, S. E.; Serra, A. C.; Popov, A. V.; Guliashvili, T.; Matyjaszewski, K.; Coelho, J. F. J., Synthesis of cationic poly((3-acrylamidopropyl)trimethylammonium chloride) by SARA ATRP in ecofriendly solvent mixtures. *Polymer Chemistry* **2014,** *5* (19), 5829-5836.

13.Matyjaszewski, K., Atom transfer radical polymerization (ATRP): Current status and future perspectives. *Macromolecules* **2012,** *45* (10), 4015-4039.

14.Schroder, K.; Matyjaszewski, K.; Noonan, K. J. T.; Mathers, R. T., Towards sustainable polymer chemistry with homogeneous metal-based catalysts. *Green Chemistry* **2014,** *16* (4), 1673-1686.

15.Zhang, Y.; Wang, Y.; Matyjaszewski, K., ATRP of methyl acrylate with metallic zinc, magnesium, and iron as reducing agents and supplemental activators. *Macromolecules* **2011,** *44* (4), 683-685.

16.Matyjaszewski, K.; Coca, S.; Gaynor, S. G.; Wei, M.; Woodworth, B. E., Zerovalent metals in controlled/"living" radical polymerization. *Macromolecules* **1997,** *30* (23), 7348-7350.

17.Abreu, C. M. R.; Serra, A. C.; Popov, A. V.; Matyjaszewski, K.; Guliashvili, T.; Coelho, J. F. J., Ambient temperature rapid SARA ATRP of acrylates and methacrylates in alcohol-water solutions mediated by a mixed sulfite/Cu(II)Br_2 catalytic system. *Polymer Chemistry* **2013,** *4* (23), 5629-5636.

18.Cordeiro, R. A.; Rocha, N.; Mendes, J. P.; Matyjaszewski, K.; Guliashvili, T.; Serra, A. C.; Coelho, J. F. J., Synthesis of well-defined poly(2-(dimethylamino)ethyl methacrylate) under mild conditions and its co-polymers with cholesterol and peg using Fe(0)/Cu(II) based SARA ATRP. *Polymer Chemistry* **2013,** *4* (10), 3088-3097.

19.Konkolewicz, D.; Wang, Y.; Zhong, M.; Krys, P.; Isse, A. A.; Gennaro, A.; Matyjaszewski, K., Reversible-deactivation radical polymerization in the presence of metallic copper. A critical assessment of the SARA ATRP and SET-LRP mechanisms. *Macromolecules* **2013,** *46* (22), 8749-8772.

20.Konkolewicz, D.; Wang, Y.; Krys, P.; Zhong, M.; Isse, A. A.; Gennaro, A.; Matyjaszewski, K., SARA ATRP or SET-LRP. End of controversy? *Polymer Chemistry* **2014,** *5* (15), 4396-4417.

21.Gois, J. R.; Konkolewic, D.; Popov, A. V.; Guliashvili, T.; Matyjaszewski, K.; Serra, A. C.; Coelho, J. F. J., Improvement of the control over SARA ATRP of 2-(diisopropylamino)ethyl methacrylate by slow and continuous addition of sodium dithionite. *Polymer Chemistry* **2014,** *5* (16), 4617-4626.

22.Percec, V.; Popov, A. V.; Ramirez-Castillo, E.; Monteiro, M.; Barboiu, B.; Weichold, O.; Asandei, A. D.; Mitchell, C. M., Aqueous room temperature metal-catalyzed living radical polymerization of vinyl chloride. *JACS* **2002,** *124* (18), 4940-4941.

23.Rosen, B. M.; Percec, V., Single-electron transfer and single-electron transfer degenerative chain transfer living radical polymerization. *Chem. Rev.* **2009,** *109* (11), 5069-5119.

24.Levere, M. E.; Nguyen, N. H.; Leng, X.; Percec, V., Visualization of the crucial step in SET-LRP. *Polymer Chemistry* **2013,** *4* (5), 1635-1647.

25.Lligadas, G.; Rosen, B. M.; Bell, C. A.; Monteiro, M. J.; Percec, V., Effect of Cu(0) particle size on the kinetics of SET-LRP in DMSO and Cu-mediated radical polymerization in mecn at 25 °c. *Macromolecules* **2008,** *41* (22), 8365-8371.

26.Nguyen, N. H.; Levere, M. E.; Percec, V., SET-LRP of methyl acrylate to complete conversion with zero termination. *J. Polym. Sci., Part A: Polym. Chem.* **2012,** *50* (5), 860-873.

27.Morandi, G.; Heath, L.; Thielemans, W., Cellulose nanocrystals grafted with polystyrene chains through surface-initiated atom transfer radical polymerization (SI-ATRP). *Langmuir* **2009,** *25* (14), 8280-8286.

28.Wu, W.; Huang, F.; Pan, S.; Mu, W.; Meng, X.; Yang, H.; Xu, Z.; Ragauskas, A. J.; Deng, Y., Thermo-responsive and fluorescent cellulose nanocrystals grafted with polymer brushes. *Journal of Materials Chemistry A: Materials for Energy and Sustainability* **2015,** *3* (5), 1995-2005.

29.Xu, Y.; Yuan, L.; Wang, Z.; Wilbon, P. A.; Wang, C.; Chu, F.; Tang, C., Lignin and soy oil-derived polymeric biocomposites by "grafting from" raft polymerization. *Green Chemistry* **2016,** *18* (18), 4974-4981.

30.Jessop, P. G., Searching for green solvents. *Green Chemistry* **2011,** *13* (6), 1391-1398.

31.Jessop, P. G.; Heldebrant, D. J.; Li, X. W.; Eckert, C. A.; Liotta, C. L., Green chemistry - reversible nonpolar-to-polar solvent. *Nature* **2005,** *436* (7054), 1102-1102.

32.Jessop, P. G.; Kozycz, L.; Rahami, Z. G.; Schoenmakers, D.; Boyd, A. R.; Wechsler, D.; Holland, A. M., Tertiary amine solvents having switchable hydrophilicity. *Green Chemistry* **2011,** *13* (3), 619-623.

33.Jessop, P. G.; Mercer, S. M.; Heldebrant, D. J., Co2-triggered switchable solvents, surfactants, and other materials. *Energy & Environmental Science* **2012,** *5* (6), 7240-7253.

34.Liu, Y.; Jessop, P. G.; Cunningham, M.; Eckert, C. A.; Liotta, C. L., Switchable surfactants. *Science* **2006,** *313* (5789), 958-960.

35.O'Neill, C.; Fowler, C.; Jessop, P.; Cunningham, M., Redispersing aggregated latexes made with switchable surfactants. *Green Materials* **2013,** *1*, 27-35.

36.Fowler, C. I.; Jessop, P. G.; Cunningham, M. F., Aryl amidine and tertiary amine switchable surfactants and their application in the emulsion polymerization of methyl methacrylate. *Macromolecules* **2012,** *45* (7), 2955-2962.

37.Su, X.; Jessop, P. G.; Cunningham, M. F., Switchable surfactants at the polystyrene–water interface: Effect of molecular structure. *Green Materials* **2014,** *2* (2), 69-81.

38.Su, X.; Fowler, C.; O'Neill, C.; Pinaud, J.; Kowal, E.; Jessop, P.; Cunningham, M., Emulsion polymerization using switchable surfactants: A route towards water redispersable latexes. *Macromolecular Symposia* **2013,** *333* (1), 93-101.

39.Su, X.; Nishizawa, K.; Bultz, E.; Sawamoto, M.; Ouchi, M.; Jessop, P. G.; Cunningham, M. F., Living CO_2-switchable latexes prepared via emulsion ATRP and AGET miniemulsion ATRP. *Macromolecules* **2016,** *49* (17), 6251-6259.

40.Shirin-Abadi, A. R.; Darabi, A.; Jessop, P. G.; Cunningham, M. F., Preparation of redispersible polymer latexes using cationic stabilizers based on 2-dimethylaminoethyl methacrylate hydrochloride and 2,2′-azobis[2-(2-imidazolin-2-yl)propane]dihydrochloride. *Polymer* **2015,** *60*, 1-8.

41.Shirin-Abadi, A. R.; Jessop, P. G.; Cunningham, M. F., In situ use of aqueous RAFT prepared poly(2-(diethylamino)ethyl methacrylate) as a stabilizer for preparation of CO_2 switchable latexes. *Macromolecular Reaction Engineering* **2017,** *11* (1), 1600035

42.Pinaud, J.; Kowal, E.; Cunningham, M.; Jessop, P., 2-(diethyl)aminoethyl methacrylate as a CO_2-switchable comonomer for the preparation of readily coagulated and redispersed polymer latexes. *ACS Macro Letters* **2012,** *1* (9), 1103-1107.

43.Darabi, A.; Jessop, P. G.; Cunningham, M. F., CO_2-responsive polymeric materials: Synthesis, self-assembly, and functional applications. *Chem. Soc. Rev.* **2016,** *45* (15), 4391-436.

44.van de Wetering, P.; Moret, E. E.; Schuurmans-Nieuwenbroek, N. M. E.; van Steenbergen, M. J.; Hennink, W. E., Structure−activity relationships of water-soluble cationic methacrylate/methacrylamide polymers for nonviral gene delivery. *Bioconjugate Chem.* **1999,** *10* (4), 589-597.

45.Zhang, Q.; Wang, W.-J.; Lu, Y.; Li, B.-G.; Zhu, S., Reversibly coagulatable and redispersible polystyrene latex prepared by emulsion polymerization of styrene containing switchable amidine. *Macromolecules* **2011,** *44* (16), 6539-6545.

46.Zhang, Q.; Yu, G.; Wang, W.-J.; Li, B.-G.; Zhu, S., Preparation of CO_2/ N_2-triggered reversibly coagulatable and redispersible polyacrylate latexes by emulsion polymerization using a polymeric surfactant. *Macromol. Rapid Commun.* **2012,** *33* (10), 916-921.

47.Mihara, M.; Jessop, P.; Cunningham, M., Redispersible polymer colloids using carbon dioxide as an external trigger. *Macromolecules* **2011,** *44* (10), 3688-3693.

48.Cunningham, M. F.; Jessop, P. G., An introduction to the principles and fundamentals of CO_2-switchable polymers and polymer colloids. *Eur. Polym. J.* **2016,** *76*, 208-215.

49.Goracci, G.; Arbe, A.; Alegría, A.; García Sakai, V.; Rudić, S.; Schneider, G. J.; Lohstroh, W.; Juranyi, F.; Colmenero, J., Influence of solvent on poly(2-(dimethylamino)ethyl methacrylate) dynamics in polymer-concentrated mixtures: A combined neutron scattering, dielectric spectroscopy, and calorimetric study. *Macromolecules* **2015,** *48* (18), 6724-6735.

50.Schmalz, A.; Hanisch, M.; Schmalz, H.; Müller, A. H. E., Double stimuli-responsive behavior of linear and star-shaped poly(N,N-diethylaminoethyl methacrylate) in aqueous solution. *Polymer* **2010,** *51* (6), 1213-1217.

51.Wang, H.-D.; Roeder, R. D.; Whitney, R. A.; Champagne, P.; Cunningham, M. F., Graft modification of crystalline nanocellulose by Cu(0)-mediated SET living radical polymerization. *J. Polym. Sci., Part A: Polym. Chem.* **2015,** *53* (24), 2800-2808.

52.Hemraz, U. D.; Campbell, K. A.; Burdick, J. S.; Ckless, K.; Boluk, Y.; Sunasee, R., Cationic poly(2-aminoethylmethacrylate) and poly(N-(2-aminoethylmethacrylamide) modified cellulose nanocrystals: Synthesis, characterization, and cytotoxicity. *Biomacromolecules* **2015,** *16* (1), 319-325.

Chapter 6. Surface Modification of Cellulose Nanocrystals via SI-RAFT-mediated Polymerization via *Grafting-to* and *Grafting-from* Approach and CO_2-Responsiveness

All the materials along with the characterization methods and specifications can be found in the Appendices A.II and B. respectively

6.1 ***Introduction***

In Chapter 5, it was demonstrated that CNC could be grafted with PDMAEMA and PDEAEMA via SI-Cu(0)-ATRP through a *grafting-from* approach, to obtain CO_2-responsive CNC.[1] This approach was capable of producing CO_2-responsive CNC that can be reversibly stabilized by sparging CO_2 into the aqueous dispersion. However, the grafted polymers were not strictly homopolymers but copolymers of PDMAEMA or PDEAEMA with PMMA due to the transesterification of the monomers with the solvent (methanol) during the grafting reaction. Furthermore, it was determined by chain-extension experiments that ATRP is not the best approach to make ATRP macroinitiators of these polymers to perform a *grafting-to* approach because of the low chain-end functionality. These drawbacks represent a considerable limitation when an assessment of the effect on CO_2-responsiveness and hydrophobicity as a function of different molecular weights of the grafted polymer chains is required.

A similar approach was performed previously by our group using the NMP approach to obtain CO_2-responsive CNC. In these reports, CNC were grafted with PMMA,[2] PDMAEMA, PDEAEMA and PDMAPMAm via *grafting-from*[3] and *grafting-to*.[4] However, using NMP for the grafting process of CNC has some disadvantages that can be easily overcome by using a RAFT approach. One of these disadvantages is that the grafted

polymers were not homopolymers, but copolymers including ~10 mol% styrene units. Styrene is commonly used as a comonomer during the polymerization of methacrylates to ensure good control and livingness of the final polymers. Experimentally, it has been shown that the polymerization of MMA with styrene yields a copolymer that exhibits a high degree of livingness, whereas the polymerization of methacrylates alone compromises the chain-end functionality due to side reactions (irreversible terminations and chain transfer to polymers).[5] However, the incorporation of styrene units in the polymer grafts could alter the final hydrophobicity of the final materials, having a direct impact on the final hydrophobicity of the polymer grafts. Consequently, pure homopolymers grafts are required to assess the effect of the molecular weight of the polymer grafts. In Chapter 4, it was demonstrated that RAFT-mediated polymerization is a good candidate to obtain pure PDMAEMA, PDEAEMA and PDPAEMA-based macro-RAFT agents with high chain-end functionalities. Moreover, compared to the ATRP and NMP approaches, the absolute molecular weight of the exclusively the dormant/living chains of PDMAEMA and PDEAEMA-based macro-RAFT agents, can be determined using GPC-UV, as the Mark-Houwnik parameters for these two monomers have been recently reported.[6]

Reports on the surface modification of CNC via RAFT-mediated polymerization are limited and all of these report on the *grafting-from* of CNC using what it is referred to as an R-approach.[7-8] As it was illustrated in Figure 2.2, there are two approaches for the immobilization of polymer chains on a solid surface, the *grafting-to* and *grafting-from* approaches. In principle, the *grafting-from* approach via RAFT-mediated polymerization can be performed in two different ways; by the R-group approach or the Z-group approach. The Z-group of the CTA (as explained in Chapter 2) mediates the propagation and

deactivation of the active species; whereas the R-group fragments from the RAFT CTA and reactivates monomer propagation. In order to perform a *grafting-from* approach by RAFT-mediated polymerization, a RAFT CTA should be attached on the surface of the substrate. This attachment of the RAFT CTA can be done from either the Z or R end of the CTA molecule. Scheme 6.1 depicts both variants of the *grafting-from* approach by RAFT-mediated polymerization, the Z-group and R-group approaches.[9] To date, there have only been two reports on the *grafting-from* CNC via RAFT-mediated polymerization,[7-8] and there are two others in which the grafting was performed on cellulose substrates.[10-11] All of these report grafted polymers by the R-group approach, including PMMA, PNIPAM, PAA and PS.

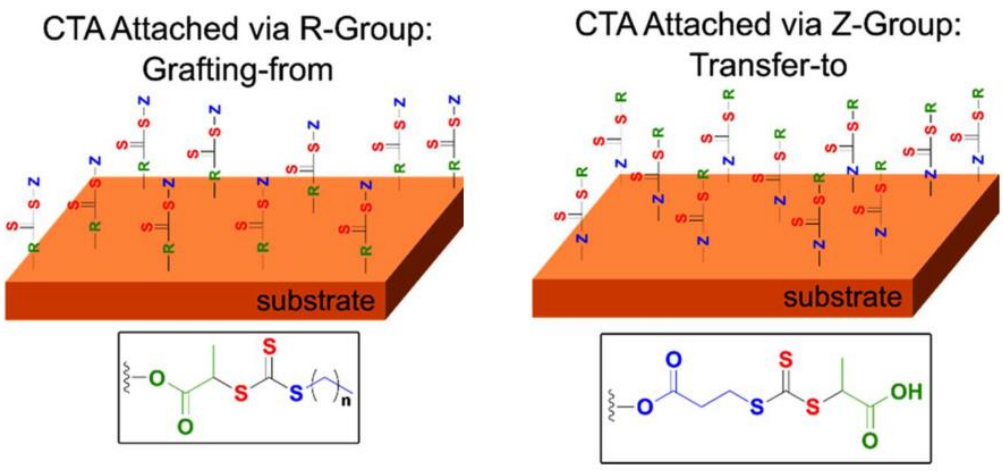

Scheme 6.1. Attachment of CTA to the substrate determines the mechanism of polymerization. If the substrate is attached through the R-group, grafting-from operates. Conversely, transfer-to is the mechanism if the CTA is attached through the Z-group.[12]

The difference between the R-group and the Z-group approaches is that when attaching polymer grafts onto a surface via the R-group approach, a radical is formed during the fragmentation step and it is attached to the substrate where monomer units can start to being

added, following the *grafting-from* definition. When grafting via the Z-group approach, propagating polymer chains will be formed in solution as the reinitiating radical (R-group) will be released into solution and will follow a grafting mechanism more similar to the *grafting-to* as depicted in Scheme 6.1. This last approach is considered as a hybrid of the *grafting-to* and *grafting-from* approaches and is commonly known as the *transfer-to* approach.[12]

Previous work reporting on the grafting of CNC with pH-responsive polymers was based on the *grafting-from* approach taking advantage of the higher graft densities that can be achieved by this route.[13-16] However, this disadvantage is counteracted by not knowing the final characteristics of the attached polymer grafts (molecular weight, dispersity, graft density). Cleavage of grafted polymers from CNC is difficult to achieve and usually requires strong acid/base conditions. In the case of poly(dialkylaminoethyl methacrylates), degradation can occur under these conditions making further analysis not viable. Consequently, there are no reports on pH-responsive CNC where the effect of the molecular weight of the polymer grafts on their hydrophobicity or colloidal stability has been assessed via a *grafting-from* approach.

The best strategy to analyze grafted materials based on fully characterized polymer grafts relies on the *grafting-to* approach. Therefore, the main objective of this chapter was to synthesize, characterize and evaluate the CO_2-responsiveness as a function of the molecular weight of the grafts via a *grafting-to* approach and to analyze any differences in CO_2-responsiveness/hydrophobicity with polymer-grafted CNC via a *grafting-from* approach (Scheme 6.2). First, the CNC surfaces were functionalized with GMA (*grafting-to)* or CTP (*grafting-from*). Then, PDMAEMA, PDEAEMA and PDPAEMA grafts were

attached to the CNC by RAFT-mediated polymerization following with thermal, spectroscopical and elemental analysis characterization. Finally, CO_2/pH-responsiveness of all the materials were assessed in terms of redispersibility in water and switchable hydrophobicity.

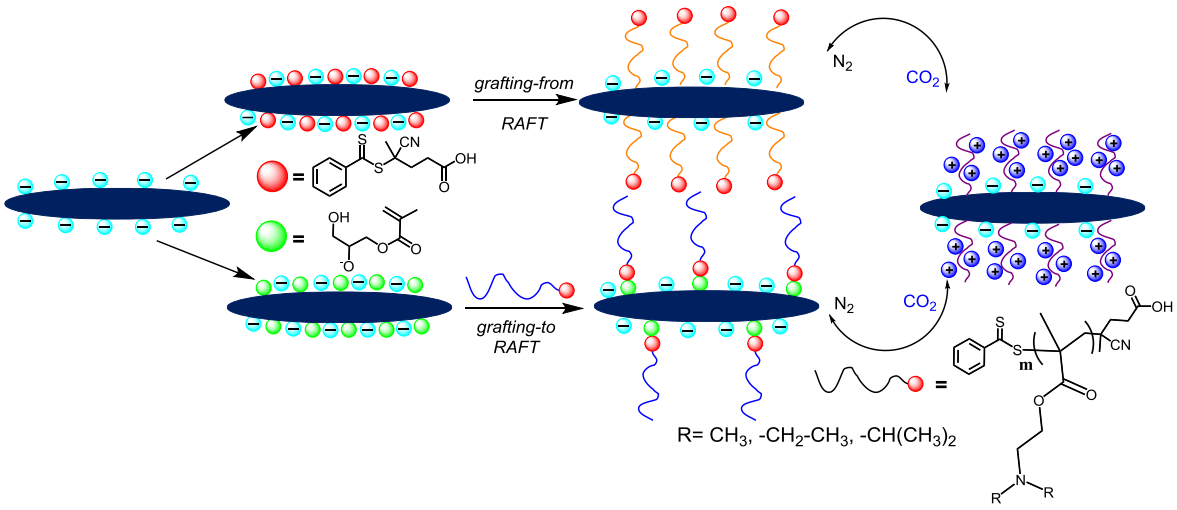

Scheme 6.2. CNC surface modification via *grafting-from* and *grafting-to* approaches.

6.2 ***Experimental***

6.2.1 *General procedure for the homopolymerization of alkylaminoethyl methacrylates*

Table 6.1 shows the recipes to prepare homopolymers via the RAFT-mediated polymerization of DMAEMA, DEAEMA and DPAEMA for three different molecular weights for each of the monomers. The monomer was first added together with tert-butanol, 4-cyano-4-((phenylcarbonothioyl)thio)pentanoic acid (CTP) and a magnetic stir bar into a 20 mL glass vial. After the dissolution of CTP, pre-weighed ACVA was added into the vial. Then, the vials were degassed by bubbling nitrogen for 10 minutes and sealed. Next, the vials were immersed in an oil bath at 70°C for 4h. The reactions were quenched at -

10°C and exposed to air. Samples were collected for ^{1}H NMR and GPC analyses. The three polymers were precipitated three times. PDMAEMA was precipitated in cold hexanes and PDEAEMA and PDPAEMA were precipitated in icy water. Finally, the three polymers were dried in a vacuum oven at 50°C overnight.

Table 6.1. Recipes for synthesizing 4 g of different macro-RAFT agents of DMAEMA, DEAMA and DPAEMA at 50% monomer conversion in solution 4mL of tert-butanol.

Target M_n[a] (Da)	CTP (mg)	CTP (mmol)	ACVA (mg)	ACVA (mmol)
2,280	279	1.00	56	0.2
4,280	140	0.50	28	0.1
6,280	93	0.33	19	0.07

[a]Target M_n = conversion x ([mon]/[CTA]) x Mw_{mon}+Mw_{CTA}. Mw_{mon} is the molecular weight of the monomer and Mw_{CTA} is the molecular weight of the CTA.

6.2.2 *General procedure for functionalizing of CNC with glycidyl methacrylate*

To a three-necked round-bottom flask, 2.2 g of CNC (36.54 mmol of hydroxyls) and 150 mL of deionized water were added. The pH was then adjusted to a value of 3 with 0.5M HCl and 200 mg of hydroquinone were added. Additionally, 5.25 g (74 mmol) of glycidyl methacrylate (GMA) were added in an addition funnel coupled to the round-bottom flask. a condenser was connected to the flask. The round-bottom flask was submerged into an oil bath at 60°C and oxygen was removed from the dispersion by bubbling nitrogen while stirring. After bubbling nitrogen, the glycidyl methacrylate was added dropwise over 1 h and then left under stirring for two additional hours. After the lapsed time, the dispersion was concentrated under reduced pressure until it formed a wet gel and the final concentrate was equally divided into 6 -50 mL centrifuge tubes. Then, 40 mL of acetone were added to each tube, followed by vortexing and centrifuging at 6000

rpm. The process was repeated several times and the final product was stored in acetone at 4°C until used.

6.2.3 *General procedure for grafting CNC via grafting-to approach by RAFT-mediated polymerization*

Table 6.2 shows the recipes that were used to perform the grafting of the PDMAEMA, PDEAMA and PDPAEMA -based macro-RAFT agents. First, the macro-RAFT agent was dissolved in 15 mL of tert-butanol and degassed by bubbling nitrogen for 5 minutes. Then, CNC-GMA (0.5 g) stored in acetone was centrifuged at 6000 rpm. The acetone was then decanted and additional 35 mL of tert-butanol were added. The CNC-GMA in tert-butanol was then vortexed and poured into a three-necked round-bottom flask with additional 35 mL of tert-butanol and a condenser and an addition funnel were coupled to the round-bottom flask. Next, the initiator was added and then, under stirring, the flask was degassed by bubbling nitrogen during 20 minutes. Then via cannula the macro-RAFT solution was transferred to the addition funnel along with an additional 15 mL of degassed tert-butanol. Next, the round-bottom flask was immersed in a pre-heated oil bath at 70°C and the macro-RAFT initiator solution was added dropwise over a period of 4h and left under stirring for an additional 20h. Then the reaction was cooled down to room temperature and the product was centrifuged. The colored solvent was decanted and then the product was exhaustively washed with THF. This process was repeated until the THF became colorless, plus additional three washing cycles. Finally, the product was decanted and stored in acetone at 4°C.

Table 6.2. Recipe for the grafting of CNC-GMA using pre-synthesized PDMAEMA, PDEAMA and PDPAEMA based macro-RAFT agents. [macro-RAFT]:[ACVA] = 5.

macro-RAFT agent	M_n[a] (Da)	macro-RAFT (g)	macro-RAFT (mmol)	ACVA (mmol)	ACVA (mg)
DM1	2,500	0.4	0.16	0.03	8.96
DM2	6,700	1.07	0.16	0.03	8.96
DM3	7,800	1.17	0.16	0.03	8.96
DE1	3,600	0.58	0.16	0.03	8.96
DE2	5,800	0.93	0.16	0.03	8.96
DE3	8,700	1.39	0.16	0.03	8.96
DP1	3,700	0.59	0.16	0.03	8.96
DP2	6,000	0.96	0.16	0.03	8.96
DP3	7,100	1.14	0.16	0.03	8.96

[a] M_n determined by GPC. PDMAEMA and PDEAEMA were determine by universal calibration using Mark-Houwnik parameters reported elsewhere.[6] M_n of PDPAEMA were obtained from relative calibration using PMMA standards.

6.2.4 *General procedure for functionalizing CNC with 4-cyanopentanoic acid dithiobenzoate*

The RAFT CTA, 4-cyano-4-((phenylcarbonothioyl)thio)pentanoic acid (CTP) was synthesized according to the following procedure reported elsewhere.[17-18] Briefly, Carbonyl diimidazole (CDI) (18 g, 111.5 mmol) was added to a 250 mL three-necked round bottomed flask with an attached 60 mL addition funnel. Then, 15 mL of fresh distilled anhydrous dichloromethane (DCM) was added via cannula. CTP (31 g, 111 mmol) was dissolved in 30 mL of fresh distilled anhydrous DCM in a septum -sealed 250 mL single necked round-bottom flask, and then the solution was transferred to the 60 mL addition funnel via cannula using nitrogen gas flow. The solution was added dropwise with constant magnetic stirring using under nitrogen atmosphere at room temperature. The reaction was then stopped after 4h once CO_2 bubbles were no longer formed as a by-product, maintaining the solution under inert atmosphere (pot 1).

Following the initial reaction between the CDI and CTP, 2.2 g (37 mmol of hydroxyl groups) of CNC were dispersed in 20 mL of freshly distilled anhydrous DMSO and stirred with a vortex agitator in a 50 mL centrifuge tube until the CNC was completely dispersed. Then, freshly distilled anhydrous DCM (30 mL) was added to the CNC dispersion, vortexed again, centrifuged (6,000 rpm) and finally decanted. The CNC cake was redispersed in 30 ml of dry DCM and then transferred with a cannula to a three-necked round -bottom flask equipped with a 60 mL addition funnel, a condenser and a stir bar (pot 2).

The Pot 1 solution was transferred via cannula to the addition funnel attached to the pot 2 mixture containing the dispersed CNC in DCM. The pot 1 solution was then added dropwise under constant magnetic stirring under nitrogen atmosphere at room temperature. Then the reaction was stirred for three days followed by a solvent exchange process with acetone. The final CNC cake was put into a coarse frit glass thimble inside a Soxhlet apparatus and left under constant acetone reflux for five days to remove any excess reactants and side products. After the Soxhlet extraction, the product was stored in ethanol at 4°C and a portion of the sample was freeze-dried for solid state NMR, FT-IR, elemental and TGA analyses.

6.2.5 *General procedure for grafting CNC via grafting-from approach by SI-RAFT-mediated polymerization*

In a 250 mL three-necked round-bottom flask, CNC-CTP (0.25 g) was dispersed in 50 mL of tert-butanol. DMAEMA (2 g, 12.72 mmol), DEAEMA (2 g, 10.77 mmol) or DPAEMA (2 g, 9.39 mmol) were dissolved in 15 mL of tert-butanol and then transferred into an addition funnel. Then, ACVA (20 mg, 0.07 mmol) was added to the flask. The round-bottom flask and the addition funnel were degassed with N_2 for 30 minutes. Finally, the round-bottom flask was submerged into a pre-heated oil bath at 70°C and then the monomers were added dropwise. The grafting reaction was left to proceed at 70°C for 24 hours. After cooling, the product was exhaustively washed with THF to remove all free polymer and then centrifuged at 6,000 rpm. These washing cycles were repeated several times. A portion of the product was vacuum dried for material characterization.

6.2.6 *General procedure for CO_2-switching*

Polymer-grafted CNC dispersions (ca. 0.4 wt.%) were prepared in 25 mL of deionized water. A three-necked round-bottom flask was adapted with a pH meter, a gas dispersion tube with a porous fritted glass tip, and a stir bar. CO_2 and N_2 was sparged through the mixture between cycles until pH readings were stable for more than 10 minutes (~10 min for CO_2; ~1 h for N_2). During the sparging of gases, the round-bottom flask was submerged in an oil bath at 25°C to maintain constant temperature.

6.3 ***Results and discussion***

6.3.1 *Homopolymerization of dialkylaminoethyl methacrylates*

Macro-RAFT agents of PDMAEMA, PDEAEMA and PDPAEMA, which were subsequently grafted onto CNC using a *grafting-to* approach, were synthesized with three different molecular weights as described in Chapter 4. Characteristics of these macro-RAFT agents are shown in Table 6.3. Additionally, chain-extension experiments were performed to demonstrate the livingness of the macro-RAFT agents. The corresponding GPC-UV traces are shown Appendix F.I. As explained in Chapter 4, during the synthesis of the macro-RAFT agents, monomer conversion was not maximized to avoid the formation of low molecular weight dead chains.

Table 6.3. Characteristics of macro-RAFT agents used for chain-extension experiments and CNC grafting.

	Monomer Conversion (%)	**M_n[a] (Da)**	**Đ**
PDMAEMA			
DM1	51	2,500	1.20
DM2	87	6,800	1.19
DM3	76	7,800	1.20
PDEAEMA			
DE1	80	3,700	1.22
DE2	71	5,800	1.22
DE3	68	8,600	1.21
PDPAEMA			
DP1	62	3,600	1.16
DP2	67	5,900	1.11
DP3	56	7,100	1.11

[a] M_n determined by GPC. PDMAEMA and PDEAEMA were determine by universal calibration using Mark-Houwnik parameters reported elsewhere.[6] M_n of PDPAEMA were obtained from relative calibration using PMMA standards.

6.3.2 *Grafting-to approach by RAFT-mediated approach*

Functionalization of CNC with glycidyl methacrylate

After preparing the RAFT-based macro-RAFT agents of each poly(dialkylaminoethyl methacrylate) with three different M_n values, the next step was to functionalize the CNC surfaces with GMA such that the macro-RAFT agent chains could be attached by reacting with the GMA double bond. GMA was first reacted with CNC under acidic conditions (Scheme 6.3), similar to a previous report by our group.[4] In acidic conditions, the epoxy group of the GMA will undergo an acid-catalyzed ring-opening mechanism from a nucleophilic attack mainly at the primary alcohols on the CNC surfaces. Due to the growing stability of a carbocation with the number of substitutions, the epoxy ring will open from the more substituted carbon on the epoxy ring, yielding as a product the structure shown in Scheme 6.3.

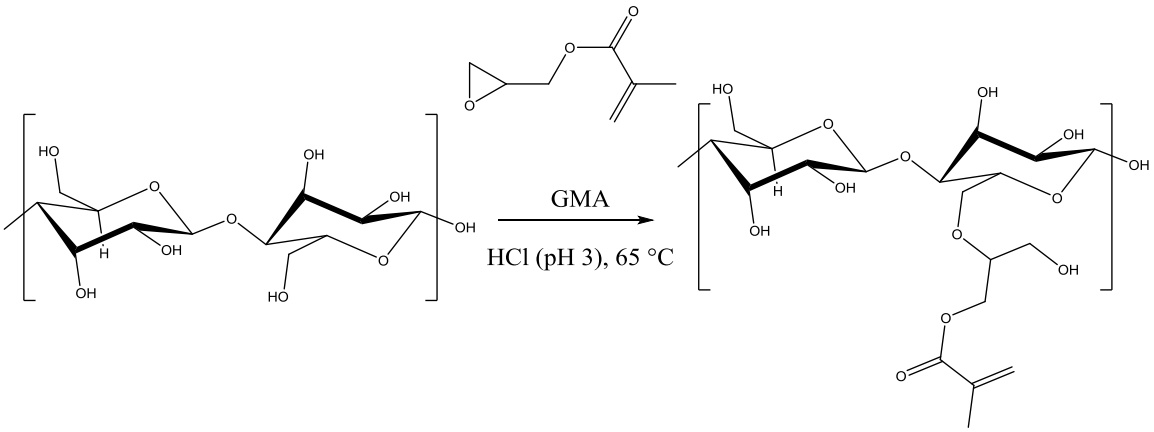

Scheme 6.3. CNC functionalization with GMA under acidic conditions (pH= 3). OH= 36.54 mmol, GMA= 74 mmol at 65°C.

Figure 6.1 shows the IR spectra of native CNC and GMA-functionalized CNC (CNC-GMA). In both spectra, it is possible to identify all of the cellulose backbone signals, which

can be divided in four main groupings: -OH stretching vibrations (3,600-3,000 cm^{-1}), -CH and $–CH_2$ symmetric and asymmetric vibrations (1,500-1,300 cm^{-1}), C-O stretching vibrations (1,200-850 cm^{-1}) and –CH skeletal vibrations (750-500 cm^{-1}). In addition to the cellulosic backbone, one signal at 1,700 cm^{-1} is observed, corresponding to the C=O bond stretching of the methacrylate carbonyl. The signal at 1,600 cm^{-1} on the native CNC corresponds to the O-H deformation vibration of residual water within the CNC crystal lattice.

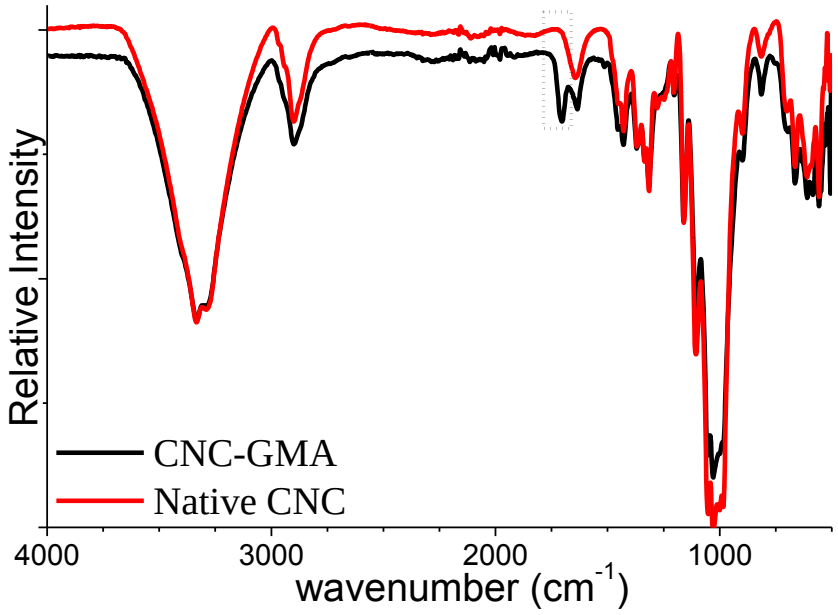

Figure 6.1 IR spectra of native CNC and CNC-GMA. The boxed region encloses the C=O stretching band at 1,700 cm^{-1} and the deformation vibration of residual water at 1,600 cm^{-1}.

TGA analysis provides additional evidence of the surface modification of CNC. In Figure 6.2, the thermal decomposition profile of native CNC and CNC-GMA are shown. It can be observed that native CNC is more thermally stable than CNC-GMA. CNC-GMA has an onset temperature of 230°C, whereas native CNC onset temperature is at 260°C,

meaning that the CNC-GMA thermal stability decreased compared to native CNC due to the presence of labile GMA groups on the CNC surfaces.

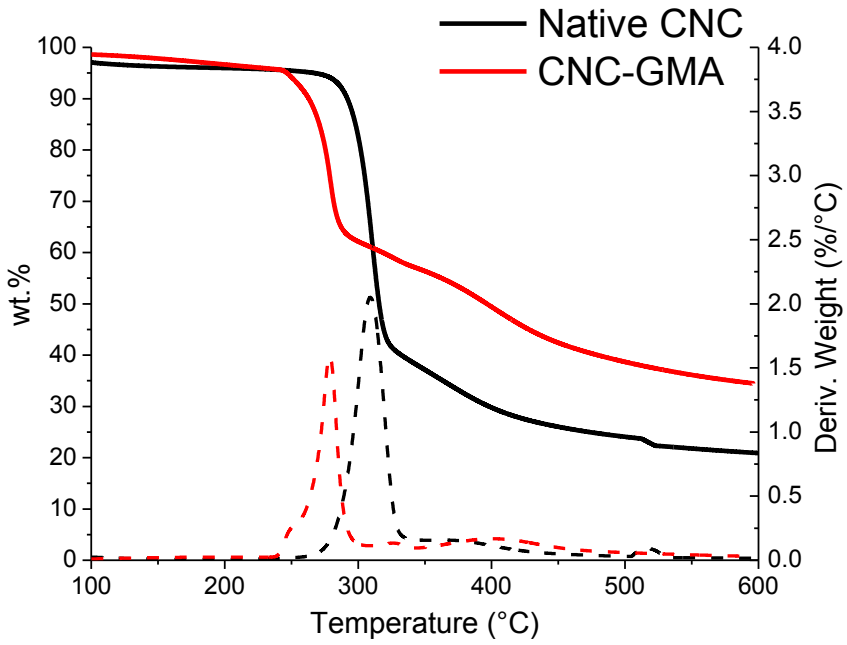

Figure 6.2. Thermogravimetric analysis of native CNC and CNC-GMA.

Grafting-to reaction of poly(dialkylaminoethyl methacrylate)s to CNC-GMA

Scheme 6.4 depicts the *grafting-to* reaction of macro-RAFT agents with CNC-GMA dispersed in tert-butanol in the presence of ACVA initiator. Primary radicals formed from the decomposition of ACVA could either react with the double bond at the surface of the CNC-GMA, or with the dithiobenzoate group of the macro-RAFT agents. In the case of the primary radical reacting with the CNC-GMA, the radical formed at the methacrylate group of the CNC-GMA will then add to the dithiobenzoate group which will in turn fragment, liberating a living propagating chain of poly(dialkylaminoethyl methacrylate). This propagating chain could react with another macro-RAFT agent, CNC-GMA or

recombine with a primary radical from the ACVA (or another propagating chain). Because the ACVA concentration was adjusted to be five times less than that of the macro-RAFT agent ([macro-RAFT]:[I] = 5:1), the probability of recombination of a propagating chain with a primary radical is reduced. In the case where the primary radical reacts first with the macro-RAFT agent, the addition-fragmentation step will produce a macro-propagating radical which can also react with the CNC-GMA, another macro-RAFT agent, or recombine with a primary radical (or other propagating chain) as well. There are, thus, multiple pathways that can lead to surface grafting.

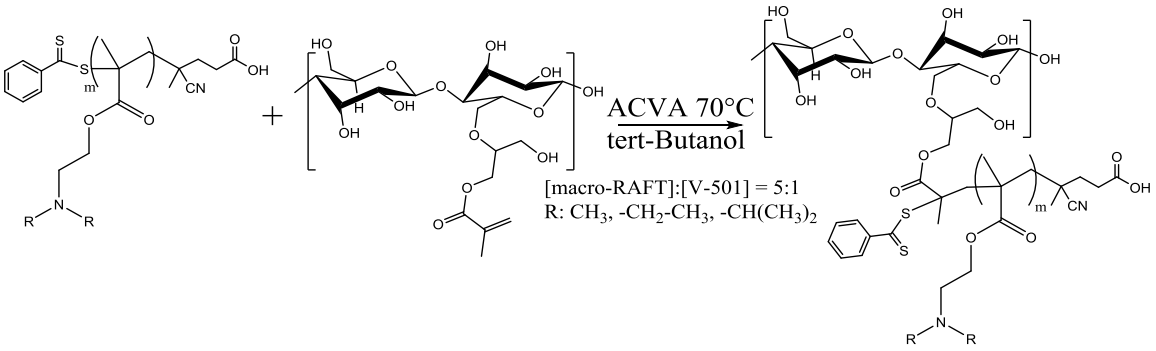

Scheme 6.4. *Grafting-to* of CNC-GMA with poly(dialkylaminoethyl methacrylates) based macro-RAFT agents in tert-butanol. [macro-RAFT]:[ACVA] = 5:1 at 70°C.

Figures 6.3-6.5 show the FT-IR spectra of surface modified CNC grafted with three different molecular weight macro-RAFT agents (Table 6.3) made of PDMAEMA (CNC-DM#), PDEAEMA (CNC-DE#) and DPAEMA (CNC-DP#). For the CNC-DM# series, the FT-IR spectra are shown in Figure 6.3. As the polymer being grafted is a tertiary polyamine, the only additional signals to be expected on the grafted CNC spectra, compared to the CNC-GMA spectrum, are the C=O stretching band of the methacrylate backbone which can be clearly observed at 1,730 cm^{-1}, and complementary C-H stretching vibrations bands which are observed at 2,960 cm^{-1}.

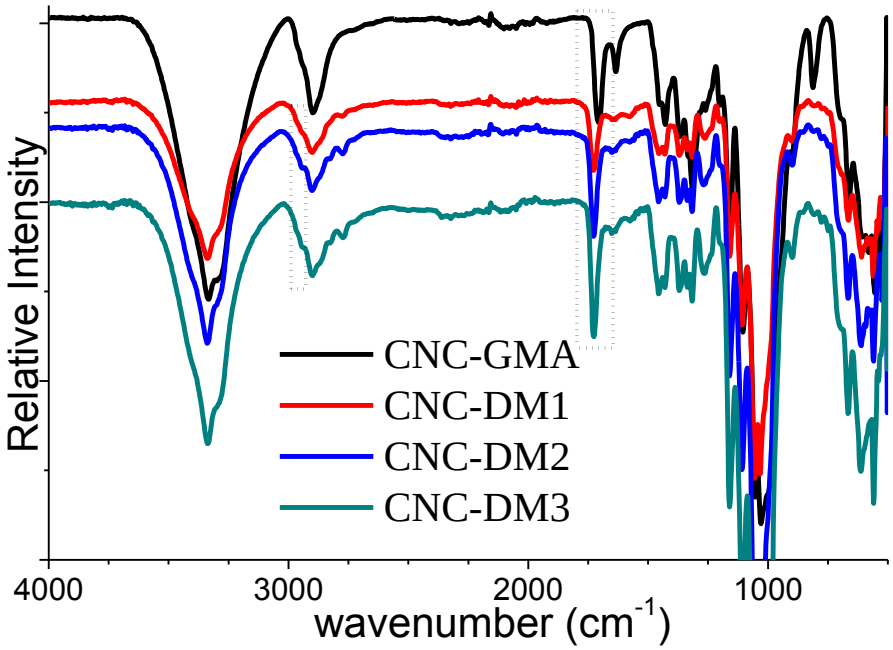

Figure 6.3. FT-IR spectra of PDMAEMA-grafted CNC (CNC-DM#) series.

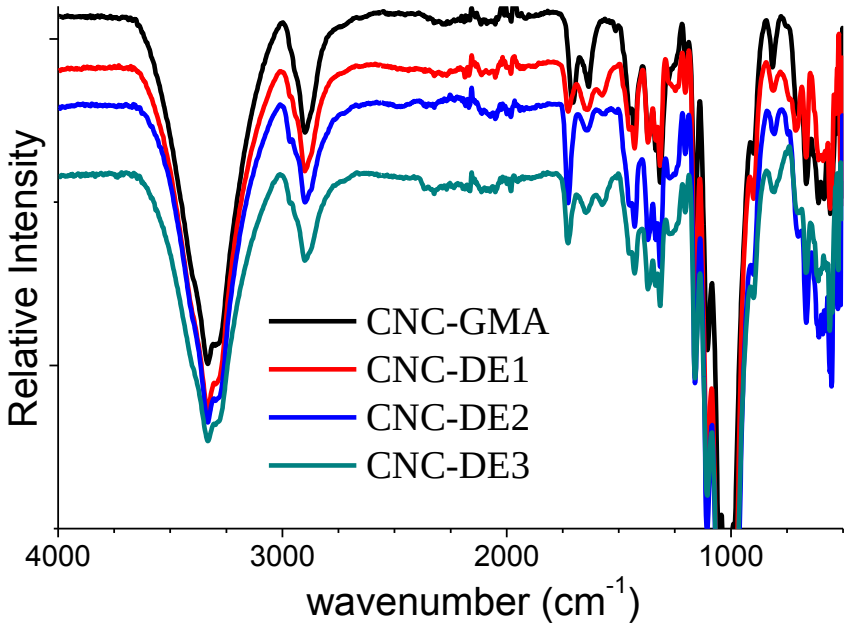

Figure 6.4. FT-IR spectra of PDMAEMA-grafted CNC (CNC-DE#) series.

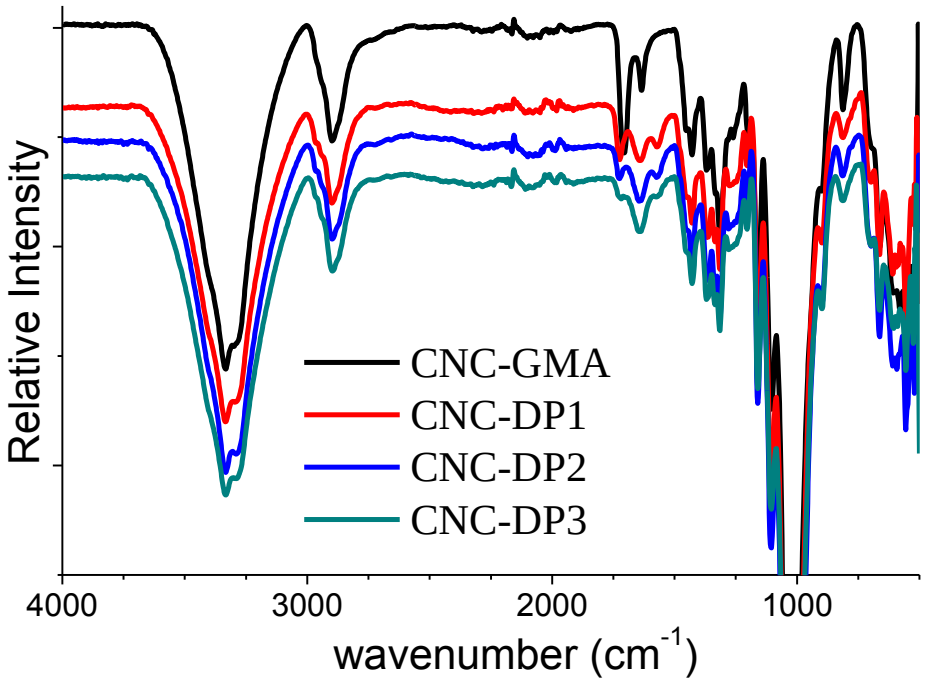

Figure 6.5. FT-IR spectra of PDMAEMA-grafted CNC (CNC-DP#) series.

Similar spectra were obtained for the CNC-DE# series (Figure 6.4) and CNC-DP# series(Figure 6.5) with the same characteristics as explained for the CNC-DM# series. For the specific case of CNC-DP# series, the carbonyl signal intensity was very low (1,725 cm^{-1}), indicating the possibility of low grafting efficiency. This was supported by elemental analysis which will be presented in a subsequent section.

TGA was performed on all of these products to confirm that the macro-RAFT agents did graft onto the CNC, and that the polymer signals observed in the FT-IR and were not the result of a physical mixture of unreacted CNC-GMA and macro-RAFT agent. Figure 6.6 shows the TGA analysis of the CNC-DM# series along with CNC-GMA and native CNC. It can be noted that native CNC exhibited an onset decomposition temperature between CNC-GMA and CNC-DM# products. Therefore, it could be concluded that the thermal stability of the grafted CNC was higher as a consequence of attaching the

PDMAEMA grafts onto the CNC. From the derivative of the wt.% trace, it can be observed that the grafted CNC did not contain any residual CNC-GMA, confirming the formation of a new different material and the absence of a physical mixture of CNC-GMA with macro-RAFT agent. Similar TGA traces were obtained for the CNC-DE# and CNC-DP# series; their thermograms can be consulted in Appendix F.II

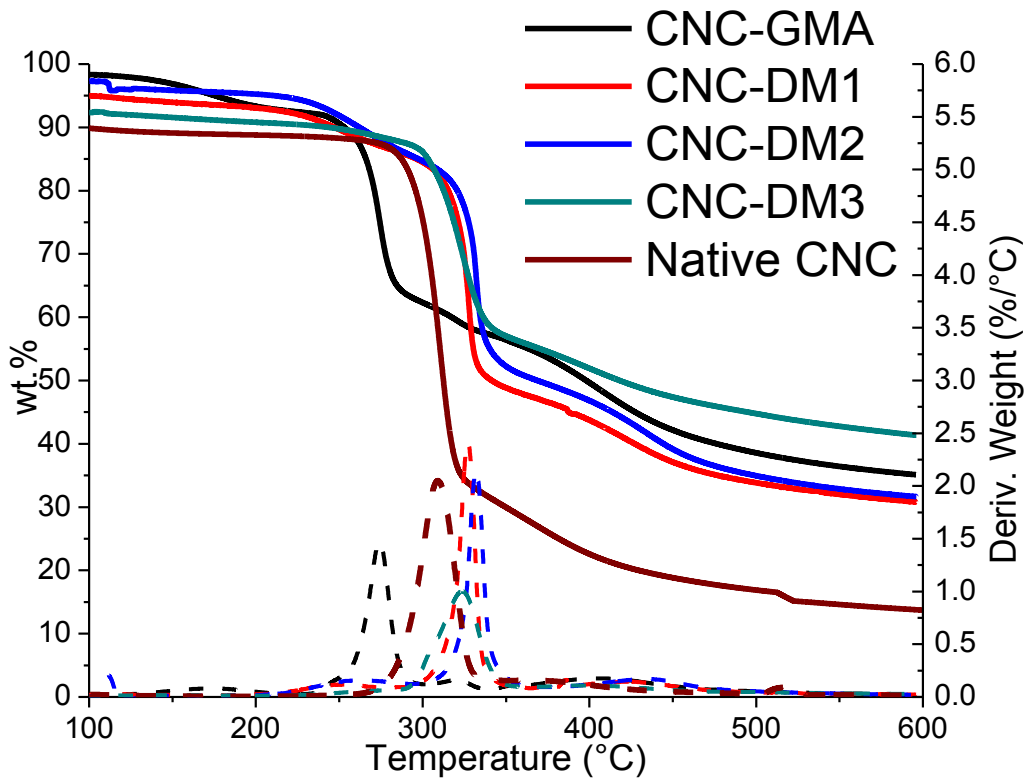

Figure 6.6. TGA analysis of native CNC, CNC-GMA and PDMAEMA-grafted CNC.

Polymer loadings of grafted CNC using different molecular weights macro-RAFT agents

The next step was to quantify how much polymer was attached to the CNC surfaces and to determine graft densities. The grafted products were analyzed by elemental analysis, for which the nitrogen mass composition was obtained. Using the amount of nitrogen per gram of grafted material, the wt.% of polymer per gram of grafted CNC can be calculated. Because the M_n of the grafted polymers is known, it is then possible to determine the graft densities of each product with different molecular weight grafts. Table 6.4 shows the elemental analysis results for all of the grafted materials.

Table 6.4. Elemental analysis, polymer content and graft densities of the CNC-DM#, CNC-DE# and CNC-DP# series.

Elemental Analysis	C%	%H	%N	N mmol/ g of CNC	wt.% of polyamine/ g of CNC[a]	M_n[b] (Da)	Chains /nm^2 [c]
CNC-DM1	43.3±0.3	6.6±0.1	0.6±0.2	0.77	11	2,500	0.050
CNC-DM2	43.4±0.2	6.7±0.1	1.8±0.0	1.63	20	6,700	0.039
CNC-DM3	44.7±0.1	6.8±0.1	1.9±0.0	1.71	21	7,800	0.036
CNC-DE1	43.3±0.6	6.3±0.1	0.9±0.0	0.78	12	3,900	0.038
CNC-DE2	43.9±0.1	6.3±0.0	0.9±0.1	0.78	12	6,300	0.023
CNC-DE3	43.5±0.1	6.4±0.2	1.0±0.1	0.88	14	9,400	0.018
CNC-DP1	43.7±0.3	6.3±0.1	0.8±0.1	0.68	12	3.700[c]	0.040
CNC-DP2	43.9±0.1	6.3±0.1	0.9±0.3	0.30	6	6,000 [c]	0.011
CNC-DP3	42.9±0.2	6.4±0.1	1.0±0.2	0.45	9	7,100 [c]	0.014
Native CNC	40.8±0.1	6.2±0.1	0.0±0.1	---	---	---	

[a] Calculated as reported by Majoinen et. al.[19] [b] M_n determined by universal calibration using Mark-Houwnik parameters reported elsewhere.[6] [c] M_n reported in PMMA equivalents.

During the grafting process of the three different series, it was attempted to obtain similar graft densities for the different grafted products by adding the same number of chains of macro-RAFT agents to react with the CNC-GMA. For the CNC-DM# series, good consistency in the graft densities was achieved, obtaining 0.036-0.5 chains per nm^2. For the CNC-DE#, the graft density of the product with the lowest molecular weight grafts was higher (DE1 =0.038 chains/nm^2) than the products with higher molecular weight grafts (DE2= 0.023 and DE3 =0.018 chains/nm^2). For the CNC-DP# series, a similar trend in graft densities to the CNC-DE# series was observed. For DP1, the grafting density was 0.040 chains/nm^2, while 0.011 and 0.014 chains/nm^2 were observed for DP2 and DP3. For all CNC grafted series, lower graft densities were obtained as the molecular weight of the macro-RAFT agent increased. Reproducibility of the grafting process was verified with the same macro-RAFT agent (DM2) and CNC-GMA. Table F.1 in Appendix F.III shows good reproducibility among three separate grafting processes using the same macro-RAFT agent and CNC-GMA, obtaining similar values of graft densities.

It is worth noting that the graft densities presented in Table 6.4 are lower when compared to other reports using *grafting-to* approach. This difference in graft density is partially attributed to steric hindrance of the macro-RAFT agents. However, a certain degree of aggregation of CNC during functionalization with GMA and/or during grafting could occur resulting in much less exposed surface area resulting in lower graft densities. Another possibility that needs to be considered is the possibility of having aggregation of CNC by polymer bridging producing discrete agglomerates. This is consistent with the AFM images presented in Chapter 5, although it cannot be assured that agglomeration did not happen during sample preparation.

6.3.3 *CO_2/pH-responsiveness of grafted CNC*

In Chapter 5, it was demonstrated that CO_2-responsive CNC obtained via SI-Cu(0)-ATRP formed a stable dispersion under CO_2 and it could be reversibly aggregated under slightly basic conditions. Similar behaviour was observed by our group in previous reports using NMP.[3-4] As we were expecting the same behaviour for the products made by the RAFT approach, CO_2-switching procedures were applied to all products following the same procedures as reported in Chapter 5.

Table 6.5. CO_2-N_2 switching of an aqueous dispersion of CNC-DM1 (0.4 wt.%). Initial pH was adjusted with 0.5 M NaOH.

	pH	Zeta Potential (mV)	Remarks
Initial	7.80	0	
100 uL NaOH	12.05	-30	Translucent
CO_2	5.62	-----	Aggregation
N_2	9.38	-25	CNC was redispersed at pH 8.3
CO_2	5.50	-----	At pH 7.3 aggregation started
N_2	9.44	-25	CNC was redispersed at pH 8.2

Table 6.5 shows how the pH and the ζ-potential behaved during the CO_2-switching process of the CNC-DM# series. The pH behaved as expected with a ΔpH of ca. ±4 units. Interestingly and unexpectedly, under CO_2, CNC-DM1 became colloidally unstable and aggregated. However, after removing the CO_2, it redispersed once again as the pH increased by sparging N_2. Figure 6.7 (a) shows the initial state of the dispersion after a slight initial pH adjustment through the addition of NaOH. CNC-DM1 was fully dispersed with a ζ-potential of -30 mV. After introducing CO_2 into the headspace of the round-bottom flask, and after a decrease in the pH to 5.62, CNC-DM1 fully aggregated (Figure 6.7 (b)). There

is no ζ-potential data during the CO_2 cycle because at the point which the grafted CNC aggregated, the ζ-potential measurements become unreliable. The process was fully reversible as the system redispersed once again after sparging N_2 at 70°C.

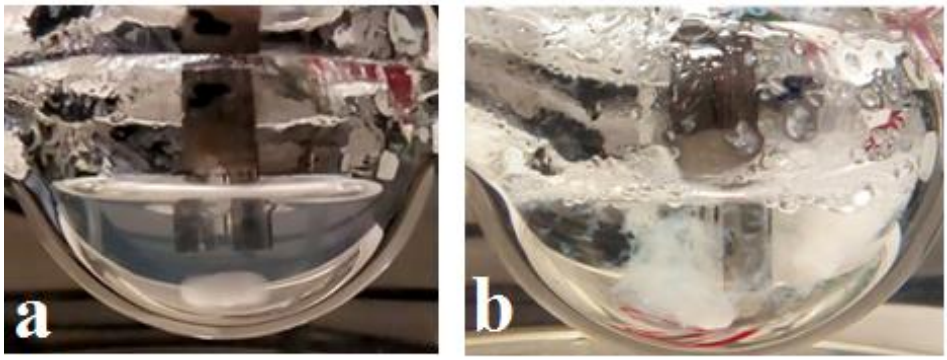

Figure 6.7. CO_2-switching of CNC-DM1 (0.4 wt.%) dispersed at neutral pH (a) and aggregated under CO_2 (b).

Similar behaviour was observed with the CNC-DM2, CNC-DM3, CNC-DE# series and CNC-DP# series. Although the CNC-DP# series did not fully aggregate**,** turbidity did increase after the pH was lowered by filling the headspace with CO_2 (Figure 6.8) This could be explained by the considerably low graft densities obtained for the CNC-DP# series, compared with the CNC-DM# and CNC-DE# (Table 6.4).

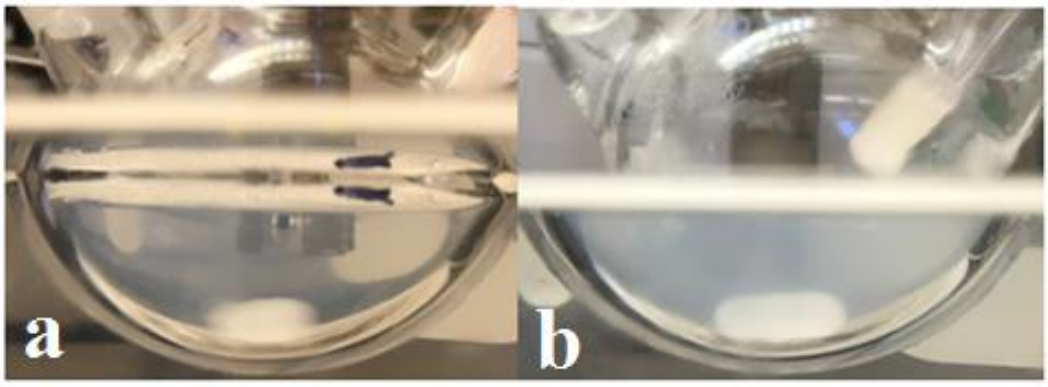

Figure 6.8. CO_2-switching of CNC-DP2 (0.4 wt.%) (a) under CO_2, (b) under N_2.

As previously mentioned, the CO_2-responsive CNC obtained by the ATRP and NMP approaches were colloidally stable under CO_2 and destabilized after sparging N_2 gas. This difference in behaviour where the grafted products made by RAFT exhibited an opposite colloidal stability could be related to the graft densities and the final molecular weight of the polymer grafts. This hypothesis will be demonstrated later, but first an assessment of the effect of the molecular weight of the polymer grafts on the dispersibility and hydrophobicity will be discussed.

Experiments, where the ζ-potential was measured as a function of pH for the grafted products, were performed by auto-titration experiments to analyze how these materials behave as a function of pH. Figure 6.9 shows how the ζ-potential of the CNC-DM# series varied as a function of pH in an aqueous dispersion. All three CNC-DM# products behave similarly at slightly basic conditions. At pH around 9, the maximum pH that could be achieved using the CO_2-N_2 switching system, all three products displayed similar ζ-potential values (ca. -20 mV). This would explain why the products were redispersible and became colloidally stable at slightly basic conditions under N_2 (Figure 6.8 (b)). However, while decreasing the pH, the ζ-potential traces showed that the products reached their isoelectric point at a pH range of 7.3-8.2. Below a pH of ca. 7, all three products started to or were already aggregated. The pH at which the isoelectric points are observed in Figure 6.9 were close to the pK_{aH} values of PDMAEMA (pK_{aH} = 7.4[20], 7.2±0.06 (Appendix F.IV)), suggesting that when the polymer grafts gets close to being 50% protonated, the CNC-grafted products become colloidally unstable. The most plausible explanation for this observation is that the positive charge density around the CNC surfaces from the protonated amine groups is not enough to produce sufficient electrostatic repulsion while protonated

under CO_2. This could be due to either low graft density, low molecular weight or a combination of both.

As previously mentioned, the ζ-potential readings are no longer reliable after the CNC have formed aggregates, as non-dispersed samples are not suitable for ζ-potential measurements. Additionally, it is worth noting that conductivity remains almost constant during the auto-titration in the pH range of interest (4-9) discarding the possibility of interference of the added HCl resulting in ion accumulation in the system.

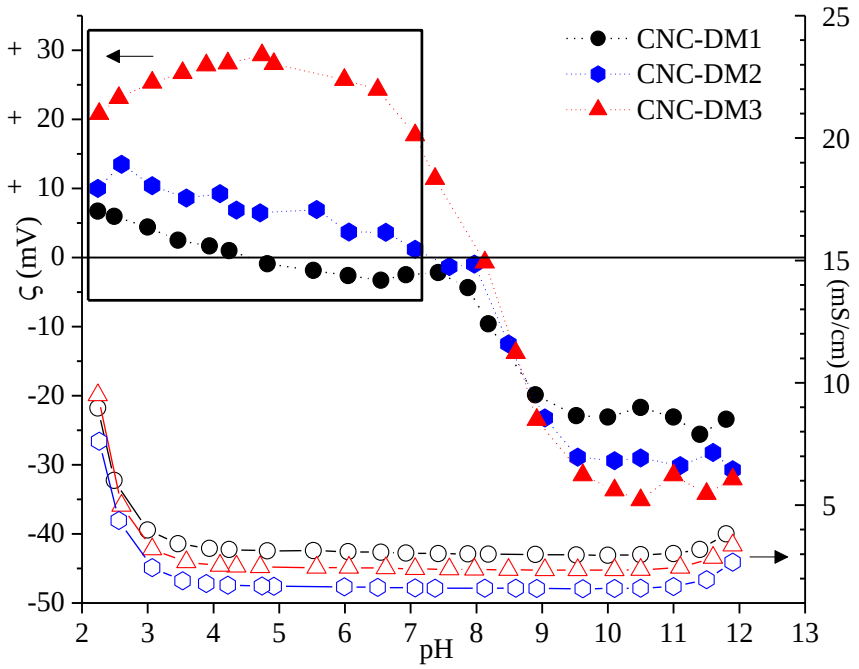

Figure 6.9. ζ-potential and ionic conductivity vs. pH of the CNC-DM# series (ca. 0.4 wt.%) going from pH 12 to 2 with 0.5 M HCl. The boxed region represents unreliable ζ-potential values as PDMAEMA-grafted CNC are aggregated at these pHs.

One of the main goals of this project was to analyze whether the molecular weight of the polymer grafts had an effect on either dispersibility or hydrophobicity, by functionalizing the CNC surfaces with CO_2-responsive polymers. As previously demonstrated, all of the CNC-DM# products behaved similarly, becoming colloidally

unstable under CO_2 regardless of the molecular weight of the polymer grafts. Phase shuttling experiments were performed on each of the CNC-DM# products to determine whether the molecular weight of the polymer grafts had an effect on the resultant hydrophobicity of the material. This assessment highlights the importance of having only pure homopolymers grafts of PDMAEMA on the CNC surfaces which was only possible using the RAFT-mediated approach. When compared to the NMP approach, having randomly distributed styrenic units along the polymer grafts could possibly have an impact on the overall hydrophobicity masking the real hydrophobic character of the polymer grafts with a determined molecular weight.

Figure 6.10 shows dispersions of the CNC-DM# series (0.2 wt.%) in 50% v/v water:chloroform mixtures dyed with the hydrophobic Nile red dye. The dispersions were adjusted to three different pH levels covering the pH range that can be achieved with the CO_2-N_2 switching system (pH = 4-9). For the CNC-DM1 at low pH (4-5), it was observed that the aqueous phase was completely transparent, suggesting that most of the grafted CNC were within the organic phase. For the CNC-DM1 dispersions at a pH of 7-8 and at a pH of 9-10, it appears that most of the CNC seemed to be in the aqueous phase as the organic phase was completely translucent. The opacity observed in the organic phases of the mentioned dispersions is due to small water droplets over the glass wall. Figure 6.11 shows CNC-DM1 dispersions showed in Figure 6.10, to which a commercial laser pointer beam was passed through the aqueous (left) and organic (right) phases. For CNC-DM1 at a mildly acidic pH, it can be noted that the intensity of the scattered light in the aqueous (upper) phases is too dim, whereas the other vials at neutral and basic pH, the intensity of the scattered light is considerably higher. For the organic (lower) phases, the laser beam is

almost unnoticeable. This partitioning behaviour appears to be counterintuitive as it was expected that in the protonated state, the CNC should have become hydrophilic. This can be explained from the fact that the polymer grafts (M_n = 2,500 Da) have a degree of polymerization (DP_n) of 16. In polyamines, 100% protonation is not easily achieved at mildly acidic conditions do to an increase of the positive charges density. Moreover, the basicity of polyamines is usually correlated to their M_n, for which the degree of protonation of short polyamine chains will be lower than longer chains. Consequently, as some of the amine groups of the polymer grafts of CNC-DM1 remained deprotonated, the grafted CNC would maintain enough of its hydrophobic character to partition into the organic phase. On the other hand, at a slightly basic pH, it would seem that most of the grafted CNC were in the aqueous phase. At a pH of 9-10, the short PDMAEMA grafts would be deprotonated, hence it would be expected that the grafted CNC would be in the organic phase. However, Figure 6.10 shows that mildly basic pH, CNC-DM1 mostly partitioned to the aqueous phase. The colloidal stability of these CNC at basic pH was most likely because the polymer grafts were too short for their hydrophobic character to counteract the hydrophilic character of the charged half-sulfate ester groups. Although the graft density could also be playing a role on the overall hydrophobicity of the grafted CNC. This explanation corresponds with the behaviour observed during the CO_2-switching where the CNC-DM# series products aggregated under CO_2 and redispersed under N_2.

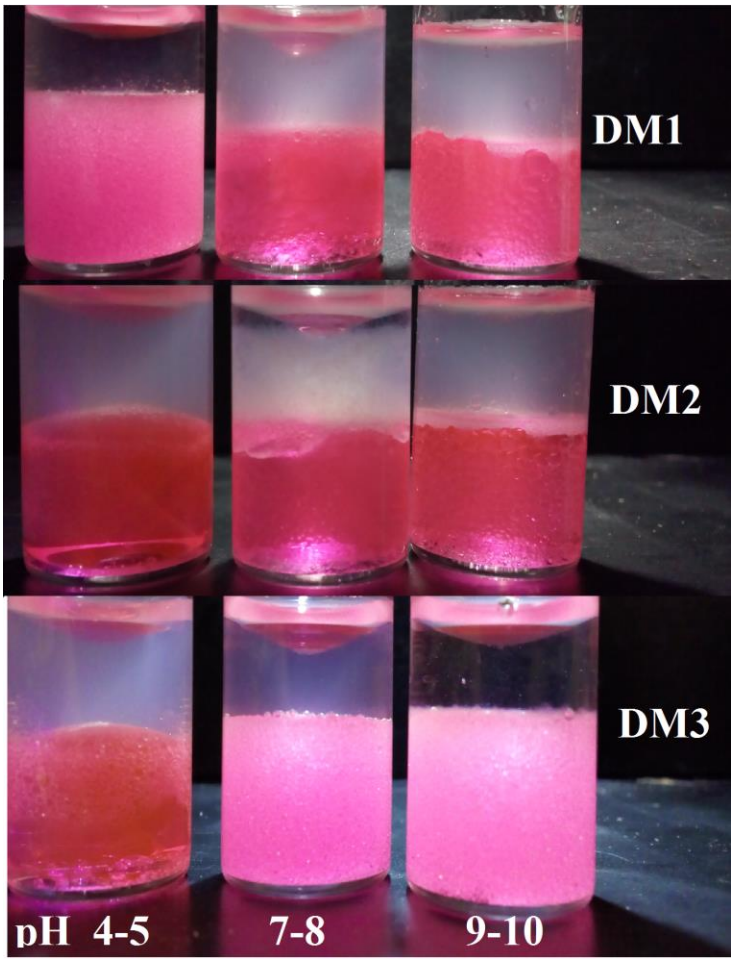

Figure 6.10. CNC-DM# dispersions (0.2 wt.%) at different pH values (DM1: pH 4-5, DM2: 7-8, DM3: 9-10) in a 50% v/v water chloroform mixture with Nile Red as hydrophobic dye.

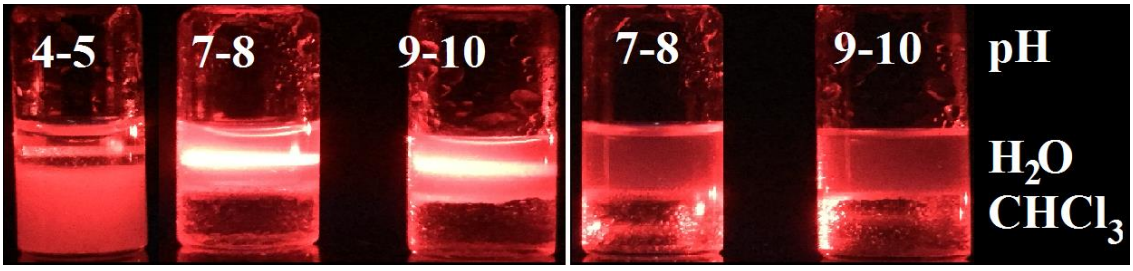

Figure 6.11. CNC-DM1 dispersion (0.2 wt.%) at three different pHs (4-5, 7-8, 9-10) in a 50% v/v water chloroform mixture with Nile Red as hydrophobic dye. A laser pointer beam was passed through the aqueous (left) an organic (right) phase. For the organic phase laser irradiation, of the dispersion in acidic pH was not shown due to a very strong light scattering of the organic phase.

With respect to CNC-DM2 dispersions (M_n 6,700 Da), where polymer grafts had a DP_n of 43, seems that most of the CNC are in the aqueous phase. For the CNC-DM2 dispersion it can be noted that the CNC were fully dispersed in the aqueous phase only in mildly basic conditions. Whereas at a pHs of 4-5 and 7-8, the CNC clearly aggregated and floated over the organic phase, leaving a clear layer of water as supernatant. This observations matched with the auto-titration curve (Figure 6.9) and the aggregation under CO_2. However, these observations suggested that CNC-DM2 is not hydrophobic enough to migrate to the organic phase neither at neutral nor acidic pH. Compared with CNC-DM1, CNC-DM2 under acidic conditions did not partitioned into the organic phase as it has larger amounts of protonable sites; which under acidic pH, the protonated amine groups might not be enough to become colloidally stable, but it is still hydrophilic enough to not migrate into the organic phase.

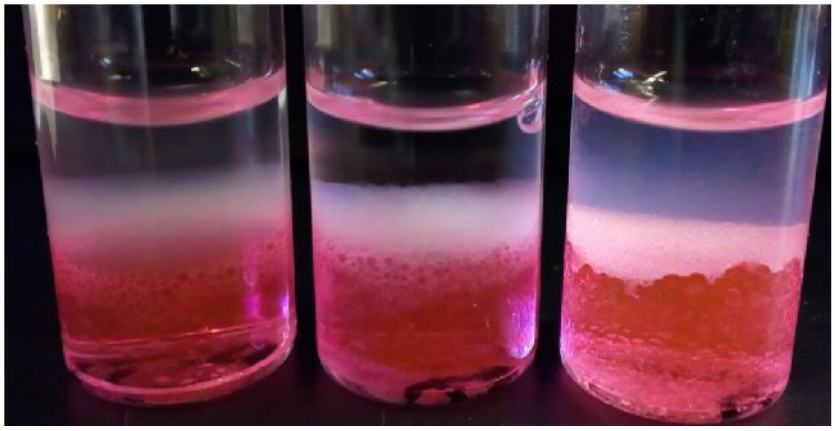

Figure 6.12. CNC-DM2 dispersion (0.2 wt.%) at three different pHs (4-5, 7-8, 9-10) in a 50% v/v water chloroform mixture with Nile Red as hydrophobic dye.

CNC-DM3 did not exhibit the same behaviour as CNC-DM1 and CNC-DM2. Under acidic pH, most of the CNC were in the aqueous phase, whereas at a pH of 7-8 and 9-10 most of the CNC were in the organic phase as no turbidity could be observed in the aqueous

phase. In Figure 6.10 it can be noted that CNC-DM3 at neutral pH, a small amount of CNC were still in the aqueous phase. Figure 6.13 shows that the scattering of the laser beam, when passed through the aqueous phase of the CNC-DM3 dispersion in acidic pH is more intense than the dispersions with neutral and mildly basic pH. Hence, most of the CNC in acidic pH are in the aqueous phase due to a higher degree of protonation of longer PDMAEMA grafts. CNC-DM3 has polymer grafts with a DP_n of 50 (M_n of 7,800), which conferred a likely sufficiently hydrophobic character to counteract the hydrophilicity of the half-ester sulfate groups, such that the CNC could partition into the organic phase. It is worth noting that the CNC-DM# products have almost the same grafting densities (Table 6.4), hence, the change in hydrophobicity between CNC-DM1 and CNC-DM3; and therefore in their partitioning, was most likely a consequence of the increase in the molecular weight of the polymer grafts. The dimmed light scattering of the neutral and basic dispersions could have been due to either unmodified CNC, tiny chloroform droplets in the aqueous phase or dust particles. A control test with just water and chloroform can be observed in Figure F.13 in Appendix F.VIII where light scattering can be noticed due to either dust particles or small chloroform droplets.

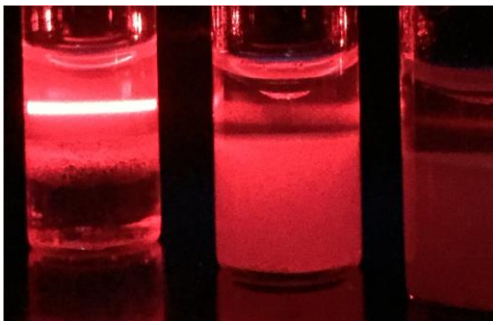

Figure 6.13. CNC-DM3 dispersion (0.2 wt.%) at three different pHs (4-5, 7-8, 9-10) in a 50% v/v water chloroform mixture with Nile Red as hydrophobic dye.

Similar trends were observed for the CNC-DE# series. Figure 6.14 shows the auto-titration curves where the ζ-potential varies as a function of pH. All of the CNC-DE# products had ζ-potential values ca. -25 mV in the pH range of 8-9. Similar to CNC-DM1 (Table 6.5), the ΔpH in between cycles was ca. 4 units. The lowest pH of 4.48 was obtained with CO_2, while a pH of 8.58 was obtained under N_2. The ζ-potential values achieved at these pH values were -14 mV and -4 mV, respectively. These values match the auto-titration curve presented in Figure 6.14. For the CNC-DE# series, the pH at which CNC aggregated was between 6-7. Therefore, similarly to the CNC-DM#, the ζ-potential measurements at pH values below 6 in the auto-titration curve were not considered to be reliable as the three products aggregate below pH 6. The conductivity behaved similarly as with the CNC-DM# series, remaining almost constant during the titration at the pH interval of interest (4-9); as the addition of HCl did not have a significant effect on the overall ionic strength of the aqueous dispersion.

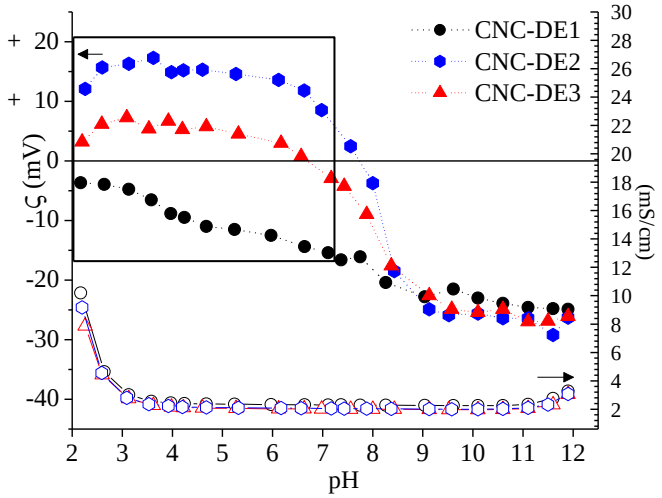

Figure 6.14. ζ-potential and ionic conductivity vs. pH of the CNC-DE# series (0.4 wt.%) going from pH 12 to pH 2 with HCl 0.5M. The boxed region represents unreliable ζ-potential values as PDMAEMA-grafted CNC aggregate in this pH region

Figure 6.15 shows the auto-titration curves of CNC-DP# series. For these products, only a change in turbidity was observed during the CO_2-switching cycles as illustrated in Figure 6.8. This behaviour corresponded to the auto-titration curves depicted in Figure 6.15 as CNC-DP2 and CNC-DP3 never reached an isoelectric point. CNC-DP1 did show an isoelectric point at a pH of 3, likely as a result of having four times more chains/nm^2 (and more total amine groups) than CNC-DP2 and CNC-DP3 (Table 6.4). In addition to the low grafting density, the basicity of the PDPAEMA grafts was also lower than PDMAEMA and PDEAEMA. PDPAEMA has a pK_{aH} of 5.7[21] (6.05, Appendix F.IV), which is almost one pH unit lower than PDMAEMA and PDEAEMA. Having a polymer graft with a lower pK_{aH} could provide the advantage of not having the need to adjust the initial pH with NaOH as was required for the grafted CNC made by SI-Cu(0)-ATRP (Chapter 5). Having a pK_{aH} of 6.05 should also ensure that at a pH of ca. 7.5-8 (maximum pH achieved during CO_2–N_2 switching system), the degree of protonation of the grafted polymers would not be as high as in the case of the grafted products made using the ATRP approach. Nevertheless, upon examination of Figure 6.15, with the graft densities obtained for the CNC-DP# series, it can be concluded that these PDPAEMA-grafted CNC are not good candidates for CO_2 switching. Figure 6.16 shows CNC-DP3 at different pHs covering the CO_2-N_2 pH switching range in which it can be noted that in any of the different pHs, the CNC did not migrate to the organic phase, as the scattering of light in the aqueous phase confirms that most of the CNC were in the aqueous phase. No light scattering was observed in the organic phase.

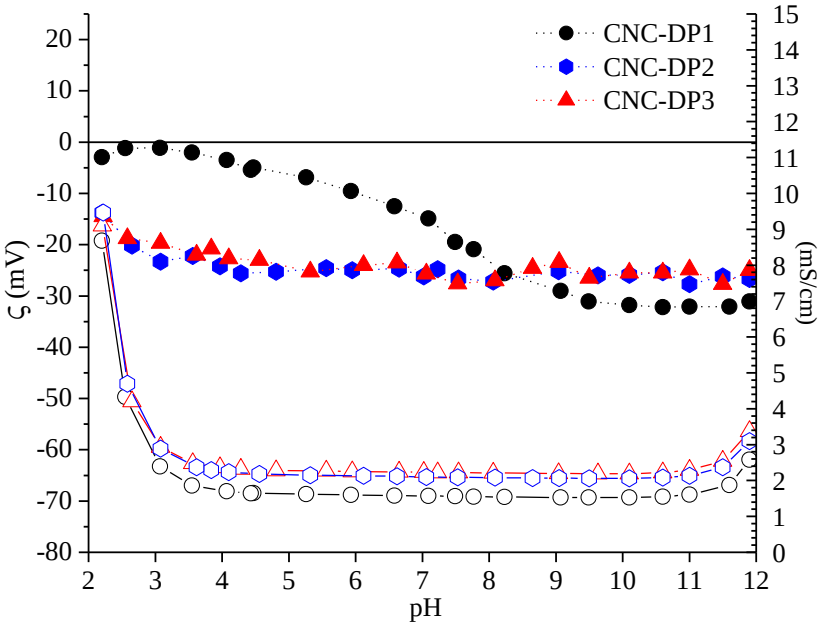

Figure 6.15. ζ-potential and ionic conductivity vs. pH of the CNC-DP# series (0.4 wt.%) going from pH 12 to pH 2 with HCl 0.5M.

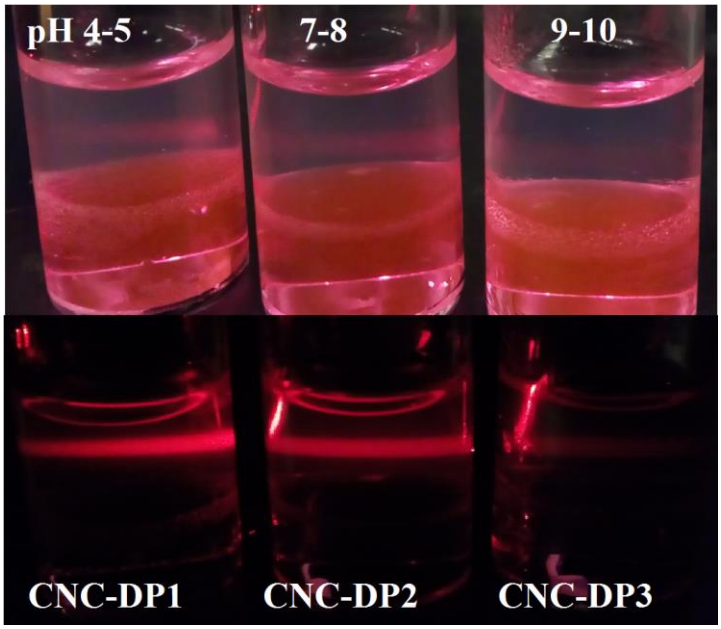

Figure 6.16. CNC-DP3 dispersion at different pHs covering the CO_2-N_2 pH range. A commercial laser pointer beam was directed through the aqueous phase in series showing the laser beam path due to light scattering generated by the CNC. The intensity of the scattered light in third vial is lower due to an attenuating effect caused by the first two vials.

From the phase shuttling experiments, it can be concluded that there is a real effect of the molecular weight of the polymer grafts on the hydrophobicity/hydrophilicity of the CNC-grafted products. However, despite having polymer grafts with a M_n close to 10,000 Da (CNC-DM3 and CNC-DE3) which can be highly protonated under CO_2, it seems that there is a combined threshold in terms of graft densities and molecular weight of the polymer grafts (i.e. total polymer content) for the CO_2-responsive CNC to be colloidally stable under CO_2.

In our published work via *grafting-from* by Cu(0)-ATRP, the highest wt.% of polyamine grafted onto CNC was 26.8% and the lowest was 14.3%,[1] whereas by the NMP approach polymer loadings varied from 36.1 wt.% up to 65.2 wt.%.[3] Unfortunately, graft densities could not be determined for the *grafting-from* results as cleavage of the polymer grafts was not possible. For the case of PDEAEMA-grafted CNC via *grafting-to* approach, Table 6.6 shows the characteristics of the products made by RAFT and NMP.[4] Graft densities varied from 0.01 to 0.06 chains/nm^2 with molecular weights ranging from 3,900 Da up to 19,700 Da respectively. These grafted CNC exhibited ζ-potential values up to +33 mV under CO_2 whereas only slightly negative ζ-potential (-13 mV) were observed under N_2, except for CNC-DE1 which was slightly more negative (-17 mV).

Table 6.6. Graft characteristics of PDEADMA-grafted CNC via RAFT and NMP.

CNC-polymer	M_n (Da)	Grafting Density (Chains/nm)^2	Polymer loading (wt.%)	Amine Groups (mmol/g)	Grafting method	Dispersed under CO_2	pH under CO_2	Average ζ (mV) CO_2	pH under N_2	Average ζ (mV) N_2
CNC-DE1	3,900[a]	0.038	13	0.8	RAFT	No	4.5	---	8.5	-17.0±2.2
CNC-DE2	6,300[a]	0.023	13	0.8	RAFT	No	4.8	---	8.6	5.3±0.5
CNC-DE3	9,400[a]	0.018	14	0.9	RAFT	No	4.8	---	8.8	-1.3±2.2
CNC-g-P(DEAEMA-co-S)1	4,200[b]	0.062	20	1.12	NMP	Yes	4.6	20.5±1.8	8.2	-6.7±1.9
CNC-g-P(DEAEMA-co-S)2	7,800[b]	0.022	14	0.7	NMP	Yes	5.1	27.6±2.6	9.0	-13.7±1.3
CNC-g-P(DEAEMA-co-S)3	19,700[b]	0.008	13	0.7	NMP	Yes	5.2	33.6±0.5	9.0	12.3±2.4

[a]M_n determined by universal calibration. [b]M_n reported in PMMA equivalents.[4]

From Table 6.6, it can be observed that no logical trends are evident to determine when a PDEAEMA-grafted CNC could be colloidally stable under CO_2. It is possible and perhaps likely, that this behaviour follows a similar trend as described by a common LCST phase diagram curve (Figure 2.4) in which a minimum graft density combined with a minimum M_n might be required for the grafted CNC to be CO_2-dispersible as proposed in Figure 6.17. From Table 6.6, it can be observed that CNC-DE1 polymer grafts have lower M_n but double the graft density of CNC-DE2 and CNC-DE3. Although having more chains/nm^2, CNC-DE1 is still colloidally unstable under CO_2. CNC-DE2 and CNC-DE3 have the same graft densities and both are still colloidally unstable under CO_2 despite the fact that CNC-DE3 polymer grafts have higher M_n. PDEAEMA-grafted CNC by NMP

(CNC-g-P(DEAEMA-co-S)2) and grafted via RAFT (CNC-DE2) have similar graft densities, but different M_n, where P(DEAEMA-co-S)2 exceeds the polymer grafts of CNC-DE2 by ca. 1,500 Da making the NMP modified CNC stable under CO_2. Another example is CNC-g-P(DEAEMA-co-S)3, whose polymer grafts have a M_n of 19,700 Da, although its grafting density is barely 0.01 chains/nm^2. However, it was colloidally stable under CO_2.

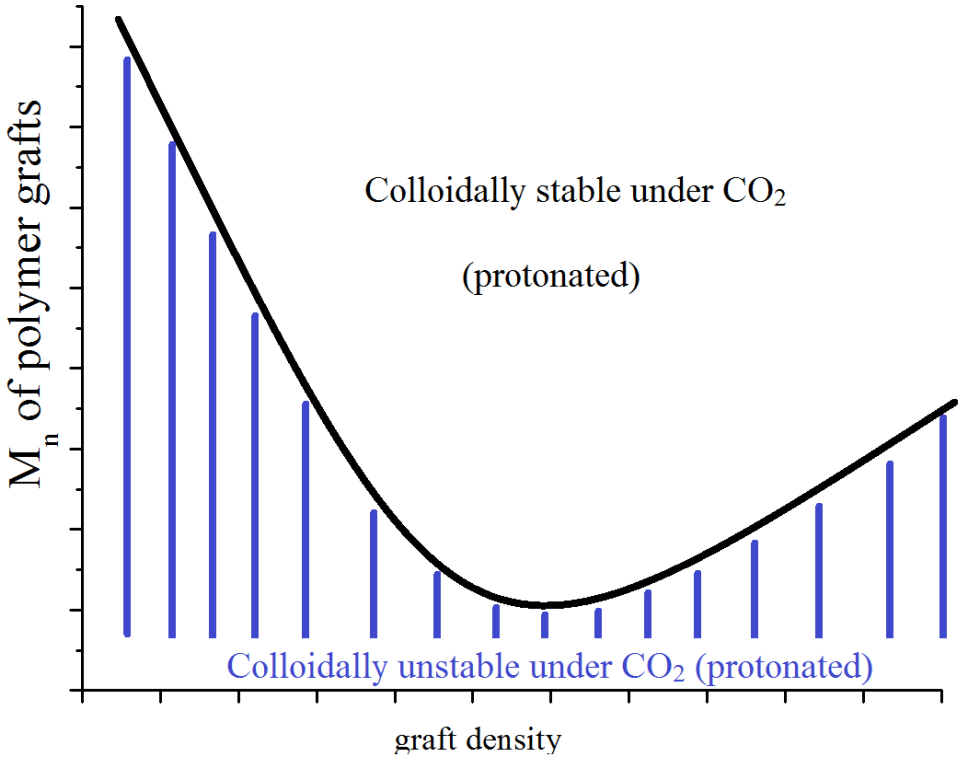

Figure 6.17. Proposed phase diagram where CO_2 stability in aqueous dispersions depends on the graft density and the M_n of the polymer grafts.

Another example that supports this hypothesis is presented in Table 6.7, which shows the elemental analysis results of two different PDMAEMA-grafted CNC. One product corresponds to CNC-DM1 of the CNC-DM# series. The other product corresponds to a different batch of PDMAEMA-grafted CNC made using the same method as the other

series and will be referred as CNC-DM1S2 (characterization and elemental analysis of this particular batch can be found in Appendix F.V). Table 6.7 shows that CNC-DM1 and CNC-DM1S2 have similar graft densities, but a considerably different molecular weight on the polymer grafts. CNC-DM1, as previously described, aggregated and sedimented under CO_2, but CNC-DM1S2 was colloidally stable under CO_2 and sedimented under N_2 (Figure 6.18). The auto-titration curves of both PDMAEMA-grafted CNC are shown in Figure 6.19. It is evident that at a pH of 4-5 (pH achieved under CO_2), the ζ-potential of CNC-DM1S2 had a value of +26 mV, while the ζ-potential of CNC-DM1 was -0.9 mV (CO_2-switching cycles of CNC-DM1S2 can be found in the Appendix F.VI). However, more experimental data is needed to know the real shape of this "phase diagram" like trace with high degree of accuracy and certainty. This is because in Table 6.4, CNC-DM1 and CNC-DM2 have similar numbers than the products presented in Table 6.7 but both products aggregate under CO_2. However, the results presented in this work and the ones presented in Table 6.6 does follow the general trend of the proposed diagram.

Table 6.7. Elemental analysis and graft densities of CNC-DM1 and CNC-DM1S2.

Elemental Analysis	C%	%H	%N	N mmol/ g of CNC	wt.% of polyamine/ g of CNC	M_n (Da)	Chains/ nm^2	#amine groups/ particle[a]
CNC-DM1S2	46.6±0.2	7.0±0.1	1.4±0.1	1.2	16	4,900	0.039	2,600
CNC-DM1	44.4±0.1	6.70±0.1	0.6±0.2	0.8	11	2,500	0.050	1,600

[a] Number of amine groups per particles was estimated assuming a crystal length of 150 nm. The radius (2.2 nm) was obtained via AFM measurements of native CNC as reported by our group elsewhere.[4]

These last experiments along with the data extracted from the NMP work published by our group,[4] and the RAFT results presented in this Chapter, support the hypothesis that there is a threshold that needs to be achieved in terms of chains/nm^2 and molecular weight of the grafts to obtain grafted CNC that could be colloidally stable under CO_2 or in mildly acidic aqueous dispersions (Figure 6.13). Additionally, grafted CNC with poly(dialkylaminoethyl methacrylates) were synthesized via *grafting-from* to analyze the CO_2-responsiveness of the grafted CNC generated from a grafting technique that allows much higher grafting densities. These results will now be discussed.

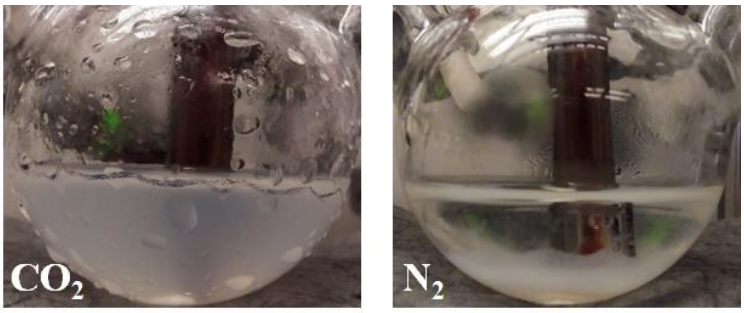

Figure 6.18. CO_2-switching of CNC-DM1S2 (0.4 wt.%). Under CO_2 it forms a stable dispersion and it sediments under N_2.

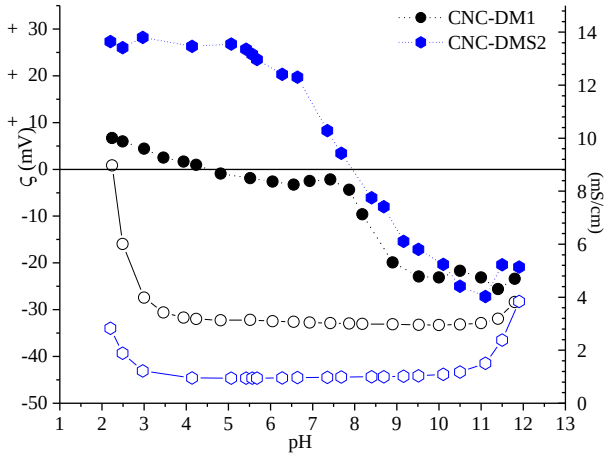

Figure 6.19. Auto-titration curves of CNC-DM1 and CNC-DM1S2 (ca. 0.4 wt.%).

6.3.4 *Grafting-from approach by SI-RAFT-mediated polymerization*

The *grafting-from* approach has been reported to be a good choice when high grafting densities are required.[19] Similarly, RAFT-mediated polymerization is also very convenient to perform the *grafting-from* approach as many RAFT CTAs contain carboxylic acids as part of the R-group which can react readily with the hydroxyl functionalities of many substrates.[12]

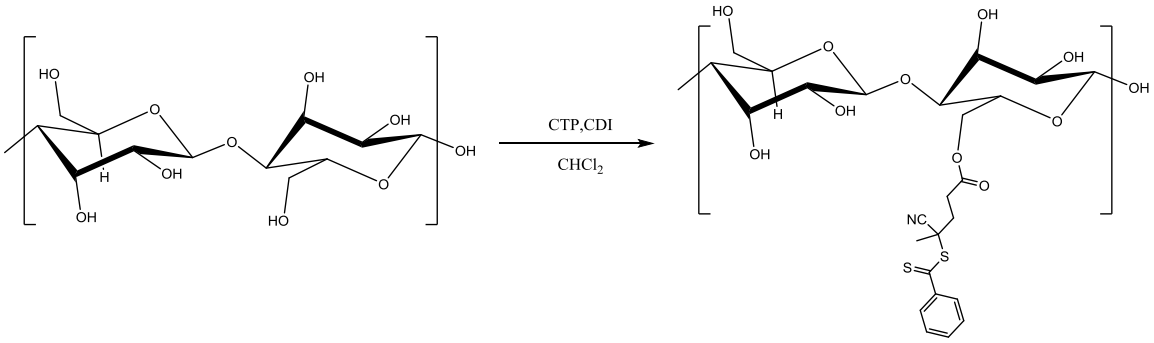

Scheme 6.5. CNC functionalization reaction with CTP and CDI at room temperature. CTP= 111 mmol, CDI= 111.5 mmol, OH= 37 mmol.

Initially, CNC surfaces were modified with CTP as the CTA to obtain a cellulose-based macro-RAFT agent (CNC-CTP) (

Scheme 6.5). Figure 6.20 shows the FT-IR spectra of both native CNC and CNC-CTP where, similar to the CNC-GMA, the only visible change in the spectra is related to the C=O stretching vibration at 1,717 cm^{-1} corresponding to the carbonyl group of the CTP structure. The aromatic skeletal vibrations are barely noticeable at 1,590 cm^{-1}, which overlaps the O-H signal of the CNC residual water at 1,640 cm^{-1}. An additional signal appeared at 1,268 cm^{-1}, which was presumed to be an aromatic deformation vibration that was not present in the native CNC.

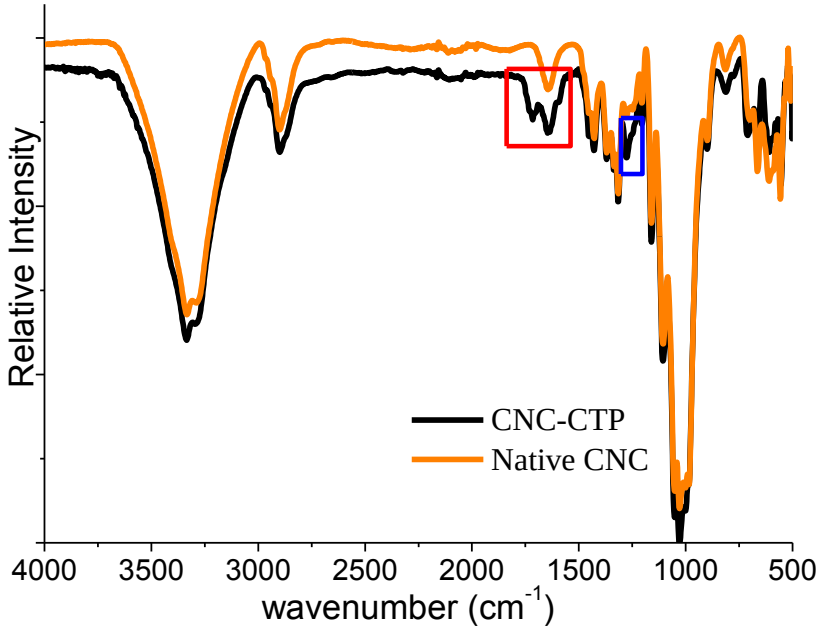

Figure 6.20. FT-IR of native CNC and CNC-CTP. The red box highlights corresponding to the carbonyl group of the CTP at 1,717 cm^{-1} structure and the aromatic skeletal vibrations at 1,590 cm^{-1} which overlaps the O-H signal at 1,640 cm^{-1}. The blue box highlights a signal at 1,268 cm^{-1} which is presumed to be an aromatic deformation vibration.

TGA analysis was also performed. Figure 6.21 shows the TGA of neat CTP, native CNC and CNC-CTP. It can be observed that CNC-CTP began to decompose at around 244°C whereas, for native CNC, the onset temperature was 267°C. The CTP onset temperature was 170°C. From the TGA trace of CTP, it was possible to confirm that there was no significant residual CTP within the CNC-CTP product, supporting the FT-IR results that the CNC surfaces have been modified with CTP.

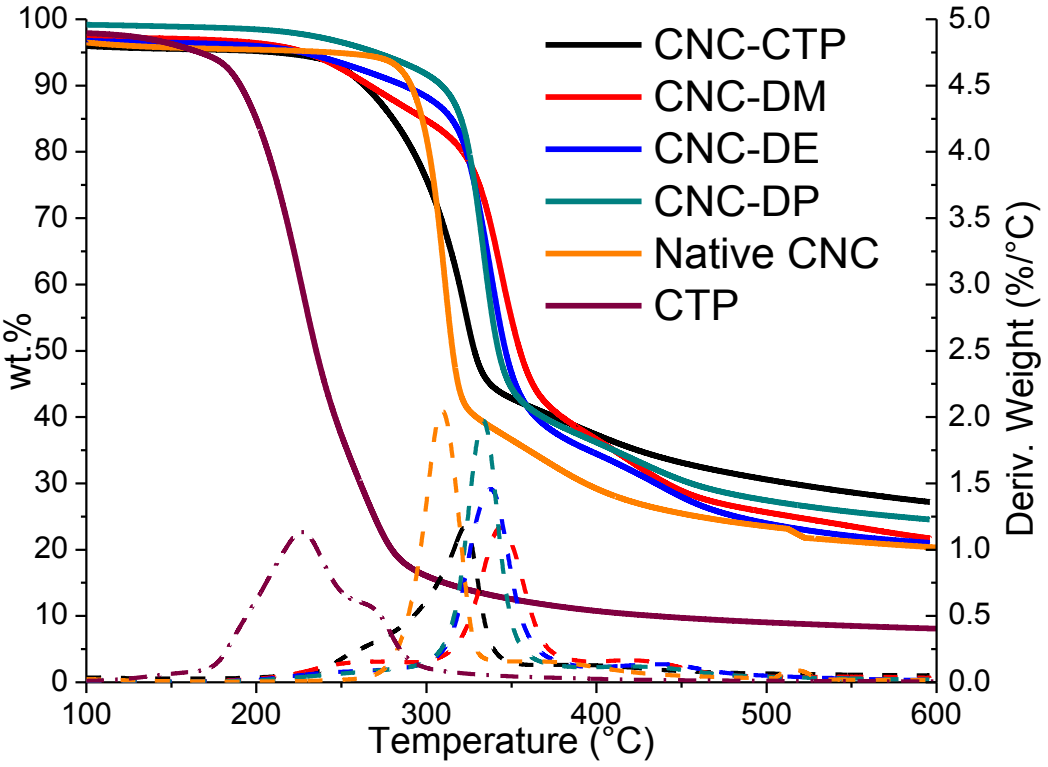

Figure 6.21. TGA analysis of CTP, native CNC, CNC-CTP and grafted CNC products via SI-RAFT polymerization.

Scheme 6.6 illustrates the *grafting-from* reaction of CNC-CTP with dialkylaminoethyl methacrylate monomers in tert-butanol in the presence of the ACVA initiator. In this case, the primary radicals coming from the ACVA will react with the dithiobenzoate at the CNC-CTP surface. After the addition-fragmentation step, the CNC-CTP will play the role of the R-group, and become a primary radical where monomeric units will start adding onto the CNC surfaces. Due to the growing polymeric chains on the CNC surfaces, steric hindrance may play an important role such that, deactivation of the growing grafts by the dithiobenzoate groups may be hindered. However, this does not represent a problem as livingness of the polymer-grafted chains is not required. Successful grafting of

PDMAEMA, PDEAEMA and PDPAEMA did occur and was confirmed by FT-IR and TGA. Solid-state CP-MAS ^{13}C NMR spectra are shown in Appendix F.VII.

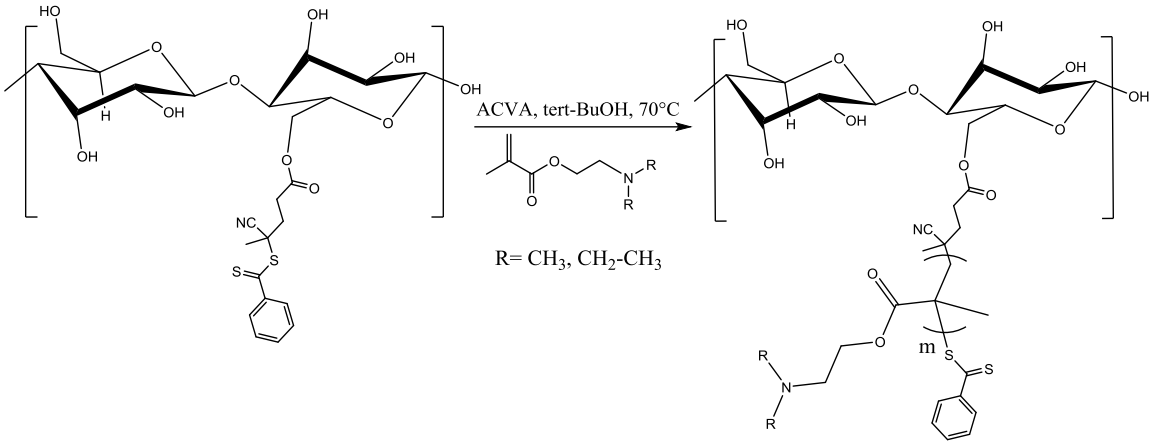

Scheme 6.6. *Grafting-from* via SI-RAFT polymerization. CNC-CTP (0.25 g), DMAEMA (12.72 mmol), DEAMA (10.77 mmol), DPAEMA (9.39 mmol), ACVA (0.07 mmol) in tert-butanol at 70°C.

Figure 6.22 shows the FT-IT spectra of all three grafted products. The cellulose backbone still has the most prominent signals in the spectra. Nevertheless, the C=O stretching of the poly(methacrylate) backbone is evident at 1,727 cm^{-1} along with the C-H stretching vibrations of the polymer backbone and the alkyl groups of the amines in the range of 2,950-2850 cm^{-1}. In Figure 6.21, the TGA traces also confirmed a successful grafting of the CNC-CTP as the thermal stability of the final products was higher than the native CNC and CTP.

Table 6.8 shows the results of the elemental analysis of the CNC-grafted products. As with the grafting-*from* products via SI-Cu(0)-ATRP, it was not possible to determine the graft densities of the products. Nevertheless, the wt.% percent of polymer per gram of CNC was higher than that of the *grafting-to* products (Table 6.4), going from 20 wt.% to 26

wt.%, while the maximum obtained via *grafting-to* was 21 wt.%, but most of those products were in the range of 10-12 wt.%.

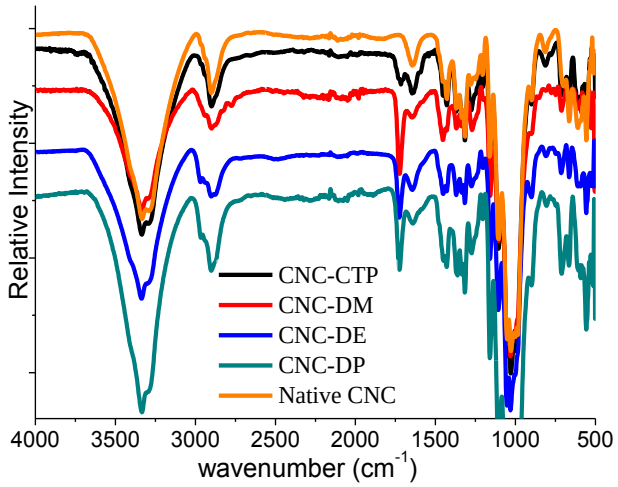

Figure 6.22. FT-IR of native CNC, CNC-CTP and polymer-grafted CNC via SI-RAFT polymerization.

Table 6.8. Elemental analysis results of CNC-grafted products via SI-RAFT polymerization.

Elemental Analysis	%C	%H	%N	N mmol/ g of CNC	wt.% of polyamine/ g of CNC[a]
CNC-DM	44.5±0.1	6.9±0.1	2.3±0.1	2.21	26
CNC-DE	44.3±0.5	6.6±0.1	1.6±0.1	1.41	18
CNC-DP	45.0±0.1	6.7±0.1	1.3±0.2	1.18	28
Native CNC	40.8±0.1	6.2±0.1	0.0±0.1	---	---

[a] Determined as reported by Hemraz *et al.*[22]

In the previous section, it was demonstrated that CNC could be grafted with CO_2-responsive polymers via *grafting-to* RAFT-mediated polymerization. Depending on the graft densities and the molecular weight of the polymer grafts, the grafted materials could form colloidally stable dispersions either under CO_2 (protonated) or under N_2 (deprotonated).

Figure 6.23 shows the auto-titration curves of CNC-DM, CNC-DE and CNC-DP where the ζ-potential varies as a function of pH. In this case, where the polymer content was considerably higher compared to the products made via *grafting-to*, it can be observed that CNC-DM and CNC-DE had an isoelectric point close to a pH of 9. This represents almost one more pH unit when compared to the *grafting-to* series. Hence, the *grafting-from* products exhibited a more basic character. As seen previously, the pH at which these CO_2-N_2 switching systems varied was in the range of 4-9. It can be noted from the auto-titration curves a pH between 8 and 9 that the ζ-potential of CNC-DM and CNC-DE were very close to zero. This is an almost identical trend with the grafted products obtained by SI-Cu(0) ATRP and presented in Chapter 5. The CO_2-switching plots for CNC-DM and CNC-DE are shown in Figure 6.24 and Figure 6.25, respectively. The minimum ζ-potential that was achieved under N_2 for CNC-DM was -2.0 mV at a pH of 8.6, whereas for CNC-DE, the ζ-potential was 18 mV at a pH of 7.12, which agrees well with the auto-titration curves shown in Figure 6.23.

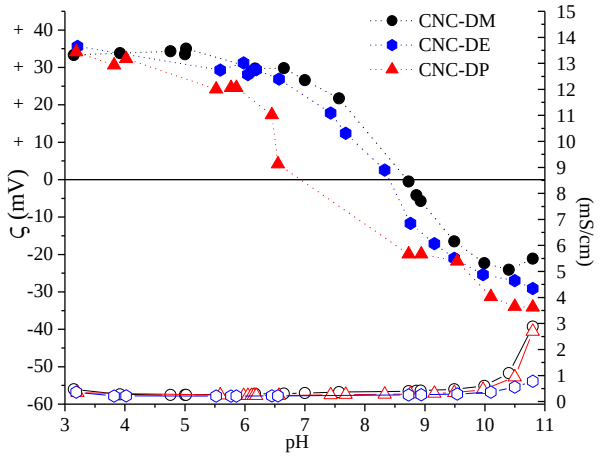

Figure 6.23. Auto-titration curves of CNC-grafted products made by SI-RAFT polymerization (0.4 wt.%).

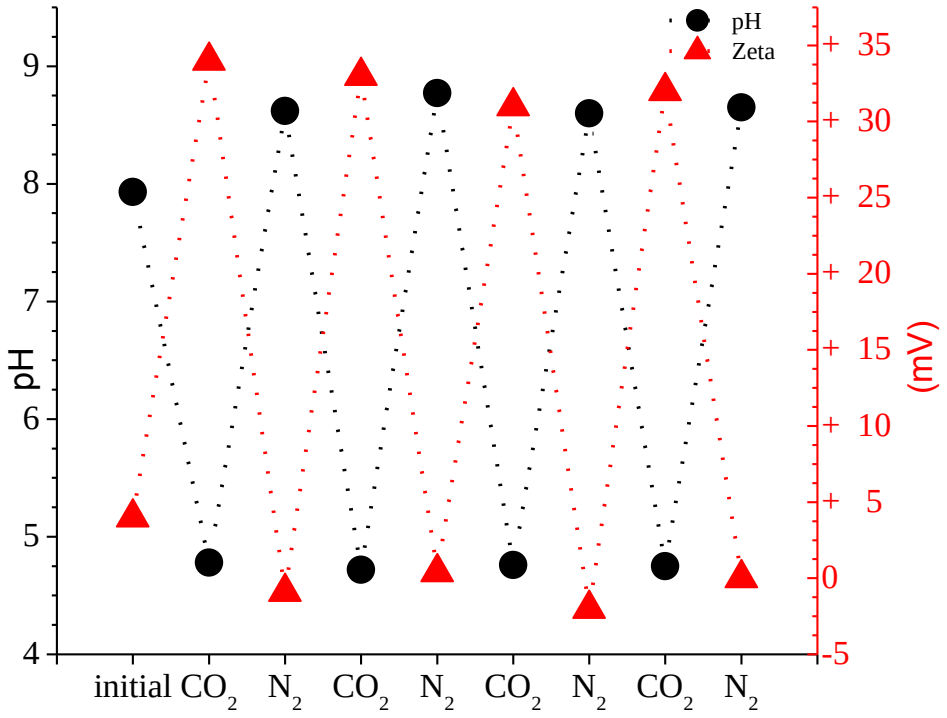

Figure 6.24. CO_2-switching cycles of CNC-DM. (0.4wt %).

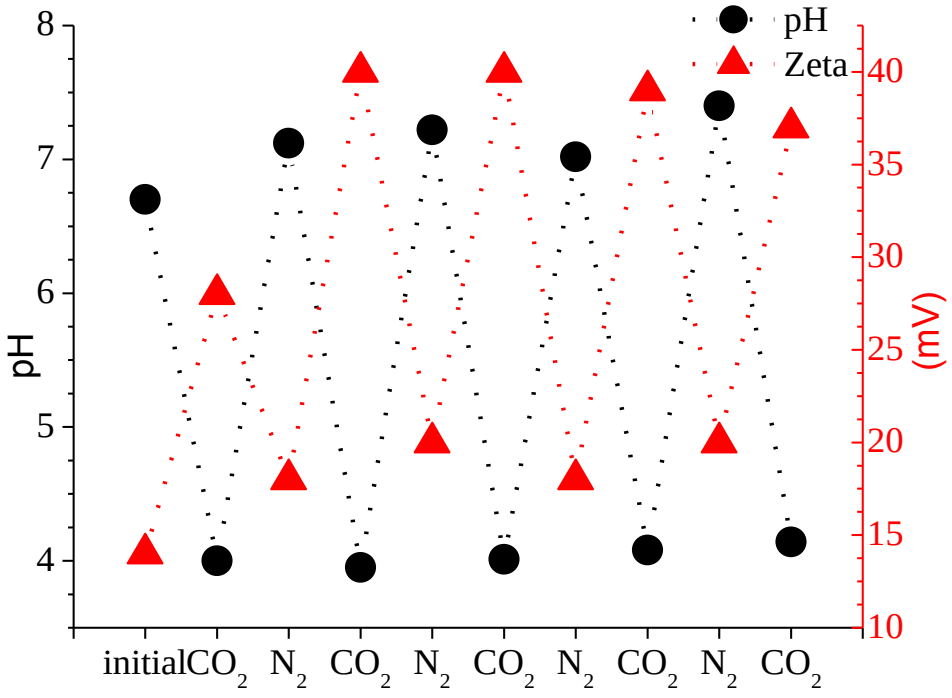

Figure 6.25. CO_2-switching cycles of CNC-DE. (0.4wt %).

For the particular case of CNC-DP, it can be observed that, this time, the ζ-potential increased to +35 mV (Figure 6.23). These results were considerably different than those obtained for the CNC-DP# series (*grafting-to approach*) and was likely due to the polymer content on the CNC surfaces, which was more than double that of the *grafting-to* products. Moreover, it is worth noting that the isoelectric point for CNC-DP occurred at a pH between 6.5 and 7. In contrast, for CNC-DM and CNC-DE the isoelectric points were almost two pH units higher (PDPAEMA is less basic, as reflected by its lower pK_{aH}).

6.3.5 *CO_2-responsive CNC as potential Pickering emulsifier agents*

In Pickering emulsions, nanoparticles are used as stabilizing agents capable to stabilizing oil in water (o/w) or water in oil (w/o) emulsions.[23] Certain types of nanoparticles can be employed as surfactants and represent a viable alternative to conventional small molecule ionic or non-ionic surfactants which are often harmful to the environment.[24] Pickering emulsifying agents have even been used to perform emulsion polymerizations as alternatives for commonly used ionic surfactants.[25-29] Recently, CNC have been used as Pickering emulsifying agents mainly due to their green characteristics (low toxicity and bio-renewability).[30-33] Tang *et al.* previously reported the formation of Pickering emulsions using PDMAEMA-grafted CNC. However, they encountered salt accumulation during repeated cycles of pH variation, typical when using strong acids/bases as pH triggers.[14-15] To the best of our knowledge, there are no reports on the use of pH-responsive CNC as Pickering emulsifying agents using CO_2 as a trigger.

While performing the phase shuttling experiments, it was observed that the PDMAEMA, PDEAMA and PDPAEMA-grafted CNC were capable of stabilizing macro-

oil droplets in the aqueous phase, preventing them from coalescing and reforming organic and aqueous layers. An example is presented in Figure 6.26 where a dispersion of ca. 0.2 wt.% of CNC-DM1 of the CNC-DM# series was mixed in a 1:1 vol/vol ratio with toluene dyed with Nile Red at three different pH levels in the CO_2-N_2 pH switching range. After shaking by hand for a few seconds, it can be observed that CNC-DM1 favoured the formation of toluene macro-droplets at mildly acidic and neutral pH. Recalling Figure 6.10, it was concluded that CNC-DM1 in the mildly acidic and neutral pH range had a hydrophobic character, while at mildly basic pH, the hydrophilic character was dominant. Despite the fact that at acidic and neutral pH, the droplets were not dispersed throughout the entire aqueous phase, the droplets were stable and did not coalesce for more than one month.

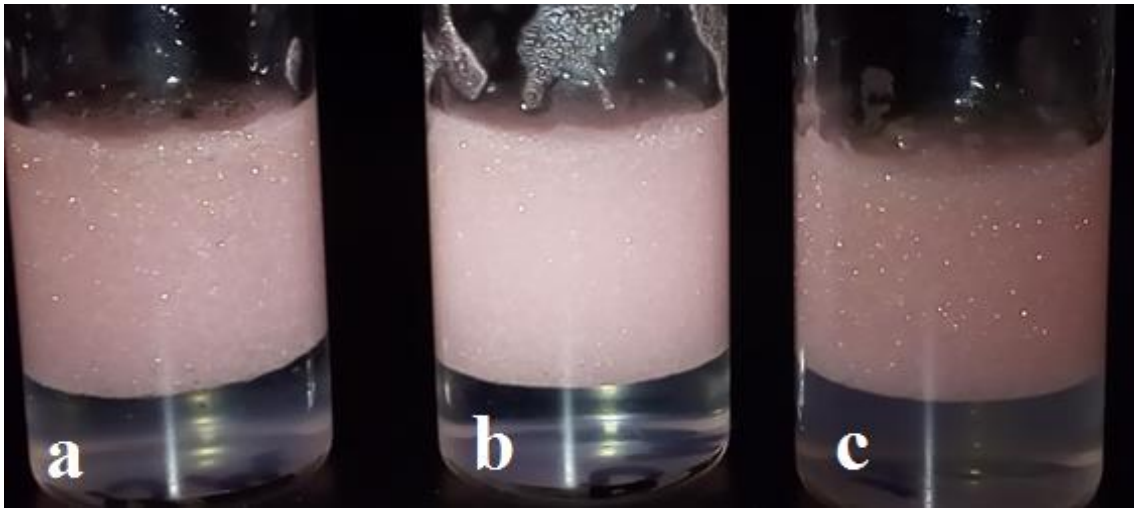

Figure 6.26. Toluene macro-droplets stabilized with CNC-DM1 (0.2 wt.%) using Nile red as dye. pH was adjusted with 0.5 M HCl and NaOH in the CO_2-N_2 pH switching range. (a) 5-6, (b) 7-8, (c) 9-10.

Figure 6.27 shows the same system as previously described, but with CNC-DM3. CNC-DM3 was grafted with higher molecular weight polymer chains and had almost the same grafting density as CNC-DM1. The mixture of CNC-DM3 in acidic media did not form stable macro-droplets of the organic phase, while in a neutral or mildly basic dispersion, smaller macro-droplets were formed in the organic phase. It is worth remembering that CNC-DM3 did not behave in the same manner as CNC-DM1 in aqueous dispersion at the same pH values, where CNC-DM1 exhibited a hydrophobic character under acidic pH and a hydrophilic character at a basic pH. These experiments confirm that the molecular weight has a notable effect on the hydrophobicity of the grafted CNC and that these materials have the potential to form CO_2-responsive Pickering emulsions.

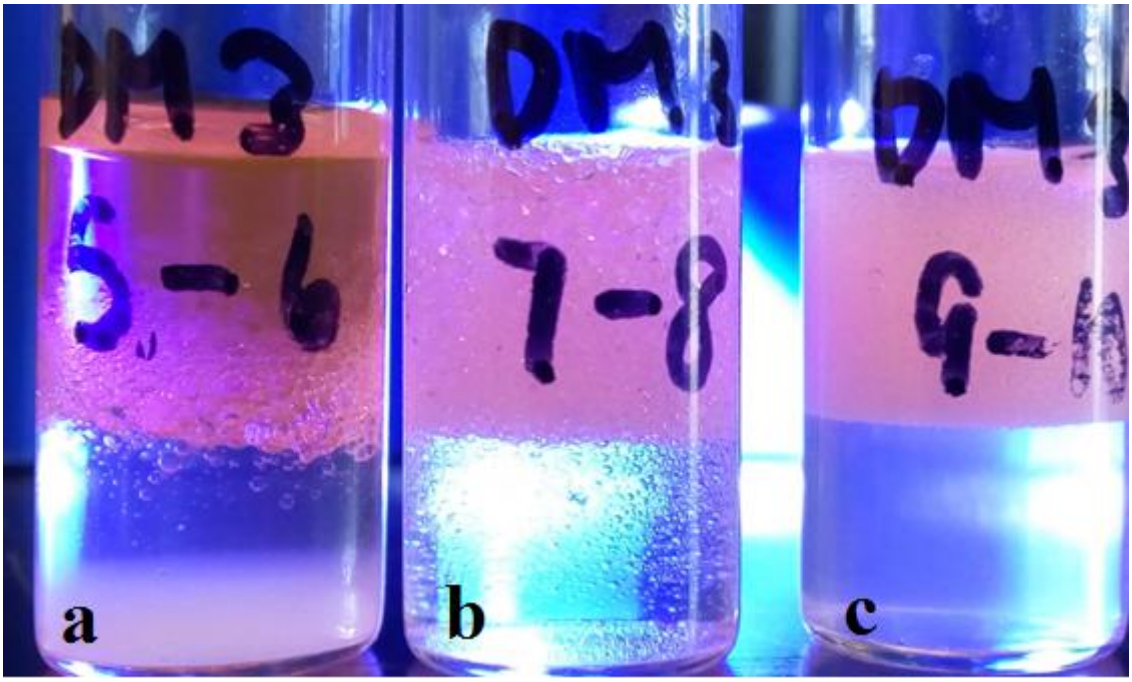

Figure 6.27. Toluene macro-droplets stabilized with CNC-DM3 (0.2 wt.%) using Nile red as dye. The pH was adjusted with 0.5 M HCl and NaOH in the CO_2-N_2 pH switching range. (a) 5-6, (b) 7-8, (c) 9-10.

The majority of polymer-grafted CNC products behaved similarly. Additional pictures of stable macro-droplets in organic solvents can be found in Appendix F.VIII. If these stabilized macro-droplets are subjected to sonication, a high viscosity emulsion results, which resembles a high-internal phase emulsion (Figure 6.28). Although no further specialized characterization methods were employed to analyze these macro-droplets and emulsions, it illustrates that these CO_2-responsive CNC offer promising potential in their use as Pickering emulsifying agents to stabilize o/w systems or to produce CO_2-responsive polymer latexes.

Figure 6.28. High viscosity emulsions of different organic solvents (chloroform, hexanes and toluene) after sonication of CNC-DM1 and CNC-DM3 aqueous dispersions (ca. 0.2 wt.%) at a pH between 7-8. The pH was not adjusted.

6.4 ***Conclusions***

CO_2-responsive CNC were obtained via RAFT-mediated polymerization using both the *grafting-to* and *grafting-from* approaches. Different grafting densities and different molecular weight grafts were attached onto CNC surfaces via *grafting-to*. It was demonstrated that depending on the graft densities, as well as the molecular weight of the polymer grafts, polymer-grafted CNC could display either a hydrophobic or hydrophilic character. Hence, poly(dialkylaminoethyl methacrylates) grafted CNC can be used in systems with different polarities as the extremely hydrophilic nature of CNC could be modified, capable of becoming either hydrophobic or hydrophilic with the particular feature to be fully reversible in aqueous dispersions. CO_2/pH-responsive CNC were capable of forming stable aqueous dispersions either under CO_2 (mildly acidic) or N_2 (mildly basic) conditions. *Grafting-from* via SI-RAFT-mediated polymerization is an efficient technique to incorporate more polymer content onto the CNC surfaces, although the grafting densities cannot be measured. Additionally, it was demonstrated that CO_2-responsive CNC have the potential to function as Pickering emulsifiers and stabilize oil/water macro-droplets and emulsions.

References

1.Arredondo, J.; Jessop, P. G.; Champagne, P.; Bouchard, J.; Cunningham, M. F., Synthesis of CO_2-responsive cellulose nanocrystals by surface-initiated cC(0)-mediated polymerisation. *Green Chemistry* **2017,** *19* (17), 4141-4152.

2.Roeder, R. D.; Garcia-Valdez, O.; Whitney, R. A.; Champagne, P.; Cunningham, M. F., Graft modification of cellulose nanocrystals via nitroxide-mediated polymerisation. *Polymer Chemistry* **2016,** *7* (41), 6383-6390.

3.Garcia-Valdez, O.; Brescacin, T.; Arredondo, J.; Bouchard, J.; Jessop, P. G.; Champagne, P.; Cunningham, M. F., Grafting CO_2-responsive polymers from cellulose nanocrystals via nitroxide-mediated polymerisation. *Polymer Chemistry* **2017,** *8* (28), 4124-4131.

4.Glasing, J.; Bouchard, J.; Jessop, P. G.; Champagne, P.; Cunningham, M. F., Grafting well-defined CO_2-responsive polymers to cellulose nanocrystals via nitroxide-mediated polymerisation: Effect of graft density and molecular weight on dispersion behaviour. *Polymer Chemistry* **2017,** *8* (38), 6000-6012.

5.Nicolas, J.; Guillaneuf, Y.; Lefay, C.; Bertin, D.; Gigmes, D.; Charleux, B., Nitroxide-mediated polymerization. *Prog. Polym. Sci.* **2013,** *38* (1), 63-235.

6.Kockler, K. B.; Fleischhaker, F.; Barner-Kowollik, C., Free radical propagation rate coefficients of N-containing methacrylates: Are we family? *Macromolecules* **2016,** *49* (22), 8572-8580.

7.Anžlovar, A.; Huskić, M.; Žagar, E., Modification of nanocrystalline cellulose for application as a reinforcing nanofiller in PMMA composites. *Cellulose* **2016,** *23* (1), 505-518.

8.Zeinali, E.; Haddadi-Asl, V.; Roghani-Mamaqani, H., Nanocrystalline cellulose grafted random copolymers of n-isopropylacrylamide and acrylic acid synthesized by RAFT polymerization: Effect of different acrylic acid contents on LCST behavior. *RSC Advances* **2014,** *4* (59), 31428-31442.

9.Roy, D.; Semsarilar, M.; Guthrie, J. T.; Perrier, S., Cellulose modification by polymer grafting: A review. *Chem. Soc. Rev.* **2009,** *38* (7), 2046-2064.

10.Roy, D.; Guthrie, J. T.; Perrier, S., Graft polymerization: Grafting poly(styrene) from cellulose via reversible addition−fragmentation chain transfer (RAFT) polymerization. *Macromolecules* **2005,** *38* (25), 10363-10372.

11.Hernández-Guerrero, M.; Davis, T. P.; Barner-Kowollik, C.; Stenzel, M. H., Polystyrene comb polymers built on cellulose or poly(styrene-co-2-hydroxyethylmethacrylate) backbones as substrates for the preparation of structured honeycomb films. *Eur. Polym. J.* **2005,** *41* (10), 2264-2277.

12.Foster, J. C.; Radzinski, S. C.; Matson, J. B., Graft polymer synthesis by RAFT transfer-to. *J. Polym. Sci., Part A: Polym. Chem.* **2017,** *55* (18), 2865-2876.

13.Kan, K. H. M.; Li, J.; Wijesekera, K.; Cranston, E. D., Polymer-grafted cellulose nanocrystals as pH-responsive reversible flocculants. *Biomacromolecules* **2013,** *14* (9), 3130-3139.

14.Tang, J.; Berry, R. M.; Tam, K. C., Stimuli-responsive cellulose nanocrystals for surfactant-free oil harvesting. *Biomacromolecules* **2016,** *17* (5), 1748-1756.

15.Tang, J.; Lee, M. F. X.; Zhang, W.; Zhao, B.; Berry, R. M.; Tam, K. C., Dual responsive pickering emulsion stabilized by poly[2-(dimethylamino)ethyl methacrylate] grafted cellulose nanocrystals. *Biomacromolecules* **2014,** *15* (8), 3052-3060.

16.Tang, J.; Quinlan, P. J.; Tam, K. C., Stimuli-responsive pickering emulsions: Recent advances and potential applications. *Soft Matter* **2015,** *11* (18), 3512-3529.

17.Mitsukami, Y.; Donovan, M. S.; Lowe, A. B.; McCormick, C. L., Water-soluble polymers. 81. Direct synthesis of hydrophilic styrenic-based homopolymers and block copolymers in aqueous solution via RAFT. *Macromolecules* **2001,** *34* (7), 2248-2256.

18.Wager, C. M.; Haddleton, D. M.; Bon, S. A. F., A simple method to convert atom transfer radical polymerization (ATRP) initiators into reversible addition fragmentation chain-transfer (RAFT) mediators. *Eur. Polym. J.* **2004,** *40* (3), 641-645.

19.Majoinen, J.; Walther, A.; McKee, J. R.; Kontturi, E.; Aseyev, V.; Malho, J. M.; Ruokolainen, J.; Ikkala, O., Polyelectrolyte brushes grafted from cellulose nanocrystals using Cu-mediated surface-initiated controlled radical polymerization. *Biomacromolecules* **2011,** *12* (8), 2997-3006.

20.van de Wetering, P.; Moret, E. E.; Schuurmans-Nieuwenbroek, N. M. E.; van Steenbergen, M. J.; Hennink, W. E., Structure−activity relationships of water-soluble cationic methacrylate/methacrylamide polymers for nonviral gene delivery. *Bioconjugate Chem.* **1999,** *10* (4), 589-597.

21.Cunningham, M. F.; Jessop, P. G., An introduction to the principles and fundamentals of CO_2-switchable polymers and polymer colloids. *Eur. Polym. J.* **2016,** *76*, 208-215.

22.Hemraz, U. D.; Campbell, K. A.; Burdick, J. S.; Ckless, K.; Boluk, Y.; Sunasee, R., Cationic poly(2-aminoethylmethacrylate) and poly(N-(2-aminoethylmethacrylamide) modified cellulose nanocrystals: Synthesis, characterization, and cytotoxicity. *Biomacromolecules* **2015,** *16* (1), 319-325.

23.Binks, B. P., Particles as surfactants - similarities and differences. *Current Opinion in Colloid & Interface Science* **2002,** *7* (1-2), 21-41.

24.Wu, J.; Ma, G. H., Recent studies of Pickering emulsions: Particles make the difference. *Small* **2016,** *12* (34), 4633-4648.

25.Bon, S. A. F.; Chen, T., Pickering stabilization as a tool in the fabrication of complex nanopatterned silica microcapsules. *Langmuir* **2007,** *23* (19), 9527-9530.

26.Bon, S. A. F., Pickering emulsion polymerization. In *Encyclopedia of polymeric nanomaterials*, Kobayashi, S.; Müllen, K., Eds. Springer Berlin Heidelberg: Berlin, Heidelberg, 2015; pp 1634-1639.

27.Bon, S. A.; Colver, P. J., Pickering miniemulsion polymerization using laponite clay as a stabilizer. *Langmuir* **2007,** *23* (16), 8316-22.

28.Cauvin, S.; Colver, P. J.; Bon, S. A. F., Pickering stabilized miniemulsion polymerization: Preparation of clay armored latexes. *Macromolecules* **2005,** *38* (19), 7887-7889.

29.Teixeira, R. F. A.; McKenzie, H. S.; Boyd, A. A.; Bon, S. A. F., Pickering emulsion polymerization using laponite clay as stabilizer to prepare armored "soft" polymer latexes. *Macromolecules* **2011,** *44* (18), 7415-7422.

30.Hu, Z.; Ballinger, S.; Pelton, R.; Cranston, E. D., Surfactant-enhanced cellulose nanocrystal Pickering emulsions. *J. Colloid Interface Sci.* **2015,** *439*, 139-148.

31.Hu, Z.; Cranston, E. D.; Ng, R.; Pelton, R., Tuning cellulose nanocrystal gelation with polysaccharides and surfactants. *Langmuir* **2014,** *30* (10), 2684-2692.

32.Hu, Z.; Marway, H. S.; Kasem, H.; Pelton, R.; Cranston, E. D., Dried and redispersible cellulose nanocrystal pickering emulsions. *ACS Macro Letters* **2016,** *5* (2), 185-189.

33.Hu, Z.; Patten, T.; Pelton, R.; Cranston, E. D., Synergistic stabilization of emulsions and emulsion gels with water-soluble polymers and cellulose nanocrystals. *ACS Sustainable Chemistry & Engineering* **2015,** *3* (5), 1023-1031.

Chapter 7. Conclusions and Recommendations

7.1 ***Conclusions and contributions***

Conducting the grafting of CO_2-responsive polymers onto CNC can be performed using different approaches. However, reliable information of the homopolymerization of the monomers of interest is required beforehand so better control of the grafting process can be obtained. In Chapter 3, the homopolymerization of DMAEMA and DEAEMA by Cu(0)-ATRP was reported for the first time. A few drawbacks were observed using this system to polymerize these monomers. Transesterification of the monomers did occur with the solvent (primary alcohols) producing copolymers of the dialkylaminoethyl methacrylates and MMA. Additionally, due to a strong interactions of the monomers with the copper catalyst, chain-end functionality and livingness of the final macro-initiators were affected. Still, from the results obtained from this study, suitable conditions were determined to perform the *grafting-from* of CNC via SI-Cu(0)-ATRP.

Looking for an alternative to polymerize dialkylaminoethyl methacrylates to obtain homopolymer chains capable to efficiently chain extend, the polymerization via RAFT-mediated polymerization of DMAMEA, DEAEMA and DPAMEA was studied. Because of the need to perform the polymerization of the mentioned monomers in a polar solvent capable of dispersing CNC, kinetics analysis as well as livingness were reported for the first time in tert-butanol and compared with the bulk system. Good livingness and control were obtained in both systems, demonstrating that the synthesized macro-RAFT agents were capable of efficiently chain extending. The main contribution of this work is a method that can provide fully characterized homopolymers based macro-RAFT agents with known

molecular weight of exclusively the living chains for the purpose of grafting them onto a substrate or for block copolymer synthesis.

Chapter 5 details the surface of modification of CNC via SI-Cu(0)-ATRP with CO_2-responsive polymers. Most of the published work on CNC grafting use conventional ATRP techniques where high concentrations of copper are usually employed. In this work, it was demonstrated that CNC can be efficiently grafted with CO_2-responsive polymers using a greener approach that requires lower amounts of copper. Moreover, by using this method, CO_2-responsive CNC capable of forming reversibly dispersible colloidal systems using a CO_2-N_2 switching system were obtained via *grafting-from* of DMAEMA and DEAMA.

In Chapter 6, using fully characterized PDMAEMA, PDEAMA and PDPAEMA macro-RAFT agents, the effect of the molecular weight of the polymer grafts on the dispersibility of the pH/CO_2-responsive CNC via *grafting-to* was reported for the first time, and then compared to the pH/CO_2-responsive behaviour of grafted CNC via *grafting-from*. It was determined that depending on either the graft density, the molecular weight of the polymer grafts or a combination of both, the grafted CNC could be colloidally stable either in acidic or basic aqueous dispersions. Moreover, when having similar graft densities of polymer grafts with different molecular weights, it was determined that the molecular weight of the polymer grafts have a real impact in the overall hydrophobic/hydrophilic character of the grafted CNC. Therefore, the hydrophobic/hydrophilic character can be accordingly tuned depending on the required pH conditions of the final dispersion. Finally, it was demonstrated that these pH/CO_2-responsive CNC have the potential to be used as Pickering emulsifying agents.

7.2 ***Recommendations for future work***

Grafted CNC with PDMAEMA, PDEAEMA and PDEAEMA proved to be CO_2-responsive and depending on the molecular weight of the grafts and/or graft densities, their hydrophobic/hydrophilic character could be easily adjusted. In Chapter 6, it was proposed that the stability of grafted CNC could have a colloidal stability profile under CO_2/N_2 similar to an LCST phase diagram. However, not enough data could be collected to fully demonstrate this hypothesis. Therefore, it would be of significant value to produce more grafted CNC batches with many more different graft densities and molecular weight to determine the limits and the graft characteristics that will confer the surface-modified CNC a colloidal stability under CO_2 in aqueous dispersions.

In this work, the surface modification of CNC was carried out using RDRP techniques such as ATRP and RAFT. A few experiments were done to graft CNC using FRP instead of RDRP techniques (See Appendix G.I). The FRP approach has the advantage that no specialty chemical reagents or catalysts are required making the process much cheaper and feasible in an industrial scale making it a valuable approach for surface modifying CNC with any type of polymers via a *grafting-from* approach. Figure G.1 shows the TGA analysis of the *grafting-from* of the monomers used in this work from CNC-GMA via FRP. The TGA traces confirms the surface modification. However, the pH/CO_2-responsive properties of these materials were not studied. Therefore, it is recommended to carry on with this approach to further analyze how to control polymer loading and pH/CO_2-responsiveness as well. The costs of the current processes to produce CNC at large scale are expensive preventing their utilization in any commercial applications. Using the surface

modification via the FRP approach does represent an important alternative to make a composite material at reasonable costs.

In Chapter 6, the potential capabilities of pH/CO_2-responsive CNC to be used as Pickering emulsifying agents were demonstrated, representing a viable alternative as emulsifying agents in the cosmetic industries due to their low toxicity and bio renewability. However, there are many factors that need to be further analyzed and properly characterized to fully understand the limitations and mechanism of action of these modified CNC to form and stabilize emulsions. Factors worthy of study include as polymer loadings, polymer hydrophobicity, phase composition, shelf time, surface coverage, and how these complex colloidal systems would behave under a CO_2-N_2 switching system. Grafted CNC could represent a possible alternative for the production of polymer latexes. Although emulsion polymerization using nanoparticles as emulsifying agents is not an unexplored field, so far there are no reports of attempting an emulsion polymerization using pH/CO_2-responsive CNC. Once it is possible to stabilize and characterize o/w emulsions using pH/CO_2-responsive CNC as Pickering emulsifying agent, the next step worth to explore is the production of CO_2-responsive polymer latexes using surface modified CNC as a stabilizing agent.

Appendix

A. Materials

A.I. ATRP

(Diethylamino)ethyl methacrylate (99%), 2-(dimethylamino)ethyl methacrylate (99%), copper (II) bromide (99%), 40 gauge copper wire, α-bromo isobutyric acid (98%), ethyl 2-bromoisobutyrate (98%), and carbonyldiimidazole (reagent grade) were purchased from Sigma-Aldrich. Monomers were dried over calcium hydride and distilled under vacuum to remove the inhibitor. Methanol (99.8%) and dimethyl formamide (99%) were purchased from ACP chemicals and used as received. Anhydrous ethanol was purchased from GreenField Specialty Alcohols and used as received. Dichloromethane and dimethyl sulfoxide were purchased from ACP Chemicals and were dried over calcium hydride and distilled under nitrogen and vacuum, respectively**.** Water used in this work was deionized using a Millipore Synergy water purification system equipped with SynergyPak purification cartridges (18.2 MΩ-cm). Cellulose nanocrystals (generated by sulphuric acid hydrolysis) were provided by FP Innovations Inc.

A.II. RAFT

2-(Diethylamino)ethyl methacrylate (Aldrich, 99%), 2-(Dimethylamino)ethyl methacrylate (Aldrich, 99%) and 2-(Diisopropylamino)ethyl methacrylate (Aldrich, 99%) were dried in calcium hydride (Aldrich, 95%), and distilled under vacuum to remove inhibitor. 1,1'-carbonyldiimidazole (Aldrich, reagent grade), phenyl magnesium bromide (Aldrich, 1M in THF), carbon disulfide anhydrous (Aldrich, 99.9%), potassium

ferricyanide (III) (Aldrich, 99%), 4,4′-Azobis(4-cyano pentanoic acid) (ACVA) (Aldrich, 98%), sodium hydroxide (Aldrich, 97%), silica gel (Aldrich, 60 Å 70-230 mesh), chloroform-D (Aldrich, 99.8 atom % D, contains 0.03 % (v/v) TMS), methanol (APC, 99.8%), ethanol (CA, absolute), tert-butanol (Aldrich, 97%), acetone (APC, 99%), dimethyl formamide (APC, 99%), ethyl acetate (ACP, 99%), n-hexanes (ACP 98.5%), tetrahydrofuran (ACP, 99%) were used as received. Dichloromethane (APC, 99%) dimethyl sulfoxide (APC, 99%) were dried under calcium hydride (Aldrich, 95%) and distilled under nitrogen and vacuum respectively. Nitrogen and Argon gas (UHP 5.0) were acquired from Praxair Inc. Cellulose nanocrystals were provided by FP Innovations. Water used in this project was in-house water (18.2 MΩ-cm) passed through a Millipore Synergy water purification system equipped with SynergyPak purification cartridges.

A.III.Synthesis of 4-cyanopantanoic Acid Dithiobenzoate

100 ml of phenyl magnesium bromide in THF (0.1 mol) was transferred via cannula to a three-necked round bottom flask previously torched under vacuum and it was submerged on an ice bath. Then 6.6 ml (0.11 mol) of carbon disulfide was added dropwise with a gas-tight syringe and it was left under stirring for two hours. Then 5 ml of deionized water were added to quench the reaction. The solution was concentrated on a rotary evaporator and then washed and extracted with 600 ml of NaOH 1M and the final solution was divided into two 500ml round bottom flasks. To each round bottom flask, potassium ferricyanide (III) (32.93 g, (0.1 mol) aqueous solution was added dropwise via an addition funnel under vigorous stirring for 2h. The red precipitate was filtered and washed with deionized water until the washing liquors became colorless. The product was dried under vacuum at room

temperature and recrystallized from ethanol. Once recrystallized and dried, 14.3 g (47 mmol) was added to a 500 ml round bottom flask along with 14.5 g (51.7 mmol) of ACVA dissolved in 350 ml of ethyl acetate. A condenser was equipped to the round bottom flask and the reaction was heated at reflux for 18h. The ethyl acetate was removed under vacuum. The crude product was purified through column chromatography (silica gel 60 Å 70-230 mesh) using ethyl acetate: hexane 1:1 as eluent. Red purple fractions were collected and concentrated under vacuum. The red oil product was placed in a freezer (-4°C) upon which it crystallized. Yield: 82%.

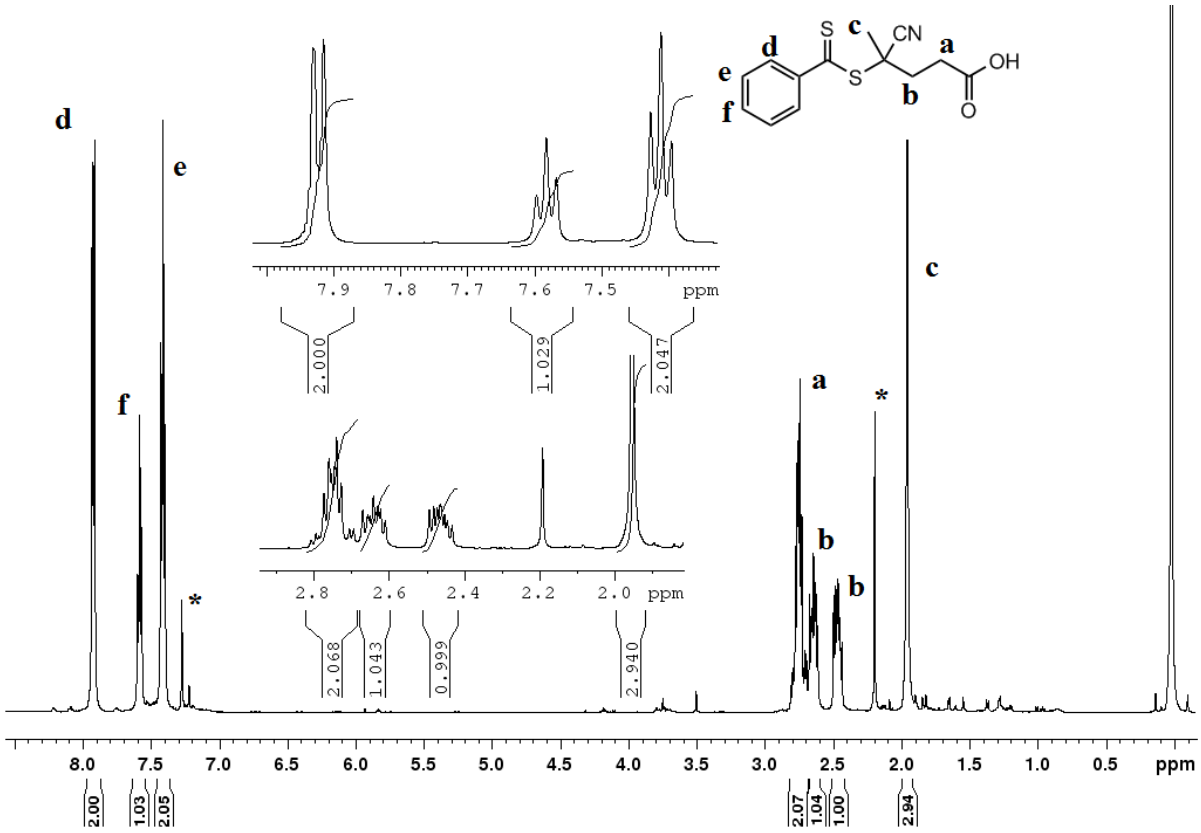

Figure A.1. ^{1}H NMR of synthesized CTP.

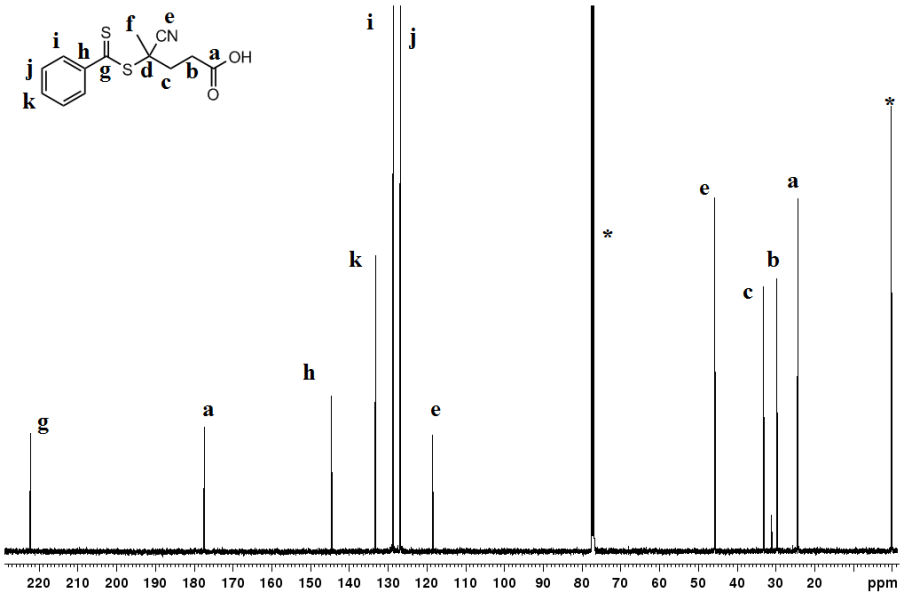

Figure A.2. ^{13}C NMR of synthesized CTP.

B. Instrumentation

B.I. Gel Permeation Chromatography

Gel Permeation Chromatography (GPC) analysis was performed in a Waters 2690 Separation Module with Waters Styragel 4.6 mm 3 300 mm columns (HR 0.5, HR 1, HR 3, and HR 4) coupled with a Waters UV detector at a wavelength of 310 nm and a Waters 410 differential refractive index detector (930 nm) operating at 35°C THF was used as the eluent with a flow rate 0.3 mL/min. All GPC data for the ATRP work are reported as PMMA equivalents. For the RAFT work, all GPC data is reported as absolute molecular weights for PDMAEMA and PDEAEMA using reported Mark-Houwnik parameters and for PDPAEMA, molecular weights are reported as PMMA equivalents, based on a calibration curve of narrow molecular weight distribution PMMA standards purchased from Polymer Standards Service-USA.

B.II. ^{1}H and ^{13}C Nuclear Magnetic Resonance Spectroscopy

Conversion measurements were made by ^{1}H NMR spectroscopy using a Bruker Avance 500 MHz spectrometer with a total of 32 scans, D1: 2 sec at room temperature in $CDCl_3$ or D_2O and DMF as internal standard. Conversion was determined by direct comparison of the internal standard and the vinyl protons of the monomers. Solid state CP-MAS ^{13}C NMR spectroscopy was performed on a Bruker Avance 600 MHz spectrometer with a spin rotation of 12 MHz, D1=2 and CT= 3 ms.

B.III. FT-Infrared Spectroscopy

Fourier Transform Infrared Spectroscopy (FT-IR): measurements were run on a Bruker ALPHA FT-IR with an ATR accessory with a total of 64 scans and a resolution of 4 cm^{-1}.

B.IV. X-ray Photo Electron Spectroscopy

The XPS spectra were measured on a Microlab 310-F spectrometer equipped with an XR-4 twin anode (Al/Mg). The manufacturer of this system is VG Scientific. The samples were mounted on a stub-type stainless steel holder using double-sided adhesive Cu tape and kept under high vacuum (10^{-8} mbar) overnight inside the preparation chamber before they were transferred into the analysis chamber (10^{-9} mbar) of the spectrometer. The XPS data were collected using MgKα radiation at 1253.6 eV (280 W, 14 kV) and a spherical sector analyzer (SSA) operating in CAE (constant analyzer energy) mode. Binding energies are referred to the C1s peak at 284 eV. The survey spectra were recorded from -5 to 1000 eV at a pass energy of 40 eV. High resolution spectra were measured for C1s, O1s,

and Br3d in the appropriate region at a pass energy of 20 eV. Samples were analyzed in triplicate at different locations.

B.V. Elemental Analysis

Elemental analysis was performed on a Perkin Elmer 2400 Series II CHNS/O System in CHN and CHNS mode using helium as carrier gas. Acetanilide or cysteine was used as a calibration standard. All the samples were freeze-dried before running the analysis.

B.VI. Thermogravimetric Analysis

Thermogravimetric analysis was performed using a TA Instruments Q500 TGA analyser setting up an isotherm at 75°C for 15 min where the sample was maintained to remove any traces of moisture, followed by a temperature ramp at 10°C/min up to 600°C. All the samples were vacuum dried before running analysis.

B.VII. Atomic Force Microscopy

Microscopy (AFM) images were taken using a Bruker Nanoscope IV multimode scanning probe microscope with an E scanner in tapping mode using silicon nitride cantilevers with a typical resonance frequency of 315 kHz, spring constants of 13-77 N/m, and a tip radius <10 nm using a scanning rate of 1 Hz. All samples were dispersed in ethanol (c.a 0.1 wt.%) and briefly sonicated. Afterwards, the dispersions were sprayed over freshly cleaved mica using a spray brush.

B.VIII. Zeta Potential and Auto-titrations

The ζ-potential measurements were measured at 25°C on a Malvern Nano ZS instrument with a 633 nm laser diode and a backscattering detection angle of 173 using DTS1070 disposable folded capillary cells. All measurements were performed in triplicate with the data presented (ζ-potential) representing the average value. For in-line measurements, a Malvern Multipurpose Titrator (MPT-2) was coupled to the ZetasizerNano.

C. ATRP homopolymerization

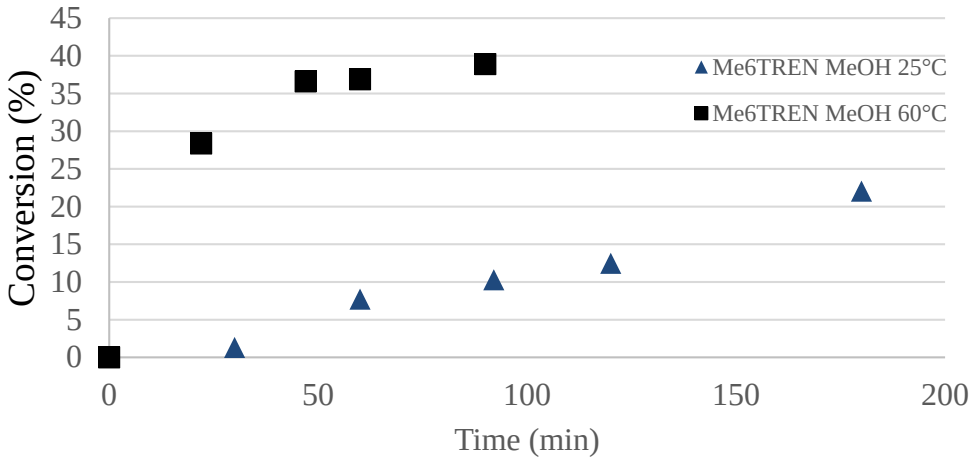

Figure C.1. Conversion vs. time profiles of DEAEMA polymerization using Me_6TREN as ligand. [$CuBr_2$]:[Me_6TREN] = 1:100, BIBA=0.2 mmol, DEAEMA= 10.8 mmol. Me_6TREN= 0.37 mmol.

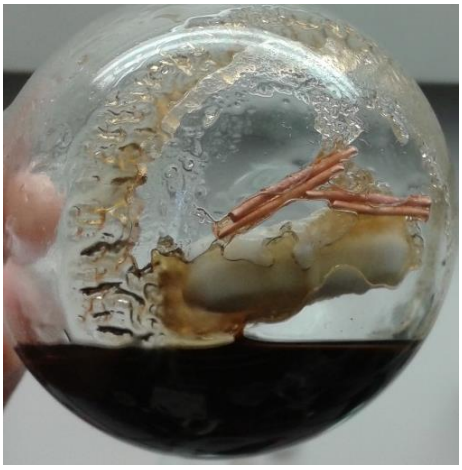

Figure C.2. DEAEMA polymerization using Me_6TREN as ligand in DMSO. [$CuBr_2$]:[Me_6TREN] = 1:100, BIBA=0.2 mmol, DEAEMA= 10.8 mmol. Me_6TREN= 0.37 mmol.

D. RAFT homopolymerization

D.I. GPC-UV traces of macro-RAFT agents and chain-extensions

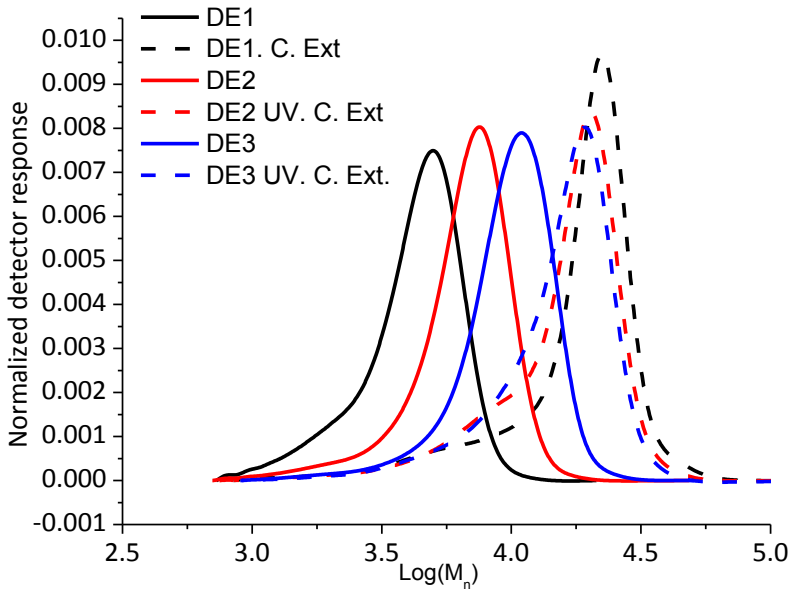

Figure D.1. GPC-UV traces of PDEAEMA macro-RAFT agent series and their chain-extension.

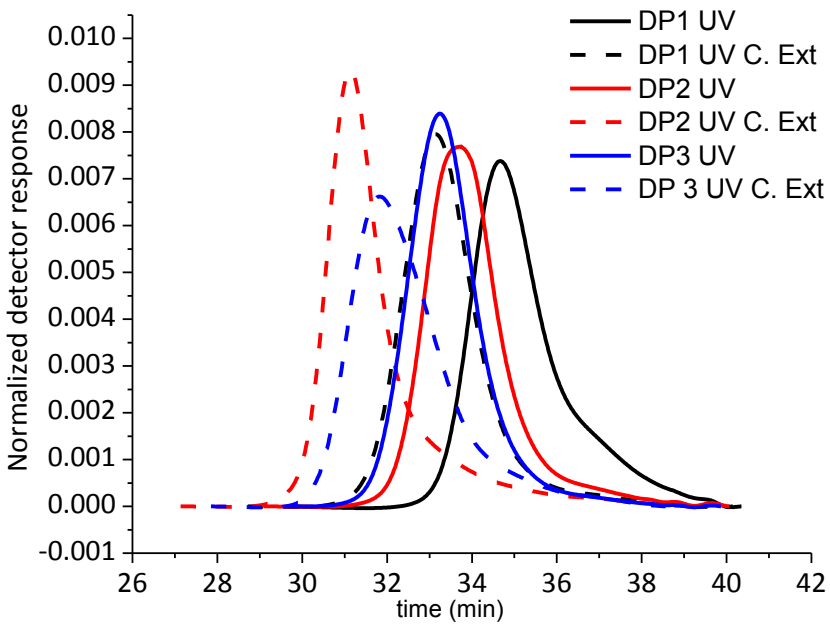

Figure D.2. GPC-UV traces of PDEAEMA macro-RAFT agent series and their chain-extension.

D.II. Multi-peak fitting.

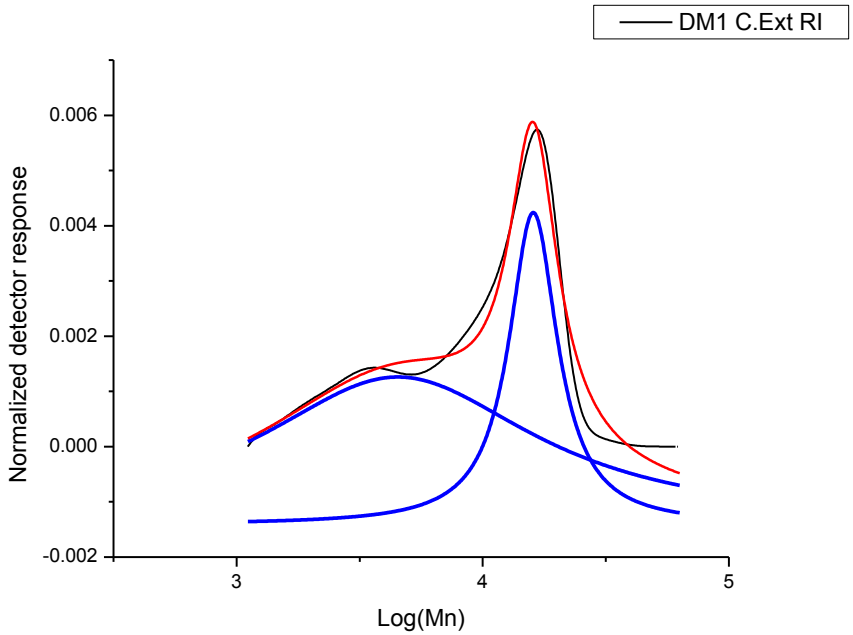

Figure D.3. Multi-peak fitting of the RI chain-extension trace of DM1.

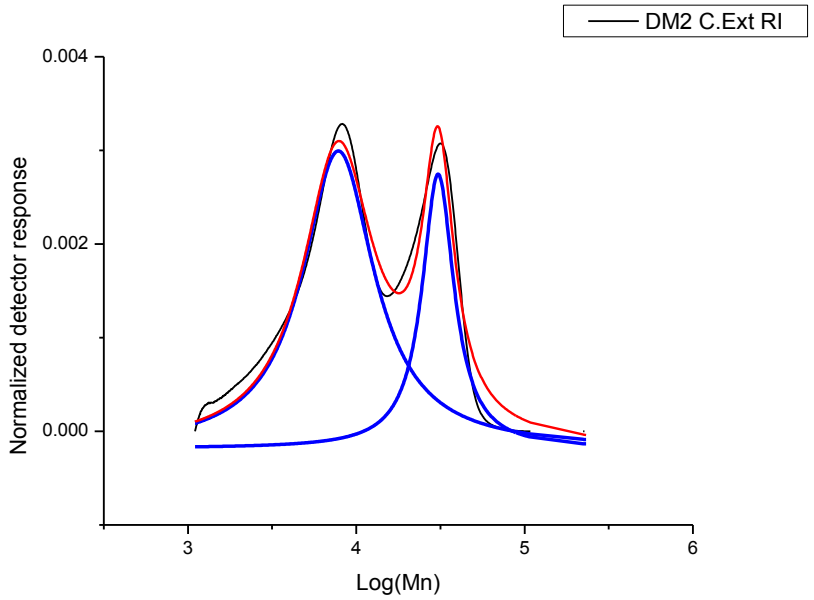

Figure D.4. Multi-peak fitting of the RI chain-extension trace of DM2.

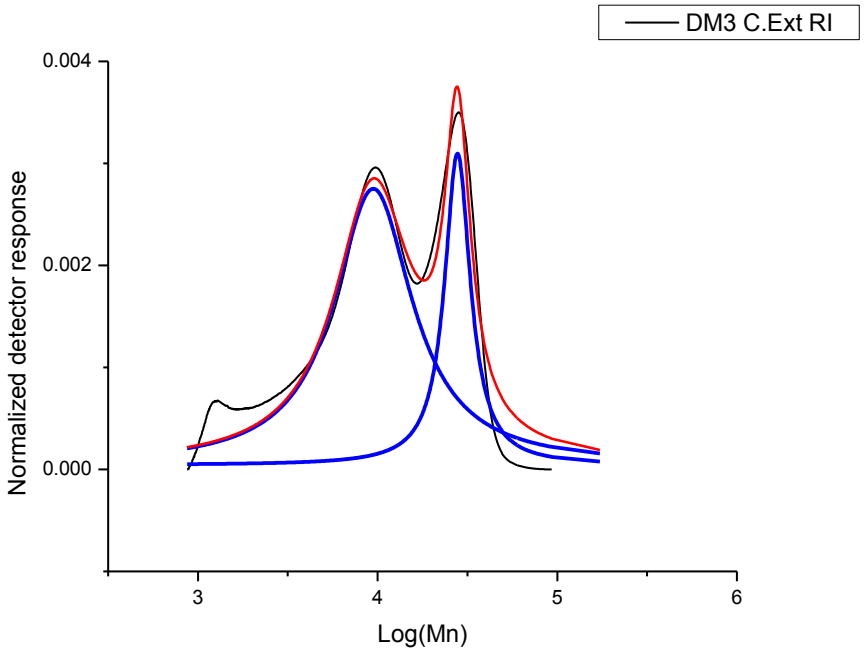

Figure D.5. Multi-peak fitting of the RI chain-extension trace of DM3.

D.III. GPC-UV-RI of PDEAEMAs series

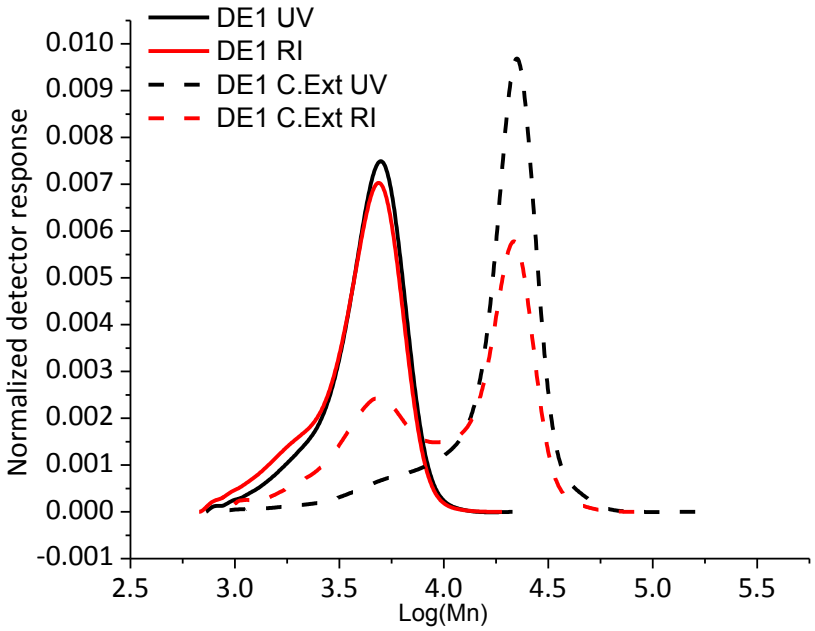

Figure D.6. GPC-UV-RI of DE1 macro-RAFT agent and its chain-extension.

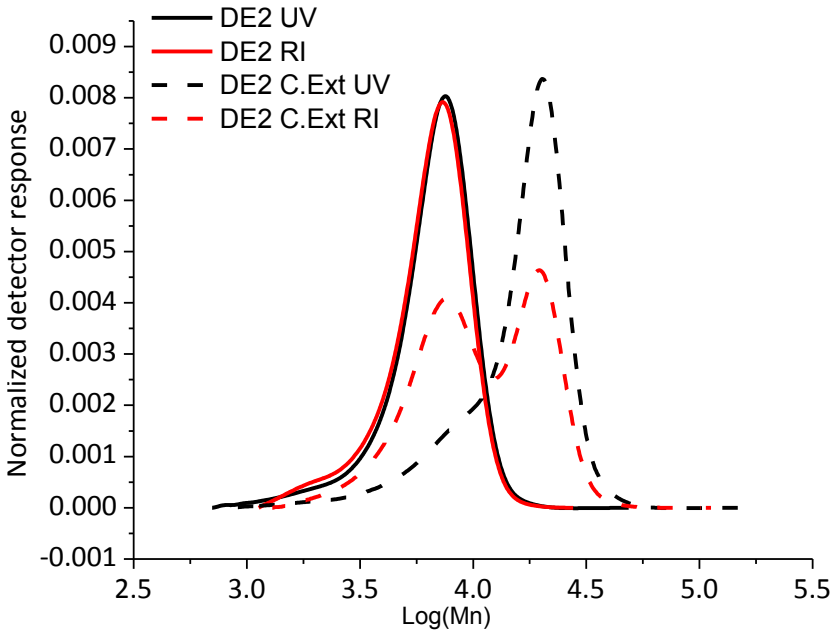

Figure D.7. GPC-UV-RI of DE2 macro-RAFT agent and its chain-extension.

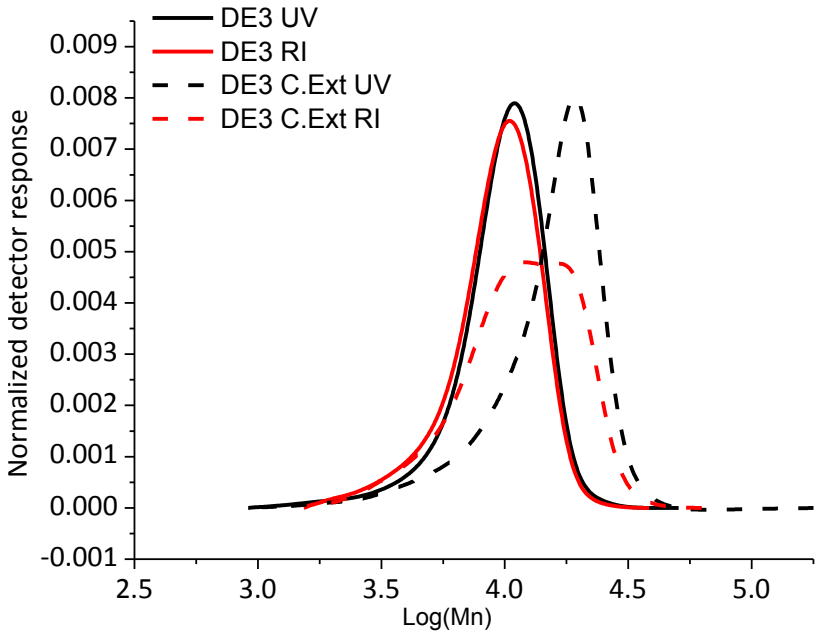

Figure D.8. GPC-UV-RI of DE3 macro-RAFT agent and its chain-extension.

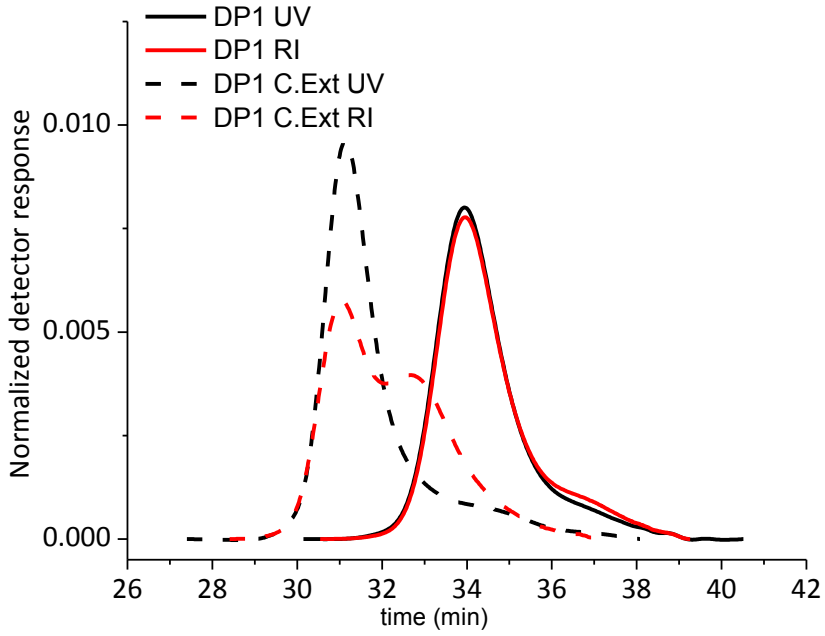

Figure D.9. GPC-UV-RI of DP1 macro-RAFT agent and its chain-extension.

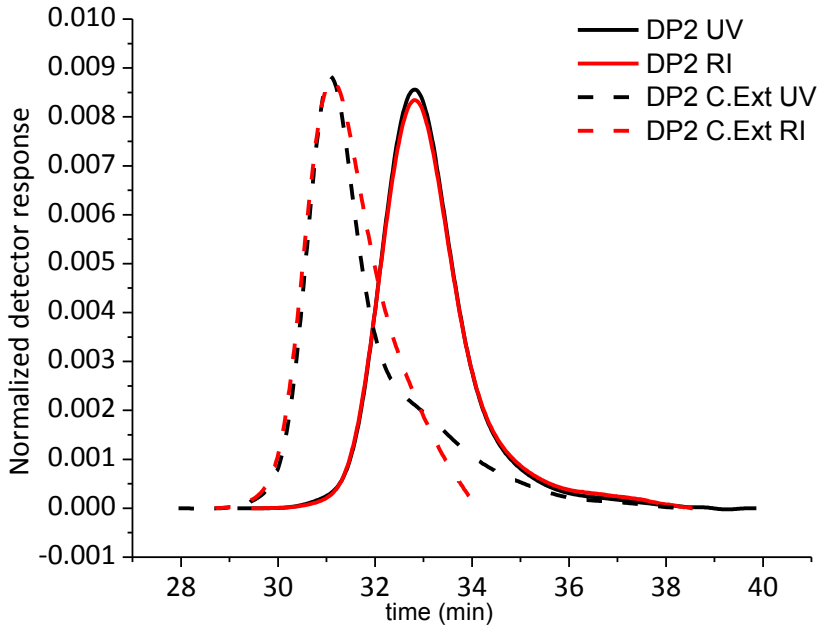

Figure D.10. GPC-UV-RI of DP2 macro-RAFT agent and its chain-extension.

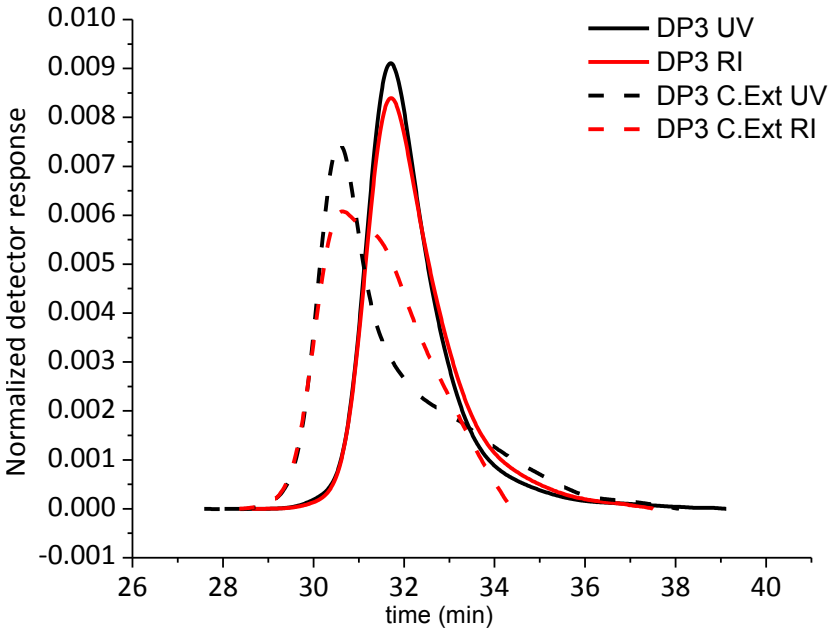

Figure D.11. GPC-UV-RI of DP2 macro-RAFT agent and its chain-extension.

E. Grafting by SI-Cu(0)-ATRP

Using the elemental analysis data of CNC-g-PDEAEMA B1 (where a 20 wt.% of polyamine was determined base on nitrogen content), the theoretical amount of carbon that should be expected if all of the grafted polymer is exclusively polyamine can be calculated. The calculation is as follows using a basis of 1 g of grafted CNC (CNC-g).

$$\frac{0.2\ g\ PDEAEMA}{g\ CNC-g} * \frac{64.77\ \%C}{1\ g\ PDEAMA} = \frac{0.13\ g\ C_{PDEAEMA}}{g\ CNC-g}$$

$$\frac{0.8\ g\ CNC}{g\ CNC-g} * \frac{41\ \%C}{1\ g\ CNC} = \frac{0.33\ g\ C_{CNC}}{g\ CNC-g}; Total\ C_{theo} = 45.8\%$$

Elemental analysis shows 54.13 %C per gram of CNC-g, indicating an excess of 8.3 %C which comes from the PMMA. Therefore,

$$\frac{1\ \text{g PMMA}}{0.599\ \text{g C}} * \frac{0.083\ \text{g C}}{\text{g CNC} - \text{g}} = \frac{0.139\ \text{g PMMA}}{g\ CNC-g}; 13.9\%\ PMMA$$

F. Grafting by RAFT

F.I. GPC-UV of DP# series macro-RAFT agents and their chain-extension

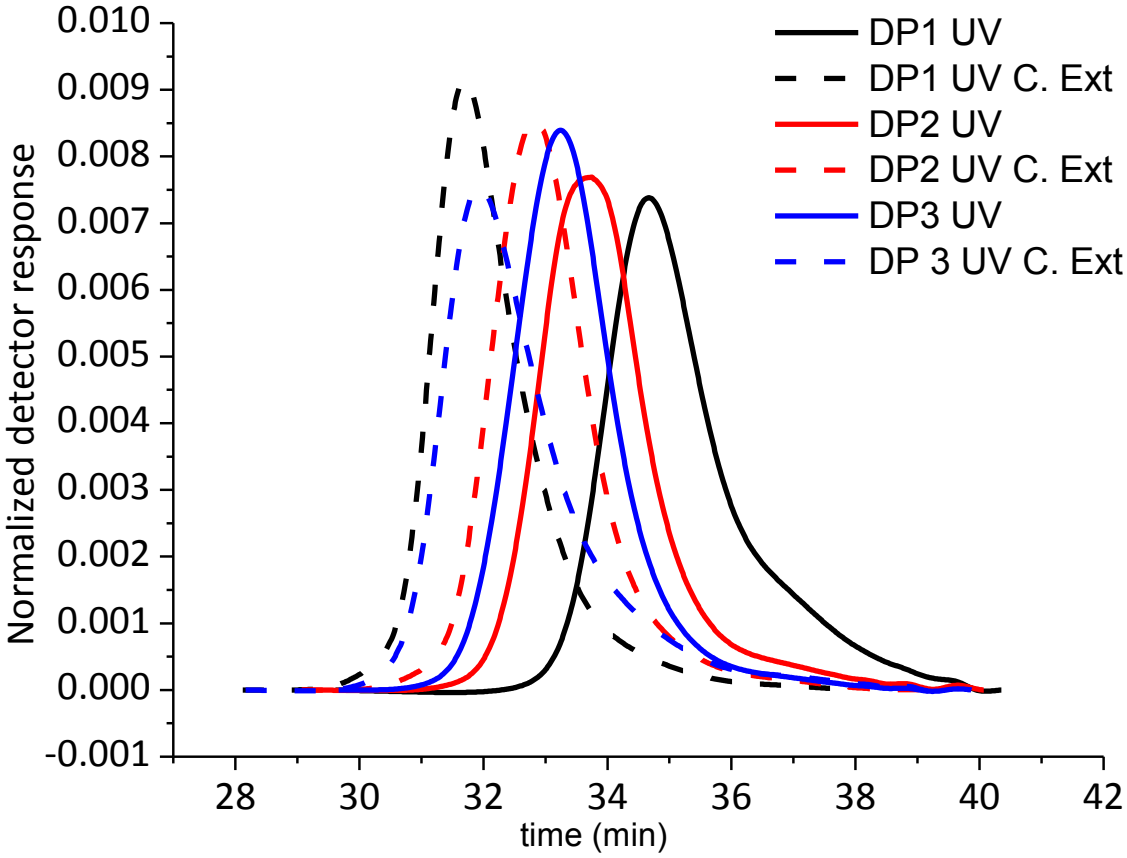

Figure F.1. GPC-UV of DP# series macro-RAFT agents and their chain-extension.

F.II.TGA plots of DE and DP grafting-to

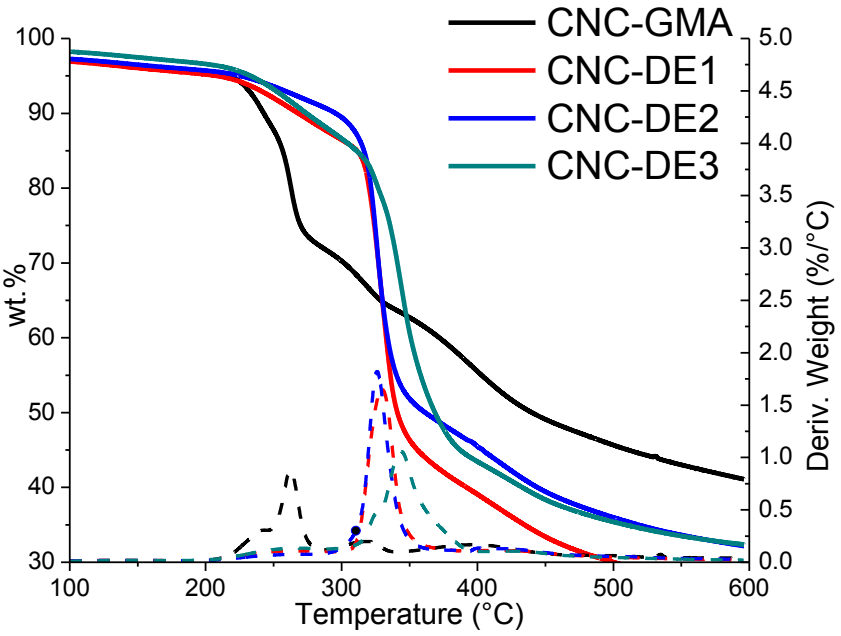

Figure F.2. TGA analysis of CNC-DE# series.

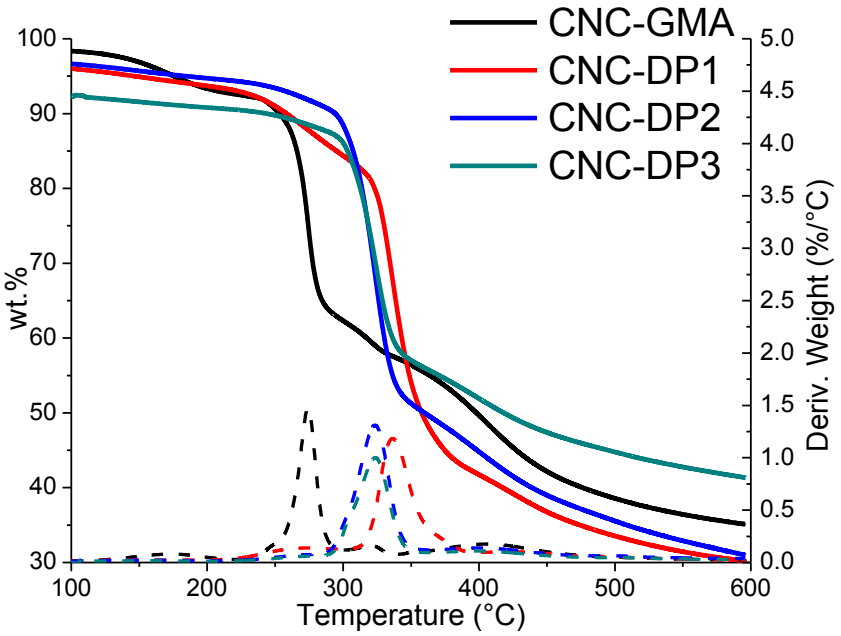

Figure F.3. TGA analysis of CNC-DP# series.

F.III.Grafting Reproducibility

Table F.1 Elemental analysis of grafting-to replicates of DM2 macro-RAFT agent

	%C	%H	%N	N mmol /g CNC	wt.% polymer/ g CNC	Chains/ nm^2
CNC-DM2 Run 1	43.5±0.1	6.8±0.1	2.0±0.1	1.86	23	0.045
CNC-DM2 Run 2	43.1±0.01	6.7±0.01	2.2±0.1	2.09	25	0.051
CNC-DM2 Run 3	44.4±0.2	6.7±0.0	1.8±0.0	1.63	20	0.039
σ[a]	±0.54	±0.04	±0.16	±0.2	±2.05	±0.005

[a]σ represents the standard deviation of the three independent replicates of the grafting-to reaction of DM2 macro-RAFT agent with the same batch of CNC-GMA

F.IV. pK_{aH} of Polymers

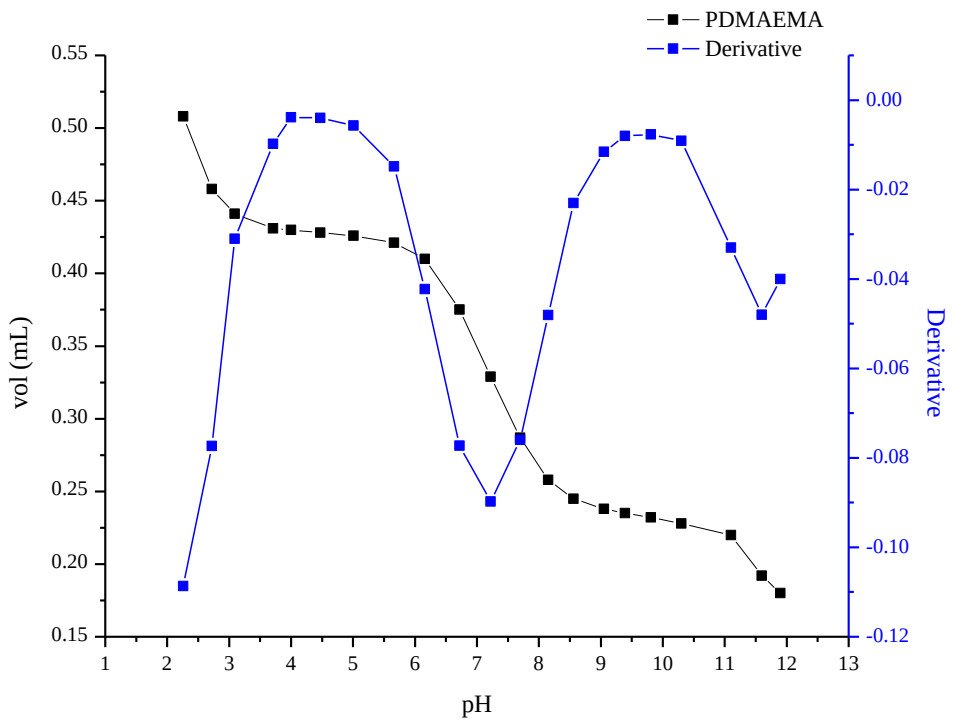

Figure F.4. Titration of PDMAEMA for pK_{aH} determination. $M_{n\ MHS}$: 14,900 Da.

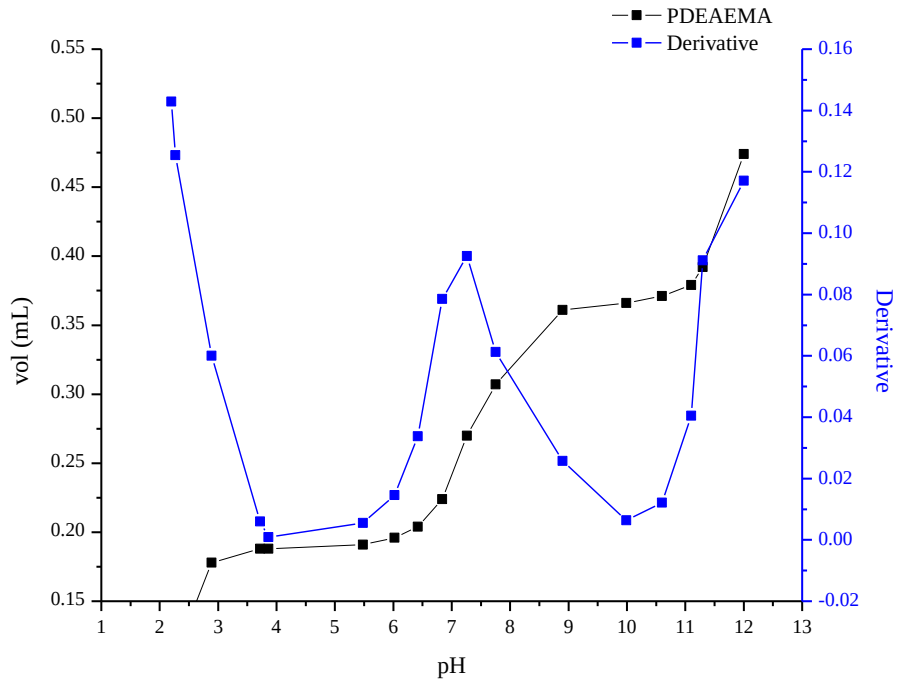

Figure F.5. Titration of PDEAEMA for pK_{aH} determination. $M_{n\ MHS}$: 12,700 Da.

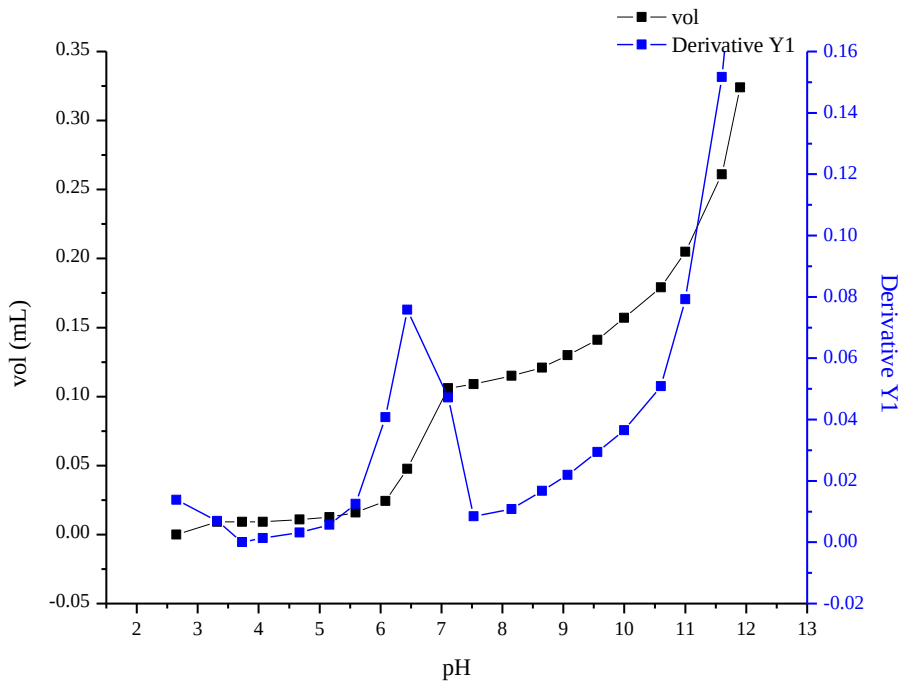

Figure F.6. Titration of PDPAEMA for pK_{aH} determination. $M_{n\ PMMA}$: 7,100 Da.

F.V. Grafting of CNC-DM# S2

Table F.2. Elemental Analysis of CNC-DM#S2 series.

	%C	%H	%N	N mmol/ g CNC	wt.% polymer/ g CNC	Density (chain/nm^2)	M_n[a] (Da)
PDM1	46.6	7.0	1.4	1.2	15.8	0.039	4,900
PDM2	45.5	6.9	1.4	1.2	15.9	0.026	7,500
PDM3	44.9	6.6	1.2	1.0	14.0	0.014	11,800

[a]M_n determined by GPC using universal calibration

F.VI.CO_2 switching of CNC-DM# S2

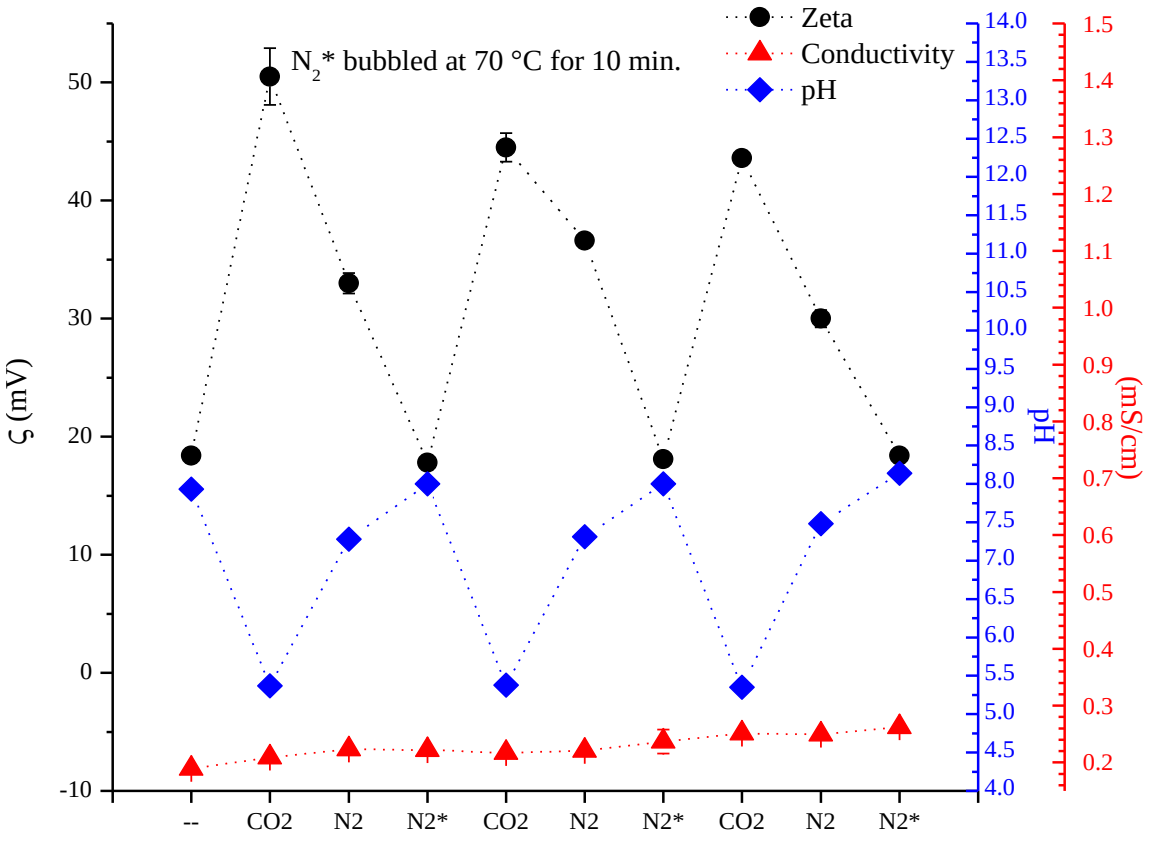

Figure F.7. CO_2-N_2 switching of CNC-DM1S2.

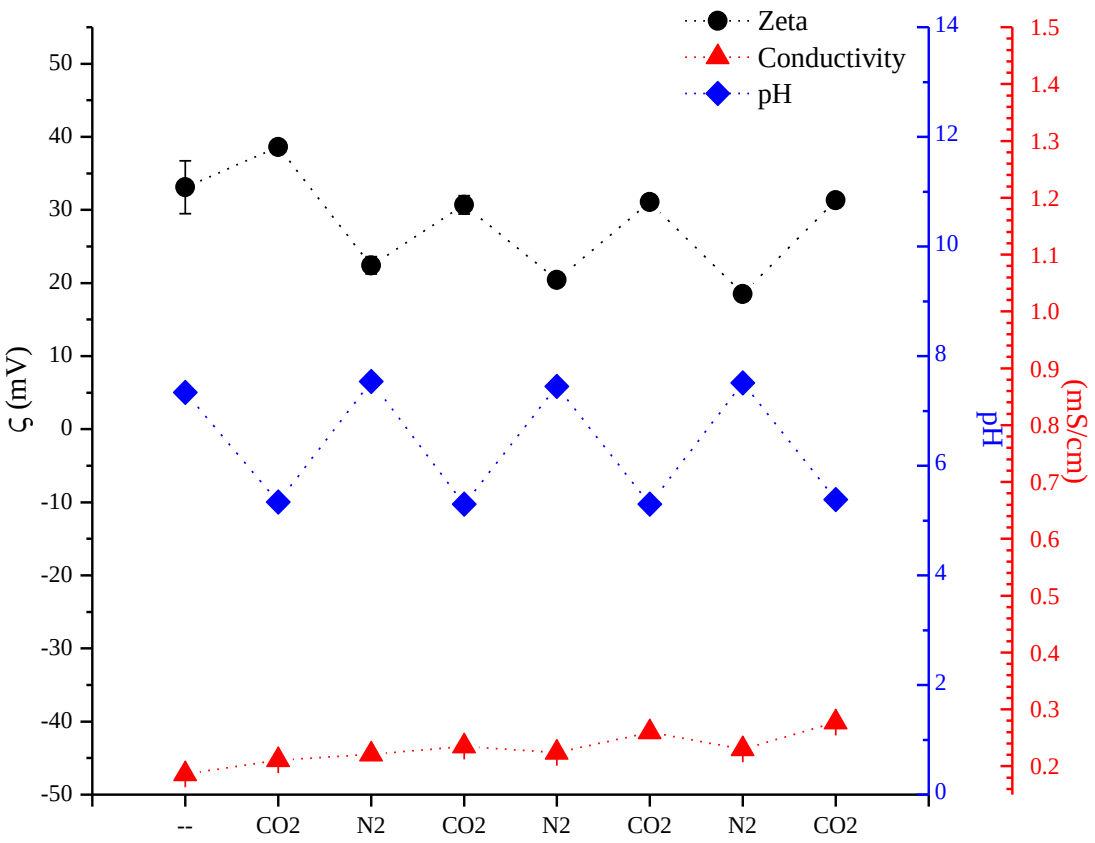

Figure F.8. CO_2-N_2 switching of CNC-DM2S2.

F.VII. ^{13}C NMR of grafting-from products

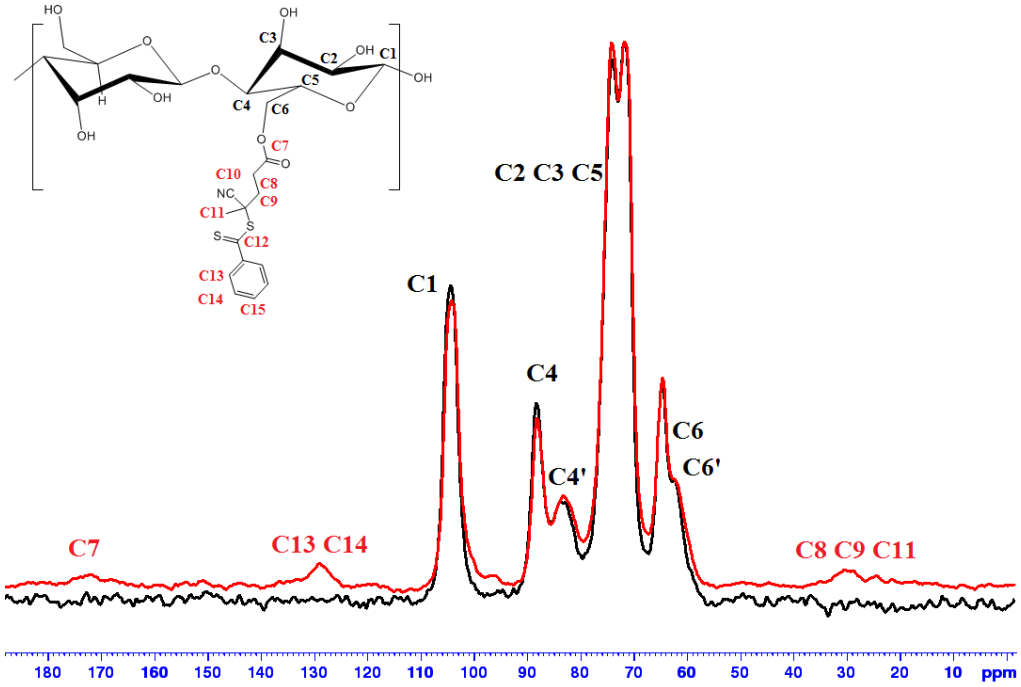

Figure F.9. CP-MAS ^{13}C NMR of native CNC (black) and CNC-CTP (red).

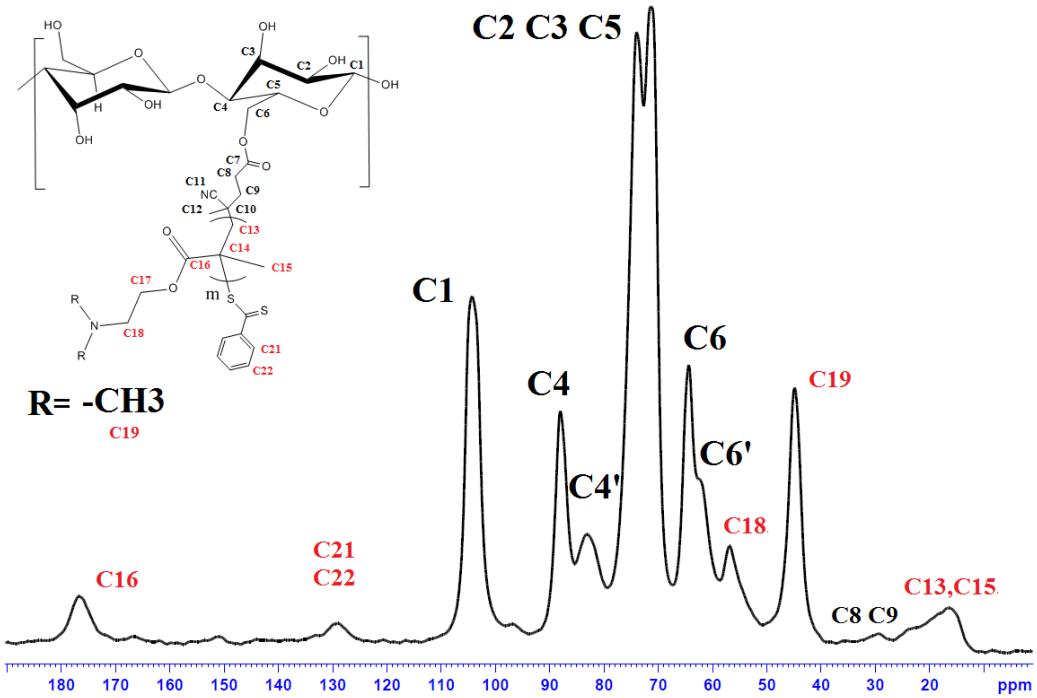

Figure F.10. CP-MAS ^{13}C NMR of CNC-DM.

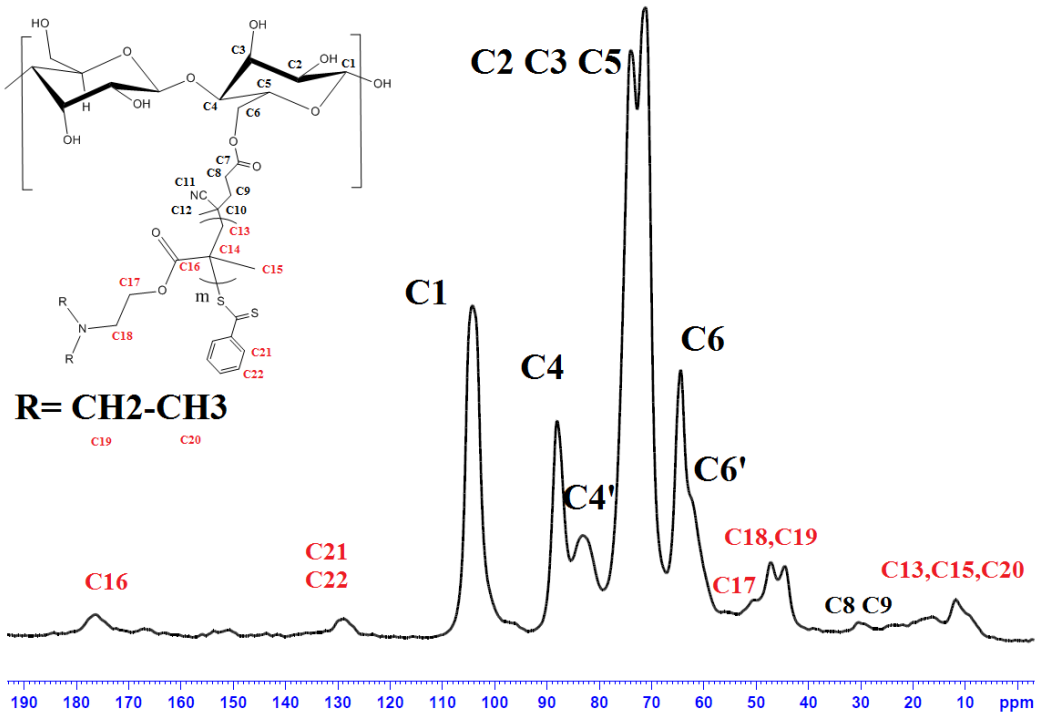

Figure F.11. CP-MAS ^{13}C NMR of CNC-DE.

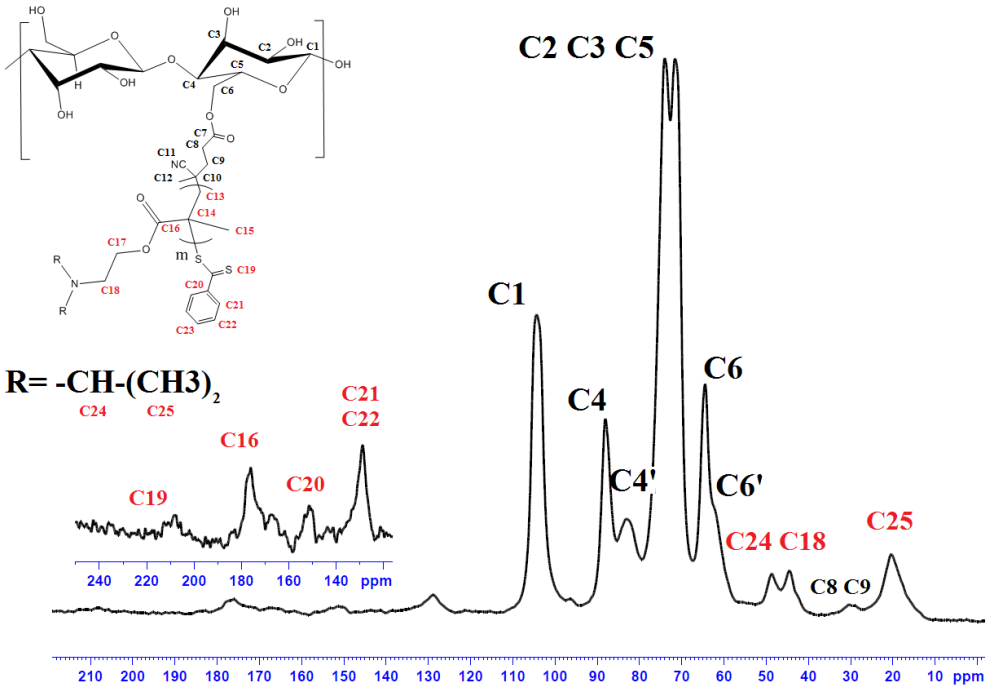

Figure F.12. CP-MAS ^{13}C NMR of CNC-DP.

F.VIII. CNC stabilized macro-droplets of organic solvents

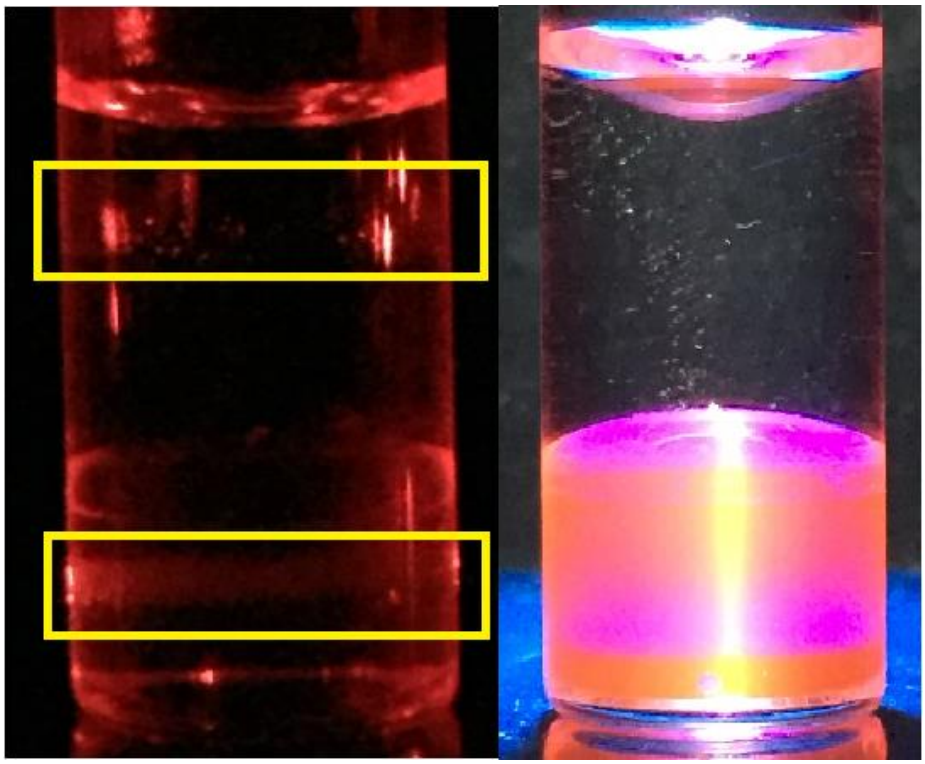

Figure F.13. Mixture of chloroform and water with Nile Red as a hydrophobic dye. Both phases show a certain level of light scattering (left).

Figure F.14. CNC-DM2 dispersions (0.2 wt.%) in dyed toluene (left) and chloroform (center) and hexanes (right) with unmodified pH. The vial on the left with each solvent was not stirred. The vial on the right was hand-shaken. No sonication.

Figure F.15. CNC-DE3 dispersion (0.2 wt.%) in dyed toluene. The pH was adjusted with 0.5 M NaOH to a value of 9-10 (left). No sonication.

Figure F.16. CNC-DE1 dispersion (0.2 wt.%) in dyed toluene. The pH was adjusted with 0.5 M HCl to a value of 2-3 (left). No sonication.

Figure F.17. Sonicated CNC-DM1, CNC-DM2, CNC-DM3 and CNC-DE2 dispersion (0.2 wt.%) in dyed toluene. The pH was adjusted with 0.5 M HCl to a value of 4-5 only for CNC-DE2 (right). The rest dispersions are at neutral pH.

G. Grafting by FRP

G.I. Procedure to perform *grafting-from* approach via FRP

To a three-necked round-bottomed flask, 0.5 g of CNC-GMA (see page 102) were redispersed in 100 mL of tert-butanol and 100 mg of ACVA were also added. Then, 2 g of dialkylaminoethyl methacrylate (DMAEMA, DEADMA or DPAEMA) were dissolved in 20 mL of tert-butanol and the solution mixture was added into an addition funnel. The CNC dispersion was degassed by bubbling nitrogen for 30 minutes and then sealed. Afterwards, the round-bottomed flask was immersed in an oil-bath at 70°C and left under stirring for 24 h. Then, the dispersion was centrifuged at 6000 rpm and solvent exchanged with THF to remove any residual free polymer in solution. This process was repeated six times. The grafted CNC was stored in acetone at 4°C.

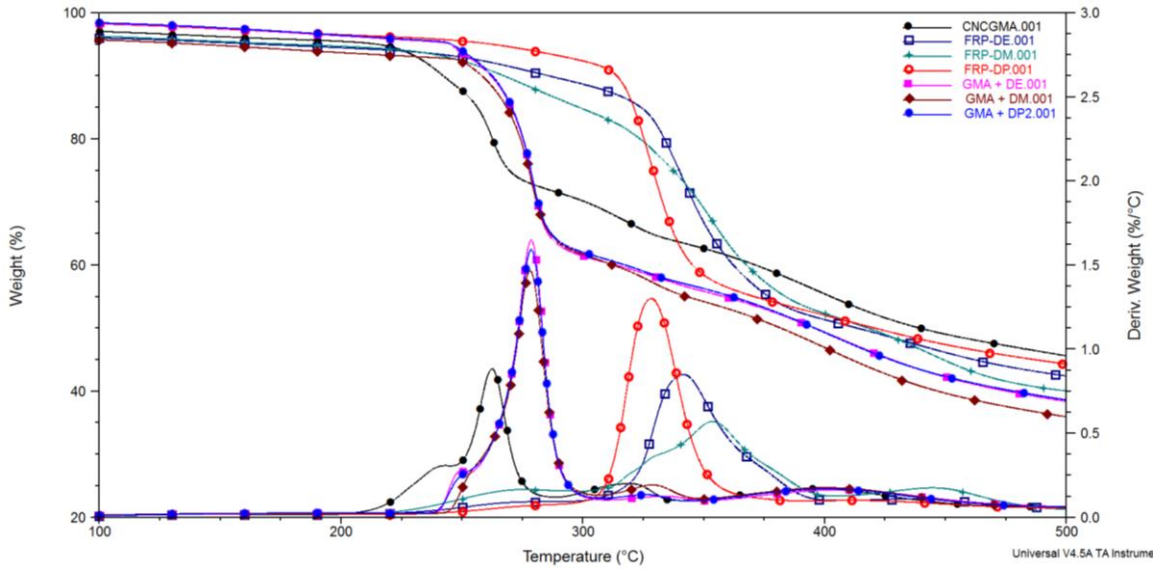

Figure G.1. TGA analysis of CNC-GMA, FRP grafted CNC and physical mixtures of CNC-GMA with homopolymers of DMAEMA, DEAEMA and DPAEMA.